

# An investigation into the molecular mechanisms of hyperbaric oxygen using a human dermal microvascular endothelial cell line and a porcine retinal explant model.

IWUAGWU, B.U.

2019

The author of this thesis retains the right to be identified as such on any occasion in which content from this thesis is referenced or re-used. The licence under which this thesis is distributed applies to the text and any original images only – re-use of any third-party content must still be cleared with the original copyright holder.

# An investigation into the molecular mechanisms of hyperbaric oxygen using a human dermal microvascular endothelial cell line and a porcine retinal explant model

BENEDICTA UGOCHI IWUAGWU

A thesis submitted in partial fulfilment of  
the requirements of the Robert Gordon  
University for the degree of Doctor of  
Philosophy

February 2019

# Declaration

I, Benedicta Ugochi Iwuagwu, hereby declare that the thesis entitled “An investigation into the molecular mechanisms of hyperbaric oxygen using a human dermal microvascular endothelial cell line and a porcine retinal explant model” is my own original research. I confirm that this thesis has not been submitted at this university or any other institution to claim any other qualification; I have cited properly the sources from the journals, books or any other unpublished articles.

**Benedicta Ugochi Iwuagwu**

# Abstract

**Background:** Diabetes is a debilitating metabolic condition with associated vascular complications that are a major cause of morbidity and mortality. Endothelial dysfunction is central to microvascular complications such as diabetic retinopathy (DR) and impaired wound healing in diabetes. Hyperbaric oxygen therapy (HBOT) is the administration of hyperbaric oxygen (HBO) which involves breathing  $\geq 95\%$  oxygen at elevated pressures. It is used for the treatment of recalcitrant ulcers in diabetes. However, the exact molecular mechanism is unclear, and there are questions about its safety, and what contribution the single components of hyperoxia and elevated pressure provide. The effect of HBO on human dermal microvascular endothelial cells (HDMEC) and porcine retinal vasculature is presented with three mechanistic pathways of transcriptional factors regulating the redox (nuclear factor type-2 (Nrf2)), pro-inflammation (Nuclear Factor kappa B; (NFkB)), and oxygen signalling (hypoxia inducible factor type 1 (HIF-1)).

**Method:** HDMEC and porcine retinal explants (a novel explant model) were exposed to treatments simulating HBOT using a bespoke HBO chamber ( $\geq 95\%$  oxygen at 2.2 absolute pressures (2.2ATA) for 105 mins), or hyperoxia alone (HYP) ( $\geq 95\%$  oxygen) or hyperbaric pressure alone (HYB) (2.2ATA) for 90 mins in low (\*LG) or high glucose (HG) concentration. HDMEC and explants were exposed to 20 mM and 25 mM D-glucose concentrations respectively for HG treatment. Post treatments, samples were incubated for 2 h (explants), 4 h (HDMEC) and up to 24 h (explants and HDMEC). HDMEC morphology and metabolic activities were determined using image analysis and the Resazurin assay respectively. Targets of the aforementioned pathways; nrf2 (HO-1), NFkB (IL-6 mRNA), HIF-1 $\alpha$  (VEGF) and PECAM-1 were examined. HIF-1 $\alpha$ , nrf2, HO-1, PECAM-1, VEGF, and NFkB levels were detected by immunocytochemical/immunohistochemistry and/or by Western blotting (WB). Total RNA was isolated from HDMEC and cDNA prepared and amplified for each treatment with IL-6 mRNA specific primers with  $\beta 2m$  as reference.

**Results:** Porcine retinal explants were established as a viable explant model. HIF-1 $\alpha$  immunoreactivity was increased in response to HG relative to LG in retinal explants. In addition, HIF-1 $\alpha$  reactivity was augmented post treatments; HBO, HYP and HYB, and further exaggerated in the presence of HG relative to control, with a corresponding increase in PECAM-1. In retinal explants, HIF-1 $\alpha$  expression post HBO was increased, including increased nuclear associated HIF-1 $\alpha$  reactivity which was sustained for up to 24 h across all retinal layers relative to control. Whilst HG was associated with profound HIF-1 $\alpha$  reactivity in retinal explants, HIF-1 $\alpha$  expression in HDMEC appeared suppressed in response to HG, which may indicate cell type differences between retinal cells and HDMEC. Mean HDMEC size was significantly varied between samples ( $p < 0.0001$ ,  $n = 8$ ), and HDMEC in HYP were significantly larger relative to control or HBO ( $p < 0.05$ ) and hyperbaric pressure ( $p < 0.01$ ), but HBO was not associated with HDMEC morphology or size alteration relative to control ( $p > 0.05$ ). Nrf2 was basal in control sample which was consistent with a homeostatic condition but, ironically nrf2 was acutely lower in HG relative to LG for HDMEC in control condition ( $p < 0.05$ ). Increased nrf2 stabilisation and accumulation was seen following HBO, HYP and HYB relative to control. In addition, nrf2 distribution post HBO and to a lesser extent in HYB were nuclear and plasma membrane associated, whilst predominantly perinuclear associated post hyperoxia relative to control.

Total HO-1 protein in HDMEC appeared elevated in response to treatments; HBO and HYP relative to control possibly via nrf2 mediated mechanism(s). In addition, HO-1 appeared more elevated in HG relative to LG in control and HBO conditions but HO-1 elevation post HYP seemed independent of glucose concentration, alluding to a predominant hyperoxia mediated effect. More so, VEGF accumulation possibly linked to HO-1 increase appeared imminent post HYP relative to control. In HDMEC, concomitant HYP and HG at 24 h were associated with downregulation of PECAM-1 relative to control, although this response appeared lacking in the retinal explants. HBO, HYP and HYB, but more so HBO were associated with significant IL-6 mRNA downregulation relative to control ( $p < 0.0001$ ). IL-6 mRNA was significantly less suppressed post HBO ( $p < 0.01$ ), whilst more suppressed post HYP ( $p < 0.0001$ ) in HG relative to LG control. This shows a significantly higher level of IL-6 mRNA was induced post HBO, whilst decreased post HYP in response to high glucose. NF $\kappa$ B (p65) appeared basal post HBO, whilst elevated post HYP and HYB but more so post HYP relative to control which is suggestive of an acute pro-inflammatory response or endothelial cell activation.

**Conclusion:** HDMEC and retinal cells appear to have different responses to HG, which highlights pertinent cell-type differences that may be fundamental in understanding dysfunctions in endothelial cells of retinal or dermal origin. Also, differential responses are evident in the expression of HIF-1 $\alpha$ , nrf2 stabilisation and possibly its target protein HO-1, and IL-6 post treatments alone and in concert with HG. Fundamentally, this demonstrates the pivotal role of high glucose on HBO mediated effects. Taken together, HBO effects in HDMEC and retinal explants are distinct and may generate a greater protective environment in relation to redox, immune-response and HIF-1 $\alpha$  expression. Further studies are needed to identify the exact mechanisms of redox (nrf2), inflammatory (NF $\kappa$ B), and HIF-1 $\alpha$  expression in HBO particularly in in-vivo setting.

**Key words:** Diabetes, Hyperglycaemia, Endothelial dysfunction, Retinal explants, Nrf2, NF $\kappa$ B, HIF-1 $\alpha$ , HBO. Abbreviations; Diabetic retinopathy (DR), hyperbaric oxygen (HBO), Hyperoxia (HYP), Hyperbaric pressure (HYB). High glucose (HG), low glucose (LG). \*The term low glucose (LG) is used to refer to basal physiological (5.5 mM) glucose level.

## Acknowledgments

Thank you heavenly Father, a Father you have been to me, a fatherless and an orphaned one. Thank you Father for sending Jesus to be my Lord and saviour, and giving me Your His Holy Spirit so I am never alone. I am thankful to my God and Saviour, the Lord Jesus Christ for His help to me all my life

and especially during this journey of my PhD. I have learned immensely that “You are the Wonderful Counsellor and the friend that is closer than a brother” (Isaiah 9 vs 6 and Proverbs 18 vs 24).

I would like to thank my father for his sacrifice and my mum– “may the names of George and Catherine be made great on the earth and be called blessed in their seeds”. My siblings have been my truest precious gift from the Father of Light; Florence, Maria-Celina, Ursula, Georgina, thank you for all you have done. I do not forget you Angela, the beautiful one, I never met you but I know you live on in His hoK2me. I would like to acknowledge and thank my nephews; Joshua, David, Timothy, and Jesse, and my nieces; Valerie, Catherine, and Chantal, and the nieces and nephews still ahead. I would like to thank all my brother in-laws, who have stepped in at various times of my life and growth; Dede, uncle Emeka, Uche, thank you for all you have done and do. I am also thanking my aunt Rose for the love she has shown. I would like to thank the Reads; James, Liz and Louise. I am thankful for your care all these year. Vivien Isiraojie and family, thank you for all the love you have shown to me and my family through friendship.

I owe my earnest gratitude to my supervisor Dr Rachel Knott, whose office door was always open to me, who listened and advised, and supported me throughout the project. I would also like to express my sincere gratitude to my supervisors Dr Stuart Cruickshank and Dr Iain Rowe for their help and guidance.

I would like to thank Mr Allan McPherson for his help in building the hyperbaric chamber.

I am thanking my past advisers, mentors and supervisors; Richard Fisher, Nidhi Patel, Dr Ning Xu Landen, Dr Ulrika Johansson, Dr Jorge Lira Ruas.

I would like to thank Dr Arthur Stewart and his family, for their prayers and friendship. I would like to thank Andrea McMillan for her hugs, a listening ear and support. I would like to thank all the colleagues (past and present) in N540 research hub for the companionship we have shared during these 4 years.

I would like to thank the Robert Gordon University (RGU) for the scholarship funding that enabled me carry out this thesis at RGU

I would like to thank all my Christian brothers and sisters at the Holburn Assembly Aberdeen, City Temple London, and in Stockholm, the ministers at City Temple, Dr Rodney and Karen Woods, Elsie Anifowose and her family, Andrew MacPhee and his family, Dr Emerald Heiland (PhD), Dr Selma Fahmi (MD), and all my friends everywhere who have supported me. I would like to remember and thank you, Martin (of Thum) for believing and encouraging my application to Karolinska Institutet, which has eventually led to this doctorate studies.

# List of publications

Iwuagwu BU, Rowe I, Cruickshank S, Knott RM (2018) Regulation of HIF-1 alpha in hyperoxia and hyperglycaemia in human dermal microvascular endothelial cells. FASEB Journal, 32 Issue 1supplement01

Iwuagwu BU, Rowe I, Cruickshank S, Knott M (2017) Use of a three dimensional porcine retinal explant model to detect HIF1 alpha for understanding DR. FASEB Journal, 31, Issue 1supplement01

Iwuagwu BU, Rowe I, Cruickshank S, Knott RM (2018). Regulation of HIF-1 $\alpha$  in hyperoxia and hyperglycaemia in human dermal microvascular endothelial cells. Experimental Biology, San Diego, USA.

Iwuagwu BU, Rowe I, Cruickshank S, Knott RM (2017) Use of a three dimensional porcine retinal explant model to detect HIF1 alpha for understanding DR. Experimental Biology, Chicago USA (2017).

Iwuagwu BU, Rowe I, Cruickshank S, Knott RM (2016) 3D Porcine retinal model to study microvascular and structural deregulation in DR. British Microcirculation Society Conference Newcastle, UK.

Iwuagwu BU, Rowe I, Cruickshank S, Knott RM (2015). Developing a retinal model for DR. 6th APS International PharmSci Conference UK.

# Table of contents

Declaration .....	i
Abstract .....	ii
Acknowledgments .....	iii
List of publications .....	v
Table of contents .....	vi
List of tables .....	x
List of figures .....	xi
Abbreviations .....	xiii
Chapter 1.0: Introduction .....	1
1.0 Introduction .....	2
1.1 Diabetes Mellitus .....	2
1.2 Diabetic complications.....	4
1.2.1 Macrovascular complications.....	5
1.2.2 Microvascular complications.....	6
1.2.2.1 Diabetic Retinopathy .....	7
1.2.2.2 Diabetic Nephropathy .....	10
1.2.2.3 Diabetic Neuropathy.....	10
1.2.2.4 Impaired wound healing of diabetes .....	11
1.3 Endothelial Perturbations.....	16
1.4 Mechanisms of diabetic complications .....	20
1.5 Oxidative Stress, Inflammation and Angiogenesis .....	26
1.5.1 Nuclear factor erythroid 2–related factor 2 (Nrf2) .....	26
1.5.1.1 Nrf2- NFkB Crosstalk .....	33
1.5.1.2 Heme Oxygenase isoform 1.....	34
1.5.2 Nuclear factor kappa-light-chain-enhancer of activated B cells .....	36
1.5.2.1 Endothelial interleukin-6 (IL-6).....	39
1.5.3 Hypoxia inducible factor -1 alpha (HIF-1 $\alpha$ ) .....	40
1.5.3.1 Vascular endothelial growth factor.....	45
1.6 Endothelial cell models.....	46
1.6.1 Human dermal microvascular endothelial cells (HDMEC).....	46
1.6.2 Porcine retinal explants .....	49
1.7 Hyperbaric oxygen .....	51
1.7.1 Hyperbaric oxygen therapy .....	52



1.7.2 Limitations of HBOT .....	58
1.8 Proposed study mechanism .....	59
1.9 Aim and objectives of the study .....	60
1.10 Objectives of the study .....	60
Chapter 2.0: Materials and methods .....	61
2.0 Materials and methods .....	62
2.1 Materials .....	62
2.2 Maintenance and propagation of HDMEC .....	62
2.3 Retinal explants .....	67
2.3.1 Methods used to validate retinal explant model .....	68
2.3.2 Measurement of matrix oxygen level .....	69
2.3.3 Measurement of a contractile response .....	69
2.3.4. Explant harvest .....	71
2.3.5 Haematoxylin and Eosin staining .....	71
2.3.6 Gomori Trichrome stain for Collagen .....	71
2.4. Immunohistochemistry and immunocytochemistry .....	72
2.5. Immunoblotting (Western blot) .....	73
2.6 Gene expression .....	79
2.7K2 Resazurin assay .....	87
2.8 Hyperbaric oxygen chamber .....	88
2.9 HDMECs size measurement .....	92
2.10 Fluorescence intensity determination .....	92
2.11 Statistical analysis .....	93
Chapter 3.0: Validation of experimental models .....	94
3.1 Introduction .....	95
3.2. Methods .....	97
3.2.1 Retinal explants .....	97
3.2.2 Hyperbaric oxygen model .....	97
3.3. Results .....	99
3.3.1. Retinal explant .....	99
3.3.2. Hyperbaric oxygen model .....	110
3.4. Discussion .....	115
3.5. Limitations .....	121
Chapter 4.0: Endothelial cell size and metabolic activity .....	122
4.1 Hypothesis .....	123
4.2 Introduction .....	123

<b>4.3 Materials and Methods .....</b>	<b>126</b>
<b>4.4 Results .....</b>	<b>128</b>
<b>4.4.1 Effect of varying glucose concentrations, oxygen tension and pressure on HDMEC morphology and size.....</b>	<b>128</b>
<b>4.4.2 Resazurin metabolic activity assay.....</b>	<b>133</b>
<b>4.5 Discussion.....</b>	<b>136</b>
<b>4.6 Limitations.....</b>	<b>140</b>
<b>Chapter 5.0: Inflammatory and Redox Responses .....</b>	<b>141</b>
<b>5.1 Hypothesis.....</b>	<b>142</b>
<b>5.2 Introduction .....</b>	<b>142</b>
<b>5.3 Materials and method .....</b>	<b>144</b>
<b>5.3.1 Cell culture and assays.....</b>	<b>144</b>
<b>5.4 Results .....</b>	<b>146</b>
<b>5.4.1 Effect of glucose concentration, oxygen tension and pressure on redox response.....</b>	<b>146</b>
<b>5.4.2 Effect of glucose concentration, oxygen tension and pressure on inflammatory response .....</b>	<b>157</b>
<b>5.5 Discussion.....</b>	<b>163</b>
<b>5.6 Limitations.....</b>	<b>167</b>
<b>Chapter 6.0: HIF-1<math>\alpha</math>, VEGF and PECAM-1 expression .....</b>	<b>168</b>
<b>6.1 Hypothesis.....</b>	<b>169</b>
<b>6.2 Introduction .....</b>	<b>169</b>
<b>6.3 Materials and Method .....</b>	<b>174</b>
<b>6.4 Results .....</b>	<b>175</b>
<b>6.4.1 Effect of glucose concentration, oxygen tension and pressure on HIF-1<math>\alpha</math>, VEGF and PECAM-1 protein expression .....</b>	<b>175</b>
<b>6.5 Discussion.....</b>	<b>190</b>
<b>6.6 Limitation .....</b>	<b>193</b>
<b>Chapter 7.0: Limitations, overall discussion and future work.....</b>	<b>194</b>
<b>7.1 Over all study limitations.....</b>	<b>195</b>
<b>7.2 Result summary .....</b>	<b>196</b>
<b>7.3 Overall Discussion and Conclusion.....</b>	<b>200</b>
<b>7.3 Further studies .....</b>	<b>209</b>

<b>Chapter 8.0: References</b> .....	210
<b>A</b> .....	211
<b>B</b> .....	212
<b>C</b> .....	215
<b>D</b> .....	217
<b>E</b> .....	219
<b>F</b> .....	220
<b>G</b> .....	221
<b>H</b> .....	223
<b>I</b> .....	226
<b>J</b> .....	226
<b>K</b> .....	227
<b>L</b> .....	231
<b>M</b> .....	233
<b>N</b> .....	235
<b>O</b> .....	236
<b>P</b> .....	237
<b>Q</b> .....	238
<b>R</b> .....	238
<b>S</b> .....	240
<b>T</b> .....	243
<b>U</b> .....	245
<b>V</b> .....	245
<b>W</b> .....	245
<b>X</b> .....	247
<b>Y</b> .....	247
<b>Z</b> .....	248

# List of tables

## Chapter 1

Table1.1 Phases of wound healing .....	12
Table 1.2 Nrf2 dependent gene .....	32
Table1.3 HIF-1 target genes. ....	44

## Chapter 2

Table 2. 1 Antibodies and ancillary materials .....	78
Table 2. 2 CDNA thermal cycler program.....	81
Table 2. 3 Primer BLAST reports.....	82
Table 2. 4 Primers and sequence details .....	83
Table 2. 5 Thermal cycler program for End-point RT-PCR reaction .....	84
Table 2. 6 Standard cycling mode for Real-time qPCR.....	85
Table 2. 7 Dissociation curve conditions (melt curve stage) for Real-time qPCR .....	85

# List of figures

## Chapter 1

Figure 1. 1 Simple diagram of the unifying mechanism .....	24
Figure 1. 2 Schematic representative structure of Nrf2 .....	28
Figure 1. 3 Nrf2 regulation in normal and stress condition .....	29
Figure 1. 4 Nrf2 and NFκB cross-talk .....	33
Figure 1. 5 Heme oxygenase -1 pathway.....	35
Figure 1. 6 Canonical (classical) NFκB signalling pathway .....	37
Figure 1. 7 Domain structure of human HIF-1α and HIF-1β .....	41
Figure 1. 8 Proposed study mechanism(s) .....	59

## Chapter 2

Figure 2. 1 Morphology of human dermal microvascular endothelial cells (HDMEC).....	63
Figure 2. 2 Three-dimension matrix formation.....	68
Figure 2. 3 Measurement of contractile response.....	70
Figure 2. 4 Standard curve of BCA protein assay .....	75
Figure 2. 5 Resolution of RNA extracted from HDMEC .....	80
Figure 2. 6 Schematic representation of treatment in chamber.....	89
Figure 2. 7 Schematic representation of HBO cycling .....	90

## Chapter 3

Figure 3. 1 Oxygen saturation at 0.5 h and 24 h.....	100
Figure 3. 2 Representative images of explants and 2D control. ....	101
Figure 3. 3 Representative Hand E results at 0.5 h and 24 h .....	102
Figure 3. 4 Representative modified Gomori results.....	104
Figure 3. 5 Illustration of contractile response (KCl) .....	105
Figure 3. 6 Representative plot profiles (KCl) at 24 h .....	106
Figure 3. 7 Representative plot profiles (Ang II) at 24 h .....	107
Figure 3. 8 Functional viability (KCl/Ang II) at 0.5 h and 24 h .....	109
Figure 3. 9 Pressure-Voltage conversion .....	111
Figure 3. 10 Oxygen meter calibration and saturation .....	113
Figure 3. 11 Media buffering capacity .....	114

## Chapter 4

Figure 4. 1 Illustration of HDMEC size measurement.....	127
Figure 4. 2 HDMEC morphology (shape and size) in control condition and HBO at 4 h .....	129
Figure 4. 3 HDMEC morphology (shape and size) in hyperbaric pressure and hyperoxia at 4 h .....	130
Figure 4. 4 Effect of treatments on HDMEC sizes .....	132
Figure 4.5 Resazurin assay optimisation .....	134
Figure 4.6 Metabolic activity of HDMEC after normalisation .....	135

## Chapter 5

Figure 5. 1 Western blots of nrf2 protein in HDMECs at 4 h .....	147
Figure 5. 2 Nrf2 protein in HDMEC in control condition at 4 h and 24 h .....	149
Figure 5. 3 Nrf2 protein in HDMEC in HBO at 4 h and 24 h.....	150
Figure 5. 4 Nrf2 protein in HDMEC in hyperoxia at 4 h and 24 h .....	151
Figure 5. 5 Nrf2 protein in HDMEC in hyperbaric pressure at 4 h and 24 h .....	152
Figure 5. 6 Nrf2 fluorescence signal intensity in HDMECs at 4 h and 24 h.....	154
Figure 5. 7 Western blots of HO-1 protein in HDMECs at 24 h .....	156
Figure 5. 8 Primer set efficiency .....	158
Figure 5. 9 IL-6 mRNA levels at 4 h .....	160
Figure 5. 10 Western blots of NFκB protein in HDMECs at 4 h .....	162

## Chapter 6

Figure 6. 1 Western blots of HIF-1α protein in HDMECs at 4 h .....	176
Figure 6. 2 Western blots of HIF-1α protein in HDMECs at 24 h .....	177
Figure 6. 3 Western blots of VEGF in HDMECs at 24 h .....	178
Figure 6. 4 ICC detection of PECAM-1 in HDMEC at 4 h and 24 h in control condition .....	180
Figure 6. 5 ICC detection of PECAM-1 in HDMEC at 4 h and 24 h in HBO .....	180
Figure 6. 6 ICC detection of PECAM-1 in HDMEC at 4 h and 24 h in hyperoxia.....	181
Figure 6. 7 ICC detection of PECAM-1 in HDMEC at 4 h and 24 h in hyperbaric pressure .....	181
Figure 6. 8 IHC detection of HIF-1α in retinal explants at 2 h and 24 h in control condition .....	184
Figure 6. 9 IHC detection of HIF-1α in retinal explants at 2 h and 24 h in HBO.....	186
Figure 6. 10 IHC detection of HIF-1α in retinal explants in hyperoxia at 2 h and 24 h .....	188
Figure 6. 11 IHC detection of HIF-1α in retinal explants in hyperbaric pressure at 2 h and 24 h .....	189

## Chapter 7

Figure 7. 1 Summary of relevant study results.....	199
--	-----

# Abbreviations

2, 3 DPG	2, 3-Diphosphoglycerate
AGE	Advanced glycation end-product
AR	Aldose reductase
ATA	Atmospheres absolute (absolute pressure)
Ang II	Angiotensin II
ANOVA	Analysis of variance
APS	Ammonium persulphate
AR	Aldose reductase
ARE	Antioxidant response element
Bak	Bcl-2 homologous antagonist killer
BCA	Bicinchoninic acid assay
Bcl-2	B-cell lymphoma 2
BFGF	Basic fibroblast growth factor
BHLH	basic helix-loop-helix
BRB	Blood-retinal-barrier
BSA	Bovine serum albumin
CBP	Creb binding protein
CdC42	Cell division control protein 42 homolog
CHD	coronary heart disease
CHIP	Carboxyl terminus of the Hsc70-interacting protein
Coup-TFII	COUP transcription factor 2
CRP	C-reactive protein
DAG	Diacylglycerol
DAPI	4', 6-diamidino-2-phenylindole
DCCT	Diabetes control and complication trial
DdH <sub>2</sub> O	Double-distilled water
DM	Diabetes mellitus
DMEM	Dulbecco's Modified Eagle Medium
DME	Diabetic macular edema
DMOG	Dimethyloxallylglycine
DN	Diabetic neuropathy
DR	Diabetic retinopathy
DTT	Dithiothreitol
EC	Endothelial cell
ECL	Enhanced chemiluminescence
ECM	Extracellular matrix protein
EDRF	Endothelium-derived relaxing factor
EDTA	Ethylenediaminetetraacetic acid
EGTA	Ethylene glycol-bis ( $\beta$ -aminoethyl ether)-N, N, N', N'-tetraacetic acid
ERK	Extra-cellular signal regulated kinase
EMT	Endothelial-mesenchymal transition
eNOS	Endothelial nitric oxide synthase
EPO	Erythropoietin
ET-1	Endothelin-1

ETC	Electron transport chain
FIH	Factor inhibiting HIF-1
FGF-2	Fibroblast Growth Factor 2
G6PD	Glucose-6 phosphate dehydrogenase
GAPDH	Glyceraldehyde 3-phosphate dehydrogenase
GCK	Glucokinase
GCL	Ganglion cell layer
GFAT	Glutamine: fructose-6 phosphate amidotransferase
GFAP	Glial fibrillary acidic protein
GLUT-1	Glucose transporter 1
GSK-3 $\beta$	Glycogen synthase kinase – 3 beta
GTP	Guanosine triphosphatases
HBO	Hyperbaric oxygen
HBOT	Hyperbaric oxygen therapy
HDMEC	Human dermal microvascular endothelial cell
HDF	Human dermal fibroblasts
HIF-1	Hypoxia inducible factor-1
HIF-1 $\alpha$	Hypoxia inducible factor -1 alpha
HKP	Housekeeping proteins
HNF1 $\alpha$	Hepatocyte nuclear factor 1 homeobox A
HNF4 $\alpha$	Hepatocyte nuclear factor 4 homeobox A
HO-1	Heme oxygenase -1
HRE	Hypoxia response element
HRP	Horseradish peroxidase
HSP	Heat shock protein
IDF	International diabetes federation
ICC	Immunocytochemistry
IF	Immunofluorescence
IGT	Impaired glucose tolerance
IHC	Immunohistochemistry
IL-6	Interleukin-6
IDDM	Insulin-dependent diabetes mellitus
INL	Inner nuclear layer
JNK	c-Jun N-terminal kinases
Keap 1	Kelch-like ECH associated protein 1
LDL	Low density lipoprotein
Lyve-1	Lymphatic Vessel Endothelial Hyaluronan Receptor 1
MAPK	Mitogen-activated protein kinase
Mfn	Mitofusion protein
MGO	Methylglyoxal
MI	Myocardial infarction
MiRNA	MicroRNA
MMPs	Matrix metalloproteinases
NADH	Nicotinamide adenine dinucleotide
NADPH	Nicotinamide adenine dinucleotide phosphate
NBF	Neutral buffered formalin
NEMO	NF-kappa-B essential modulator
NF $\kappa$ B	nuclear factor kappa-light-chain-enhancer of activated B cells



NIDDM	Non-insulin dependent diabetes mellitus
NO	Nitric oxide
Nrf2	Nuclear factor erythroid 2–related factor 2
Nrp2	Neuropilin2
NSAID	Non-steroidal anti-inflammatory
OCT	Optimal cutting temperature
ODDD	Oxygen-dependent degradation domain
ONL	Outer nuclear layer
PA-1	Plasminogen activator inhibitor
PARP	Poly (ADP-ribose) polymerase
PCR	Polymerase chain reaction
PDGF	Platelet-derived growth factor
PECAM-1	Platelet endothelial cell adhesion molecule -1
PDR	Proliferative diabetic retinopathy
PFKP3	6-Phosphofructo-2-kinase/fructose-2,6-bisphosphatase-3
PHD	Prolyl hydroxylases
PI3K	Phosphoinositide 3-kinase
PI	Protease inhibitor
PKC	Protein kinase C
PBS	Phosphate buffered saline
PMRS	Plasma membrane redox system
PMSF	Phenylmethylsulfonyl fluoride
PPP	Pentose phosphate pathway
PVD	Peripheral vascular disease
PVDF	Polyvinylidene difluoride
pVHL	von Hippel-Lindau
Prox-1	Prospero homeobox 1
QPCR	Real-time polymerase chain reaction
QRT-PCR	Quantitative reverse transcription polymerase chain reaction
RAC1	Ras-related C3 botulinum toxin substrate 1
RAC3	Ras-related C3 botulinum toxin substrate 3
RAGE	Receptors for AGE
RFU	Relative fluorescent unit
RIPA	Radio-immunoprecipitation assay
ROS	Reactive oxygen species
RPE	Retinal pigment epithelium
RT	Room temperature
SDS	Sodium dodecyl sulphate
SEM	Standard error of mean
SMaf	Small musculoaponeurotic fibrosarcoma
SOD2	Superoxide dismutase 2
Sox1	SRY-Box 1
Sox18	SRY-Box 18
T1DM	Type 1 Diabetes mellitus
T2DM	Type 2 Diabetes mellitus
TBS	Tris buffered saline
TEMED	Tetramethylethylenediamine
TG	Tris-Glycine

TGFβ1	Transforming growth factor beta 1
TGS	Tris-Glycine-SDS
TNF	Tumour necrosis factor
TPS	Total protein loading staining
UCP-1	Uncoupling protein -1
UKPDS	United Kingdom prospective diabetes study
VEGF	Vascular endothelial growth factor
VEGFR3	VEGF receptor 3
WB	Western blot
WHO	World health organisation
WR	Working reagent

# Chapter 1.0: Introduction

# 1.0 Introduction

Diabetes is a debilitating metabolic syndrome whose prevalence has gained significant grounds in recent years. Diabetes is associated with vascular complications that are a major cause of morbidity and mortality. Endothelial dysfunction is central to microvascular complications such as diabetic retinopathy (DR) and impaired wound healing in diabetes. Hyperbaric oxygen therapy (HBOT) involves the use of hyperbaric oxygen (HBO) which entails breathing  $\geq 95\%$  oxygen at elevated pressures and is used for the treatment of recalcitrant ulcers in diabetes. However, the exact molecular mechanism is unclear, and there are questions about its safety, and what contribution the single components of hyperoxia and elevated pressure provide. The effect of HBO on human dermal microvascular endothelial cells (HDMEC) and porcine retinal vasculature is presented with three mechanistic pathways of pro-inflammation (Nuclear Factor kappa B; (NF $\kappa$ B)), redox (nuclear factor type-2 (Nrf2)), and oxygen signalling (hypoxia inducible factor type 1 (HIF-1)).

## 1.1 Diabetes Mellitus

Diabetes mellitus (DM) is a metabolic syndrome of multiple aetiology characterised by chronic elevated glucose (hyperglycaemia) (WHO 1999, ADA 2014). Diabetes was first described 3500 years ago by the Ancient Egyptians. Aretaeus (120 AD) described the condition as 'fortunately rare', but 'short will be the life of the man in whom the disease is fully developed' (Reed 1954). The loss of normal hyperglycemic control in diabetes is attributed to deficiencies in insulin secretion, insulin action or a combination of both (ADA 2014, Herman 1999). Diabetes is generally divided into type 1 diabetes mellitus (T1DM), type 2 diabetes mellitus (T2DM) and as well as Gestational diabetes (IDF 2018a). The current diagnostic criteria for DM are a fasting plasma glucose  $\geq 7.0\text{mmol/l}$  ( $126\text{mg/dl}$ ) or 2h post prandial plasma glucose of  $11.1\text{mmol/l}$  ( $200\text{mg/dl}$ ) (WHO 1999, Herman 1999). T1DM, also known as 'juvenile' diabetes, is characterized by autoimmune destruction of the insulin-secreting  $\beta$ -cells of the islets of Langerhans in the pancreas (Solari et al 2009). In T2DM, there is varying degree of  $\beta$ -cell failure relative to insulin resistance that results in the loss of insulin action or an effect owing to metabolic exhaustion (Fotino et al 2010, Cnop et al 2005). T2DM is marked by increased insulin resistance, hyperinsulinemia, and pancreatic  $\beta$ -cell failure and alpha cell deregulation, immune deregulation, with pro-inflammation (reviewed in Chatterjee et al 2017).

Exogenous insulin is the mainstay of life-sustaining therapy in T1DM and late stage T2DM, in addition to oral drug therapy for management of blood glucose and micro- or macrovascular complication predominantly in T2DM. In our times, Aretaeus' description about diabetes is far from true as the incidence of diabetes has doubled every 20 years since 1945 (Barnett 1998). About 425 million people world-wide are currently living with diabetes mellitus with two-thirds of those in the adult working population affected (IDF 2017b). This figure is expected to reach 700 million by 2045 owing to an aging population, increasing trends of sedentary lifestyle with inadequate physical activities and obesity-associated diets. There is a strong genetic constituent to T1DM and T2DM susceptibility that can be measured by single nucleotide polymorphism (SNP) genotyping (reviewed in Oram et al 2016). Genome wide association studies (GWAS) have identified some commonly affected genes; *HNF-1 $\alpha$* , *HNF-4 $\alpha$* , and *GCK* (Thanabalasingham et al 2012) of glycemic traits in T2DM but these variants only account for 10% of total trait variance, suggesting that there are more rare (unidentified) variants which are important (Grarup et al 2014). Although the epidemiology of T2DM is affected by genetic and environment factors, genetic factors exert their effect more following exposure to environmental factors such as a sedentary lifestyle and excessive sugar and fat consumption (Chatterjee et al 2017). The financial burden of diabetes mellitus is high with a total global expenditure of \$727 billion per annum (IDF 2017). In addition, the daily management of T1DM and T2DM is burdensome to patients and their families made worse by long-term complications such as microvascular (retinopathy, neuropathy and nephropathy) and macrovascular such as coronary heart disease (CHD), myocardial infarction (MI) and peripheral vascular diseases (PVD) which have caused the most morbidity and mortality in DM (NDDG 1985, Deckert et al 1978).

## 1.2 Diabetic complications

Hyperglycaemia sufficient to cause tissue damage can be present without clinical symptoms for many years before diagnosis and this is particularly relevant in T2DM (Herman 1999). Severe hyperglycaemia ( $\geq 10$  mM of chronic elevated glucose) causes excessive urination (polyuria) and thirst (polydipsia), weight loss, and blurred vision. Acute, life threatening hyperglycaemia causes ketoacidosis and non-ketotic hyperosmolar syndrome with increased vulnerability to certain infections. Long term, hyperglycaemia results in retinopathy (with potential blindness), nephropathy, peripheral neuropathy (increased risk of diabetic recalcitrant ulcers, amputation, and Charcot joints), autonomic neuropathy (with gastrointestinal, sexual, and bladder dysfunction), and greatly increased risk of atheroma in large vessels (Herman 1999).

A link between developments of long-term complications (retinopathy, neuropathy and nephropathy) and cardiovascular complications and high glucose (hyperglycaemia) has long been documented resulting from studies in animal models and clinical observations showing a causal link between chronic hyperglycaemia in the pathogenesis of long-term complications with diabetes mellitus (NDDG 1985, Deckert 1978). Yet, clinical trial data did not demonstrate any consistent beneficial effect of intensive blood-glucose control on DM complications, until two pivotal clinical studies; the diabetes control and complication trial (DCCT 1993) and the United Kingdom prospective diabetes study (UKPDS1998) were carried out.

The DCCT (1993) study was a clinical study conducted from 1983 to 1993 and funded by the National Institute of Diabetes and Digestive and Kidney Diseases (USA and Canada). This study showed that intensive control of blood glucose levels slows the onset and progression of retinopathy, nephropathy, and neuropathy in diabetes for T1DM. The follow-up study, Epidemiology of Diabetes Interventions and Complications (EDIC) study (2005) also showed intensive blood glucose control has long-term beneficial effects on lowering the risk of cardiovascular disease in patients with T1DM. In addition, the Kumamoto study (1995) showed intensive blood glucose control in insulin treated T2DM over six years lowered relative risks of retinopathy, nephropathy, and neuropathy. Similarly, the Stockholm diabetes Intervention Study demonstrated a beneficial effect of intensive blood glucose control in patients with established microvascular complications, although there was crossover of conventional control group patients to intensive therapy during the trial (Reichard et al 1999).

The United Kingdom Prospective Diabetes Study (UKPDS) was the largest and longest study ever undertaken in diabetes; median follow-up was 10 years (UKPDS1991). The study demonstrated that intensive therapy effectively delays the onset and slows the progression of DR, nephropathy, and neuropathy in patients with IDDM (UKPDS1998a). In addition, the group determined that intensive blood-glucose control by either sulphonylureas or insulin substantially decreases the risk of microvascular complications, but not macrovascular disease, in patients with T2DM (UKPDS 1998b). Furthermore, the Action in Diabetes and Vascular Disease: Preterax and Diamicon Modified Release Controlled Evaluation (ADVANCE 2008), and the Veterans Association Diabetes Trial (VADT) (Duckworth et al 2009) are other large randomised control trials like the UKPDS which have helped to establish the benefits of intensive glucose management on microvascular complications, such as retinopathy, nephropathy, and neuropathy. In effect, what these large randomised clinical trials (RCTs) showed was that improved glycaemic control prevents/reduces diabetic complications, especially microvascular complications.

## 1.2.1 Macrovascular complications

Macrovascular complications in diabetes are coronary heart disease (CHD), myocardial infarction and peripheral vascular diseases (PVD). The Framingham study first identified CHD as a macrovascular diabetes complication (Kannel and McGee 1979). Studies have shown the risk of myocardial infarction (MI) in people with diabetes is equivalent to the risk in nondiabetic patients with a history of previous MI (Haffner et al 1998). This culminated in the classification of diabetes as coronary artery disease by the American diabetes association (ADA) and the American Heart Association (Buse et al 2007). The process of atherosclerosis in arterial macro vessels is central in diabetes associated macrovascular dysfunction. Atherosclerosis results from chronic inflammation in the endothelium and insults in arterial vessels of the peripheral or coronary vascular system.

As a result of endothelial barrier dysfunction, oxidized lipids from low density lipoproteins (LDL) particles infiltrate and accumulate in the endothelial wall of arteries. Inflammatory cells such as monocytes extravasate into the arterial wall and differentiate into macrophages which produce foam cells from accumulated oxidized lipids. Once formed, foam cells stimulate macrophage proliferation and increased recruitment of T-lymphocytes. Recruited T-lymphocytes induce smooth muscle proliferation in the arterial walls and collagen accumulation. Consequently, a lipid rich atherosclerotic plaque with a fibrous cap is formed in the arterial wall and the rupture of this lesion may precipitate an acute vascular infarction (Boyle 2007).

In T2DM, there is impaired nitric oxide generation and increased free radicals (reactive oxygen species) (ROS) generation in platelets with altered calcium regulation which promotes platelet aggregation and hypercoagulability. Elevated levels of plasminogen activator inhibitor type 1 (PAI-1) in diabetic patients further impairs fibrinolysis. This combined incidence of increased coagulation and impaired fibrinolysis increases the risk of vascular occlusion and cardiovascular events in T2DM (Beckman et al 2002).

## 1.2.2 Microvascular complications

Microvascular complications in diabetes relates to diabetes specific damage to microvessels in the retina of the eye, the glomerulus of the kidney, and vasa nervorum of the peripheral nerves which share similar pathophysiologic characteristics and hyperglycaemia is the central instigator and driver in all types of diabetic microvascular disease (reviewed in Brownlee et al 2016). In addition, there is also a genetic determinant of susceptibility to microvascular complication due to polymorphisms that have been observed in several protein-coding genes. Furthermore, the involvement of regulator non-coding microRNAs (miRNAs) on different biological and cellular pathways in diabetic complications is now increasingly evident. In the whole retina, diabetes has been associated with increased levels of NFkB responsive miRNAs such as miR-21, miR-132, miRNA-155, and miRNA-146, while a specific downregulation of miRNA-146a in retinal microvessels endothelial expression due to high glucose has been reported (Kato et al 2013). These aspects shed light on the complexity of diabetes and its complications. In the following paragraphs, pathophysiologic features of DR, nephropathy and neuropathy are reviewed with detailed attention to retinopathy. In section 1.4, the mechanisms associated with high glucose mediated toxicity and damage are reviewed.



### 1.2.2.1 Diabetic Retinopathy

Diabetic retinopathy (DR) is initiated from injury and insults to the retinal microvasculature and it is one of the commonest microvascular complications with a frequency of 75%, and a common cause of blindness in those aged 25-74 years (reviewed in Klein et al 1989). Poor glycaemic control is a strong risk factor for the development and progression of DR which affects all three parts of the retinal vessel (reviewed in Knott and Forrester 2003). Retinal damage appears to precede clinical manifestations of diabetes in T2DM, and retinopathy may already be in existence as early as 7 years in patients with T2DM before clinical diagnosis is made (Fong et al 2004). Several mechanisms have been put forward for the development of diabetes associated retinopathy. Increased flux of the polyol pathway and activation of the enzyme Aldose reductase (AR), which catalyses the initial step in glucose conversion to sorbitol, is the most implicated pathway in the development of retinopathy (mechanism is covered in section 1.4). The polyol pathway is attendant with increased free radical formation due to depletion of the two major non-enzymatic anti-oxidants; ascorbate and glutathione.

In animal models of retinopathy, sugar alcohols such as sorbitol accumulation were linked to microaneurysm formation, thickening of the basement membranes, and loss of pericytes (Fong et al 2004, Gabbay 1975 and 2004). In view of that, anti-oxidant treatments were found to be associated with decrease of polyol-pathway induced deleterious effects on the retina (Knott and Forrester 2003, Obrosova et al 2005). In-vitro evidence also corroborated this positive role of anti-oxidant treatment on amelioration of polyol-induced effects on the retina with the observation of decreased retinal capillary cell apoptosis in high glucose in the presence of vitamin D3 (Lu et al 2018). Sorbitol accumulation in cells through the polyol pathway precipitates osmotic stress, and this may also contribute to onset and development of retinopathy. AR inhibitors were expected to have excellent outcomes in retinopathy, but treatment studies with AR have so far not been successful (Fong et al 2004, Gabbay et al 1975 and 2004, reviewed in Brownlee 2016), although interest remains. DR is associated with pericytes coverage loss in retinal capillaries leading to acellular capillaries due to hyperglycaemia induced apoptotic pericytes and endothelial cell death (Cogan et al 1961, Kuwabara et al 1960 and 1963, Shepro and Morel 1993, Robison et al 1983 and 1986, Frank et al 1983, Das et al 1990). Consequently, microvasculature autoregulation, which is essential for regulation of nutrient and oxygen, and modulation of vascular tone in the microvasculature, is lost.

Glycoproteins are injurious to endothelial cells and elevated high glucose concentrations in the retinal microvasculature can promote non-enzymatic formation of advanced glycosylated end products (AGEs). AGEs associated microaneurysm and pericyte loss resulting in retinal blood retinal barrier (BRB) have been demonstrated in animal models and drug targets of AGEs are effective to some degree. Aminoguanidine, the first known AGE inhibitor was effective but it is now overtaken by second generation derivatives such as albiglutam (ALT-711), an aminoguanidine and thiazolidine derived compound but clinical developments of albiglutam was discontinued due to safety and/or a lack of efficacy concerns (Freedman et al 1999, reviewed in Furlani et al 2015). A lead compound, bis-2 Aminoguanidine has been developed and it is expected to exhibit superior AGE inhibition, although it is yet to make it into clinical trials (Furlani et al 2015).

In diabetic retina, sustained elevated high glucose instigates protein kinase C (PKC) activation which drives vascular endothelial growth factor (VEGF) expression and raised levels of the vasoconstrictor, endothelin-1 (ET-1), both of which culminates in retinal vessel vasoconstriction and ischaemia (Park et al 2000, Matsuo et al 2009, reviewed in Zhongwei and Khalil 2018). In addition, due to hypoxia stemming from retinal ischaemia in the diabetic retina, VEGF is over-expressed leading to uncontrolled angiogenesis, which is common cause of blindness in DR (Semenza 2008, Nussenbaum and Herman 2010). In animal models of DR, suppressed VEGF production is associated with reduced progressive retinopathy (Keenan et al 1995, Fong et al 2004). VEGF is a classical mediator of BRB breakdown in DR because it increases retinal neovascularisation and increased retinal vessel permeability (Keck et al 1989). In addition to VEGF, increase in levels of several growth factors including transforming growth factor  $\beta$  (TGF $\beta$ ), and angiostatic factors such as Tie 2 play important roles in the development of DR (Hammes et al 2011).

The successful use of anti-VEGF agents for age-related macular degeneration helped to showcase the important role of anti-VEGF in the treatment of ocular treatments (Lim et al 2012). Anti-VEGF indications have since been expanded to encompass diabetic macular oedema (DME) and proliferative DR (PDR). Among the four anti-VEGF agents (ranibizumab, bevacizumab, pegaptanib, and aflibercept), ranibizumab has been most thoroughly tested in clinical trials (Cheung et al 2014). A novel in-vitro candidate (RC28-E), with VEGF and fibroblast growth factor 2 (FGF2) blockade activity has recently been reported to decrease retinal cell apoptosis, nonspecific reactive change of glial cells (gliosis), leakage and pro-inflammatory microenvironment in early DR (Yang et al 2018), and it is still undergoing development.

Hyperglycaemia induced oxidative stress plays a key role in cellular injury in DR because high glucose stimulates free radical production and ROS formation. The concept of hyperglycaemia induced oxidative damage in diabetes is supported by several in-vivo and in-vitro evidences. Vitamin E and C administration were associated with amelioration of oxidative stress in diabetes (reviewed in Kastelan et al 2013). In addition, in-vivo administration of vitamin E is associated with decline of macro-vascular dysfunctions in diabetes, but not on the development and progression of microvascular complications including retinopathy (Kunisaki et al 1995, Fong et al 2004). An in-vitro example is the inhibition of oxidative stress, nitrotyrosine formation, NF $\kappa$ B activation, and apoptosis in retinal capillary cells with antioxidants (N-acetyl cysteine and  $\alpha$ -lipoic acid) (Kowluru 2005).

Inflammatory processes have a considerable role in the pathogenesis of DR with multiple studies showing associations between increased levels of systemic and local (vitreous and aqueous fluid) inflammatory factors and the progression of DR. Inflammation is key in retinal vessel permeability and neovascularisation (PDR), both of which leads to vision loss in diabetes (reviewed in Kastelan et al 2013). Raised levels of tumour necrosis factor  $\alpha$  (TNF- $\alpha$ ) in vitreous, serum, and ocular fibrovascular membranes of patients with DR in comparison to non-DR subjects have been found (Limb et al 1996, Jousen et al 2002). Consequently, TNF- $\alpha$  is now regarded as a novel biomarker to assess the degree of DR (Costagliola et al 2013). Furthermore, increased interleukin-6 (IL-6) level in the vitreous has been shown to significantly correlate with DR severity and progression (Funatsu et al 2003, Mocan et al 2006, and Feng et al 2018). Therefore, the use of anti-inflammatory agents such as steroidal corticosteroids; triamcinolone, fluocinolone and dexamethasone and non-steroidal anti-inflammatory (NSAIDs) drugs in experimental research and in the clinic in DR has strong molecular basis (reviewed in Kastelan et al 2013).

### 1.2.2.2 Diabetic Nephropathy

Diabetic nephropathy is the main cause of renal dysfunction in the United States and is predominant in both T1DM and T2DM. It is defined by proteinuria > 500 mg in 24 h in the setting of diabetes, preceded by lower degrees of proteinuria, or microalbuminuria a state characterized by albumin excretion of 30-299 mg/24 h (Fowler 2008). Microalbuminuria is correlated with increased glomerular extracellular matrix in both T1DM and T2DM and it is present in 7% of T2DM patients at diagnosis (Osterby 1992, Osterby et al 1993 and Gross et al 2005). High glucose (hyperglycaemia) is dominant in the pathogenesis of diabetic nephropathy since the development of diabetic nephropathy is faster in patients with poor metabolic control (Ayo et al 1990, Schleicher and Nerlich 1996), and significant structural changes particularly the thickening of glomerular basement membrane and mesangial expansion occurs only after several years of diabetes. Diabetic nephropathy affects both the glomerulus and the tubular interstitium of the kidney. Non-enzymatic pathways are set off by high glucose which results in glycation end-products (Brownlee et al 1988), oxidative stress activation via AGE/RAGE pathway (Bierhaus et al 1998). Moreover, hyperglycaemia-induced formation of ROS leading to increased apoptosis has been shown with cultured renal endothelial cells (Du et al 1998). The biochemical mechanisms of high glucose mediated toxicity are discussed further in section 1.4.

### 1.2.2.3 Diabetic Neuropathy

Diabetic neuropathy (DN) has a high prevalence (45–50%) in diabetes (Shaw and Zimmet 1999). Several studies have shown the presence of neurological involvement in impaired glucose tolerance (IGT). Neurological symptom such as small fibre neuropathy characterised by intra-dermal nerve fibre loss is found in IGT (Sumner et al 2003, Polydefkis et al 2003). In DN, microangiopathies such as increased capillary density, decreased capillary luminal area and increased basement membrane are precipitated by IGT and exist in parallel with nerve fibre loss and endothelial cell swelling (Thrainsdottir et al 2003). This scenario is compounded in diabetes because vascular supply of peripheral nerves is sparse and lacks autoregulation which makes peripheral nerves vulnerable to IGT associated vascular hypoxia and ischaemia (Smith et al 1977, Yagihashi et al 2011). In addition, sustained elevated blood glucose triggers pathways; polyol pathway, AGE, oxidative stress, PKC activity and the activation of polyADP-ribose polymerase (PARP) enzyme, all which contribute to the initiation and progression of neuropathy (Yagihashi et al 2011), as outlined in the glucotoxicity pathways in section 1.4.

Hyperglycaemia driven polyol pathway activation causes NADPH depletion resulting in impaired nitric oxide (NO) synthesis or reduced glutathione regeneration. Impaired NO synthesis and decreased glutathione can precipitate vascular insufficiency and over-production of free radicals respectively. Consequently, the treatment of streptozotocin-induced diabetic rats with butylated hydroxytoluene, a lipophilic radical scavenger and trientine, a heavy metal chelator was found to significantly reduce nerve denervation highlighting the role of free radical in neural/neurovascular deficits (Love et al 1996). Furthermore, the distribution of AR enzyme in Schwann cells supports the role of hyperglycaemia induced polyol pathway activation in nerve damage in DN. Ischaemia/poor reperfusion in distal peripheral nerves of diabetic patients' cause polyol activation which exacerbates DN (reviewed in Yagihashi et al 2011). Moreover, the mitogen-activated protein kinase (MAPK) pathway causes functional and structural deregulation of peripheral nervous system in DN (Sima and Sugimoto 1999, Tomlinson 1999). Thus, the flavonoid baicalcein was reported to alleviate DN in C57B16/J mice models through the inhibition of the polyol-sorbitol accumulation which culminated with the reduction of the p38 MAPK and oxidative nitrosative stress pathways (Stavniichuk et al 2011).

### 1.2.2.4 Impaired wound healing of diabetes

Diabetes is the commonest cause of non-traumatic lower limb amputation and 15–20% of all foot ulcers will ultimately require amputation (Mulder et al 1994). Diabetic foot ulcers (DFUs) are common and serious complications of diabetes due to its high prevalence and impairment of wound healing. The risk factors for DFUs are peripheral neuropathy, peripheral arterial disease and trauma but, impaired wound healing is the main complication that results in the development of chronic wounds, which often lead to amputations. Wound healing is a dynamic complex process that begins when tissue integrity is disrupted and can be divided into four partly overlapping phases: coagulation, inflammation, migration-proliferation (including matrix deposition) and remodelling (reviewed in Falanga 2005, Guo and Dipietro 2010). Acute wounds go through the linear progression of overlapping biological and molecular events as outlined in table 1.1 below. Although, in reality, even in normal wound healing process, complications such as infection, thrombosis and ischaemia can occur and this can confound the linear progression outlined.

**Table 1. 1 Phases of wound healing** Major cells types involved in each phase with selected specific events of wound healing (Adapted from Falanga 2005).

Time	Phases	Main cell types	Specific events
<div> <div>Hours</div> <div>Days</div> <div>Weeks to months</div> </div>	a). <b>Coagulation</b> Fibrin plug formation, release of growth factors, cytokines, hypoxia	Platelets	Platelet aggregation and Release of fibrinogen fragments And other pro-inflammatory mediators
	b). <b>Inflammation</b> Cell recruitment and chemotaxis, wound debridement	Neutrophils, monocytes	Selectins slow down Blood cells and binding to integrins- diapedesis
	c). <b>Migration/proliferation</b> Epidermal resurfacing, fibroplasia, angiogenesis, ECM deposition, contraction	Macrophages Keratinocytes Fibroblasts, Endothelial cells	Hemidesmosome Breakdown – keratinocyte migration  Cross-talk between MMPs, integrins, cells cytokines – cell migration, ECM production
	d). <b>Remodelling</b> Scar formation and revision, ECM degradation, further contraction and tensile strength	Myofibroblasts	Phenotypic switch to Myofibroblasts from fibroblasts

Inflammation with subsequent coagulation sets in early after an acute wound for haemostasis and wound protection (a and b), giving rise to fibrin plugs around the wound site which aids to ward off bacteria. Platelets within the fibrin plug release pro-inflammatory cytokines and growth factors such as platelet derived growth factor (PDGF) and transforming growth factor (TGF)  $\beta$ 1. Endothelial cells express selectins, and leucocytes are slowed down in the bloodstream and are able to extravasate through endothelial gaps via binding to integrins into the extracellular space (diapedesis) (Martin 1997). In non-diabetic wounds, these recruited inflammatory cells (especially neutrophils and macrophages) aid wound debridement and recruited neutrophils secrete tissue growth factors that drives wound repair process (Singer and Clark 1999).

The local vessels in the vicinity of acute wounds are acutely hypoxic as a result of damage to blood vessel. This temporary hypoxia drives the third stage of wound healing; migration and proliferation (C). Hypoxia increases keratinocyte migration, early angiogenesis, and fibroblasts proliferation, in addition to increased production of PDGF and TGF $\beta$ 1 (Falanga 2004). Matrix metalloproteinase (MMPs) and other enzymes (tissue plasminogen activator, tPA and urokinase plasminogen activator, uPA) break down the stable structures around cells so they are free to migrate. For instance, the hemidesmosomes, a highly organized structure which provide anchorage of the basal keratinocytes to the underlying basement membrane are broken down by MMPs for the purpose of keratinocyte cell migration. Recruited monocytes which are now differentiated as macrophages, fibroblasts and endothelial cells forms the early granulation tissue that initiates wound contraction process, overlapping with the fourth stage (Remodelling) (D). Within weeks to months of an acute wound, inflammatory responses are resolved. This aspect distinguishes an acute from a chronic wound as in diabetes ulcers where there is low-grade chronic inflammation which drives aberrant gene expression (Tang et al 2013).

Angiogenesis, contraction and extra-cellular matrix (ECM) deposition are critical for this last phase of acute wound healing. ECM proteins such as collagen, fibronectin, and vitronectin are laid down to provide substrate for cell attachment via integrins to enable cell-cell communication and migration (Falanga 2002, Santoro and Gaudino 2005). In addition, wound contraction which is vital for wound closure is made possible by the newly formed ECM, granulation tissue and newly formed myofibroblasts. Integrins are essential in wound healing because they support cell-cell, cell-ECM communication and migration. Diabetic wounds do not follow the wound progression and resolution outline in table 1.1 (Loots et al 1998 and 2002), due to Intrinsic factors and extrinsic factors which complicates wound healing in diabetes (reviewed in Falanga 2005). In diabetic wounds, the basement membrane is thickened so migrating leucocytes cannot extravasate into extracellular spaces (i.e. diapedesis is slowed down) which contributes to infection (Martin 1997). Also due to endothelial dysfunction, endothelial nitric oxide synthetase (eNOS) expression is reduced which contributes to blood flow maldistribution although true luminal occlusion of small vessels does not occur (LoGerfo and Coffman 1984). As a consequence, microvessels autoregulatory capacity required for meeting local needs of cells in response to cellular demands are impaired (Dinh and Veves 2005, Zong et al 2017).

In diabetic wounds, wound contraction and closure is impaired and the impairment is worsened by the presence of infection in diabetic wounds. More so, excessive collagen and fibronectin (ECMs) deposition has been identified in diabetic wounds, which causes ECM stiffening, and hampering cell movement (Falanga 2004). As stated previously, acute local hypoxia in wound vicinity is necessary for early angiogenic response, however, there is chronic hypoxia in diabetic wounds due to vascular inefficiencies that are often characteristic of diabetes (Catrina et al 2004). Oxygen is critical in tissue healing and oxygen tension is a major controlling factor in bacterial killing, resistance to infection, collagen synthesis, angiogenesis, and epithelisation. Oxygen tension in diabetic wounds are low and ranges from 5 to 20 mm Hg (1.1% - 4.2%), which limits the leukocyte's function, which requires an optimal oxygen tension of 45 to 80 mm Hg (9.5% - 17%) relative to sea level conditions for bacterial lethality (Hodges et al 2003).



Furthermore, fibroblasts mediated matrix deposition e.g. in collagen synthesis required for angiogenesis and tissue remodelling are impaired in chronic hypoxia (Niinikoski 1972, Hunt and Pai 1972, Hunt et al 1974, Siddiqui et al 1996). In wound healing the signalling activity of the hypoxia inducible factor -1 alpha (HIF-1 $\alpha$ ) is necessary for expression of multiple angiogenic growth factors, and recruitment of endothelial progenitor cells (Kelly et al 2003, Catrina et al 2004). But the stability of HIF-1 $\alpha$ , the regulated subunit of HIF-1 is impaired by hyperglycaemia with very low levels of HIF-1 $\alpha$  expression in ulcerated diabetic foot biopsies (Catrina et al 2004, Fadini et al 2006, and Gao et al 2006). Accordingly, HIF-1 $\alpha$  stabilization and consequently HIF-1 activation and signalling have been shown to reverse pathological processes in hyperglycaemia associated diabetic wound impairment (Botusan et al 2008).

Low-grade chronic inflammation in diabetes and diabetic wound also drives aberrant gene expression in diabetic wounds (Tang et al 2013). The activation of the Poly (ADP-ribose) polymerase (PARP), a nuclear enzyme which is activated by hyperglycaemia induced ROS which causes oxidative DNA damage leads to cell necrosis and changes in microcirculatory reactivity (reviewed in Falanga 2005). This suggested a role for anti-oxidant therapy in diabetic wound healing. A recent study demonstrated the beneficial effect of the nuclear factor-E2- related factor (nrf2)-mediated antioxidant response in treating diabetic skin ulcer (Long et al 2016), which supported the implied role of ROS in cell necrosis and changes in microcirculatory reactivity.

Taken together, hyperglycaemia, hypoxia, oxidative stress and impairment of neutrophil and macrophage function can result in endothelial dysfunction and are some of the key drivers in diabetic wound impairment (Catrina et al 2004, Patel et al 2005, reviewed in Falanga 2005, Long et al 2016).

Infection is an important cause of morbidity and hospitalisation, amputation, and impaired healing in DFUs, although it is unclear whether it plays a role in DFUs development. The combination of stress and pressure sites is said to favour overgrowth of bacteria (Ctercteko et al 1981). In addition, decreased macrophage and neutrophil function in diabetic wounds encourages infection because these cells produce ROS using oxygen derived radicals to kill bacteria (Knighton et al 1984, Naghibi et al 1987, Alien et al 1997 and Zykova et al 2000).

## 1.3 Endothelial Perturbations

The thin single layered specialized squamous epithelial cells lining the luminal surfaces of blood and lymphatic vessels are referred to as the endothelium or endothelial cells. Endothelial cells also line the heart cavity. They form an interface separating circulating lymph or blood in the vessel from the rest of the vessel wall. The endothelium is involved in the maintenance of vessel wall permeability and regulation of blood flow (Fishman et al 1982). Glucotoxicity induced endothelial dysfunction is present in the earliest stages of diabetic metabolic syndrome and insulin resistance, and may be established prior to any clinical diagnosis of T2DM by several years (Ruderman et al 1992, Brownlee et al 1989, reviewed in Sena et al 2013). Acute, transient and sustained hyperglycaemia impairs endothelial function of both micro and macro vascular beds (Ceriello 2010). Endothelial dysfunction in diabetes worsens diabetes-associated vasoconstriction, inflammation, and thrombosis (Beckman et al 2002, Nesto 2004).

Insulin dependent stimulation of NO in endothelial cells via activation of the endothelial NO synthase (eNOS) PI-3K dependent pathway is impaired by insulin resistance, and consequently NO is diminished while insulin resistance drives MAPK signalling (Kim et al 2006). This culminates in increased production of endothelin -1 (ET-1), and the plasminogen activator inhibitor (PAI-1), which increases endothelial platelet adhesion expression (Muniyappa and Sowers et al 2013). Ultimately, hyperglycaemia driven insulin resistance culminates in chronic low-grade inflammation with persistent elevated serum levels of IL-6, PAI-1, ET-1, and sensitive C-reactive protein (CRP) (Kim et al 2006). Enhanced cytokine mediated endothelial dysfunction in diabetes is well known (Aoki et al 1989, Kim et al 2006). Heightened NF $\kappa$ B signalling occurs early in vascular dysfunction via cytokine mediated signal transduction, including interleukin -6 (IL-6) (Castell et al 1988, Pober 1999). Moreover, endothelial contraction and impaired microvascular function due to the presence of vasoconstrictors such as ET-1 and Ang II are linked to increased levels of IL-6 and TNF $\alpha$  in the endothelium (Iversen et al 1999, Weis et al 1999, Peng et al 2018).

Blood flow is regulated, in part, through secretion and uptake of vasoactive substances by the endothelium that act in a paracrine manner to constrict and dilate specific vascular beds in response to vasoconstriction stimuli such as Ang II, endotoxin, and ET-I or vasodilators such as NO and prostacyclin (reviewed in Cines et al 1998, Cameron and Cotter 1999). In normal circumstance *in vivo*, Ang II regulates capillary perfusion in retinal capillaries by inducing abluminal retinal pericytes contraction and thereby constricts microvessels lumen (Zhang et al 2011, Kawamura et al 2004). This response is also seen *in-vitro* where Ang II induced stimulation of pericytes in cultured retinal microvessels resulted in vessel depolarisation and constriction, an effect that was vessel-type/site dependent (Kawamura et al 2004).

In diabetes, vascular tone modulation by Ang II is lost because of glucotoxicity induced cell death of retinal endothelial cells and pericytes (Nakaizumi et al 2012). In view of that, high glucose was shown to inhibit contractile response in cultured bovine retinal capillary pericytes (Gillies and Su 1993). Polyunsaturated fatty acids are a major target for ROS. Hence in diabetes, there is reduced availability of essential fatty acids and this is worsened in the presence of hyperglycaemia associated increased ROS production. ROS causes vascular endothelium dysfunction via impairment of NO-mediated vasodilatation which is made worse in the presence of reduced synthesis of prostanoids such as the vasodilator, prostacyclin while Ang II and ET-1 production are enhanced (Cameron and Cotter 1999).

In the diabetic endothelium, uncontrolled angiogenesis is potentiated by VEGF, FGF, PDGF and TGF- $\beta$  (Mackay 2001, Jackson et al 1997, Naldini et al 2003, Carmeliet 2000). High glucose (15mM) induced upregulation of TGF- $\beta$ 1 in human retinal endothelial cells (HREC) has been documented highlighting that glucose may regulate TGF- $\beta$ 1 and play a role in the growth and proliferation of HREC in a similar manner as DR (Pascal et al 1999). In endothelial cells, chronic high glucose results in pseudohypoxia which is characterised by increased cellular cytosolic ratio of free NAD<sup>+</sup> to NADH and is distinct from true hypoxia because it is initiated under non-hypoxic condition in the absence of any vascular compromise (Williamson et al 1993, reviewed in Catrina et al 2004). Subsequently, hyperglycaemia driven pseudohypoxia in diabetes may lead to enhanced TGF- $\beta$  and VEGF expression and collagen synthesis (Williamson et al 1993, Marfella et al 2002). Thus, pseudohypoxia is a likely driver of endothelial dysfunction (Williamson et al 1993).

Theoretically a hyperglycaemic microenvironment should be stimulatory for VEGF production because of pseudohypoxia but this effect appears to be selective (Kim et al 2002). For instance, vascular endothelial cells are renewed by angiogenesis and this is dysfunctional in diabetes with reduced revascularisation and impaired wound healing (Martin et al 2003). However, in the retina there is over-expression of VEGF and uncontrolled angiogenesis in the later stages of DR (Aiello 2005). Thus, pseudohypoxia driven VEGF expression is a cell-type dependent response.

Hyperglycaemia is also associated with true cellular hypoxia in the endothelium via increased production of mitochondrial ROS (Brownlee 2005, Nishikawa et al 2000, Cameron and Cotter 1999), and subsequent to aquaporin-1 suppression (Sada et al 2016). ROS is produced by all layers of the endothelium. The mitochondrial electron transport chain (ETC) (Chance et al 1979, Jezek and Hlavata 2005, Turrens 2003), NADPH oxidase (Griendling et al 1997, Ray and Shah 2005, Soccio et al (2005), xanthine oxidase (Cai and Harrison 2000, Suzuki et al 1995) are all sources of ROS in the endothelium, in addition to the ROS generated by uncoupled eNOS (Cai and Harrison 2000). NADPH oxidases produce ROS in response to cytokines, and mechanical stimuli (shear stress and stretch), and in response to Ang II and ET-1 (De Keulenaer et al 1998, Schramm et al 2012). ROS production is further augmented in the diabetic endothelium due to insulin resistance (INRS), which impairs protein tyrosine phosphatase non-receptor type 1 (PTPN1/PTP1B) (Tiganis 2011) and nuclear factor-erythroid derived 2-like (NFE2L2/NRF2) redox function (KEAP 1) (Kobayashi and Yamamoto 2006). Consequently, oxidative stress impairment of endothelium-dependent vasodilatation is the earliest consequence of hyperglycaemia (Cai and Harrison 2000). Several mitochondrial antioxidant systems are in place to protect against ROS-induced damage in the endothelium. Nonetheless, anti-oxidant systems can be overwhelmed leading to ROS deleterious effect, as is the case in the diabetic endothelium (reviewed in Sena et al 2013).

The heme oxygenase is an example of endothelial anti-oxidant defence protein with an indirect antioxidant function through its action of free heme breakdown to carbon monoxide, biliverdin and bilirubin metabolites (Perrella and Yet 2003). Also, its HO-1 isoform is involved in an adaptive cytoprotective role in endothelial cells in response to oxidative stress (Hoekstra et al 2004).

In the early stages of vascular development, junction formation initially involves rather weak adhesion complexes required for cell-cell recognition. Endothelial cell-cell adhesion molecules are expressed by the endothelium and are necessary for vessel sprouting and extension. A classic example of cell-cell mediator molecule in endothelial cells is the platelet endothelial cell adhesion molecule -1 (PECAM-1), also referred to as the cluster of differentiation 31 (CD31) (Albelda et al 1991). ECs express two isoforms of PECAM that mediate cell adhesion that differ in their requirement for divalent cations and sulphated proteoglycans. The VE-cadherin isoform (cadherin-5) of PECAM, is found almost exclusively on ECs, and promotes endothelial cell adhesion via a calcium-dependent homotypic mechanism (Dejana 1996). Hence, in the presence of calcium, VE cadherin from one endothelial cell binds to the VE-cadherin expressed on an adjacent cell. As vessel matures, stronger connections such as tight junctions and gap junctions are formed depending on the vessel type (reviewed in Cines et al 1998). In addition to cell adhesion functions, PECAM-1 undergoes phosphorylation and activation on tyrosine residues following mechanical or biochemical stimulation (reviewed in Ilan et al 2000, Fleming et al 2005). Furthermore, PECAM-1 presence in endothelial cells is associated with decreased/absence of endothelial-mesenchymal transition (EMT) and MMP-2 expression (Enciso et al 2003). Moreover, PECAM-1 is involved in maintenance of endothelial cell junctional integrity (Privratsky and Newman 2014).

High glucose disturbs endothelial integrity via disruption of tight junction proteins such as Occludin and Zona Occludin protein -1 (ZO-1) (Yan et al 2012). In addition, high glucose disrupts endothelial VE-cadherin junctions causing increased endothelial junction paracellular permeability, and consequently blood-retinal barrier (BRB) breakdown in DR (Gillies et al 1997, Peng et al 2016). Direct in vitro evidence shows high glucose induced toxicity and BRB breakdown in DR. Incidentally; these high glucose mediated effects were ameliorated in diabetic mice with vitamin D3 administration, suggesting a role of glucose induced oxidative damage on BRB breakdown (Lu et al 2018).

In addition to junctional compromise, endothelial morphology (size/shape) is affected by hyperglycaemia. Diabetes associated hyperglycaemia and ROS are associated with endothelial cell phenotype (shape/size) transformation in-vivo and in-vitro (Bowden and Adamson, 1974, Crapo et al 1980, Attaye et al 2017, Hempel et al 1997, and Peng et al 2016). In addition, diabetes associated dysregulation of vascular flow and shear stress, altered pro-inflammatory cytokine activity, and endothelial derived factors such as endothelin-1 (ET-1) are associated with alterations in endothelial cell size and shape (Barbee et al 1994, Malek and Izumo 1996, Chung et al 2000). Moreover, high glucose is linked with endothelial switch to mesenchymal phenotype (spindle shaped) in the endothelial mesenchymal transition (EndMT). The physiological consequence of EndMT and alterations in endothelial cell morphology is increased endothelial paracellular permeability via disruption of VE-cadherin, and consequently blood retinal-barrier breakdown (Gillies et al 1997, Peng et al 2016). Therefore, hyperglycaemia associated glucotoxicity and interaction with various other factors fosters the development and progression of endothelial dysfunction. In the following paragraphs the four biochemical pathways implicated in the various diabetes induced hyperglycaemia driven deregulations/complications are outlined.

## 1.4 Mechanisms of diabetic complications

Diabetes mellitus initiates retinopathy, neuropathy and nephropathy (DCCT 1993, UKPDS 1998). Hyperglycaemic injury is meted on endothelial cells in vascular walls including microvascular walls of the retina (reviewed in Rask-Madsen and King 2013), renal glomerular endothelium (reviewed in Arora and Singh 2013), and in neurons and Schwann cells of peripheral nerves (Cameron and Cotter 1999, reviewed in Yagihashi et al 2011). All diabetic cells are exposed to high plasma glucose levels but high glucose damage to the endothelial, mesangial, neurons and Schwann cells is selective (Brownlee et al 2016). Non-insulin dependent glucose transporter-1 (GLUT-1) mediated facilitated diffusion is the mechanism by which glucose enters endothelial and smooth muscle cells (Takata et al 1997). However, glucose transport into endothelial cells is not auto-regulated as in smooth muscle cells, and unlike smooth muscle cells, endothelial cells cannot downregulate glucose transport when exposed to extracellular high glucose. Instead, GLUT1 in retinal endothelial cell operates at near saturation levels at normal physiological blood glucose concentration. Consequently, it is not positively regulated by glucose (Brownlee 2001 and Brownlee et al 2016).

Therefore, diabetes induced hyperglycaemia drives increase in intracellular glucose in cells which produce harmful effects in cells via the following four biochemical pathways.

- a) Increased flux of glucose via the polyol pathway
- b) Increased intracellular production of AGEs
- c) Protein kinase C (PKC) activation
- d) The hexosamine pathway

The polyol pathway is regulated by the enzyme aldose reductase (AR) which converts glucose to sorbitol. Under normal condition AR converts the toxic aldehydes into non-toxic alcohol. But in hyperglycaemia, there is persistent elevated intracellular glucose, and glucose is diverted into the polyol pathway. Increased intracellular glucose is reduced by AR to sorbitol using nicotinamide adenine dinucleotide phosphate (NADPH) as a co-factor. Sorbitol is further converted to fructose by the enzyme sorbitol dehydrogenase (SDH) which utilises nicotinamide adenine dinucleotide (NADH) as a reducing intermediate. Therefore, the polyol pathway when activated disturbs cellular redox balance because NADPH and NADH which are required for glutathione regeneration, a key antioxidant needed for counteracting ROS in the cell are made unavailable (reviewed in Sena et al 2013). Thus the normal endogenous protection offered by glutathione is limited by the competing requirement of NADPH for AR activity in diabetes induced polyol pathway activation.

This underlines the role of anti-oxidant mechanism in ameliorating hyperglycaemia derangement in polyol pathway associated cellular redox imbalance. Lead inhibitors of AR pathway; Sorlini, Kinostat, ARI-809 and Ranirestat have been developed and are proposed for use in the prevention of microvascular complications (Zhu 2013). Recent animal studies conducted in dogs showed that AR activity inhibition had more profound effect on prevention of DN, but the inhibition of this enzyme was not as effective in preventing retinopathy or capillary basement thickening in the retina (reviewed in Brownlee et al 2016).

Hyperglycaemia causes damage via increased production of advanced glycation end-product (AGEs). AGEs are a diverse group of metabolites resulting from the intracellular auto-oxidation of glucose to three reactive dicarbonyl intermediates; glyoxal, methylglyoxal and 3Deoxyglucosone (Taguchi and Brownlee 2003), which subsequently react with amino groups of both intra/extracellular proteins and other macromolecules such as nucleic acids to form AGEs (Degenhardt et al 1998, Wells-Knecht et al 1995, Thornalley 1990).

AGEs modifies intracellular and extracellular protein, and growth factors including basic fibroblast growth factor (bFGF) in bovine endothelial cells (Giardino et al 1994). In addition, extracellular (ECM) matrix proteins such as collagen I, IV and laminin are modified by AGEs, resulting in alteration of ECM structures which are critical for endothelial cell adhesion and migration (Falanga 2004). More so, the methylglyoxal detoxifying enzyme glyoxalase I, an enzyme necessary for macromolecule endocytosis is also altered by AGEs (Shinohara et al 1998). Furthermore, AGEs modifies cell associated receptors culminating in the upregulation of receptors for AGEs (RAGE) leading to increased gene expression of cytokines, growth factors, pro-inflammatory and pro-coagulatory molecules. Moreover, RAGE activation results in increased production of ROS by stimulating specific signalling cascades such as NF $\kappa$ B (Daffu et al 2013). Due to the complex nature of the receptor and multiple intersecting pathways, the AGE/RAGE signalling mechanism is still not well understood (reviewed in Kay et al 2016).

The protein kinase C (PKC) family members ( $\alpha$ ,  $\beta$ ,  $\delta$ ,  $\epsilon$ ,  $\zeta$ ) are activated by hyperglycaemia and PKC signalling activity is upregulated in diabetic vascular tissues including the retina (Suzuma et al 2002, Geraldles et al 2009). Hyperglycaemia stimulates PKC signalling via de novo synthesis of diacylglycerol (DAG) from glyceraldehyde 3-phosphate and phosphatidic acid or from non-esterified fatty acids. DAG is also accumulated via the glycolytic pathway due to the inhibition of GAPDH by PARP in high glucose concentrations (Du et al 2003). Hyperglycaemia indirectly stimulates PKC- $\beta$  via the binding of AGE receptors (e.g. RAGE) and by increased polyol pathway flux, apparently by increasing ROS (Portilla et al 2000, Keough et al 1997). PKC $\beta$  activation leads to inhibition of NO (Ishii et al 1996), increased ET-1 (Yokota et al 2003), and vascular permeability which were associated with altered retinal blood flow and increased vascular permeability (Behzadian et al 2000), and angiogenesis via upregulation of VEGF expression (Rask-Masden and King 2013).

Further hyperglycaemia induced PKC activation drives pro-inflammatory and redox imbalance response via upregulation of NF $\kappa$ B and ROS overproduction (reviewed in Evcimen and King 2007). More so, PKC activation drives increased matrix protein e.g. fibronectin, collagen IV, and TGF- $\beta$  accumulation in retinal vessels leading to basement membrane thickening and capillary occlusion (Studer et al 1993, Craven et al 1997, Pieper and Riaz-ul-Haq 1997, Kuboki et al 2000, Ganz and Seftel 2000). Activation of PKC signalling causes vascular occlusion via upregulation of the fibrinolytic inhibitor PAI-1 (Ahn et al 2001). In that respect, human studies with Ruboxistaurin, a PKC inhibitor demonstrated beneficial clinical effect by limiting the progression of macular oedema and albuminuria levels in patients with T2D (Aiello et al 2005). However, Ruboxistaurin has not made it to the market yet (NICE 2018).



Glycolytic conversion of glucose first to glucose-6-phosphate, fructose-6-phosphate and subsequently into metabolic intermediates of the glycolytic pathways is the norm for glucose metabolism. Some of the fructose-6-phosphate is diverted into the signalling pathway in which glutamine: fructose-6-phosphate amidotransferase (GFAT) catalyses the conversion of fructose-6-phosphate to glucosamine-6-phosphate and finally to uridine diphosphate (UDP) N-acetyl glucosamine. Consequently, N-acetyl glucosamine is incorporated into serine and threonine residues of transcription factors. In hyperglycaemia driven high intracellular glucose flux, glucose enters endothelial, mesangial, neuron and Schwann cells indiscriminately. Fructose-6-phosphate conversion is shunted to N-acetyl glucosamine resulting in over-modification of glucosamine which causes pathologically aberrant changes in gene expression, lesions and pathological damage, and increased endothelial cell protein modification (Kolm-Litty et al 1998, Sayeski and Kudlow et al 1996, Wells and Hart 2003, Clark et al 2003, Federici et al 2002). A single unifying hypothesis of ROS overproduction as the unifying instigator for the four biochemical pathways of glucotoxicity in diabetes was proposed (Brownlee 2005, Nishikawa et al 2000). In support of this hypothesis, Brownlee and co (2005) showed that the four hyperglycaemia driven glucotoxicity pathways were blocked by mitochondrial superoxide blockade via (UCP-1 and SOD2 over-expression (Nishikawa et al 2000). The unifying mechanism of hyperglycaemia mediated complications as hypothesised by Brownlee et al (2005) is illustrated in a simplified diagram below (fig 1.1). According to this theory, hyperglycaemia associated inhibition of GAPDH results in increased intracellular glucose (which drives the four biochemical pathways already outlined). This results in the overproduction of superoxide (ROS) and increased intracellular ROS in the mitochondria which induces DNA strand breaks, consequently leading to the activation of poly ADP (ribose) polymerase (PARP) enzyme (Brownlee 2001). Activated PARP catalyses  $\text{NAD}^+$  breakdown into nicotinic acid and ADP-ribose and subsequently PARP induced polymerisation of GAPDH with ADP-ribose, thereby inactivating GAPDH and other nuclear proteins (Du et al 2003). Thus, glycolytic intermediates accumulate which drives increased polyol flux, PKC pathway, AGEs and RAGE production with increased ROS and oxidative stress in the cells.

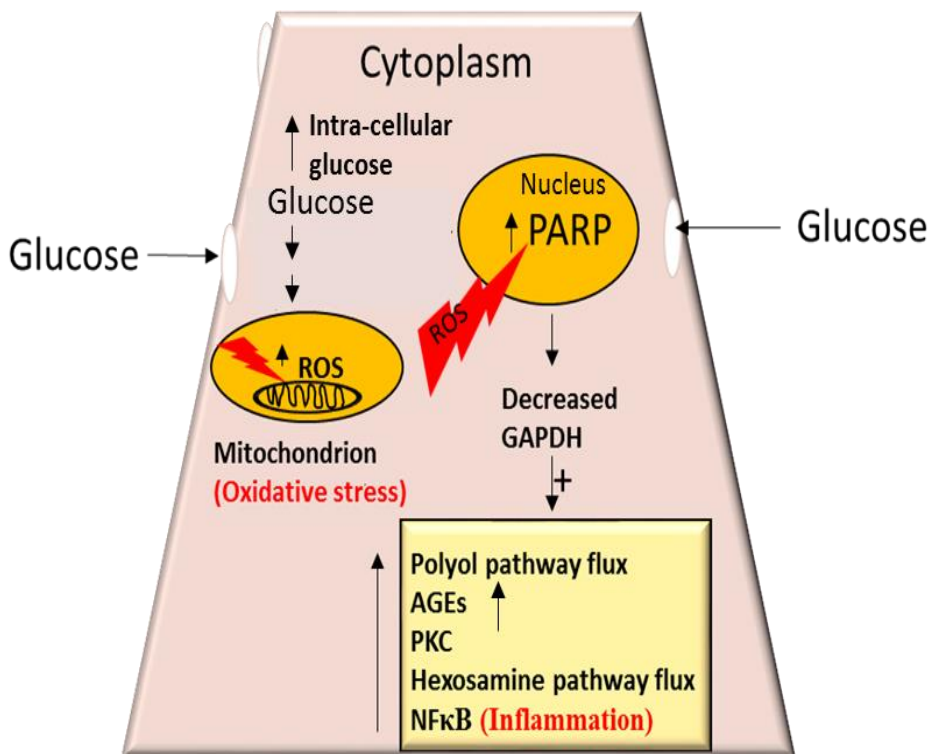


**Figure 1.1 Simple diagram of the unifying mechanism**

Persistent high glucose in diabetes drives uncontrolled glucose entry into selectively susceptible cells such as endothelial cells. Increased intracellular glucose exerts oxidative stress in the mitochondria via increased mitochondrial ROS. ROS drives the four damaging pathway; polyol, AGEs, PKC, and hexosamine flux pathway via PARP-dependent inhibition of GAPDH. Increased ROS initiates DNA strand breaks which activates PARP enzyme in the nucleus. PARP makes ADP-ribose polymers which are added unto GAPDH inactivating the enzyme, and glycolytic intermediates accumulates leading to more activation of polyol pathway flux, PKC activation, hexosamine pathway flux, and inflammation via NFκB activation.

An inflammatory theme is proposed as the instigator for the derangement seen in DR (Adamis 2008). Microscopic manifestations of inflammation in retinal vessels are vessel dilatation, altered flow, fluid exudation, leukocyte accumulation and migration (Gallin and Snyderman 1999, reviewed in Chatterjee et al 2017). A causal link between CD18/ICAM-1 mediated leukocyte adhesion and blood-retinal barrier (BRB) breakdown have been shown (Adamis 2008, Jousseaume et al 2004). Hallmark features of DR such as acellular capillaries and leukocyte adhesion were inhibited in CD18/ICAM-1<sup>-/-</sup> knockout mice with ameliorated pericytes loss (Jousseaume et al 2004).

Various mechanisms have been put forward to explain the damaging effects of inflammatory leukocytes in the pathogenesis of DR. Leukocytes may exert a direct damage to endothelial cells, leading to endothelial cell death. They are likely to exert an indirect effect on endothelial cells by damaging endothelial supportive cells such as pericytes. Leukocytes are known to induce tight junction opening and endothelial fenestrae via leukocyte mediated release of permeability factor such as VEGF, thereby impairing endothelial barrier (Adamis 2002, Jousseaume et al 2004). In addition, leukocytes adhesion may promote receptor mediated endothelial apoptosis (Jousseaume et al 2004).

The role of inflammation in DR is strengthened by the role of anti-inflammatory agents in ocular diseases. Administration of high dose aspirin, a non-steroidal anti-inflammatory (50mg/kg), meloxicam (a cyclooxygenase 2 inhibitor) and etanercept (a soluble tumour necrosis factor  $\alpha$  receptor) significantly inhibited diabetic retinal ICAM-1 expression, leukocyte adhesion, and BRB breakdown through a mechanism involving TNF- $\alpha$  suppression (Jousseaume et al 2002). In addition, Ozurdex (dexamethasone) (NICE 2015) and Iluvien (fluocinolone acetonide) (NICE 2013), both corticosteroidal anti-inflammatory drugs are in clinical use for treatment of chronic diabetic macular oedema in adults.

## 1.5 Oxidative Stress, Inflammation and Angiogenesis

Three cardinal themes; oxidative stress, inflammation and angiogenesis are evident from glucotoxicity of the endothelium. In normal physiological conditions, these events are under the control of three transcriptional factors; the nuclear factor (erythroid-derived 2)-like 2 (nrf2), the nuclear factor kappa-light-chain-enhancer of activated B cells (NFκB), and the hypoxia inducible -1 (HIF-1) respectively. Discussion of these transcription factors important in responses of endothelium to glucotoxicity is presented in the following paragraphs.

### 1.5.1 Nuclear factor erythroid 2–related factor 2 (Nrf2)

The nuclear factor erythroid 2-related factor (Nrf2) is a cytoprotective transcription factor which regulates the expression of genes coding for anti-oxidant, anti-inflammatory and detoxifying proteins, in addition to modulation of species longevity and in cellular metabolism (Kansanen et al 2013, Mitsuishi et al 2012, Negi et al 2011, and Siewart et al 2013, Heiss et al 2013). The vertebrate nrf2 belongs to Cap 'n' Collar (Cnc) bZIP family of transcription factors and shares a high homology with SKN-1 from *Caenorhabditis elegans* or Cnc found in *Drosophila melanogaster* (reviewed in Hu et al 2011). Nrf2 has seven functional domains (Neh1-7) which are important for its stability and its transcriptional activity (fig 1.2).

The N-terminal domain is the interaction site for nrf2 and Kelch-like ECH associated protein 1 (Keap 1) (Chen et al 2012). The Neh5 domain regulates nrf2 cellular localisation (Namani et al 2014, Krajka-Kuźniak et al 2017), while the Neh6 domain controls Keap 1-independent nrf2 degradation. Nrf2 binds to its target antioxidant response elements (AREs) sequences via the Neh1 domain which represents a platform for modulation of nrf2 protein stability (Keum and Choi 2014). The nuclear localisation signal required for nrf2 nuclear translocation is located on the Neh1 domain and is unmasked after Keap 1 dissociation. Co-activators of the ARE-dependent gene transcription complex such as chromo-ATPase/helicase DNA-binding protein (CHD6) interact with nrf2 via the Neh3 domain (Namani et al 2014, Krajka-Kuźniak et al 2017, and Xiang et al 2014).

Similarly, Neh4 and Neh5 are domains for targets that facilitate nrf2 transcription by binding to the co-activator cyclic adenosine monophosphate –responsive element-binding protein (CBP/p300) such as NFκB (Xiang et al 2014). Nrf2 nuclear cofactor, Ras-related C3 botulinum toxin substrate 3 protein (RAC3) interacts with Neh4 and Neh5 domains resulting in the enhancement of nrf2-targeted ARE gene expression (Namani et al 2014, Krajka-Kuźniak et al 2017, and Xiang et al 2014).

The repression of nrf2 activity by retinoic acid receptor alpha takes place in the Neh7 domain (Bai et al 2016). The Nfe2l3 gene promoter also contains ARE-like sequences providing a positive feedback mechanism which amplifies nrf2 when bound to AREs (Kwak et al 2002). The adaptor molecule, beta-transducin repeat containing E3 ubiquitin protein ligase (B-TrCP), regulates nrf2 in a Keap1-independent manner via glycogen synthase kinase 3 (GSK-3 $\beta$ )-mediated phosphorylation of the Neh6 domain (Rada et al 2011 and 2012). PKC activity promotes nrf2 activation via phosphorylation of the serine residue (Ser40) in Neh2 domain of nrf2 (Steinberg 2015), highlighting a possible link by which nrf2 activity may be induced by signals that induce PKC, such as high glucose or ROS induced oxidative stress. The phosphoinositide-3 kinase (PI3K), PKC, MAPK, and the extracellular signal regulated kinase (ERK) also enhance nrf2 activity through inhibition of GSK-3 $\beta$ , in addition to the Notch signalling pathways (Kaidanovich-Beilin et al 2011, Wakabayashi et al 2010). Another potential regulator for nrf2 is the musculoaponeurotic fibrosarcoma oncogene homolog small Maf (sMaf) proteins which are co-transcription activators for nrf2 with capacity to dimerize with nrf2 or self-dimerize. Ironically, over-expression and self-dimerization of sMaf is associated with impairment of nrf2 transactivation because sMaf dimers are incapable of mediating transcriptional activation with nrf2 (Motohashi et al 2010). The nrf2 functional domains are shown in fig 1.2.

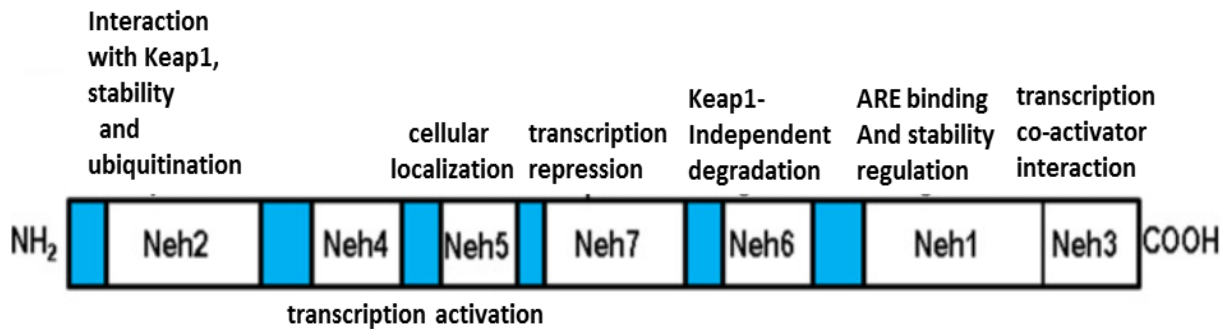


**Figure 1. 2 Schematic representative structure of Nrf2**

Nrf2 has seven functional domains (Neh1-7). Neh1 (N-terminal) is nrf2-Keap 1 interaction domain and represents the platform for Keap 1 mediated nrf2 degradation via ubiquitination. Nuclear localisation site for nrf2 on Neh1 domain is unmasked after Keap 1 dissociation. Neh5 regulates nrf2 cellular localisation and Neh6 is the site for Keap 1-independent nrf2 degradation. Nrf2 interacts with co-activators that transactivate ARE-dependent genes after chromatin remodelling, while CBP binding co-activators such as NFκB interacts with nrf2 via Neh4 and Neh5 domains. Nrf2 is repressed by retinoic acid receptor via Neh7 domain. (Reproduced with permission from Bellezza et al 2018).

Nrf2 protein is distributed in the cytosol and translocate to the nucleus upon its stabilisation and activation, and there is small evidence that nrf2 might be distributed in the plasma membrane (HPA, 2018). Owing to its global role in the activation of vast arrays of genes, nrf2 level is well regulated in cells. During cell homeostasis, although nrf2 is constitutively expressed in the cytoplasm, it is isolated via two molecules of Kelch-like ECH associated protein 1 (Keap 1) under normal conditions (Chen et al 2012). Keap 1 promotes ubiquitination and degradation of nrf2, thus Keap 1 modulates nrf2 protein stability, maintaining basal levels in unstressed cell states. However, nrf2 is constitutively expressed in some disease states such as in acute myeloid leukaemia (AML) (Fuse and Kobayashi 2017). The half-life of nrf2 in the cytosol in normal condition is approximately 20 min (Kobayashi and Yamamoto 2006). In conditions of excess oxidants or electrophiles e.g. ROS, nrf2-dependent cellular defence response is activated, and Keap 1 is oxidised at its cysteine thiol groups. Both nrf2 and Keap 1 undergo post-translational modification and the oxidation of Keap 1 cysteine group allows for nrf2 dissociation from Keap 1 and its subsequent stabilisation.

In human cell lines, Keap 1 knock down is associated with nrf2 accumulation (Wakabayashi et al 2003, Devling et al 2005), and stabilisation of nrf2 protein is reported to increase its half-life to 200 mins (Canning et al 2015). With increased residence time, nrf2 translocate to the nucleus where it binds with specific DNA-recognition sequence antioxidant response elements (AREs) as a heterodimer with sMaf resulting in activation of transcription to induce anti-oxidant and metabolic gene expression (Katsuoka et al 2005, Bellezza et al 2018). Nrf2 regulation in normal and stress condition is illustrated in figure 1.3.

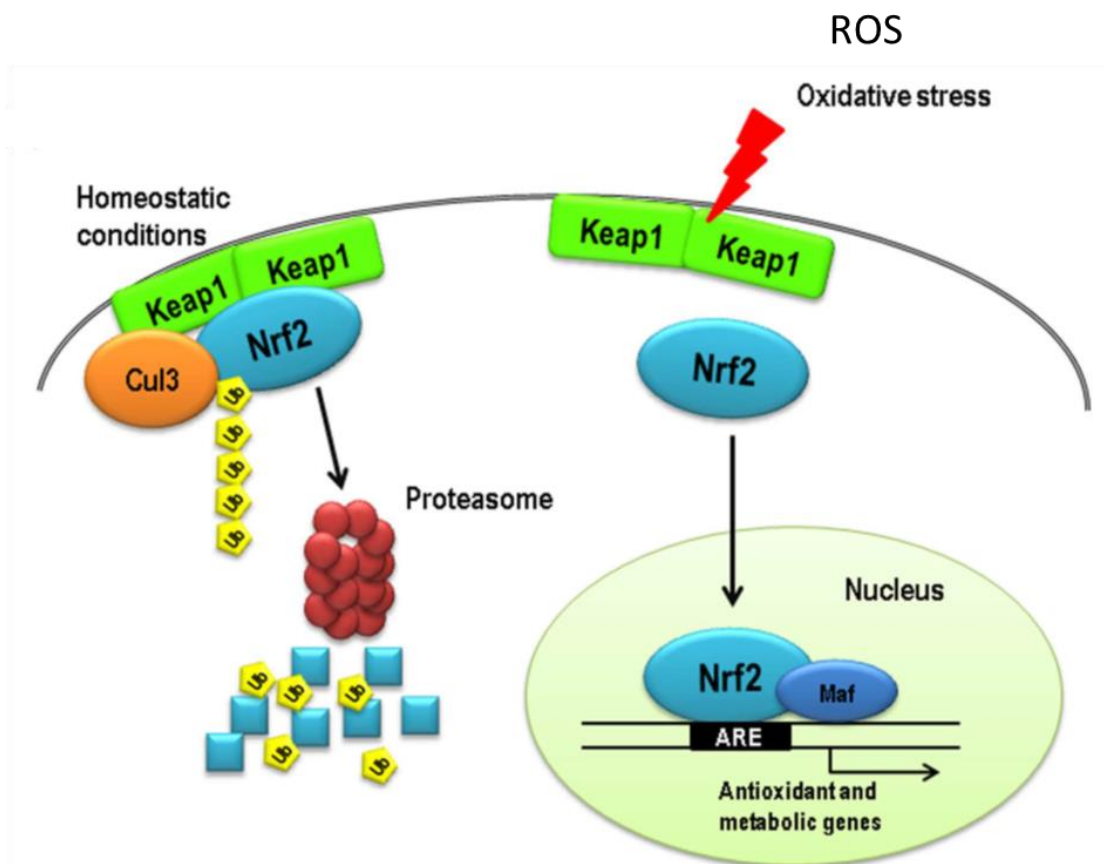


**Figure 1. 3 Nrf2 regulation in normal and stress condition**

In normal (homeostatic) condition, nrf2 (light blue) is bound tightly by Keap 1 via F-actin cytoskeleton (Velichkova and Hasson 2005, Bellezza et al 2010). In homeostatic condition nrf2 levels are kept very low via proteasomal (red) mediated ubiquitination (yellow) and degradation. Stress signals such as oxidative stress causes nrf2 to separate from Keap 1 and translocate to the nucleus where it heterodimerizes with sMaf proteins (blue) and the nrf2-Maf heterodimer binds to AREs (black) to induce anti-oxidant and metabolic gene expression (Reproduced with permission from Bellezza et al 2018).

Nrf2 is a mechanosensitive transcription regulator in endothelial cells (ECs) (reviewed in McSweeney et al 2015). Increased shear stress in ECs is accompanied by ROS generation and increased expression of adhesion molecules which may explain the activation of nrf2 during increased shear stress in ECs presumably to mediate the expression of anti-oxidant response genes and proteins (reviewed in McSweeney et al 2015). Mechanical stress associated ROS enhancement also indirectly mediates nrf2 activation via ROS activation of the p38 and c-Jun N-terminal (JNK) activity leading to NFκB activation. Activated NFκB cross-talks with nrf2 via guanosine triphosphatases (GTPase) Rac1 (Ras-related C3 botulinum toxin substrate 1) resulting in nrf2 activation and the inducement of nrf2 cytoprotective genes and protein such as the heme oxygenase -1 (HO-1) (Bellezza et al 2012, Minelli et al 2009, and Cuadrado et al 2014) (fig 1.4 and 1.6).

The effect of nrf2 in cells is predominantly protective. Recently, the over-expression of nrf2 in endothelial progenitor cells (EPCs) of diabetic mice was shown to be associated with increased protection against oxidative stress (Wang et al 2018). Although, hyperglycaemia induced endothelial dysfunction is associated with ROS production and oxidative stress and several of the glucotoxicity effects are driven from the build-up of glycolytic intermediates, the activation of the pentose phosphate pathway (PPP) is reported to counter hyperglycaemia induced metabolic dysfunction (Babaei-Jadidi et al 2003, Hammes et al 2003, and Berrone et al 2006). What was not evident at the time was the link between the PPP and nrf2 redox system because several of the PPP enzymes including glucose-6 phosphate dehydrogenase (G6PD) are under the control of nrf2. Accordingly, Nrf2 activation has been shown to prevent metabolic dysfunction in endothelial cells via increased expression of transketolase (Xue et al 2008). Recently, vitamin D3, was shown to downregulate intracellular ROS and inhibited TRX-interacting protein (TXNIP)/NOD-like receptor family, pyrin domain-containing 3 (NLRP3) inflammasome pathway activation in diabetic mice and human retinal microvascular endothelial cells, which strengthens the association of the redox system controlled by the transcriptional factor, nrf2 (Lu et al 2018).



Nrf2 is also involved in cell membrane homeostasis. High glucose also increases PMRS activity but PMRS activity is not observed in low glucose (Leiser and Miller 2010). Activation of the nrf2 is associated with up-regulation of plasma membrane redox system (PMRS) activity which is linked with cell survival under stress conditions (Hyun et al 2006, Saraswat and Rizvi 2017). In dwarf cells, elevated nrf2 protein levels with increased PMRS resulted in decreased stress-induced lipid peroxidation (Leiser and Miller 2010). There are not many studies that have examined plasma membrane associated nrf2 activation in endothelial cells.

Nrf2 pathway signalling activates over 200 antioxidant and cytoprotective genes (Godman et al 2010). Nrf2 regulated pathway regulates the expression of cytoprotective genes including antioxidant genes e.g. heme oxygenase -1 (HO-1), ferritin, and SOD, genes encoding enzymes that participate in glutathione synthesis and regeneration such as G6PD, glutathione peroxidase (GPx), glutathione S transferase (GST), glutathione reductase (GR) and  $\gamma$ -glutamylcysteine ligase, in addition to the xenobiotic detoxifying pathway. A list of examples of genes/pathways regulated by nrf2/Keap 1 pathway is presented in table 1.2 (reviewed in Loboda et al 2015).

**Table 1.2 Nrf2 dependent genes.** Examples of the cytoprotective genes regulated by nrf2 (adapted from Loboda et al 2015)

<u>Genes</u>	<u>Abbreviation</u>	<u>Major function</u>
Heme oxygease-1	HO-1	Degrades heme and generates the antioxidant molecules, biliverdin and CO
Ferritin	Fn	Sequesters free iron
Glucose -6-phosphate Dehydrogenase	G6PD	Provides NADPH to glutathione reductase
Glutathione peroxidase	GPx	Detoxifies peroxides and Hydroperoxides
Superoxide dismutase	SOD	Catalyzes the dismutation of the superoxide radical (O <sub>2</sub> <sup>-</sup> ) into molecular oxygen (O <sub>2</sub> ) or hydrogen peroxide (H <sub>2</sub> O <sub>2</sub> )
Glutathione reductase	GR	Catalyzes the reduction of glutathione disulfide (GSSG) to the sulfhydryl form of glutathione (GSH)
γ-Glutamylcysteine ligase	GCL	Catalyzes the rate limiting step in the cellular glutathione (GSH) biosynthesis pathway

### 1.5.1.1 Nrf2- NFκB Crosstalk

Nrf2 pathway performs a pro-survival role via its cross-talks with the nuclear factor kappa-light-chain-enhancer of activated B cells (NFκB) pathway which ameliorates the pro-death ROS-mediated JNK activation signalling pathway (Bellezza et al 2018) (fig 1.4). This interaction between nrf2 and NFκB is made possible by the presence of an NFκB binding site on the promoter region of nrf2. Both nrf2 and NFκB compete for CBP/300 binding in the nucleus, dependent on the relative amounts of NFκB or nrf2 as shown in fig 1.4 (A), and in the presence of simultaneous nuclear increases in these two transcription factors, NFκB (p65) antagonizes nrf2-induced gene transcription (Bellezza et al 2018).

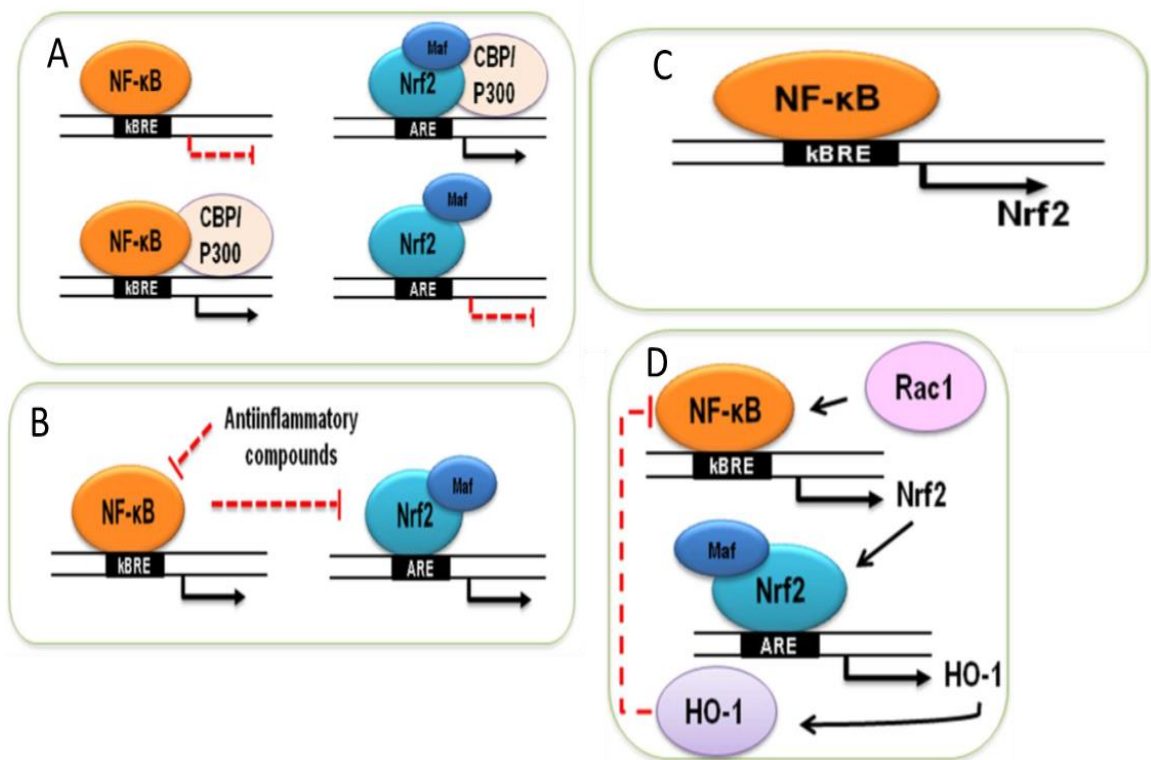


**Figure 1. 4 Nrf2 and NFκB cross-talk**

Nrf2 and NFκB compete for CBP/P300 binding in the nucleus (A). When NFκB is more in abundance, it upsets nrf2 gene transcription. But if NFκB activity is suppressed by anti-inflammatory molecules, then nrf2 activity is activated (B). When NFκB is activated it binds on κB response elements (κBRE) on nrf2 promoter region, causing nrf2 induction (C). Rac1 activates NFκB which stimulates nrf2 and upregulates HO-1 (D). HO-1 goes back and inhibits NFκB. (Reproduced with permission from Bellezza et al 2018).

On the other hand, compounds with anti-inflammatory properties indirectly activate nrf2 by suppressing NFκB activity, which relieves NFκB competition for CBP/p300 with nrf2 (Grottelli et al 2016, Li et al 2008, Kim et al 2013, and Minelli et al 2012). Ironically, NFκB also shows protective anti-inflammatory activity by activating nrf2 activity via GTPase Rac1 (C) (Cuadrado et al 2014). Activated nrf2 induces HO-1 which inhibits further NFκB activity (Bellezza et al 2012, Minelli et al 2009, and Cuadrado et al 2014). NFκB mediates this effect on ROS via its effect on the expression of several antioxidant proteins including nrf2. Secreted cytokines are also able to stimulate nrf2. Kharazmi et al (1989) showed that secretory cytokines including IL-6 and TNFα are able to auto-activate (prime) macrophages and increase their production of superoxide anion, and TNFα cell lethality is in part due to TNFα induced oxidative free radical damage.

In-vivo studies have evidenced the role of nrf2 in mediating inflammatory signals. In nrf2-deficient (*Nrf2*<sup>-/-</sup>) mice, increased plasma TNFα and decreased levels of glutathione in the retina were documented versus their wild-type (*Nrf2*<sup>+/+</sup>) diabetic equivalents at 8 weeks of diabetes (Xu et al 2014). Consequently, these *Nrf2* knockout mice exhibited early onset of blood–retina barrier dysfunction and exacerbation of neuronal dysfunction in diabetes demonstrating nrf2 has a protective transcription factor in DR and suggests enhancement of the nrf2 pathway as a potential therapeutic strategy (Xu et al 2014).

### 1.5.1.2 Heme Oxygenase isoform 1

Nrf2 regulated pathway regulates the expression of cytoprotective genes including anti-oxidant heme oxygenase -1 (HO-1) (reviewed in Loboda et al 2015). The heme oxygenase-1 (HO-1, *HMOX1*) is regulated by nrf2 (Alam et al 1999, Kansanen et al 2013). HO-1 is an inducible 32-kDa protein found in mammals and it is distinct from the constitutive HO-2 isoform of heme oxygenase (HO). HO-1 functions as an anti-oxidant, anti-inflammatory and anti-apoptotic microsomal stress response protein (Otterbein et al 1999, Chen et al 2012). It is expressed as an integral protein of the smooth endoplasmic reticulum but localises to caveolae, mitochondrion and the nucleus (Yoshida and Sato 1989), Yoshida et al 1991, Jung et al 2003, Slebos et al 2007, and Sacca et al 2007). HO-1 is upregulated by a number of stimuli including heme, nitric oxide, heavy metals, growth factor, cytokines, and NFκB in response to oxidative stress (ROS) (reviewed in Loboda et al 2008, Bellezza et al 2018).

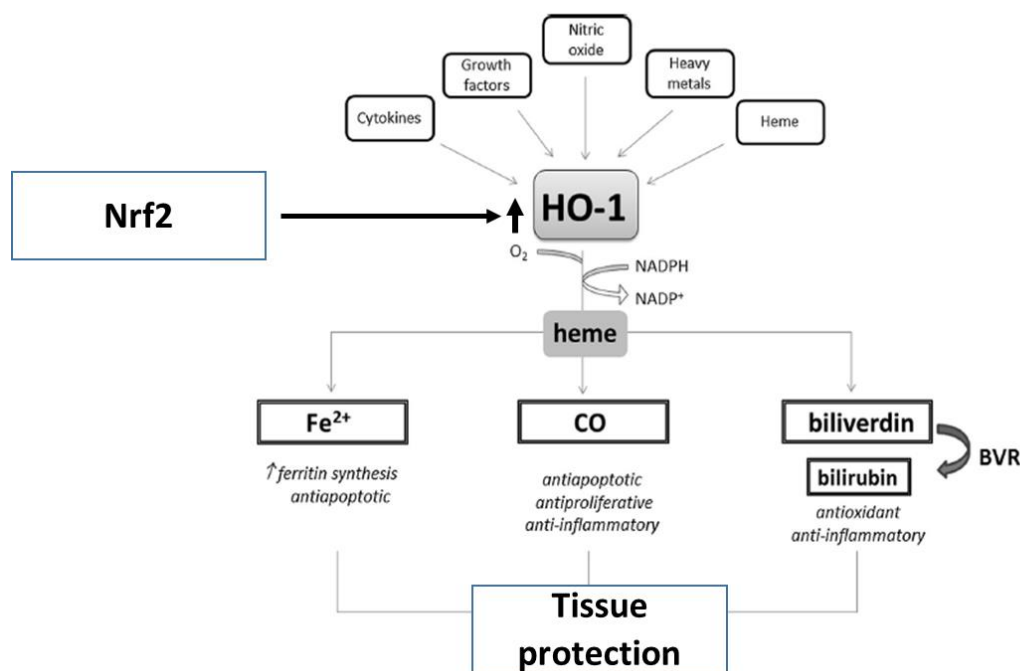


**Figure 1. 5 Heme oxygenase -1 pathway**

Nrf2 stabilisation, accumulation and activation may result in the induction of HO-1 protein. HO-1 enzyme when induced co-operates with NADPH cytochrome P450 to degrade heme, to three bioactive intermediates; iron ions, carbon monoxide and biliverdin. Biliverdin is rapidly converted to bilirubin by biliverdin reductase (BVR). All three metabolites of HO-1 elicit functions that are pro-angiogenic, anti-oxidant or anti-inflammatory (Adapted from Loboda et al 2015).

HO-1 catalyses the breakdown of heme to; iron, carbon monoxide (CO) and biliverdin in a catalytic reaction aided by NADPH cytochrome P450. The enzyme, biliverdin reductase (BVR) reduces biliverdin to bilirubin, which confers anti-oxidant and anti-inflammatory protection. In addition, free iron released as a by-product of heme breakdown induces and enhances ferritin, an iron scavenger in endothelial cells (Balla et al 1992). Therefore, enhanced ferritin levels reduces availability of redox-active iron from participating in the Fenton reaction, thereby preventing the generation of highly reactive and DNA-damaging hydroxyl radical (Tenhunen et al 1968, Choi et al 1996, Elbirt and Bonkovsky 1999, and Otterbein et al 1999). Moreover, ferritin elevation also confers anti-apoptotic protection to endothelial cells (reviewed in Loboda et al 2015). Furthermore, carbon monoxide, another heme metabolite is associated with anti-inflammatory and anti-proliferative and protective effects especially in vascular dysfunction (Loboda et al 2015).

In addition to Keap 1, nrf2 is regulated via GSK-3 $\beta$  mediated phosphorylation. GSK-3 $\beta$  phosphorylation is associated with increased proteasomal degradation of nrf2 (Biswas et al 2014). Initial studies identified the translocation of a truncated (28-kDa) enzymatically inactive HO-1 with nrf2 into the nucleus during times of oxidative injury (Otterbein et al 1999). Later studies suggested the truncated HO-1 interacts with activator protein 1 (AP-1) consensus sequences on nrf2 during oxidative stress consequently stabilising nrf2 against GSK-3 $\beta$  mediated phosphorylation and that HO-1/nrf2 interaction in the nucleus prolongs nrf2 nuclear residence and provides sustained tolerance against oxidative injury, thus increasing cell survival (Dennery 2013). The importance of HO-1 enzyme is demonstrated by some of the effects of HO-1-deficiencies which include marked systemic inflammation, abnormalities of the coagulation/fibrinolysis system, developmental failure, and iron-deficiency anaemia, intravascular haemolysis with fragmented erythrocytes, nephropathy, and vascular endothelial injury (Yachie et al 1999).

## 1.5.2 Nuclear factor kappa-light-chain-enhancer of activated B cells

The nuclear factor kappa-light chain-enhancer of activated B cells (NF $\kappa$ B) and its activating receptors were first described in immune cells. They are a five member family of transcription factors with a Rel-homology (RHD) domain that is critical for DNA binding and dimerization. Three of the five NF $\kappa$ B members; Rel A, (also known as p65), Rel B and cRel, have a C-terminal transcription activation domain (TADs) that serves to positively regulate gene expression, while the P105 and p100 members are synthesised as inactive precursor proteins that are cleaved to the smaller p50 and p52 subunits which lack TADs. Unlike the Rels with transactivational C-terminals, the C-terminals of P105 and p100 subunits have inhibitory ankyrin repeats. However, they are able to associate with the Rel proteins to form transcriptionally active heterodimers.

In normal conditions, NF $\kappa$ B is sequestered in the cytoplasm by inhibitors of  $\kappa$ B (I $\kappa$ B). I $\kappa$ B possesses potent nuclear export signal (NES), hence their capability to export nuclear NF $\kappa$ B. In addition, I $\kappa$ B inhibits NF $\kappa$ B by binding to NF $\kappa$ B DNA binding, thereby excluding any NF $\kappa$ B target gene binding and gene expression. Phosphorylation of I $\kappa$ B by upstream I $\kappa$ B kinases (IKKs) targets it for ubiquitination and proteasomal degradation, thus unmasking the DNA binding activity of the p50/Rel A heterodimer. NF $\kappa$ B is regulated via canonical (fig 1.6) and non-canonical pathways but canonical NF $\kappa$ B regulation is more relevant physiologically versus non-canonical pathway.

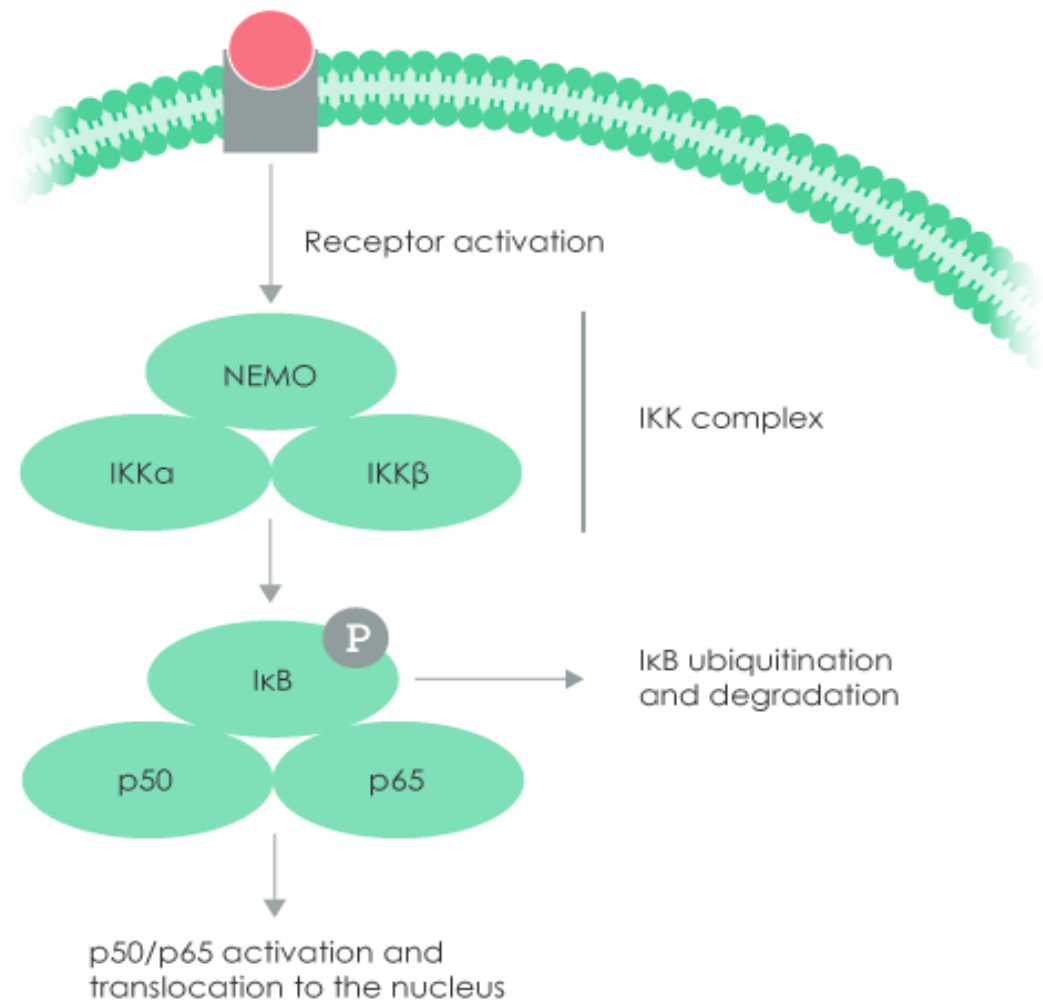


### Figure 1. 6 Canonical (classical) NFκB signalling pathways

Ligands such as IL-6 or ROS bind to cytokine and TLR receptors on NFκB respectively. IKK alpha and/or IKK beta catalytic subunits and two molecules of NFκB essential modulator (NEMO) are recruited forming the IKK complex. The IKK complex phosphorylates IκB leading to degradation by the proteasome. NFκB heterodimer (Rel A (p65)/c-Rel/p50) complex translocate to the nucleus to activate target genes. Source: Abcam- <https://www.abcam.com/research-areas/overview-of-NFκB-signaling> 11.45pm/ 13th September 2018.

The canonical and non-canonical NF $\kappa$ B pathways share a common regulatory step of activation of an I $\kappa$ B kinase (IKK) complex consisting of catalytic kinase subunits (IKK $\alpha$  and/or IKK $\beta$ ) and the regulatory non-enzymatic scaffold protein, NF $\kappa$ B essential modulator (NEMO) also known as IKK $\gamma$ . In the canonical route, Rel A/c-Rel/p50 NF $\kappa$ B complex translocate to the nucleus where it activates the transcription of its target genes (Hayden and Ghosh 2008, Karin and Ben-Neriah 2000). In the non-canonical pathway, p100 is degraded to p52, allowing a Rel B/p52 complex to translocate from the cytoplasm to the nucleus (Xiao et al 2001).

NF $\kappa$ B is important for regulation of inflammatory responses. In addition to mediating induction of various pro-inflammatory genes in innate immune cells, NF $\kappa$ B regulates the activation, differentiation and effector function of inflammatory T cells (Tak and Firestein 2001, Lawrence 2009). NF $\kappa$ B also has a role in regulating the activation of inflammasome (Sutterwala et al 2014). Furthermore, NF $\kappa$ B exerts a protective role in oxidative stress by suppressing ROS accumulation via nrf2 activation and directs host response to environmental stress (Hayden et al 2004 and Bellezza et al 2018). For instance, NF $\kappa$ B is a mediator of mechanotransduction in several cell types including endothelial cells (Barkett and Gilmore 1999, Dolcet et al 2005). Mechano-transduced signals at focal endothelial cell adhesion stimulates NF $\kappa$ B in response to shear stress via Rac1 and cell division control protein 42 homolog (Cdc42) activation (Khachigian et al 1995, Chien et al 1998, and Tong and Tergaonkar 2014).

Thus, basal NF $\kappa$ B activity is critical for the regulation of inflammatory response, cellular growth, permeability and apoptosis in endothelial cells (Barkett and Gilmore 1999, Dolcet et al 2005). Moreover acute Inflammation is a protective response of the host to infections and tissue damages, necessary for cell response to infection or tissue injury. Hence, inflammation can be beneficial to the host if resolved in a timely manner; however, deregulated inflammatory responses can cause excessive or long-lasting tissue damages, contributing to the development of acute or chronic inflammatory diseases. Indeed chronic deregulated NF $\kappa$ B activation is a hallmark of chronic inflammatory diseases including diabetes. In the diabetic endothelium, chronic NF $\kappa$ B expression is promoted and augmented due to hyperglycaemia induced PKC activation which drives pro-inflammatory and redox imbalance response via chronic upregulation of NF $\kappa$ B and ROS overproduction (reviewed in Evcimen and King 2007).



Endothelial cells (ECs) direct leukocyte traffic through regulation of adhesion molecules, chemokines, and cytokines (Galley and Webster 2004, Zhang and Frei 2001, Aoki et al 2001, and Badrichani et al 1999). Pro-inflammatory cytokines have profound effect on endothelial function, including their regulation of vascular tone, permeability, and leukocyte diapedesis (Aoki et al 1989, Galley and Webster 2004, Lush et al 2000). The pro-inflammatory cytokine, interleukin 6 (IL-6) and ROS activate canonical pro-inflammatory NF $\kappa$ B (p65) activation in endothelial cells via cytokine receptors and toll-like receptors (TLRs) respectively (Castell et al 1988, Pober 1999, Morgan and Liu 2011).

### 1.5.2.1 Endothelial interleukin-6 (IL-6)

Interleukin-6 (IL-6) is a pleiotropic cytokine with functions in acute phase protein response, autoimmunity in addition to driving chronic inflammation and endothelial dysfunction. IL-6 was molecularly cloned in 1986 as a B-cell stimulatory factor by the group of (Hirano et al 1986). Human IL-6 is made up of 212 amino acids, including a 28-amino-acid signal peptide, and its gene has been mapped to chromosome 7p21 (Kobayashi et al 2012). It is also associated with factors including myeloid blood cell differentiation-inducing protein indicating its other roles in addition to immune response (reviewed in Schaper and Rose-John 2015, and Barnes et al 2011). IL-6 is synthesized and secreted by several cell types including endothelial cells (ECs), monocytes, T-cells and fibroblasts (Schaper and Rose-John 2015). Accordingly, IL-6 mRNA and protein were shown to be upregulated in endothelial cells (HUVECs) independent of LPS or contamination (Kobayashi et al 2012).

The vascular endothelium, particularly the lymphatics constitutively synthesize IL-6 which offers immune surveillance and protection in readiness for acute phase protein activation (Castell 1988, reviewed in Gabbay 2006). IL-6 signalling takes place via classic (a membrane bound receptor) or soluble receptor (trans) signalling mechanisms and the biological effects of these two mechanisms are separate (reviewed in Schaper and Rose-John 2015). Membrane bound IL-6 receptors (IL-6R) are not expressed in ECs hence IL-6 signalling in ECs occurs via trans signalling has been observed (Romano et al 1997). IL-6 trans signalling is associated with pro-inflammatory and stress response to restore homeostasis (Schaper and Rose-John 2015). In addition, IL-6 promotes endothelial tube formation and proliferation (Sato et al 2016), and neoangiogenesis (Tartour et al 2011). However, IL-6 overstimulation in the endothelium is linked to increase in the expression of adhesion molecules such as ICAM-1 and VCAM-1 and endothelial cell dysfunction (reviewed in Barnes et al 2011). IL-6 was recently shown to increase migration and proliferation of human dermal microvascular endothelial cells (HDMECs) without inducing endothelial-mesenchymal transition (EndMT) (Kevin et al 2018).

IL-6 has been shown to exhibit both pro-inflammatory and anti-inflammatory functions mediated predominantly via NFκB in cells (reviewed in Scheller et al 2011, Sato et al 2016). NFκB binding sites are found on functional *cis*-regulatory elements in human IL-6 gene 5' flanking region demonstrating the regulation of the IL-6 gene transcription by NFκB (Tanaka et al 2014). Stretch induced IL-6 responses in ECs are dependent on sequential IKKs and NFκB activation in a ROS dependent manner (Kobayashi et al 2003).

IL-6 is regulated predominantly at the transcriptional level (Castell et al 1988). In vivo IL-6 mRNA is unstable and has a half-life of 30 mins due to AU-rich instability elements in its 3' untranslated region and serum IL-6 is rapidly cleared (Paschoud 2006, Saitoh et al 2000, and Ramakers et al 2009). However, in in-vitro experiments using human pulmonary artery endothelial cells (HPAECs) and HUVECs, IL-6 was stable (> 2 h) indicating serum IL-6 and IL-6 mRNA may be cleared in-vivo by mechanisms which may be lacking in-vitro (Kobayashi et al 2012). Non-coding regulatory microRNAs (miRNA) are suggested to be associated with IL-6 mRNA instability in-vivo. MiRNA are small non-coding regulatory RNA, 22-24 nucleotide long that silences gene expression at post-transcriptional level by base pairing with the 3'-untranslated region (3'-UTR) of complementary sequences within coding mRNA molecules, thereby suppressing gene expression (Bartel 2004, Xu et al 2011). Base-pairing silences the target mRNA either by destabilization of the mRNA through shortening of its poly(A) tail, cleavage, or decreased translation of the mRNA into proteins by ribosomes. Interaction of miRNA-146a/b and -223 was shown to indirectly suppress transcription of IL-6 by respectively targeting IL-1 receptor-associated kinase 1 and signal transducer and activator of transcription 3 (STAT3) (Chen et al 2012, Zilahi et al 2012).

### 1.5.3 Hypoxia inducible factor -1 alpha (HIF-1α)

Hypoxia-inducible factor -1 (HIF-1) is the major transcription factor regulating genes that facilitate adaptation and survival of cells and the whole organism from normoxia (~ 21% oxygen) to hypoxia (~ 1% O<sub>2</sub>) (Wang et al 1995, Semenza 1998). HIF-1 was discovered by the identification of a hypoxia response element (HRE; 5'-RCGTG-3') in the 3' enhancer of the gene that codes for erythropoietin (EPO) hormone (Goldberg et al 1988, Semenza et al 1991). HIF-1 is a heterodimer complex consisting of a regulated subunit, HIF-1α and a constitutively expressed subunit, HIF-1β, also known as the aryl hydrocarbon nuclear translocator (ARNT) (fig 1.7) (Semenza et al 1991, Wang and Semenza 1993). HIF-1α isoforms; HIF-2α and HIF-3α and splice variant inhibitory PAS (IPAS) have been described (Semenza et al 1991, Wang and Semenza 1993). The human HIF-1 gene is found on chromosome 14 (14q21-q24), while HIF-1β gene is located on chromosome 1 (1q21).

HIF-1 $\alpha$  and HIF-1 $\beta$  are large proteins composed of 826 basic helix-loop-helix motifs (bHLH) and the bHLH and PAS motifs are requisite for HIF-1 $\alpha$  and HIF-1 $\beta$  heterodimer formation (Semenza et al 1991, and 1993). The downstream basic region is required for binding to the HRE DNA sequence (Wang et al 1995, Crews 1998). HIF-1 $\alpha$  (HIF-1 $\alpha$ , HIF-2 $\alpha$ , HIF-3 $\alpha$ , and inhibitory Per-ARNT-Sim (IPAS) and HIF-1 $\beta$  belong to the Per-ARNT-Sim (bHLH-PAS) protein family (Wang et al 1995). The HIF-1 $\alpha$  subunit has two transactivation domains (TAD); the N- and C-terminal transactivation domains: NTAD and CTAD, found between residues 531-575 and 813-826 respectively (Ruas et al 2002). The NTAD motif overlaps with a larger O<sub>2</sub>-dependent degradation domain (ODDD), which confers control on HIF-1 $\alpha$  in response to O<sub>2</sub> concentration (Pugh et al 1997). The main function of CTAD is to recruit transcriptional co-activators; CBP/P300, SRC-1 and TIF-2 (Kung et al 2000, Lando et al 2002b, and Hirota and Semenza 2006).

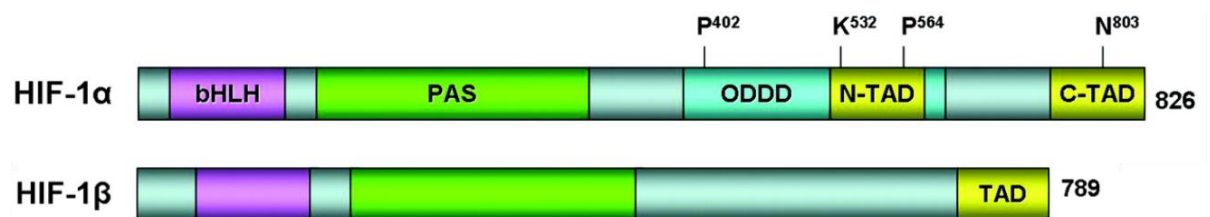


**Figure 1. 7 Domain structure of human HIF-1 $\alpha$  and HIF-1 $\beta$**

HIF-1 $\alpha$  and HIF-1 $\beta$  belong to the bHLH (purple) and PAS (green) protein family. HIF-1 $\alpha$  contains an ODDD that mediates HIF-1 $\alpha$  regulation based on O<sub>2</sub> concentration via hydroxylation of two proline residues which is absent in HIF-1 $\beta$ . HIF-1 $\alpha$  contains two transactivation domains; C-TAD and N-TAD, whereas HIF-1 $\beta$  has only one TAD. HIF-1 $\alpha$  has a total of 826 amino acids (AA), whilst there are 789 AAs in HIF-1 $\beta$  (Adapted from Ke and Costa 2006).

HIF-1 $\beta$  is constitutively expressed and its mRNA and protein levels are maintained at a constant level regardless of oxygen availability (Kallio et al 1997). The transcription and synthesis of HIF-1 $\alpha$  is constitutive and unaffected by oxygen levels (Wang et al 1995, Kallio et al 1997). However, in normoxia de novo synthesized cytoplasmic HIF-1 $\alpha$  is degraded within a half-life of ( $t_{1/2}$  of ~ 5 min) resulting in very low levels of HIF-1 $\alpha$  protein (Wang et al 1995). In converse, HIF-1 $\alpha$  is stabilized in hypoxia or other relevant stimuli, and translocate to the nucleus where it dimerizes with HIF-1 $\beta$  forming a transcriptionally active complex. HIF-1 $\alpha$  and HIF-1 $\beta$  heterodimer bind to hypoxia response elements (HREs) in the regulatory regions of target genes. Transcriptional co-activators such as the CBP/P300 are recruited to the HIF-HRE complex which activates transcription (Ruas et al 2002).

HIF-1 $\alpha$  stability and the subsequent transactivational function of HIF-1 are controlled mainly via post-translational modifications including hydroxylation, ubiquitination, acetylation, and phosphorylation. Translation modification of HIF-1 $\alpha$  is also known. In normal oxygen tension (normoxia), two proline; Pro402 and Pro564 residues at the ODDD undergo hydroxylation which promotes HIF-1 $\alpha$  association with the tumour suppressor protein von Hippel–Lindau (pVHL) ubiquitin E3 ligase complex. The VHL tumour suppressor protein is a substrate recognition element of the E3 ubiquitin ligase complex proteasomal pathway and pVHL labels HIF-1 $\alpha$  with ubiquitin tag marking HIF-1 $\alpha$  for degradation via the ubiquitin-proteasomal degradation pathway (Srinivas et al 1999). Mutation of both proline 402 and 564 disrupts HIF-1 $\alpha$  interactions with pVHL, resulting in increased HIF-1 $\alpha$  protein stability in normoxia (Masson et al 2001).

HIF-1 $\alpha$  activity is also controlled via modulation of HIF-1 $\alpha$  transactivation domains, NTAD and CTAD. Transactivation domains function to recruit co-activators such as with cyclic adenosine monophosphate –responsive element-binding protein (CBP/P300) for example (Arany et al 1996).

In normoxia, the factor inhibiting HIF-1 $\alpha$  (FIH) hydroxylates asparagine (Asn) residue 803 (Asn803) in C-TAD of HIF-1 $\alpha$ , thereby preventing HIF-1 $\alpha$  interaction with CBP/300 (Lando et al 2002). But hypoxia abrogates FIH mediated Asn803 hydroxylation in a reaction requiring 2-oxoglutarate dependent dioxygenase, iron and ascorbate as coactivators (Lando et al 2002a). The distribution of FIH-1 is mainly cytoplasmic, but a nuclear fraction is documented (Metzen et al 2003). Hence, FIH is able to disrupt HIF-1 $\alpha$  transactivation domains in both nuclear and cytoplasmic compartments.

In regards to post-translational regulation, HIF-1 $\alpha$  protein levels are maintained low by prolyl hydroxylases (PHDs), more so by PHD2 in comparison to PHD3 and PHD1 (Huang et al 2002). PHD2 is primarily located in the cytoplasm but also shuttles between the cytoplasm and the nuclear compartment, thus regulating HIF-1 $\alpha$  in both compartments, suggesting HIF-1 $\alpha$  may still be degraded in the nucleus by PHD2 unless HIF-1 $\alpha$  is stabilized. In addition to sub-cellular distribution, PHDs also differ in their tissue distribution which may enable a graded or tissue-specific response to hypoxia, thereby promoting the O<sub>2</sub>-dependent degradation of HIF-1 $\alpha$  (Baek et al 2005).

The name ‘hypoxia inducible factor’ sometimes seems at odds for studies involving the use of physiologically higher than normal oxygen levels (hyperoxia). This conundrum has long been addressed by the understanding that HIF-1 is also stimulated by oxygen independent mechanisms including ROS (Haddad et al 2001 and 2002), growth factors via PI3K, serine/threonine kinase AKT (protein kinase B), and FKBP-rapamycin associated protein (FRAP) (Zhong et al 1998). The PI3K/AKT/mTOR pathways play important roles in the regulation of angiogenesis in normal and cancerous tissues as well as in endothelial cells, thus linking HIF-1 $\alpha$  with regulation of angiogenesis in endothelial cells (Karar and Maity 2011).

HIF-1 $\alpha$  expressions in hyperbaric oxygen (HBO) are regulated by a PHD-VHL independent, HSP70, or RAC1 mediated mechanisms (Catrina et al 2008). Physiological activation of HIF-1 $\alpha$  is observed during embryogenesis and in wound-healing processes. However, HIF-1 $\alpha$  activation in cancer is associated with malignancy and poor prognosis.

There are more than 100 HIF-1 downstream target genes. HIF-1 regulates the expressions of these genes by binding to a 50 base pair (*bp*) cis-acting HIF-1 response element (HRE) located in their enhancer and promoter regions (Semenza et al 1991). The table below (table 1.3) adapted from Ke and Costa (2006) outlines some relevant HIF-1 target genes. HIF-1 activity increases virtually all glycolytic enzymes and glucose transporters. Several of these intermediate if not all e.g. hexokinase and the GAPDH for instance are implicated in the four biochemical pathways leading to diabetic complications (Brownlee 2005). Consequently, HIF-1 signalling is implicated in high glucose-induced blood-retinal barrier breakdown (Yan et al 2012). In DR, hypoxia and over-expression of VEGF precipitates vessel-overgrowth and blood-retinal barrier breakdown resulting in vision loss. This posits the indirect role of HIF-1 signalling mediated VEGF accumulation in DR. Accordingly, activation of PHD2 prevented high glucose (30mM)-induced BRB breakdown in human retinal microvascular endothelial cells (HRMECs) and in retina of STZ-induced DR rats via increased PHD2-mediated HIF-1 $\alpha$  degradation and consequently, the downregulation of HIF-1 $\alpha$ -VEGF signalling pathway (Liang 2015). This aspect highlights the likelihood for a HIF-1 targeted therapy in the treatment of BRB in DR.

HIF-1 regulates erythropoiesis and iron metabolism via its regulation of the erythropoietin (EPO) gene required for the formation of blood cells and HIF-1 was first discovered by the identification of HREs in the enhancer region of EPO (Goldberg et al 1988, Semenza et al 1991). As a result, HIF-1 regulates not only vascular integrity but also vascular function since HIF-1 acts in concert with hypoxia to stimulate EPO (Semenza et al 1991).

**Table 1.3 HIF-1 target genes.** Examples of relevant target genes regulated by HIF-1 and the references (Adapted from Ke and Costa 2006)

Function	Gene abbreviations	References
<b>Angiogenesis</b>	Vascular endothelial growth factor (VEGF) Endocrine-gland-derived VEGF (EG-VEGF) Transforming growth factor- $\beta$ 3 (TGF- $\beta$ 3)	<a href="#">Levy et al 1995</a> <a href="#">LeCouter et al 2001</a> <a href="#">Scheid et al 2002</a>
<b>Vascular tone</b>	Nitric oxide synthase (NOS2) Heme oxygenase 1 Endothelin 1 (ET1)	<a href="#">Melillo et al 1995</a> <a href="#">Lee et al 1997</a> <a href="#">Hu et al 1998</a>
<b>Matrix metabolism</b>	Matrix metalloproteinases (MMPs) Plasminogen activator receptors and inhibitors (PAIs) Collagen prolyl hydroxylase	<a href="#">Ben-Yosef et al 2002</a> <a href="#">Kietzmann et al 1999</a> <a href="#">Takahashi et al 2000</a>
<b>Glucose metabolism</b>	Aldolase-A,C (ALDA,C) Enolase-1 (ENO1) Glucose transporter-1,3 (GLU1,3) Glyceraldehyde phosphate dehydrogenase (GAPDH) Hexokinase 1,2 (HK1,2) Lactate dehydrogenase-A (LDHA) Pyruvate kinase M (PKM)	<a href="#">Semenza et al 1996</a> <a href="#">Semenza et al 1996</a> <a href="#">Chen et al 2001</a> <a href="#">Graven et al 1999</a> <a href="#">Mathupala et al 2001</a> <a href="#">Semenza et al 1996</a> <a href="#">Semenza et al 1994</a>
<b>Erythropoiesis/ iron metabolism</b>	Erythropoietin (EPO)	<a href="#">Semenza et al 1991</a>

### 1.5.3.1 Vascular endothelial growth factor

The vascular endothelial growth factor (VEGF) is a diffusible endothelial cell-specific mitogen that potently stimulates angiogenesis, vasodilatation, and microvascular hyperpermeability (Hood et al 1998). VEGF is a 46 KD dimer of two identical disulphide-linked subunits (Klagsbrun and Soker 1999), with at least six isoforms produced through alternative splicing (Ferrara et al 2003). VEGF directly participates in angiogenesis by recruiting endothelial cells and endothelial progenitor cells (EPCs) into hypoxic and avascular area and stimulating endothelial proliferation (Rafii and Lyden 2003). VEGF signalling in endothelial cells is activated after VEGF binds to the receptor via activation of phospholipase C-gamma which results in increased activity PKC and entry of intracellular calcium, activation of the PI3K-dependent Akt/ protein kinase beta (PKB) and inducing MAPK via Ras/Raf stimulation.

VEGF functions to induce endothelial proliferation, differentiation, permeability, vascular tone, sprouting, migration and tube formation (Kroll and Waltenberger 1999, Ferrara et al 2003). It is also a potent survival factor for endothelial cells during physiological angiogenesis by inducing the expression of anti-apoptotic proteins including B-cell lymphoma 2 (Bcl-2) and Bcl-2 related protein (Gerber et al 1998). Hypoxia is not the only mechanism for VEGF upregulation in wound, hyperoxia as used in HBO also stimulates VEGF expression (Sheikh et al 2000). In addition, endothelial cytokine molecules such as the platelet derived growth factor (PDGF), epidermal growth factor (EGF), basic fibroblast growth factor (bFGF), and the transforming growth factors (TGF) also induce VEGF expression (Ferrara et al 2004). Moreover, VEGF and PECAM-1 are induced in response to mechanical stimulus (Fujiwara 2006, Tzima et al 2005) via VEGF receptor-2 (VEGFR-2) (Mahajan et al 2017).

Endothelial cells renewal by angiogenesis is dysfunctional in hyperglycaemia and diabetes, possibly via VEGF downregulation (Enciso et al 2003). In diabetic wounds, HIF-1 $\alpha$  stability is impaired due to hyperglycaemia with very low levels of HIF-1 activity in ulcerated diabetic foot biopsies leading to VEGF downregulation, decreased angiogenesis and impaired wound healing (Catrina et al 2004, Fadini et al 2006, and Gao et al 2006). But HIF-1 $\alpha$  stabilization reverses diabetic wound impairment possibly via HIF-1 induced VEGF upregulation (Botusan et al 2008). VEGF causes increased paracellular permeability in endothelial cells through the formation of intercellular gaps, vesico-vascular organelles, vacuoles and fenestration (Bates et al 2002). In addition, VEGF exerts potent vasodilatation effects via induction of the endothelial nitric oxide synthase (eNOS), thereby increasing NO (Kroll and Waltenberger 1999).

Over-expression of VEGF is associated with uncontrolled signalling of cytokine growth molecules such as bFGF, PDGF, TGF $\beta$  in the diabetic endothelium which drives vascular complications (Mackay 2001, Jackson et al 1997, Naldini et al 2003, Carmeliet 2000). This presents an aspect of VEGF in diabetes that is not desirable as in DR. Animal studies and observations in human patients provide convincing evidence of the role of VEGF in the development and progression of DR via several of these mechanisms involving cytokine growth factor molecules (Keck et al 1989, Hammes et al 2011, Mackay 2001, Jackson et al 1997, Naldini et al 2003, Carmeliet 2000). Accordingly, ocular anti- VEGF therapy represents one of the most significant advances in DR (Cheung et al 2014).

## 1.6 Endothelial cell models

### 1.6.1 Human dermal microvascular endothelial cells (HDMEC)

Endothelial cells (ECs) form an interface separating circulating lymph or blood in the vessel from the rest of the vessel wall. Blood and lymphatic endothelium have cell-cell contact at the capillary level, thus ECs express common lineage markers such as PECAM-1 (Podgrabinska et al 2002, Robichaux et al 2010). However, lymphatic endothelial cells (LECs) which originate from venous endothelial cells express lymphatic specific markers such as lymphatic vessel endothelial hyaluronan receptor 1 (Lyve1), prospero homeobox 1 (Prox1), high levels of Neuropilin2 (Nrp2), VEGF receptor 3 (VEGFR3) and podoplanin, whilst blood endothelial cells (BECs) express blood lineage markers such as laminin and cluster of differentiation 34 (CD34). In mouse embryonic stage (E9.0 upwards), some venous ECs in the paired cardinal vein initiate Lyve1 and SRY-Box 18 (Sox18) expression culminating subsequently in the upregulation of Prox1 within a subset of venous ECs via SRY-Box 1 (Sox1) and COUP transcription factor 2 (Coup-TFII) activity. Prox1 positive cells migrate out of the cardinal vein to form the primary lymph sacs. Upon the appearance of LECs, the expression of VEGFR3 (the main growth factor receptor on LECs) thereafter is restricted to lymphatic vessels, and prior blood vascular makers such as CD34 and laminin on these progenitors decreases (reviewed in Neufeld et al 2014).



The constitutive phenotype of endothelial cells (ECs) is unstable and their behaviour change rapidly once explanted in-vitro. As a result, there is no resting endothelial cell model that perfectly replicates typical in-vivo endothelial behaviour (Grant et al 1989). For instance, in static in-vitro culture, ECs exhibit a non-aligned polygonal cobblestone appearance which is different from their in-vivo alignment with flow in vessels (Phillips et al 1988, Malek and Izumo 1996, Chung et al 2000, Leung et al 2002, and Potter et al 2011). Structurally, lymphatic capillaries are larger than the blood capillaries; they have an irregular or collapsed lumen with no red blood cells, a discontinuous basal lamina, overlapping intercellular junctional complexes and anchoring filaments that connect the lymphatic endothelial cells to the extracellular matrix (Witte et al 2001). In addition, lymphatic vessels lack pericytes coverage and hence may not play a role in hyperglycaemia induced pericytes loss in retinal capillaries in comparison to blood endothelial cells (Fong et al 2004, Gabbay 1975 and 2004). The pro-inflammatory cytokine, IL-6 is expressed in all vascular endothelium, but lymphatic endothelium are more primed for IL-6 expression necessary for immune surveillance, antigen presentation and initiation of adaptive responses in comparison to blood endothelial cells (Witte et al 2001, Förster et al 2008, Pflücke and Sixt 2009, Girard 2012, Ataie-Kachoie et al 2016). Interleukin 6 is described as a lymphangiogenic inflammatory cytokine (McKimmie et al 2013). In-vitro observation also supports this view because the expression and effect of IL-6 in lymphatic cell lines such as the human dermal lymphatic endothelial cell (HDLECs) has been documented to be significantly higher versus blood endothelial cells (BECs) (Sato et al 2016).

Ironically, a lot of the studies in vascular biology have used the umbilical endothelial cells (HUVECs) which have provided phenomenal insights into vascular biology, but they are derived from a type of vessel that is rarely affected by common human vascular disorders including diabetes (reviewed in Cines et al 1998). In-vivo, it is likely that EC heterogeneity may contribute to adaptive processes as well as the development of disorders restricted to specific vascular beds. Therefore, cell models that are more akin to in-vivo endothelial behaviour from vessel types related to what is being studied are advantageous (Oberringer et al 2007). Endothelial cells (ECs) of different lineage differ in some aspects of their function, gene expression profiles, markers and phenotypic characteristics (Podgrabinska et al 2002, Petrova et al 2002).

Primary human dermal microvascular endothelial cells (HDMECs), which are composed of 83% human dermal lymphatic endothelial cells (HDLECs) and 17% blood lineage (BECs) endothelial cell therefore represent a model of the microvascular bed that prototypes lymphatic and blood endothelial lineage characteristics (Oberringer et al 2007). Several targets; HIF-1, VEGF and PECAM-1 (Podgrabinska et al 2002), inflammatory markers; NFκB (Hauser et al 2017), IL-6 (Sato et al 2016, Ataie-Kachoie et al 2016), nrf2 and HO-1 (Loboda et al 2016) are expressed by HDMEC. In addition, endothelial cells such as HDMEC do not inter-convert so they are a good model to understand how endothelial cells of different vascular beds respond, which may give information that is akin to that of blood and lymphatic endothelium cell-cell contact (junctions) at the capillary level (Kriehuber et al 2001, Mäkinen et al 2001, Robichaux et al 2010).

Normal wound healing represents an ideal process to study regeneration whereby there is interplay of endothelial cells, fibroblasts, epithelial cells, myocytes, immunocompetent cells and stem cells, however wound biopsies or experimentation with a diseased human eye are difficult to acquire, if not impossible since one cannot remove tissue/retina required for the healing/sight itself (reviewed in Oberringer et al 2007). Although, interactions between different cell types as obtainable with biopsies are absent with single cell model, cell cultures such as HDMECs can be used to mimic wound trauma and cellular responses (Amadeu et al 2003). Furthermore, owing to their native in-vivo location in the endothelium, ECs such as HDMEC are adapted to respond to oxygen tension and pressure. Moreover, HDMEC being of microvascular lineage may display easily some of the glucotoxicity effect since high glucose is known to be injurious to endothelial cells of microvascular beds (Brownlee et al 2005). Consequently, HDMECs are good models to study EC response to glucose concentration, oxygen and pressure levels.

## 1.6.2 Porcine retinal explants

Despite the several advantages of using single cell culture and in particular HDMECs as outlined above, single cell systems do not allow the analysis of intercellular interactions (Oberringer et al 2007). Although, human studies are useful for generating data in regards to development of DR, they are not adaptable for the elucidation of mechanistic details due to several limitations, e.g. complexity and ethical issues (Jo et al 2013, Lai and Lo 2013). Moreover, in-vivo animal studies are limited by high costs and the need for ethical approval (Jo et al 2013, Lai and Lo 2013). More so, metabolic homeostasis induced upon the initiation of systemic diabetes in *in-vivo* diabetic models can confound interpretation of results (Matteucci et al 2015, Costa and Andrade 2015). Thus, ex vivo/in-vitro study models are needed for examining endothelial response in the retina in order to further appreciate molecular mechanisms in DR (Jo et al 2013, Lai and Lo 2013).

Organotypic cultures of explanted retinal tissue preserves whole retina architecture and vessel networks (Matteucci et al 2015, Costa and Andrade 2015). Hence, a better picture of endothelial cells is gained when endothelial cells are studied in situ versus when explanted (Grant et al 1989). Therefore, explanted retinas give an added advantage for native endothelial cell examination in the context of relevant cell-cell interactions with resident cell types such as neurons and glial cells (Matteucci et al 2015, Costa and Andrade 2015). Also, because retinal vasculature is of microvascular bed, the endothelial response examined in this context gives relevant insight into endothelial characteristic or dysfunctions in retinal microvascular associated complications especially when examined in the relevant context of high glucose.

Retinal explants can be maintained in-vitro without the need for tissue slicing. Whole intact retina preserves retinal architecture and most intraretinal connections, thereby facilitating the study of generalizable biological processes as well as those that are retinal-specific (Matteucci et al 2015). However, upon sacrifice, there is separation of the ocular bulb from the main retinal blood vessels and the optic nerve resulting in a lack of circulation and innervations (Ferrer-Martin et al 2014), which leads to early demise of the photoreceptors and physiological thinning of the ganglion cell layer (GCL) (Gancharova et al 2013, Thangaraj et al 2011). The porcine retina bears close resemblance in size, basic retinal structure and vasculature to that of the human eye, with some differences noted (Sanchez et al 2011, Lai and Lo 2013). Retinal explant culture began in the mid-twentieth century with the early work by Tansley (1933), Ames and Hastings (1956), and several workers have since utilised organotypic retinal explant to examine retinal development, central nervous system regeneration, cell death and neuroprotection, electrophysiological activity, and genetic modification (reviewed in Bull et al 2011).

Mechanistic and cell-specific studies have also been carried out (Caffe et al 1989 and 2001, Rzezinski et al 2006, Gaddini et al 2009, Thangaraj et al 2011, reviewed in Matteucci et al 2015) including endothelial cell response in retinal angiogenesis (Knott et al 1999). The roles of high glucose on the retina have also been examined. Accruing results from different studies provide evidence of the susceptibility of retinal explants to extracellular high glucose in culture (He et al 2013, Matteucci 2015). In one study, a time-dependent decrease in HO-1 expression in retinal explants was seen in response to high glucose which showed that hyperglycaemia causes reduction in antioxidant capacity in a time-dependent manner (He et al 2013). In addition, retinal photoreceptors reactivity to high glucose in diabetic animals has been documented (Du et al 2013). In ns2Akitamouse model of retinal complications, photoreceptor death was found to precede amacrine and ganglion cell death (Hombrebueno et al 2014). These studies demonstrated the effects of high glucose on the retina and retinal cells but a precise time-course of high glucose induced retinal cell death/deregulation has not yet been fully characterised (Matteucci et al 2015).

Explants (vessels) are anchorage dependent (Barr-Nea and Barishak 1970, Caffe et al 1989, Discher et al 2005, Gaddini et al 2009, Kato et al 1983, Caffe et al 2001). Consequently, several methods of culture of explanted retinas have been developed in order to address this critical requirement for anchorage. Provision of substrates on which retinal tissues are placed for support have been used as well as three dimensional (3D) culture of explanted retina (Barr-Nea and Barishak 1970, Caffe et al 1989, Gaddini et al 2009, Kato et al 1983, Caffe et al 2001). Three dimensional (3D) cultures are more native to in-vivo milieu in comparison to two-dimensional (2D) cultures for many tissue and cell-types (Tibbitt and Anseth 2009).

Extra cellular matrix (ECM) proteins are molecules that present physical sites for cellular attachment and mediate key processes such as migration, proliferation, adhesion, differentiation and cell death (Tibbitt and Anseth 2009, Stendahl et al 2009). In addition, they modulate the binding and storage of growth factors, cytokines and soluble signalling molecules, thus regulating cell signalling. Moreover, they provide biomechanical interactions that are critical to cell development and differentiation (Stendahl et al 2009). Fundamentally, ECMs provide anchorage to retinal cells during development (Galli-Resta et al 2008). Simple natural hydrogel (e.g. agarose) are inert and when incorporated with ECM protein such as collagen, mimics native ECM (Lake et al 2011). Complex matrices such as matrigel with several ECM protein mixtures can confound conclusions with experiments, although matrigel has a pivotal place in some studies such as in human embryonic stem cell studies (Hughes et al 2010). Here, explanted retinas from the porcine eye were cultured within biologically compatible and inert agarose (Lake et al 2011) incorporated with collagen type I protein, as a 3D matrix and used to study endothelial cells responses in depth in the context of cellular-interactions.

## 1.7 Hyperbaric oxygen

The air we breathe contains 21% oxygen, 78% nitrogen, with the remaining 1% being contributed by the noble gases and carbon dioxide at normal sea level barometric pressure of 1 atmosphere of pressure absolute (ATA) which corresponds to 760 mm of mercury (760 mmHg). Under these conditions, the partial pressure of oxygen ( $P_{aO_2}$ ) is 100 mmHg which supplies about 0.3 ml of oxygen per 100 ml of blood including haemoglobin bound oxygen (HBOT Trust 2018). Normally, the concentration of oxygen in the air we breathe in is sufficient for normal body metabolism and repair in tissue injury or illness (HBOT Trust 2018). Owing to their position within blood vessels, endothelial cells are exposed to arterial oxygen content of 75–100 mmHg (10–14%).

Tissue oxygen (11%-1%) levels are lower in comparison to blood levels and descend to about 4% in the mitochondrion (Wangsa-Wirawan and Linsenmeier 2003, Yu et al 2001, and Carreau et al 2011). In retinal microvasculature, the oxygen level in inner segments of photoreceptors (mitochondria-rich) after dark adaptation is between 0 and 5 mmHg (0.7%) increasing up to 20 mmHg after light adaptation and reaching up to 20 mmHg in the inner retina. Hence, normal oxygen levels (normoxia) depend on the area of retina and dark/ light state (Wangsa-Wirawan and Linsenmeier 2003). Sustained local hypoxia (1.1%- 4.2% oxygen) in wound vicinity due to vascular compromise as well as hyperglycaemia-induced tissue pseudohypoxia is present in diabetes and these are associated with impaired wound healing. On the other hand, hypoxia drives vessel over-growth and uncontrolled angiogenesis which leads to vision loss in the retina (Williamson et al 1993, Catrina et al 2004). Low oxygen tension in the diabetic wound impairs collagen synthesis, epithelization, and leukocyte function which require an optimal oxygen range of 45 to 80 mm Hg (9.5% - 17%) to function (Knighton et al 1984, Naghibi et al 1987, Alien et al 1997 and Zykova et al 2000). In essence, tissue and cellular oxygen needs and oxygen availability is dependent upon tissue/cell type and how healthy the tissue/cell is.

Physiologically relevant increase in  $P_{aO_2}$  is attained at twice atmospheric pressure (2 ATA) breathing of 100% oxygen as this increases blood oxygen content to 3 ml oxygen in 100ml of blood (HBOT Trust 2018). This means the gradient of transport of free oxygen in blood into tissue increases by 10-fold (HBOT Trust 2018). Essentially oxygen dissolution increases with pressures higher than the stipulated 2 ATA. For instance, plasma oxygen concentrations of up to 1804 mmHg was achieved in with barometric pressures of 2.5 ATA with 95% oxygen ( $O_2$ ) (Hodges et al 2003). In clinical settings, hyperoxia is achieved by inhaling high levels of oxygen as in neonatal intensive care unit (Carreau et al 2011). Increased oxygen delivery to the tissue also forms the basis for hyperbaric oxygenation therapy (HBOT) for recalcitrant wound healing in diabetes and other indications (Godman et al 2010, Löndahl et al 2013, and Akgu" et al 2014).

### 1.7.1 Hyperbaric oxygen therapy

Hyperbaric oxygen therapy (HBOT) is an adjunct treatment modality involving the use of hyperbaric oxygen (HBO) which entails breathing in  $\geq 95\%$  oxygen at a pressure greater than the atmospheric pressure absolute (1 ATA) at sea level to provide sufficient tissue/plasma oxygenation (Godman et al 2010, Löndahl et al 2013, Akgu" et al 2014, HBOT Trust 2018). In the clinics, the treatment/session is administered in three phases; compression, treatment and decompression and the total duration is 60-90 mins with sessions repeated. The amount of oxygen dissolved in the plasma is directly related to the applied pressure although there are limits for treatments in human patients ( $\sim 2.0$  -2.5 ATA) depending on local prescribing guidelines (HBOT Trust 2018). The Scottish clinical protocol for HBOT entails the use of three cycles of 30 mins exposure to pressures not exceeding 3 ATA with  $\geq 95\%$  medical gas (oxygen) with 5 mins air-breathing intervals for a total of up to 2 hours per session, with repeated sessions (Ritchie et al 2008).

Compressed air has been used medically with variable success and little understanding of its mechanistic details. HBO was used clinically as early as mid-1800s. But, it was not until 1930s that it began to be safely used for the treatment of decompression illness in deep-sea divers. Clinical trials in the 1950s uncovered a number of beneficial outcomes from exposure to HBO, and HBO as a therapy in wound healing was first administered following the 'chance' discovery that coal miners poisoned with carbon monoxide healed faster when exposed to HBO. The Undersea and Hyperbaric Medical Society legislates and reviews clinical indications for HBOT through its committee on Hyperbaric Oxygen Therapy. HBO therapy is currently indicated for gas/air embolism, decompression illness and carbon monoxide poisoning. It is also used for necrotizing soft tissue infection, and non-healing wounds, clostridial myonecrosis, sports injury and autism (HBOT Trust 2018).

HBO is indicated as an adjunct treatment for chronic recalcitrant ulcers for patients with diabetes. There are several randomised clinical trials (RCTs) reporting on HBO benefit in recalcitrant ulcer healing and reduction in incidences of amputations (Doctor et al 1992, Duzgun et al 2008). A meta-analysis data associated HBO with improved healing and reduced risk of major amputations in patients with diabetic foot ulcers (DFUs) (Liu et al 2013). But the efficacy and safety profile of HBO in patients with diabetic foot ulcer has been obscured by controversy, mainly due to absence of clear mechanistic details (Zhao et al 2017). But based on the results of studies so far, this controversy has not proven true. Nine randomised clinical trials in 2017 involving 526 patients found significant increase in the incidence of healed ulcers (risk ratio [RR] = 2.22;  $P = 0.32$ ), decrease in minor amputations (RR = 0.95;  $P = 0.91$ ), decrease in major amputations (RR = 0.47;  $P = 0.14$ ), and decrease in adverse events (RR = 1.00;  $P = 0.99$ ) with HBO in comparison to standard therapy (ST) groups (Zhao et al 2017).

In addition, HBO was associated with a greater reduction in the ulcer wound area versus ST (standard mean difference = 1.12;  $P = 0.04$ ), demonstrating that HBO is a clinically meaningful adjuvant therapy for patients with diabetic foot ulcer (Zhao et al 2017). A Cochrane review found that HBO improved the rate of ulcer healing (Kranke et al 2015), which was consistent with the finding of Zhao et al 2017. There are a small number of studies that did not unravel HBO associated benefits; Kalani et al 2002, and Londahl et al 2010. As a caution, the population size for these studies were small and limiting, and larger population studies may be required to increase the statistical power and significance of these studies (Zhao et al 2017). In addition, it is also likely some patient factors such as poor glycemic control or immunological status may have contributed to the lack of response(s) in these studies. HBO is reported to decrease blood glucose levels post treatment (Karadurmus et al 2010) but it is pertinent to understand what effect(s) a patient's glycemic control might have on the outcome of HBO therapy since poor glycemic control is associated with increased endothelial dysfunction; poor wound prognosis, heightened oxidative stress and inflammatory reactivity, with increased incidence of infection in wounds. In addition, it is important to understand the likely effects of poor glycemic status on outcomes in other indications for which HBO is utilised.

HBO effect is due to the compounding effects of physiological and biochemical changes resulting from hyperoxia and mechanisms due to gas laws (Akgu"et al 2014). In converse to HBO, breathing in  $\geq 95\%$  of oxygen ( $O_2$ ) at 1 ATA (hyperoxia) or breathing atmospheric air at greater than 1 ATA (hyperbaric pressure) are not considered HBO and the current question is just how different/alike each of these components are to HBO. In-vivo, breathing in  $O_2$  at  $> 1$  ATA is associated with increased production of ROS, a collective term for  $O_2$ -derived free radicals as well as  $O_2$ -derived non-radical species such as hydrogen peroxide and hypochlorous acid (reviewed in Thom 2011). ROS and reactive nitrogen species (RNS) facilitate transduction cascades are possible molecular basis of HBO (reviewed in Thom 2011). HBO improves tissue oxygenation and many of its beneficial effects such as reduction of regional and local ischaemia can be linked to this, although there is variability in patient outcomes post HBO (Unfirer et al 2008, CADTH 2005, Fife et al 2007, and Roeckl-Wiedmann et al 2005).

In patients, HBO stimulates oxygen-dependent wound processes such as collagen synthesis, epithelization, and leukocyte mediated wound repair, release of bone marrow stem cells, and enhancement of host antimicrobial responses (Knighton et al 1984, Naghibi et al 1987, Alien et al 1997 and Zykova et al 2000, Kalani et al 2002, and Sheehan et al 2003). Increased insulin sensitivity in HBO treated patients equivalent to that observed following moderate weight loss has also been reported (Wilkinson et al 2012). However, the possible use of HBO in retinal complication is still novel owing to a theoretical risk of a possible HBO-induced retinal neovascularisation, although accruing evidence appears to suggest otherwise. HBO-associated amelioration of retinal and macular occlusion has been reported (Oguz and Sobaci 2008). In addition, exposure of diabetic animal models to HBO was associated with amelioration of blood-retinal barrier breakdown (Chang et al 2006). Furthermore central retinal artery occlusion (CRAO) in diabetic patients was reportedly enhanced following HBO (Soares et al 2017).

The role of HBO in diabetic foot ulcers is better defined in comparison to its role in DR. Chronic wounds are associated with low oxygen tensions and it is likely that HBO enhanced oxygen tension in wound tissue is a key mechanism for beneficial outcome (Doctor et al 1992, Duzgun et al 2008, Kranke et al 2015, Liu et al 2013, and Zhao et al 2017). Some of the mechanisms associated with HBO benefit in wound healing include; promotion of wound closure and increase in the number of endothelial progenitor cells (Gallagher et al 2006), increased cell proliferation (Boykin and Baylis 2007), improved insulin sensitivity at wound site (Wilkinson et al 2012), activation of cellular proliferation pathways (Niu et al 2013), enhancement of neutrophil activity and antibiotic effectiveness, fibroblast activity, collagen synthesis and angiogenesis (Akgu"et al 2014), and the stabilization of HIF-1 $\alpha$  protein (Sunkari et al 2015).



Increased stabilization of HIF-1 $\alpha$  leading to HIF-1 activation and signalling post HBO is linked with improved wound healing in diabetic mice via VEGF upregulation (Sunkari et al 2015). Furthermore, increased nrf2 activation and induction of nrf2-mediated genes including HO-1 following HBO has been reported (Godman et al 2010). In contrast, hyperoxia did not elicit a similar effect in the same samples, although hyperoxia is a known activator of the nrf2 pathway via ROS activation (Bellezza et al 2010), which may indicate that HBO and hyperoxia have different outcomes in regard to nrf2 accumulation and stabilisation. Enhanced plasma antioxidant defence is evident post HBO and may contribute to wound healing resolution. In addition, angiogenesis and normal vascular tone may be restored via increased HBO-associated increase in NO, VEGF, IL-6 and decrease in ET-1 (Sureda et al 2016).

The role of the immune response of the individual undergoing HBO is important. Immunosuppression via downregulation of pro-inflammatory cytokines such IL-6, IL-1 and TNF-alpha post HBO have been reported (Benson et al 2003, Al-Waili 2006), while increased plasma IL-6 post HBO has also been reported (Sureda et al 2016). In contrast, hyperoxia was associated with enhancement of pro-inflammatory cytokine transcription and translation (Jensen et al 1992, Johnson et al 1997, Weisz et al 1997).

Taken together, HBO continues to demonstrate positive benefit in several clinical and experimental settings. What is still needed is continued elucidation of its exact mechanism(s). An understanding of endothelial response to HBO is important in seeking to understand how HBO may mediate its effect. The lumina of all blood vessels are lined with endothelial cells (ECs), hence they play crucial roles in haemostasis, vascular tone, inflammation, and angiogenesis and they are central to the consideration of a response to HBO (Salgado et al 1994, Tjarnstrom et al 1999). EC morphology is closely associated with function and physiology and changes in EC morphology is linked with cellular events. The role of HBO on endothelial size and shape is not well studied yet, although the effects of hyperoxia on pulmonary endothelial cells and shear stress with elevated pressure have been the subject of several studies.

In-vivo ECs that populate the luminal surface of blood vessels in areas of high laminar shear stress are elongated and aligned while those in low shear stress areas are randomly orientated (Chung et al 2000, Potter et al 2011). In vivo, ECs of all origin change their shape and size (contraction and retraction) leading to cell size decrease in response to shear stress (Barbee et al 1994, Malek and Izumo 1996, Chung et al 2000). Although ECs in static culture are polygonal, they become uniformly aligned when exposed to increased flow and shear stress (Malek and Izumo 1996). Increase in intracellular calcium via tyrosine kinase activity and actin microtubule rearrangement are some of the mechanisms leading to ECs size and shape change in response to flow/mechanical stress (Malek and Izumo 1996). In-vivo, elevated pressure as relevant in HBO may not equate to increased shear stress from modified flow. However, hyperbaric conditions can increase perfusion and so this might have a knock on effect on shear stress.

The effect of hyperoxia on pulmonary EC morphology has been documented. In pulmonary vascular beds for example, and in-vitro with cultured endothelial cells, hyperoxia is associated with enlarged EC sizes and alterations in morphology. It is notable that most of the works of hyperoxia-associated endothelial cell enlargement were carried out in endothelial cells of pulmonary origin. The mechanism includes hyperoxia mediated induction of ROS and oxidative stress in cultured endothelial which mediates increased endothelial  $[Ca^{2+}]$  levels and actin cytoskeleton rearrangements. Consequently, hyperoxia induced ROS mediated actin rearrangement causes EC size enlargement (Bowden and Adamson 1974, Crapo et al 1980, Phillips et al 1988, Brueckl et al 2006, Roan et al 2012, and Attaye et al 2017). In the alveolar, hyperoxia is associated with increased ROS production leading to activated alveolar capillary endothelium which is characterised by increased adhesiveness causing accumulation of neutrophils. In addition, increased levels of ROS are linked with increased vascular permeability, coagulation, and collagen deposition and irreversible changes occurring within the alveolar space. Hyperoxia-associated vasoconstrictive effect on vascular endothelium is reported. In renal and mesenteric microvascular beds, hyperoxia is associated with decrease in EC size as a result of hyperoxia mediated decrease in endothelial nitric oxide (NO) and increased vasoconstrictors such as cyclooxygenase (Attaye et al 2017). Hyperoxia-induced vasoconstriction in human retina is reported to occur via hyperoxia-induced ET-1 upregulation (Dallinger et al 2000). Moreover, hyperoxia has been associated with cerebral vasoconstriction (Floyd et al 2003).

Increased EC paracellular permeability and breakdown of the blood-retinal barrier in DR are some of the in-vivo effects of high glucose toxicity on endothelial cells (Gillies et al 1997). Diabetic mouse models such as db/db mice showed altered endothelial cell morphology as a result of sustained exposure to high glucose (> 30 mM) (Peng et al 2016). This observation has also been documented in cultured endothelial cells, where high glucose was associated with whole EC phenotypic change in a glucose dependent mechanism involving PKC $\alpha$  activation (Hempel et al 1997).

The endothelium releases ROS and vasoactive molecules such as Ang II and ET-1 in response to mechanical stimuli (shear stress/stretch) (De Keulenaer et al 1998, Schramm et al 2012). Permeability factors such as the endothelium derived contracting factors such as ET-1 and Ang II and inflammatory cytokines induce endothelial size change (contraction and retraction, also termed 'rounding'), and this phenotype of rounding in cultured HUVEC cells was associated with increased endothelial junction permeability which enhanced trans-endothelial passage (Sandoval et al 2001, Leung et al 2002).

The effects of HBO or its single components on EC metabolic activity appear to be divergent. A dose-dependent hyperoxia mediated decrease in cell viability and proliferation was documented in human dermal microvascular endothelial cell (HMVEC) (Attaye et al 2017). Similarly, a hyperoxia associated decline in liver sinusoidal endothelial cells (LSECs) metabolic activity in comparison to normoxia is documented (Martinez et al 2008). HBO on the other hand was associated with a protective and stimulatory effect on metabolic activity using immortalized human microvascular endothelial cell Line-1 (HMEC-1) after challenge with HBO and an organic peroxide, *t*-butyl hydroperoxide (*t*-butyl OOH) (Godman et al 2010). The role(s) of hyperbaric pressure on endothelial cell metabolic activity is unclear and there have not been many reported studies on its role.

## 1.7.2 Limitations of HBOT

At present there is no consistent clinical protocol for using HBO as a therapy (HBOT), with pressure and oxygen dose(s) and duration being largely variable (Ritchie et al 2008). Thus, many of the reported side effects of HBO, some of which are life threatening are often dose-related. Pulmonary complications such as pulmonary embolism and pneumothorax although rare (1:50,000-60,000) are the most severe potential side effect of HBO treatment (Löndahl et al 2013). In addition, oxygen toxicity such as seizures which are self-limiting with an end-treatment resolution has been reported albeit rare, with an incidence of 1 in every 10,000 treatment cases (Löndahl et al 2013). Reversible myopia and cataract are more common (Löndahl et al 2013) and HBOT poses a risk for hypoglycaemic episodes for patient managed on insulin (Löndahl et al 2013). Incidentally increased insulin sensitivity following HBO exposure is reported (Wilkinson et al 2012). Due to the highly pressurized environment, there is a risk of severe middle ear trauma which can lead to a non-reversible loss in hearing in patient. Environmental hazards such as fire in the chamber are a potential risk with the presence of high oxygen levels in the pressurised environment and should be minimized by strict adherence to protocols. These complexities justify the need for more research to understand the pivotal mechanisms in HBO, in order to develop a more evidence-based practice especially for application in newer indications.

## 1.8 Proposed study mechanism

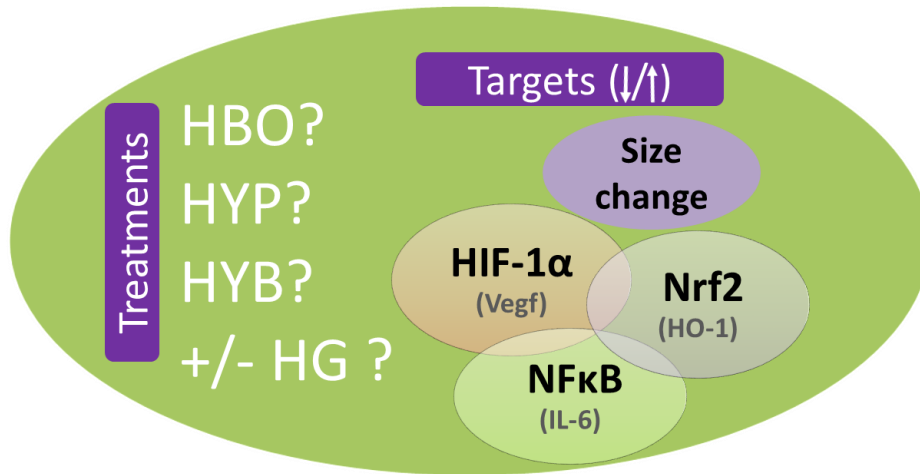


**Figure 1.8 Proposed study mechanism(s)**

This schematic diagram illustrates key concepts in this study. The effects of changing glucose concentration, oxygen tension, pressure levels (i.e. treatments) on HDMECs targets; size change, and effects on transcription factors (decrease or increase) responsible for redox (Nrf2), inflammatory (NFκB) and oxygen-sensing response (HIF1-α) are examined. In addition, targets of these pathways; IL-6 (at mRNA level) (NFκB), HO-1 (Nrf2), and VEGF (HIF-1α) are studied and the expression of a specific endothelial cell marker, PECAM-1 is utilised for identifying endothelial specific response(s). Treatments administered; HBO = hyperbaric oxygen, HYP = hyperoxia, HYB = hyperbaric pressure or controls with or without (+/-) HG = high glucose.

## 1.9 Aim and objectives of the study

This study aims to investigate the mechanisms of hyperbaric oxygen therapy in endothelial cells by examining endothelial cell responses to-inflammation, redox and HIF-1 $\alpha$  signalling using a primary human dermal microvascular endothelial cells and a developed and validated porcine retinal explant cultured in three-dimensional matrices in the context of high glucose to simulate endothelial response to normal and disease context (diabetes) in HBO. The second overarching aim is to decipher what each component of HBO does in relation to pro-inflammation, redox response and HIF-1 signalling, in order to understand the mechanism(s) of HBOT more.

## 1.10 Objectives of the study

1. Develop and validate a retinal explant model of explanted retina from porcine cultured in an agarose-collagen bilayer three-dimensional matrix.
2. Validate a developed HBO unit modelled after a clinical HBO therapy
3. Determine the effect(s) of hyperbaric oxygen (HBO), hyperoxia (HYP), and hyperbaric pressure (HYB) or control condition (controls) in basal glucose or in combination with high glucose (HG) on three mechanistic pathways of pro-inflammation (Nuclear Factor kappa B; (NF $\kappa$ B)), redox (nuclear factor type-2 (Nrf2)), and oxygen signalling (hypoxia inducible factor type 1 (HIF-1)) using human dermal microvascular endothelial cells (HDMEC) and retinal endothelial cells.

## Chapter 2.0: Materials and methods

## 2.0 Materials and methods

### 2.1 Materials

Primary human dermal microvascular endothelial cells (HDMEC), and reagents required for the maintenance and propagation of the cells were purchased from PromoCell (PromoCell, UK). Quality control tests were carried out by PromoCell prior to supply. Proprietary endothelial growth media MV (5.5 mM D-glucose) was used for HDMEC propagation and is outlined in detail in section 2.2. For high glucose treatment, HDMEC were exposed to 20 mM of D-glucose by supplementation of growth media (5.5 mM glucose) with 14.5 mM D-glucose to give a final concentration of 20 mM D-glucose. Retinal tissues used in explant culture were derived from porcine ocular globes kindly donated by a local abattoir from animals aged between 18-28 weeks weighing 70-80kg of both sex. Ocular globes ( $N \geq 10$ ) were transported on ice and were received in the lab for dissection within 1-2 hour of kill. All experiments were performed in accordance with UK legislation. Dulbecco's modified eagle media (DMEM); 5.5 mM (low) or 25mM (high) D-glucose (ThermoFisher Scientific) was used for explant culture. Detailed methods used and the development of this model are outlined in section 2.3. Chemicals and reagents were purchased from a number of different companies and specific reference to each company is made the first time that chemical/reagent is used.

### 2.2 Maintenance and propagation of HDMEC

Cryopreserved proliferating primary HDMEC from an adult donor at Passage two (P2) containing  $\geq 500,000$  viable cells in Cryo-SFM serum-free freezing medium transported on dry ice and subsequently stored in liquid nitrogen tanks were obtained from PromoCell. Cells were aseptically thawed at 37°C in a water bath, and transferred to a 25cm<sup>2</sup> (T25) culture flask (Nunc) with 10 ml of pre-warmed proprietary (PromoCell) HDMEC growth media composed of: 0.05 ml/ ml foetal calf serum, 0.004 ml/ ml endothelial cell growth supplement, 10 ng/ ml recombinant human epidermal growth factor, 90 µg/ ml heparin and 1 µg/ ml hydrocortisone. Cells were incubated overnight in a standard 5% CO<sub>2</sub> incubator (Hera Cell 150, HeraCeus) for cell attachment.



Media was replaced after 16 hours and every two days thereafter. Cells were sub-cultured once they reached confluence (see Fig. 2.1) according to protocol (PromoCell). Cells were routinely expanded in T75 flasks (75cm<sup>2</sup>) for sub-culturing or in 24-well plate (1.9cm<sup>2</sup>) (Nunc) for treatment at a cell density of 10,000-20,000 cells/cm<sup>2</sup> as recommended (PromoCell) in pre-warmed growth media supplemented with 1% Penstrep (10, 000 U/MI) (Life Technologies). All live cell-related work was aseptically performed in class II laminar flow cell culture cabinet (Aura 2000, HeraCeus). Routinely, cells were propagated in HDMEC growth media MV which contains low (5.5mM) of D-glucose which is physiological glucose level in-vivo.

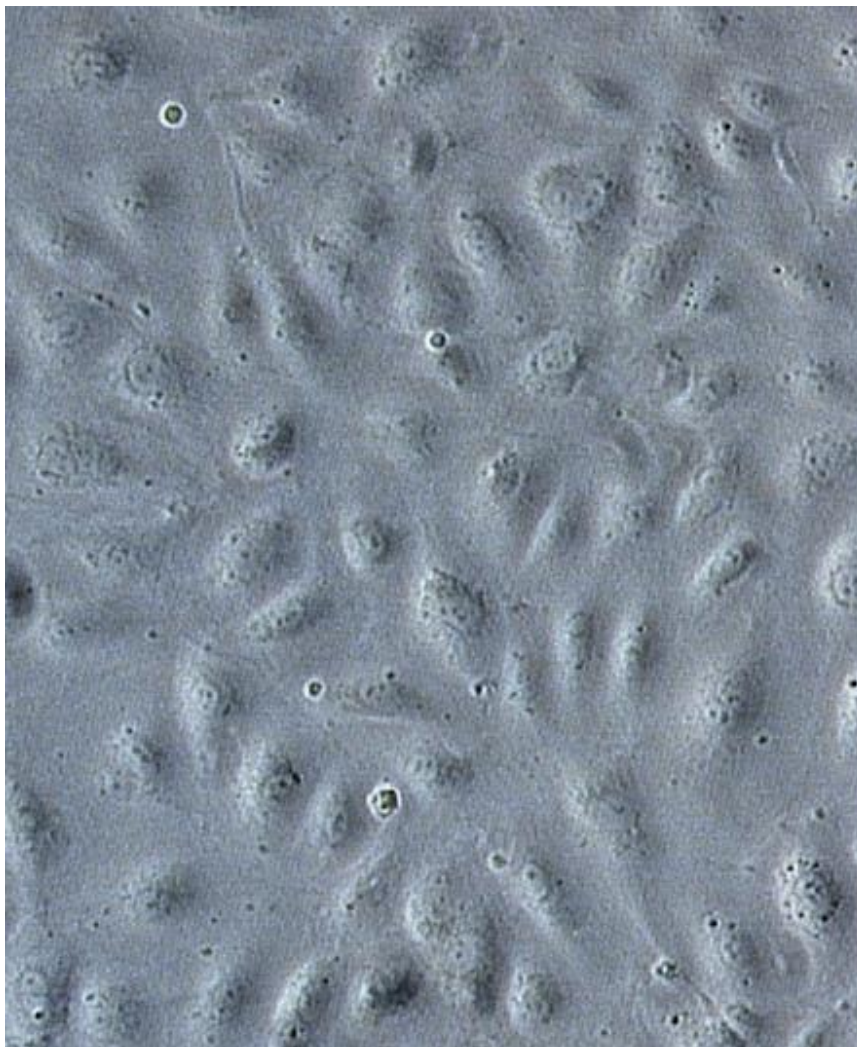


**Figure 2. 1 Morphology of human dermal microvascular endothelial cells (HDMEC)**

Selected micrograph shows HDMEC monolayer at passage 5 at 80-90% confluence. HDMEC are characterised by the cobble stone appearance. Image was taken at magnification of 10X and scale bar represents 500  $\mu$ m

HDMEC were sub-cultivated using proprietary Detach kit (PromoCell): Hepes BSS, 0.025% Trypsin/0.01% EDTA solution and Trypsin Neutralization solution (0.05% trypsin inhibitor/0.1% BSA) as recommended. Trypsinization kit was equilibrated to room temperature prior to use. Spent HDMEC growth media composed of: 0.05 ml/ ml fetal calf serum, 0.004 ml/ ml endothelial cell growth supplement, 10 ng/ ml recombinant human epidermal growth factor, 90 µg/ ml heparin and 1 µg/ ml hydrocortisone was discarded and HDMEC monolayer rinsed gently with 100 µl Hepes BSS solution per cm<sup>2</sup> of culture flask surface, and aspirated. HDMEC monolayer were incubated with 100 µl Trypsin/EDTA solution per cm<sup>2</sup> of culture flask for no longer than 10 minutes at room temperature, and examined under a light microscope (Leica DMIL) for cell detachment. Remaining adherent cells were dislodged by gently tapping the sides of the culture plate.

Trypsinization was halted with 100µl per cm<sup>2</sup> of vessel surface of Trypsin Neutralization solution. Cell suspensions were pelleted at 220 xg (Biofuge Primo R, HeraCeus) for 4 mins and supernatant discarded. Cell pellet was re-suspended in an appropriate volume of pre-warmed growth media. HDMEC were counted (see next paragraph) and seeded in 75cm<sup>2</sup> (T75) flasks or in 24-well plates and incubated in a humidified 5% CO<sub>2</sub> incubator at 37°C. Cell counts were carried out to ensure accurate cell concentration seeding at sub cultivation and cryopreservation. HDMEC suspension in Eppendorf tubes were mixed and 20µl of cell suspension pipetted unto a Haemocytometer (Neubauer, Germany) filling the chamber completely by means of capillary action. Cells were counted under a light microscope with a 100x (10x ocular and 10x objective) magnification. Four sets of 16 squares in a Haemocytometer were counted with a handy tally counter applying the same system of count to all the 4 sets of count. The average of the total of the 4 sets of counts was taken and cell count was determined with the equation below (Equation2.1):

$$\begin{aligned} & \textbf{Total cell count} \\ &= \textbf{Average cell count} \times \textbf{dilution factor} \times 10^4 - - \\ & - \textbf{Equation 2.1} \end{aligned}$$

The factor  $10^4$  is a conversion factor reflecting the volume of the cell suspension present in one set of squares ( $1\text{mm}^2$  area) of the haemocytometer and is used to convert  $10^{-4}$  ml to 1ml. Volume of one large square =  $1\text{mm} \times 0.1\text{mm} = 0.1\text{cm} \times 0.1\text{cm} \times 0.1\text{cm} = 10^{-4}\text{cm}^3 = 10^{-4}\text{ml}$ . Trypan blue exclusion criteria was used to estimate cell viability. Cell suspension was mixed thorough by gentle pipetting with 0.4% v/v trypan blue dye at a 1:1 ratio and left to stand for no longer than 2mins to allow the dye to penetrate non-viable cells. Non-viable cells retain the blue dye which permeates damaged cell membrane, whilst intact membranes in only viable cells will prevent passive diffusion of dye. Haemocytometer (Neubaur, Germany) was filled with cell /trypan blue suspension by placing approximately 20ul of suspension near the edge of glass cover slip over the chamber and allowed to fill the chamber by means of capillary action. Cells were observed under the microscope with a 100x magnification (10x ocular and a 10x objective lens). Non-viable cells (which stained blue) were counted using the same systems as the live cell count and percentage (%) cell viability was calculated with the equation below (Equation2.2):

$$\text{Cell viability (\%)} = \frac{\text{Total cell count}}{\text{Total dead cells (stained)}} \times 100$$

— — — **Equation 2. 2.**

Routinely cells were > 95% viable. For cryopreservation, cells in suspension obtained after trypsinization were pelleted by centrifugation at 220 x g for 3 minutes, and the supernatant was discarded. Cell pellets were re-suspended in appropriate volume of proprietary cryopreservation medium, Cryo-SFM (PromoCell) at a concentration of 0.1 – 1 million cells/ml. Cell suspension was transferred to sterile Cryogenic-vials (Nunc, ThermoFisher) and frozen down gradually (-1°C/minute) in isopentane kept in a -80°C freezer overnight and subsequently stored long-term in liquid nitrogen tanks.

HDMEC at passages P4-7 were seeded in six-well replicates (sixplicates) per sample in 24 well plates at cell concentrations of 35,000-38,000/well in normal HDMEC growth media MV for western blot and PCR assays, and for immunocytochemistry (ICC) in duplicates. Cells reached 70% confluence after 48 hours. Live cell photomicrographs of HDMEC prior to treatment were acquired at 200X for baseline size determination prior to treatment. For Resazurin assay, HDMEC were plated at a density of  $6 \times 10^3$  cells/per well in clear 96-well plates in sixplicates reaching 70% confluence after 48 hours. Post treatments, HDMEC were imaged and live micrographs documented. For western blot and PCR assays, six identical wells from a 24-well plate were pooled per sample.

For ICC, HDMEC in duplicates were stained with the relevant antibody per sample. HDMEC were exposed to high glucose by supplementing normal HDMEC growth media (containing 5.5 mM D-glucose) with 14.5 mM D-glucose to give a final concentration of 20 mM glucose (Botusan et al 2008, Gadad et al 2013). One molar (1M) stock solutions of D-glucose (Sigma-Aldrich) were made up in HDMEC growth media and sterile filtered with 0.45microns syringe filter (Millipore) and stored at 4°C until use. Throughout the body of text, wherever reference is made to low (5.5 mM) glucose with HDMEC, physiological glucose level is implied.

## 2.3 Retinal explants

Three dimension (3D) matrices were prepared using equal volumes of melted 1% agarose (BIOLINE) and collagen (0.5mg/ml) (Gibco, Life Technology) in low glucose (5.5 mM) Dulbecco's modified essential medium (DMEM) (ThermoFisher Scientific) were mixed at room temperature (RT) to give 0.5% agarose-collagen (0.25 mg /ml) (AC) co-gel scaffold (matrix) solution subsequently referred to as the matrix solution. A volume of 1.8ml of matrix solution was added per well of a 6-well plate, allowed to cool and solidify, forming the 'bed-matrix'. Bed matrices were prepared on the day of experiments approximately 120 minutes before use and were kept in an incubator at 37°C (5% CO<sub>2</sub>, 95% air) until use. Matrix solution for high glucose treated explants was made using high glucose (4.5 g/L i.e. 25 mM) DMEM media. Ocular globes were aseptically cleaned of the muscle and fat tissue around the eye ball, sterilised in 70% ethanol and rinsed in ice-cold 0.1M phosphate buffered saline (PBS). Retinal tissues were extracted from ocular globes as described by Rzezinski et al (2005) and Johnson and Martin (2008).

Each globe was cut circumferentially at the Ora Serrata (corneo-scleral junction) with the tip of a sharp micro scissor, opening the retina into two halves. The anterior chamber made up of the cornea, lens and vitreous were removed and discarded. The posterior half with the retina attached to the optic nerve was briefly rinsed with sterile PBS to moisten and assist the removal of retinal tissues from the retinal epithelial layer (RPE). PBS was removed and the retina was gently scraped off the RPE, but left attached at the optic disc. A cut was made from the equator to the optic disc, without severing the retina. The optic nerve was pinched with forceps and held over the matrix bed. A sharp scissor was used to cut whole retina loose from the base of the optic disc (optic nerve head), and the retinal tissue was laid flat on the bed matrix. Retinal tissues were overlaid with cooled matrix solution at 37°C and allowed to solidify in a 5% CO<sub>2</sub> 37°C incubator forming a sandwich (henceforth referred to as explants) (fig 2.2 below). In this orientation, the inner and outer retina is in immediate contact with the biomechanical support of the matrices. Explants in duplicates were overlaid with pre-warmed serum-free media low (1g/L) (5.5 mM) glucose or high (4.5g/L) (25 mM) glucose DMEM media. Explants were incubated briefly at 37°C in 5% CO<sub>2</sub> for approximately 30 minutes and exposed to treatment as specified in the relevant experiments.

Post treatment, samples (HDMEC/explants) were maintained in their respective media and were harvested for post-culture assays at 2 h (retinal explants) or 4 h (HDMEC) and 24 h (retinal explants and HDMEC). Throughout the body of text, wherever reference is made to low (5.5 mM) glucose with explants, physiological glucose level is implied.

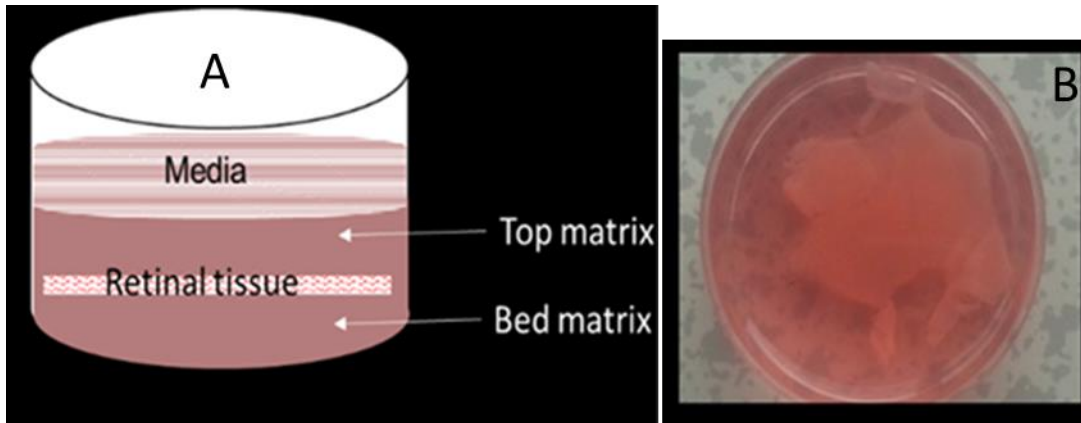


**Figure 2. 2 Three-dimension matrix formation**

A schematic diagram of retinal explant model (A), showing retinal tissue sandwiched in bilayer of a matrix composed of bed and top matrices, and overlaid with media. Full matrix depth as measured with a meter ruler is ~ 7mm. Equal amounts of scaffold solution (0.5% agarose-collagen (0.25mg/ml) (AC) co-gel was used to make both bed and top matrices, hence each matrix is ~ 3.5 mm. B) Overhead micrograph of explant showing retinal tissue sandwiched between layers of agarose-collagen bi-layer matrices.

### 2.3.1 Methods used to validate retinal explant model

The sections in 2.3.2 to 2.3.6 are the methods and initial experiments carried out on retinal explants for model validation. The results of these validations are reported in chapter 3.0 (validation of experimental model) in section 3.3.1. In order to determine the viability of the retinal vessels and the integrity of retinal tissues during culture (0 – 24 h), these confirmatory assessments listed below were performed. This included:

- a) Determination of the level of oxygen (%) within the matrices at 4 mm depth as an estimation for oxygen concentration available to retinal tissues at approximately 4mm depth.
- b) Microscopic observation of explants (tissues and vessels)
- c) Measurement of response of explant vessel to a depolarising agent (potassium chloride, KCl) and a receptor agonist (angiotensin II, Ang II). Viability was also examined by the incorporation of collagen I from matrix within retinal layers.
- d) Determination of explant structural integrity using haematoxylin and eosin (H and E) staining.

## 2.3.2 Measurement of matrix oxygen level

A Microx TX3 micro (140  $\mu\text{m}$ ) fibre optic oxygen (PSt1) meter (PreSens) was used to measure oxygen level (%  $\text{O}_2$  saturation) at 4 mm depth of the matrix at 0.5 h and 24 h. At this depth, the oxygen electrode was beyond 3.5 mm depth, where the retinal tissue was laid but the electrode was not placed directly on the tissue. Measurements were taken by holding the electrode static with the electrode inserted into the media for 30s for baseline %  $\text{O}_2$  level (controls). The electrode was lowered to 4 mm depth with a micromanipulator and measurements taken for 30 s. Because the electrode fibre optic fine-tip was easily damaged, only one-time readings were taken as attempts to re-insert the electrode to obtain replicates resulted in electrode damage. Measurements were carried out on six independent occasions ( $n = 6$ ).


## 2.3.3 Measurement of a contractile response

Functional viability of explant vessel was ascertained with contractile response to 80mM of potassium chloride (KCl) and 0.5 $\mu\text{M}$  of angiotensin II (Ang II) (Ishizaki et al 2009, Kawamura et al 2004) as recommended. Phosphate buffered saline (PBS) was used as control. Sequential application of treatment (PBS/KCl, or PBS/Ang II) on selected vessel was performed in order to reduce variability. A 7 mins lag was allowed after each treatment (PBS/KCl/Ang II) to allow adequate permeation of the treatments through the matrix to the explant vessels. KCl and Ang II treatment were carried out separately with PBS used as control. Once a treatment (e.g. PBS) was completed, equivalent volume of the treatment added in was removed and replaced with fresh media containing the next treatment (e.g. KCl or Ang II). This ensured minimal disturbance to the video capture. Hence contractile responses may also reflect residual effect from a previous treatment. Contractile responses were captured with video recording with a light microscope (Leica DM4000B) and an integrated camera (Leica DFC300-FX).

A total of 24 vessels were tested with KCl ( $n = 8$ ) and Ang II ( $n = 16$ ) at 0.5 h and 24 h post culture on  $n = 8$  independent occasions. Video recordings of contractile responses were stored and analysed with Image J software (<https://imagej.nih.gov/ij/>). A straight line tool was placed on a selected vessel as shown in fig 2.3 below to measure the vessel diameter which was used to generate plot profile/histogram/bar chart. In addition, from the straight line measurement of the vessel diameter, Image J calculates the mean grayscale and pixels across the selected area. Mean grayscale and pixel values were converted into microns ( $\mu\text{m}$ ) to derive vessel dimension before and after control or treatments using a global scale of 0.44 pixels/microns. Actual vessel dimension was obtained by dividing the values in microns ( $\mu\text{m}$ ) with the objective magnification at which the contractile response recording was taken. Selected exemplary plot profiles and summary bar chart of contractile responses are presented in the result section.

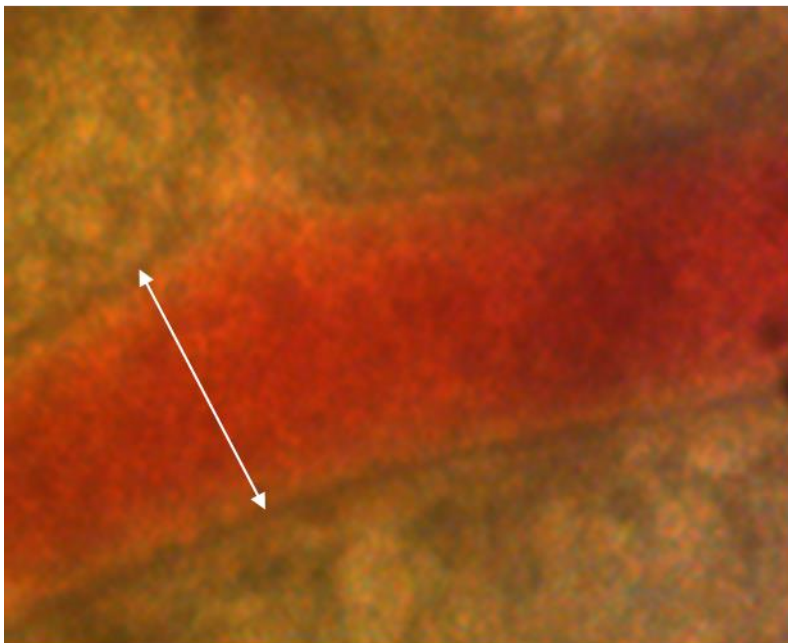


### Figure 2. 3 Measurement of contractile response

Image J straight-line tool was laid across a selected vessel with the line spanning adjacent ends as shown in the diagram. Mean grayscale and pixel values for the line measured is converted into microns ( $\mu\text{m}$ ) with a global scale (0.44 pixels = 1 microns) and actual vessel diameter obtained by dividing value in microns with the objective lens magnification (100X). Scale bar 500 $\mu\text{m}$  



### 2.3.4. Explant harvest

Explants in 6-well plates were gently washed within the wells with PBS three times (3X) for 5 minutes on gentle rotation. A total of 5ml of 10% neutral buffered formalin (NBF) was added per well and incubated overnight at 4°C. Holes were made through the matrix bilayer without disrupting the retinal tissue to facilitate penetration of the fixative. Explants were washed 3X in PBS and the matrices dismantled. Retinal tissues were embedded with optimal cutting temperature (OCT) medium (Tissue-Tek). Retinal tissues were cryosectioned into 20µm thick sections on Superfrost Plus and Colourfrost slides (Thermo Scientific) and stored in -20°C until use. Series of optimisations were carried out to achieve optimal harvest of retinal tissues from explants, cutting temperatures and section sizes.

### 2.3.5 Haematoxylin and Eosin staining

Sections were air-dried prior to use. Serial sections (20 µm) were stained with 0.1% Mayer haematoxylin (Sigma-Aldrich) for 10 mins, rinsed for 5mins in distilled water (ddH<sub>2</sub>O) and dipped briefly in 0.5% Eosin (Sigma-Aldrich). Samples were mounted with Histomount (National Diagnostics) and retinal morphology was visualised with an inverted light microscope with an attached camera (Leica DM4000B/DFC300-FX) at 200X magnification. Three different fields of view (micrographs) per section were obtained and experiments were repeated on more than nine independent experiments.

### 2.3.6 Gomori Trichrome stain for Collagen

Serial sections (20 µm) were briefly air-dried and incubated for 1 hour at 56°C in Bouin's fixative (5%/9%/0.9% acetic acid/formaldehyde/picric acid) (Sigma Aldrich) in an oven. Modified Gomori trichrome stain was made in-house with the recipe; 0.6% Chromotrope 2R/ 0.3% Fast green FCF/ 0.8% phosphotungstic acid with glacial acetic acid (National Diagnostics) in distilled water according to protocol (Gomori 1950). Specimens were washed thoroughly to remove the yellow Bouin's stain and incubated with Modified Gomori (Green) trichrome solution for 20 mins as a contrasting stain to identify collagen; cytoplasm (red), fibrin (pink), collagen (green), and erythrocytes (red) (Garvey et al 1996). Specimens were rinsed and the stain differentiated in 0.5% acetic acid for 2 mins. Slides were mounted with Histomount (National Diagnostics) and visualized with a light microscope with an attached camera (Leica DM4000B/DFC300-FX) at 200X magnification. Three fields (micrographs) per section was captured and experiments were repeated on more than nine independent occasions.

## 2.4. Immunohistochemistry and immunocytochemistry

A standard protocol for immunohistochemistry (IHC) (Abcam) was utilized to examine the expression of targets; hypoxia inducible factor (HIF) 1 alpha ( $\alpha$ ) and platelet endothelial cell adhesion molecule, PECAM-1) also referred to as cluster of differentiation (CD31). Serial sections (20  $\mu$ m) were air-dried and specimens blocked with 10% normal serum (Goat) with 1% bovine serum albumin (BSA) (Santa Cruz) in Tris buffered saline (TBS) for 2 h at room temperature (RT). Specimens were incubated overnight at 4°C with mouse monoclonal primary antibodies supplied after validation by the manufacturers (see Table 2.1 for full list of antibodies and manufacturers/suppliers). Manufacturer's product codes are included in table 2.1 which can be used to obtain specific information on the antibodies. Specimens were washed gently three times (3X) for 5mins in TBST.

Non-specific endogenous peroxidase was blocked with 0.3%  $H_2O_2$  in TBS for 15 mins at RT. Primary antibodies were detected with fluorescently labelled DyLight 488 Goat directed against the heavy (H) and light (L) chains of mouse immunoglobulin (anti-mouse IgG (H+L)) Highly cross adsorbed secondary antibody (1:200) (ThermoFisher Scientific) incubated for 1 h in RT. Specimens were washed 3X with TBS and counterstained with 1  $\mu$ g/ml of 4',6-diamidino-2-phenylindole (DAPI) for 15 mins at RT. Slides were mounted with water soluble Histomount (Vector Labs) and visualized with an inverted fluorescent microscope (Leica DMIL) at 200X magnification and documented. Three fields (micrographs) per target were captured and experiments were repeated on more than 15 independent occasions. Target antigen on cell/tissue was labelled with an unconjugated specific mouse monoclonal primary antibody and Green fluorophore conjugated DyLight 488-Conjugated goat anti-mouse secondary antibody directed against the primary antibody was used for detection.

Immunocytochemistry (ICC) (immunofluorescence, IF) staining of human dermal microvascular endothelial cells (HDMEC) was carried out as recommended (ThermoFisher Scientific) to study the expression of targets; HIF-1 $\alpha$ , vascular endothelial growth factor (VEGF), nuclear factor erythroid 2-related factor 2 (nrf2), and PECAM-1. HDMEC were fixed with 100% methanol for 5 mins at RT and washed briefly with PBS. Cells were permeabilized and non-specific interaction blocked with an in-house one-step permeabilization/blocking solution according to recipe; 1% BSA (Santa Cruz) /10% normal goat serum (Invitrogen) /0.3M glycine (Sigma-Aldrich) in 0.1% PBS (Sigma Aldrich) /0.1% Tween-20 (Bio-Rad). Blocking solution was removed and wells blotted dry.

Cells were incubated with primary antibodies overnight at 4°C as outlined in table 2.1. Cells were washed 2X with PBS and incubated with Goat anti-mouse IgG, DyLight 488 conjugated highly cross-adsorbed secondary antibody (1:500) in the dark for 60 mins at RT, washed and counterstained with 4', 6-diamidino-2-phenylindole (DAPI) (1:1000; Invitrogen, ThermoFisher Scientific, UK) for 15 mins (Fig. 2.3). Samples were washed twice in PBS. The last wash was left in the wells and cells were imaged using Leica DMIL microscope with an integrated camera (Leica DC200) at 400X magnification. Series of optimization were carried out to ascertain primary and secondary antibody dilutions and incubation prior to experimental studies. PECAM-1/CD31 expression was studied in both IHC and ICC. To avoid confusion, the name PECAM-1 is used in all instances. All IHC and ICC assays with samples set up in duplicates were repeated at least 3 times ( $n \geq 3$ ). For imaging, at least three fields of views were taken per well per target.

## 2.5. Immunoblotting (Western blot)

Six identical wells of human dermal microvascular endothelial cells (HDMEC) in 24-well plates were pooled per sample. Total cell and sub-cellular lysates were prepared. HDMEC were lysed in Radio immunoprecipitation buffer (RIPA) (Cell signalling Technology) as recommended. RIPA buffer was supplemented with 1mM phenylmethylsulfonyl fluoride (PMSF) (Sigma-Aldrich) prior to use. Adherent HDMEC were rinsed with ice-cold PBS scraped off the culture plate dish using a cold plastic cell scraper with a lysis buffer, radio-immunoprecipitation assay (RIPA) buffer into pre-cooled micro-centrifuge tubes. Lysates were sheared on ice for 3s at a power setting of 2-continuous and maintained on constant agitation for 30 min at 4°C. Cells were pelleted for 20 min at 16,000 x g at 4°C, the supernatant was carefully removed and placed in a fresh tube on ice and stored long-term at -20°C. Sub-cellular lysates were prepared with fractionation buffers using differential centrifugation according to protocol (Abcam).

Fractionation buffer was prepared in-house: 20mM (4-(2-hydroxyethyl)-1-piperazineethanesulfonic acid) (Hepes, pH 7.4) (Sigma-Aldrich), 10mM Potassium chloride (KCl) (Sigma-Aldrich), 2mM Magnesium chloride ( $MgCl_2$ ) (Sigma-Aldrich), 1mM Ethylenediaminetetraacetic acid (EDTA) (Sigma-Aldrich) and 1mM Ethylene glycol-bis ( $\beta$ -aminoethyl ether (EGTA) (Sigma-Aldrich), nuclear fraction; Tris buffered saline (TBS) in 0.1% sodium dodecyl sulphate (SDS) (Sigma-Aldrich). Prior to use, buffer was supplemented with 1mM Dithiothreitol (DTT) (Sigma-Aldrich) and 1X Protease inhibitor (PI iii) (Sigma-Aldrich).

HDMEC were scraped from plates with appropriate volumes of buffer into Eppendorf tubes. The cell suspensions were passed through a 1 ML 27 gauge needle until cells were lysed ( $\geq 10$  times). Lysates were incubated on ice for 20 minutes and were centrifuged at 720 xg (MultiFuge1, HeraCeus) for 5 mins. Supernatant and pellets were separated and stored on ice. The supernatant containing all cellular components (cytosolic) minus the nuclei (pellet) was briefly agitated (3 seconds on ice at a power setting of 2-continuous) and stored at  $-20^{\circ}\text{C}$  until use. The pellets containing the nuclei were washed in appropriate volume of fractionation buffer, dispersed with a pipette and passed through a 25 gauge needle 10 times. The suspension was centrifuged at 720 xg for 10 minutes, the supernatant discarded and the pellet containing the nuclei was re-suspended in TBS with 0.1% SDS and sonicated briefly to shear genomic DNA and homogenize the lysates (3 s on ice at a power setting of 2-continuous). All lysates were incubated on ice prior to storage and were stored long-term at  $-20^{\circ}\text{C}$  until use.

Bicinchoninic acid assay (BCA) kit was used to determine sample protein concentration according to protocol (Sigma-Aldrich). Stock (2 mg/ml) BSA protein standards were serially diluted with de-ionised MiliQ water; 0 (blank), 200, 400, 600, 800 and 1000  $\mu\text{g} / \text{ml}$  in duplicates in clear 96-well plate on ice. BCA working reagent (WR) was prepared by mixing 50 parts of BCA Reagent A with 1 part BCA Reagent B (50:1, Reagent A: B). Protein standards were mixed with BCA working reagent at a ratio of 1:8, i.e. 25  $\mu\text{l}$  of protein standard was mixed with 200  $\mu\text{l}$  of working reagent in clear 96-well plate, covered and mixed, and incubated for 30 minutes at  $37^{\circ}\text{C}$ . Optical density was read at 562nm with Synergy HT (Biotek) microplate reader spectrophotometer (Gen 5 vs 2.04).

Standard curve of net absorbance versus protein concentration was plotted and a line of best-fit drawn through the points (Fig. 2.4) and equation of relationship between absorbance (nm) and protein concentration ( $\mu\text{g}/\text{ml}$ ) derived (Equation 2.3). To quantify the protein concentration of the unknowns, samples were diluted with appropriate volumes of MiliQ water on ice. Samples in duplicates were incubated with BCA working reagent (50:1, Reagent A: B) at a ratio of 1:8 (according to manufacturer's instruction) in clear 96-well plate and mixed. The plate was incubated for 30 minutes at  $37^{\circ}\text{C}$ . Optical density was read and sample protein concentrations were determined using the BCA standard curve equation 2.3.

$$Y = 0.001x + 0.0152 \text{ --- Equation 2.3}$$

( $R^2 = 0.9964$ , Where Y = average optical density and X equals to protein concentration in  $\mu\text{g/ml}$ )

### Bicinchoninic Acid (BCA) Protein Assay

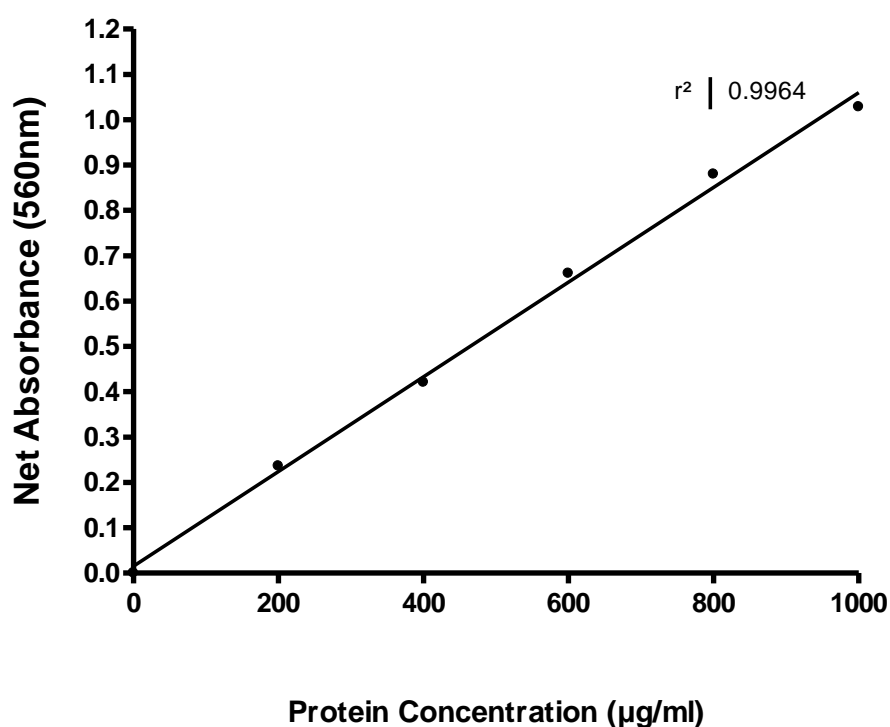


**Figure 2. 4 Standard curve of BCA protein assay**

Stock BSA (2 mg / ml) was diluted in pure MiliQ water to serial dilutions; 0, 200, 400, 600, 800 and 1000  $\mu\text{g}$  / ml. Optical density (OD) (absorbance) was measured at 560 nm wavelength. OD was corrected by subtracting blank OD (zero standard) from blank and standards, and samples. Corrected OD (net absorbance, nm) was plotted against BSA standard protein concentrations. A line of best fit was drawn through the points. Concentrations of unknown samples were determined by reference to the equation 2.3 from the standard plot.

Samples were denatured in 2X Laemmli buffer (Bio-Rad); 65.8 mM Tris-HCl pH 6.8, 26.3% (w/v) glycerol, 2.1% SDS, and 0.01% bromophenol blue with 2- $\beta$ -mercaptoethanol (Bio-Rad) for 6 mins at 95°C. Lysed protein samples were separated on an in-house hand-casted 8% separation gel (separation range, 25-200kDa) (MiliQ H<sub>2</sub>O, 30% acrylamide (Bio-Rad), 1.5M Tris pH8.8, 10% SDS (Bio-Rad), 10% Ammonium persulphate (APS)(Sigma-Aldrich), and tetramethylethylenediamine (TEMED) (Bio-Rad) and 6% stacking gel (stacker) (MiliQ H<sub>2</sub>O, 30% acrylamide (Bio-Rad), 0.5M Tris pH6.8, 10% SDS (Bio-Rad), 10% Ammonium persulphate (APS)(Sigma-Aldrich), and TEMED (Bio-Rad). A total of 30  $\mu$ g of total cell and cytosolic lysates, and 25 $\mu$ g of nuclear lysates were used. Pre-stained dual colour molecular weight marker (10-250 kDa) (Bio-Rad) was included to estimate protein band sizes. Samples were electrophoresed in a Bio-Rad MINI-PROTEAN system in 1X running Tris-Glycine SDS (TGS) buffer (Bio-Rad) initially at low voltage; 90 Volts until samples reached the end of the stacker, to make sure proteins entered the separation gel with minimal disruption.

Voltage was increased to 150 volts until samples reached end of the run. Electrophoresed protein in SDS-PAGE gels were blotted onto an Amersham Hybond™ P 0.45 $\mu$ m 150mm x 4mm Polyvinylidene difluoride (PVDF) membrane (GE Healthcare, LifeSciences) in a 1X transfer Tris-Glycine (TG) buffer (Bio-Rad) at ambient temperature for 150 mins at 100 Volts. These were found to be optimal conditions of transfer following prior use of a range of transfer times and voltages to ensure the majority of the protein had transferred to the membrane. Protein-bound PVDF membranes were blocked in 3% bovine serum albumin (BSA) (Santa Cruz) in 1X Tris buffered saline (TBS) on gentle rotation for 60 mins at room temperature (RT) to reduce non-specific binding.

Membranes were incubated overnight in mouse monoclonal primary antibodies diluted in 1.5% BSA/TBS at 4°C (see list in table 2.1). Antibodies after the first use were supplemented with 0.02% sodium azide (Sigma-Aldrich) to inhibit microbial growth. The optimal antibody concentration was determined prior to use and is reported along with a full list of antibodies, and ancillary products in Table 2.1. Membranes were washed 3X in Tris buffered saline-0.1% Tween 20 (TBST) (20mM Tris, 150mM NaCl, pH 2.2) for 5 mins and incubated in 1:1000 Goat anti-mouse IgG\_ Horseradish peroxidase (HRP) conjugated secondary antibody diluted in 1.5% BSA/TBS for 120 mins at RT. Membranes were washed 10X with TBST for 5 mins each wash and detected protein was visualised by exposure to enhanced chemiluminescence (ECL) luminol-peroxide substrate (ThermoFisher Scientific) for 5 mins. Excess ECL substrate was blotted off and membranes were carefully placed in a chemiluminescent image acquisition charge-coupled device (CCD), PeqLab Fusion FX7 camera (Vilber, Germany). Results were documented and stored as micrographs of blots. Each band on the micrograph represents a sample of pooled population of HDMEC from 6-identical wells (sixplicates) of a 24-well plate format. All experiments with western blots were repeated a minimum of 3 times ( $n \geq 3$ ).

**Table 2. 1 Antibodies and ancillary materials**

<b>Description of antibodies</b>	<b>Type</b>	<b>Dilutions used (1xTBS)</b>	<b>Manufacturer</b>
Anti-HIF1 $\alpha$ mouse monoclonal IgG <sub>1</sub>	Primary	<b>IHC (1:20)</b>	ThermoFisher Scientific (UK) (MA1-516)
		<b>IF (1:50); WB (1:100)</b>	Santa Cruz Biotechnology (USA) (28b:sc-13515)
Anti-Nrf2 mouse monoclonal (IgG2a)	Primary	<b>IF (1:50)</b>	Abcam (ab89443)
Anti-Nrf2 mouse monoclonal (IgG <sub>1</sub> )	Primary	<b>WB (1:100)</b>	Santa Cruz Biotechnology (USA) (A-10: sc-365949)
Anti-VEGF mouse monoclonal (IgG <sub>1</sub> )	Primary	<b>IF (1:50); WB (1:100)</b>	Santa Cruz Biotechnology (USA) (C-1: sc-7269)
Anti-CD31 monoclonal mouse IgG	Primary	<b>IF (1:50); IHC (:20)</b>	Sigma- Aldrich (P8590)
Anti-NF $\kappa$ B p65 (IgG <sub>1</sub> )	Primary	<b>WB (1:100)</b>	Santa Cruz Biotechnology (USA) (F-6: sc-8008)
Anti-HO-1 (IgG <sub>1</sub> )	Primary	<b>WB (1:100)</b>	Santa Cruz Biotechnology (USA) (A-3: sc-136960)
Anti- $\beta$ -actin monoclonal mouse IgG <sub>1</sub>	Primary	<b>WB (1:500)</b>	St John's Laboratory (STJ96941)
Goat anti-mouse IgG DyLight 488 conjugated	Secondary	<b>IHC (1:200), IF (1:1000)</b>	Thermo Scientific (35503)
Goat anti-mouse IgG-HRP monoclonal	Secondary	<b>WB (1:1000)</b>	Santa Cruz (D1614)
Normal goat serum	-	<b>10%</b>	Invitrogen (ThermoFisher Scientific) (PCN5000)
DAPI NuBlue fixed cell stain ready probe reagent	-	<b>1<math>\mu</math>g/ml</b>	Molecular probes, Life Technology (R37606)
BSA	-	<b>2 mg / ml (stock)</b>	Santa Cruz



## 2.6 Gene expression

All RNA and PCR-related work were carried out in a laminar flow cabinet fitted with HEPA-filtered air (MDH, Zurich). Total RNA was extracted using the guanidium thiocyanate-phenol-chloroform extraction method Chomcynski and Sacchi (1987) with a total volume of 800µl of Trizol reagent (Life Technology) per sample. Six identical wells were pooled per sample and homogenised by gently pipetting several times in Trizol, at room temperature (RT) for 5 mins in order for the complete dissociation of the nucleoprotein complex to take place. Chloroform (160µl) (ThermoFisher) was added and mixed thoroughly for 60s and incubated at RT for 3 mins. Samples were centrifuged at 12,000 x g (MultiFuge1, HeraCeus) for 15 mins at 4°C. Homogenates separated into a clear upper aqueous phase, which contains RNA, a middle layer (interphase-white), and a red lower organic phase, containing DNA and proteins.

Approximately 50% of the total volume of the aqueous phase was removed into a fresh Eppendorf. RNA was precipitated with 400µl of 100% isopropanol (Thermo Fischer), incubated at RT for 10 mins and centrifuged at 12,000 xg for a further 10 mins at 4°C. The supernatant was carefully removed, leaving the RNA pellet (gel-like) on the side and bottom of the tube. Pellets were washed with 800 µl of 75% ethanol, vortexed briefly and centrifuged at 7,500 xg for 5 mins. The wash was discarded and pellets briefly air-dried for 10 minutes. Total RNA was quantified spectrophotometrically with a ultra-violet (UV) spectrophotometer (NanoDrop LifeSciences) at 260 nm. RNA purity using the 260/280 nm ratio documented with NanoDrop were routinely found to be 2.0 indicating a high quality of RNA. The RNA was also resolved within a 1% agarose gel in 1X Tris-borate-EDTA (TBE) (ThermoFisher Scientific (Fig. 2.5).

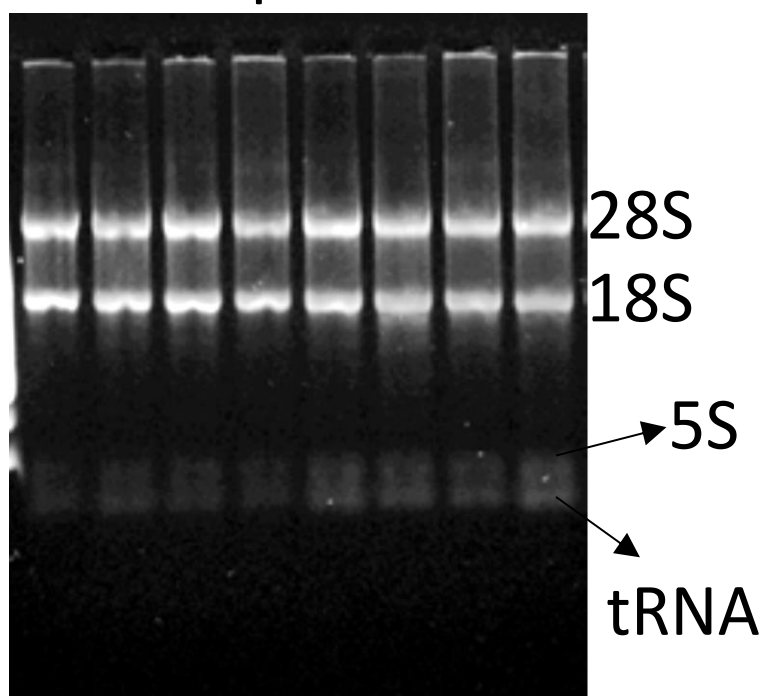


**Figure 2. 5 Resolution of RNA extracted from HDMEC**

Resolution of RNA extracted from HDMEC within a non-denaturing 1% agarose gel and electrophoresed with 1X Tris/Borate/EDTA (TBE) buffer (Sigma-Aldrich) at 80 volts for 50 minutes and visualised with PeqLab Fusion using 1X Gel Red nucleic acid gel stain (Biotium) as filter. Blot image shows 28S:18S band ratios that were roughly 2:1 with a high intensity signal at 28S vs 18S and 5S rRNA. The ratios of RNA samples were routinely 2.0.

A total of 0.5µg of RNA per sample was reverse transcribed to complementary DNA (cDNA) using a high capacity cDNA reverse transcription kit catalysed by 1X rMoMuLV MultiScribe Reverse Transcriptase (50 U/µL) as recommended (ThermoFisher Scientific) (CatLog # 4368814) using conditions outlined in table 2.2.

**Table 2. 2 CDNA thermal cycler program**

	Step 1	Step 2	Step 3	Step 4
Temperature (°C)	25	37	85	4
Time (min)	10	120	5	∞

The cDNA was used for end-point Reverse Transcriptase PCR (RT-PCR) and Real-Time Quantitative PCR (qPCR). A reaction master mix (2X) containing; 2X RT buffer, 8mM dNTP mix, 2X RT random primers (ThermoFisher Scientific) were mixed in nuclease-free water (BIOLINE) in single Eppendorf tubes. The tubes were centrifuged briefly at 4°C to spin down the content and to eliminate air-bubbles and reverse transcription carried out in iCycler thermal cycler using validated thermal cycle program (Table2.2). Samples (cDNA) were diluted to appropriate volumes in Rnase/DNase-free water and stored at -20°C. End-point reverse transcriptase polymerase chain reaction (PCR) (RT-PCR) was used to detect mRNA in cDNA transcripts from RNA samples (Schmittgen et al 2000). Appropriate volumes of 10 ng of template (cDNA) in PCR-grade RNase-free water were used.

RT-PCR reaction was catalysed by Taq DNA polymerase in a 2X concentrate REDTaq ReadyMix PCR kit with 0.2mM magnesium chloride (MgCl<sub>2</sub>) and 80µM 99% pure deoxynucleotides in a red inert dye (Sigma-Aldrich), with 0.25 µM of forward and reverse primers for; B2m, HIF-1α, IL-6, and TNFα. Primers were designed using primer design software accessed via the National Centre for Biotechnology Information (NCBI) website (<https://www.ncbi.nlm.nih.gov>). Specificity was confirmed by follow up with Basic Local Alignment Search Tool (BLAST) also available from NCBI to ensure there was no cross identity with other sequences within the genome. BLAST results showing gene accession numbers, sequence similarity index to ensure specificity which confirmed identity (%), BLAST score of the match (%), gaps score (%) query score (%) and E value (which describes random background noise) are listed in table 2.3 below. Primer name, sequence, accession number, melting temperature T<sub>m</sub> and size (bp) are listed in table 2.4 below.

**Table 2. 3 Primer BLAST reports**

a) Homo sapiens beta-2-microglobulin (B2M), mRNA, Accession number <u>NM_004048.2</u> . Blast Results showing regions of similarity between FASTA sequence of gene of interest and other sequences; 100% identity (987 out of 987), a score of 1823 out of 1823 query, 0% gaps (0/987), E value = 0.0
b) Homo sapiens hypoxia inducible factor 1 alpha subunit (HIF1A), transcript variant 1, mRNA Accession number <u>NM_001530.3</u> ; 100% identity (4082 out of 4082), a score of 1823 out of 1823 query, 0% gaps (0/4082), E value = 0.0
c) Homo sapiens interleukin 6 (IL6), transcript variant 1, mRNA, Accession number <u>NM_000600.4</u> ; 100% identity (1197 out of 1197), a score of 2211 out of 2211 query, 0% gaps (0/1197), E value = 0.0
d) Homo sapiens tumour necrosis factor (TNF), mRNA, Accession number <u>NM_000594.3</u> ; 100% identity (1686 out of 1686), a score of 1823 out of 3114 query, 0% gaps (0/1686), E value = 0.0.

All targets as retrieved with their accession numbers had gaps scores of 0 %, E-values of 0.0 and scored 100% for identity and match scores. Full list of primer names, amplicon size (bp) and sequences, melting temperature (annealing temperature, TM), accession numbers are listed in the table 2.4.

**Table 2. 4 Primers and sequence details**

Oligo name	Primer sequence (5'-3')	Tm	Accession #	Size (bp)
B2M Beta-2-microglobulin	F: 5'-GGGCATTCTGAAGCTGACA-3' R: 5'-TGGAGTACGCTGGATAGCCT-3'	67.6 63.7	NM_004048	109
HIF1A Hypoxia inducible factor 1 alpha subunit	F: 5'-GAGGGAGCCAGCGCTTAG-3' R: 5'-ACTTATCTTTTCTTGTCGTTTCGC-3'	65.2 63.4	NM_001530	116
IL6 Interleukin 6	F: 5'-TCAATATTAGAGTCTCAACCCCA-3' R: 5'-TTCTCTTTCGTTCCCGGTGG-3'	64.4 68.2	NM_000600.4	90
TNFA Tumour necrosis factor	F: 5'-TCCCCAGGGACCTCTCTCTA-3' R: 5'-GGGTTTGCTACAACATGGGC-3'	65.0 66.3	NM_000594.3	108

F, forward primer; R, reverse primer.

PCR reaction mix was gently vortexed, centrifuged and amplified using a 2-step PCR cycling parameters as set out in table 2.5. Samples of amplified DNA were loaded directly onto a 1% agarose gel and electrophoresed with 1X Tris/Borate/EDTA (TBE) buffer (Sigma-Aldrich) at 80 volts for 50 minutes and visualised with PeqLab Fusion using 1X Gel Red nucleic acid gel stain (Biotium) as filter. Results are documented as micrographs of PCR products (bands). A sample (band) on micrograph represents pooled population of HDMEC from 6-identical wells (sixplicates). All experiments with end-point PCR were repeated a minimum of 3 times ( $n \geq 3$ ). Real-time PCR was performed on duplicate samples using Applied Biosystems 7900HT Real-Time PCR System with 0.25  $\mu$ M of human IL-6 and B2m primers (table 2.4), and 2X SYBR Green with ROX reference dye (Applied Biosystems, catalogue # 4309155) with a total of 10ng of cDNA template in a final volume of 20 $\mu$ l in 96-well optical plate format (Applied Biosystems). Thermal cycle and amplification parameters are set out in table 2.6 and 2.7.

**Table 2. 5 Thermal cycler program for End-point RT-PCR**

	Step	Temperature	Duration	Cycles
1.	Initial denaturation	95°C	1 min	1x
2.	Amplification	95°C	1 min	40x
	-Denaturation	65°C	1 min	
	-Anneal			
3.	Final extension	68°C	7 min	1x
	Hold	4°C	-	-

**Table 2. 6 Standard cycling mode for Real-time qPCR**

Step	Temperature	Duration	Cycles
UDG activation	50°C	2 mins	Hold
Dual-Lock DNA Polymerase	95°C	2 mins	Hold
Denature	95°C	15s	40
Anneal/Extend	60°C	1 min	

**Table 2. 7 Dissociation curve conditions for Real-time qPCR**

Step	Ramp rate	Temperature	Time
1	1.6°C/s	95°C	15s
2	1.6°C/s	60°C	1min
3	0.15°C/s	95°C	15s

Melt curve was analysed with RQ manager 1.2 software (Applied Biosystems) to discriminate between specific products having a melting temperature ( $T_m$ ) of  $\geq 78^\circ\text{C}$  and non-specific primer-primer products with a  $T_m$  of  $\leq 78^\circ\text{C}$ . Assessment of Real-time qPCR products were based on melting curve results only. Data were normalized to human B2m mRNA levels as an endogenous control and expressed relative to untreated control (calibrator) using the formula  $2^{-\Delta\Delta C_T}$  (fold change) where  $C_T$  is the threshold cycle number since, B2M and IL-6 primers were at equivalent efficiencies ( $\geq 90\%$ ) (Winer et al 1999, Schmittgen et al 2000). Untreated samples in 5% CO<sub>2</sub> normal incubator conditions in 5.5 mM glucose media were assigned calibrator (Livak and Schmittgen 2001). Change in expression was determined with equation 2.4, and fold change calculated using equation 2.5. Six identical wells of HDMEC in a 24-well plate format were pooled per RNA sample. Real time assays were set up in duplicates, and repeated  $n = 3$  independent occasions.

$$\begin{aligned}
 & \text{Change in expression } (\Delta\Delta Ct) \\
 &= \text{Average Ct}(\text{Target treated}) \\
 &- \text{Average Ct}(\text{Target untreated}) \\
 &\text{-----Equation 2.4}
 \end{aligned}$$

$$\text{Fold change} = 2^{-\Delta\Delta Ct} \text{-----Equation 2.5}$$



## 2.7 Resazurin assay

Resazurin (CST) was used to examine cell metabolic activity post treatments (Ahmed et al 1994, Nakayama et al 1997 and Nociari et al 1998). Resazurin (7-hydroxy-3H-phenoxazin-3-one 10-oxide) assay is based on the ability of metabolically viable cells to reduce blue Resazurin dye to a highly fluorescent and measurable pink resorufin in a reaction catalysed by dehydrogenase (Ahmed et al, 1994, Nakayama et al 1997, Zalata et al 1998, Perrot et al 2003). In Resazurin assay, fluorescence is proportional to cell metabolic activity and because Resazurin is only reduced to fluorescent resorufin in metabolically viable cells, the assay can be used to estimate the impact of treatments on cell metabolic activity (Ahmed et al, 1994).

Resazurin assay was performed only with HDMEC samples and explants were not analysed for metabolic activities. Control experiments were carried out by seeding cells according to the general guidelines (10,000-20,000cells/cm<sup>2</sup>) given by PromoCell, although this was not specific for Resazurin assay. HDMEC were seeded in clear 96-well plates (surface area of 0.32cm<sup>2</sup>) plates at a density of 1,000, 2,000, 5,000, 6,000 and 10,000cells per well in 100 µl of normal growth media. Blank (no cell) control contained 100-µl media but with no cells incubated. Fluorescence from no-cell control sample was subtracted from cell-incubated wells to obtain the relative fluorescence units (RFU), an indicator of metabolic activity expressed in  $\times 10^4$ . Samples in triplicates were incubated at 37°C in a 5% CO<sub>2</sub> incubator and reached approximately 70% confluence after 48 hours, and were treated with 10µl Resazurin (10X) solution (CST) per well in the dark. Fluorescence was measured at 0, 6, and 24 h using a Synergy HT microplate reader (Biotek) at 530-570nm excitation wavelength and 585-590nm emission wavelength. Prior to treatment, growth media were refreshed with 100µl of media containing 5.5 / 20 mM D-glucose.

For experiments, HDMEC were exposed to treatments with equivalent controls (untreated) incubated in a normal 5% incubator. A no-cell blank control was included as blank to derive RFU values. HDMEC media were mixed with 10% Resazurin, and incubated in the dark in a 5% CO<sub>2</sub> incubator for 24 h. Fluorescence was read at 530-570nm excitation wavelength and 585-590nm emission wavelength using a Synergy HT microplate reader (Biotek). RFU was obtained by subtracting average RFU values of no-cell control from samples. All experiments were repeated at least 3 times ( $n \geq 3$ ) and data as reported in the relevant result section represents mean OD  $\pm$  SEM.

## 2.8 Hyperbaric oxygen chamber

Treatment of samples (HDMEC or explants) was carried out within a bespoke validated hyperbaric oxygen (HBO) unit developed in-house in collaboration with Mr Allan McPherson from the School of Engineering department at Robert Gordon University and underwent full safety testing prior to use. The figure, 2.6 is a schematic diagram detailing the procedures undertaken in setting up the HBO unit. All procedures were performed in an air-tight hyperbaric unit (chamber) made from Perspex. Perspex (Poly (methyl methacrylate)) also known as acrylic glass is a transparent thermoplastic lightweight or shatter-resistant alternative to glass. Samples undergoing treatments were placed inside the chamber. The anterior and posterior ends of the chamber are fitted with air-tight inserts for gas inlet with a pressure-voltage converter patch lead and an outlet for monitoring oxygen levels. Two gas supply cylinders; a 95/5% O<sub>2</sub>/CO<sub>2</sub> (hyperoxia) medical gas (BOC) (orange) and a 21% O<sub>2</sub>/Air/Nitrogen (normoxia) (ARC) (green) were used (1). Gas cylinders were connected to the chamber via a Y-shaped tube (green and orange). A Y-shaped gas inlet was necessary for the administration of HBO since gas cycling between hyperoxia and normoxia was required for HBO. To alternate between gases, a clamp was used to shunt gas supply from the cylinder that was not in use. For instance, if the gas in use at the time was medical gas, the gas inlet for Air/Nitrogen was shunted and vice versa.

A Honeywell gauge gas pressure sensor mounted on the anterior end of the unit transduces pressures (up to 150psi) to measurable units of voltage (1.5-12V) using a voltammeter. A data logger (Pico Technologies) was used to record and document output of gas pressures. Once samples were placed within the chamber, the chamber posterior end was tightly secured at the end with six steel Ki8.8 bolts and six steel washers and chamber placed within a 37°C incubator. The gas cylinder in use was switched on and the posterior gas outlet tube was attached to a Frith's stone fully inserted into a beaker of water kept at 37°C. Gas saturation in the beaker of water was monitored with a Strathkelvin oxygen meter until saturation was reached (validations determined time taken for oxygen meter to reach saturation was  $2.2 \pm 0$  mins,  $n = 6$ ). This was rounded up to 3 mins. After 3 mins, the outlet tube was securely closed by folding it over and clamping.

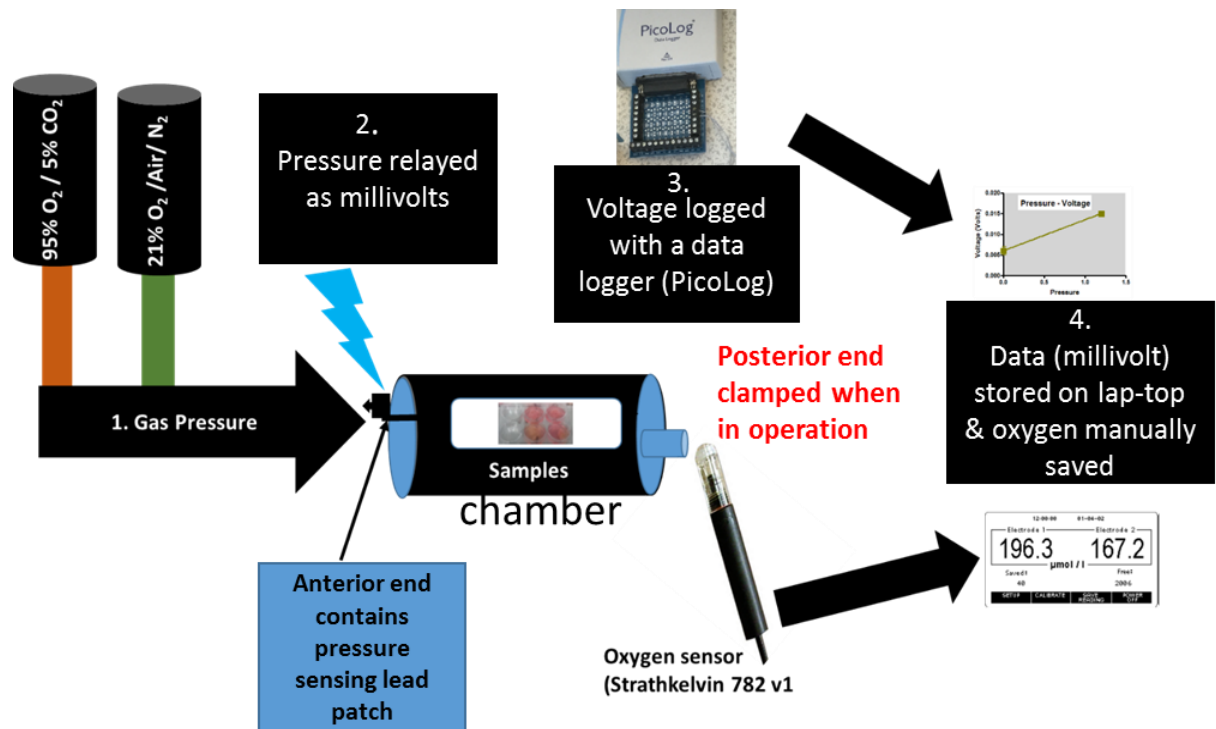


**Figure 2. 6 Schematic representation of treatment in chamber**

Samples were incubated in the chamber on a stable platform. Chamber was tightly secured and outlet tube was placed into a glass beaker of water at 37°C containing a calibrated oxygen electrode (Strathkelvin 782 v1). Two separate gas cylinders containing medical gas (95% O<sub>2</sub>/ 5% CO<sub>2</sub>) (orange) and 21% O<sub>2</sub>/ Air/N<sub>2</sub> (green) were connected via a Y-tube to a central tube into the chamber. The gas in use was released to flush and saturate chamber for 3 mins prior to use, while the gas not in use was turned off by clamping gas tube. Pressure was either maintained at 0 bar (1 ATA) or elevated to + 1.2 bar (2.2 ATA) using gas gauge switch for the appropriate cylinders. The gas gauge for hyperoxia alone treatment was maintained at 0 bar, while medical gas was used to flush and saturate chamber and for the entire incubation duration. The gas gauge was elevated to + 1.2 bar (2.2 ATA) in combination with medical gas during the hyperoxia cycle (HBO). During, the air breathing cycle, the medical gas was clamped and 21% O<sub>2</sub>/Air/N<sub>2</sub> gas (normoxia) was used to flush the chamber for 3 mins. The chamber was secured thereafter and pressure elevated to 2.2 ATA with 21% O<sub>2</sub>/Air/N<sub>2</sub> gas for additional 5mins to complete a cycle of hyperbaric oxygen. Three cycles of hyperoxia with elevated pressure, and 2 cycles of normoxia with elevated pressure was carried out per HBO procedure. The physical element (i.e. pressure) within the chamber was relayed via a pressure sensing lead patch to a voltmeter. Pressure – voltage (Volts) was logged with PicoLog and saved on hard disk of a laptop computer. Oxygen readings with Strathkelvin are manually documented. Once oxygen saturation was reached, the outlet tube was tightly secured until treatments were completed.

Samples were exposed to hyperoxia at normobaric (0 bar relative to atmospheric pressure) or hyperbaric pressure (+ 1.2 bar relative to atmospheric pressure = 2.2 atmospheric pressure absolute, (ATA)) in normoxia for 90 mins or combinations of both hyperoxia and hyperbaric pressure (2.2 ATA) (HBO) for 3 cycles of 30 mins duration with 2 cycles of 8 mins intermittent 'air' (normoxia) at 2.2ATA, giving a total treatment duration of 106 minutes. This procedure was consistent with current clinical protocol in the United Kingdom (Bennett et al 2016). However, the normal 5-mins air breathing (Bennett et al 2016) was adjusted to 8 mins in this study. The additional 3 mins allowed for proper chamber saturation with incoming gas when alternating between gases (e.g. when changing from hyperoxia to normoxia, and vice versa). Equivalent samples were incubated in a normal 5% CO<sub>2</sub> incubator (Control samples). Hyperoxia and hyperbaric pressure treatment alone were controls for HBO to examine the effects of the single components. Post incubation, gas gauges were turned off and cylinder (s) switched off. The unit was de-assembled, and returned to a normal 5% CO<sub>2</sub> incubator. The figure (2.7) below is a schematic representation of the HBO procedure which involved gas cycling and alternation between hyperoxia and normoxia at hyperbaric pressures.

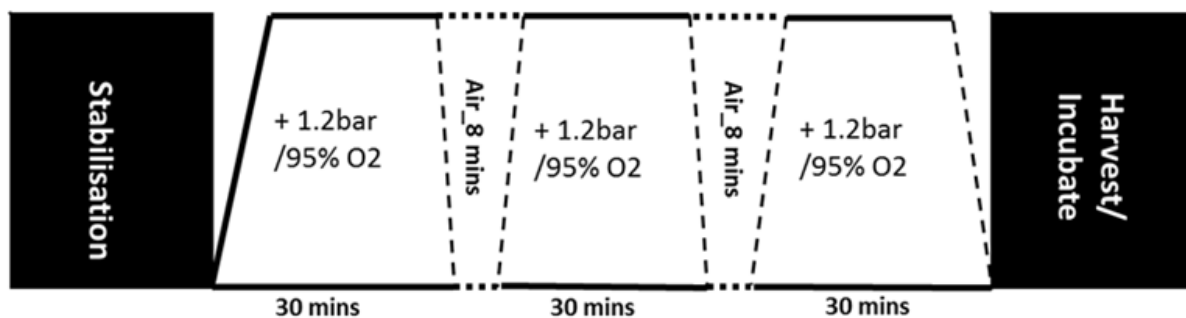


**Figure 2. 7 Schematic representation of HBO cycling**

The HBO procedure as shown in the schematic diagram above was closely aligned to the UK HBOT clinical protocol (Bennett et al 2016). A single inlet/outlet system was used, and protocol was adjusted to include an additional 3 mins before and after 5-mins of Air/Nitrogen gas (21% oxygen) to allow for complete saturation of the chamber with the relevant gas.

HDMEC require 5% CO<sub>2</sub> for optimal incubation and a bench control (exposed to 21% O<sub>2</sub>/Air/N<sub>2</sub>) was set up to assess the effect of using less than 5% CO<sub>2</sub> for up to 90 mins incubation. Bench controls were kept within a bench top incubator at 37°C concurrently with hyperbaric pressure samples, but not within the pressurised chamber. Thus 'Bench' controls differed from hyperbaric pressure samples only in respect to elevated pressure, 2.2 ATA. A Honeywell gauge gas pressure sensor, of up to 150psi (1.5-12V) was used to convert gas pressure to voltage (Volts, recorded as millivolts, mV). Data (mV) were logged via a data logger (Pico Technologies) connected to a Lenovo laptop. To demonstrate the data logger was sensitive to the pressure-voltage variation, a series of test runs were performed. Based on these initial validation (see Fig. 3.9, A), the data logger was sensitive to pressure –voltage variations at 1 ATA (0 bar) or 2.2 ATA (+ 1.2 bar). Subsequently, validations (control experiments, N = 6) (Fig. 3.9, B) were carried out to ascertain the relationship between gas pressure and voltage. External variations that might increase pressure (in addition to the applied gas pressures) include relative humidity and any substantial changes in the atmospheric pressures on the days of experiments. To determine voltage at zero bar (1 ATA), the gas pressures of 21% O<sub>2</sub> (Air/Nitrogen) or 95% O<sub>2</sub>/5% CO<sub>2</sub> at 1 ATA were monitored and recorded with a data logger. Pressure was elevated by +1.2 bar (i.e. 2.2 ATA), and voltage readings recorded. Average voltage value at 0 and +1.2 bar were 6mV (SD 0.001) and 15mV (SD 0.000) respectively. A straight line graph was plotted to determine the equation of relationship (Equation 2.6) between voltage and pressure using GraphPad Prism:

$$Y = 0.0075X + 0.006 \text{ --- Equation 2.6.}$$

Where Y equals the independent variable, voltage and X equals the dependent variable, Pressure.

The equation above shows the relationship between pressure (bar) (a physical property) and a measurable quantity, voltage (Volts). Thus, the gas pressures relayed were correlated to the voltage measured. External factors such as relative humidity and atmospheric pressure affect total gas pressure in the chamber. Hence, in order to help reduce external variations, the chamber was made airtight by securing tightly. Results of the various validations undertaken in setting up the hyperbaric oxygen unit are reported in chapter 3.0 sections 3.3.2.

## 2.9 HDMEC size measurement

Live cell (HDMEC) images were captured before (baseline) and 4 h post treatment using a light microscope (Leica DM4000B) and an attached camera (Leica DFC300-FX) at 200X magnification. Experiments were repeated on five independent occasions. Photomicrographs were independently coded. Inclusion and exclusion criteria were set prior to measurements and used for all images. Coded images of HDMECs were analysed with an Image J program with a global scale was set to 0.22pixels/ $\mu\text{m}$ . The perimeter (size), i.e. the total distance around cells (HDMEC) with clearly defined borders were traced and measured with the Image J free-hand drawing tool. Sample identities were revealed post image analysis. Statistical analysis was carried out with Graph Pad Prism vs 5.0.

## 2.10 Fluorescence intensity determination

The fluorescence intensities of stained photomicrographs of HDMEC captured at 4 h and 24 h post treatment of nrf2 were measured with Image J program. Photomicrographs with debris and non-specific (non-cell associated) fluorescence were excluded. Photomicrographs were captured at 400X magnification, and a global scale of 0.44 pixels / micron ( $\mu\text{m}$ ) was used. Photomicrographs measured were from 2-3 fields (micrographs) captured from more than three independent experiments as reported in the ICC method section (2.4).

## 2.11 Statistical analysis

Data were statistically analysed using GraphPad Prism 5.0 software (GraphPad Software Inc. USA). The normality of data from HDMEC size and metabolic activity assay where replicates were  $n \geq 18$  was ascertained with a Shapiro-Wilk's test for Gaussian distribution. Column statistics option was used to determine mean, standard error of mean (SEM) at 95% confidence intervals (CI) for fluorescence intensity and real-time PCR data where replicates were  $n \leq 18$ . Data reporting matrix oxygen measurement, contractile responses, and hyperbaric model validations are presented as mean  $\pm$  SD. Cell work data reporting HDMEC sizes, metabolic activity and mRNA expression are presented as mean  $\pm$  SEM. The SEM was chosen for cell (biological) data, not standard deviation (SD) which provides an idea of the variability of a single observation, in order to represent the spread of the mean so as to give indication of the reliability of the mean of the data as the experiments were repeated  $n \geq 3$  independent occasions. Where SD is used to report data, it is clearly noted in the relevant section, otherwise SEM is implied. One way (1way) analysis of variance (ANOVA) was used to test the means between all samples (\*), and Tukey's post hoc test to compare all columns (samples) was performed if 1way ANOVA was successful with overall p value; \* $p < 0.05$ , \*\* $p < 0.01$ , \*\*\* $p < 0.0001$ . Student t-test was used to make comparison between samples in the same treatment group for glucose effect where relevant. Bonferroni's post hoc analysis was used to compare selected columns of samples for metabolic activity analysis; low glucose samples: HBO versus hyperoxia versus hyperbaric pressure, and high glucose samples: HBO versus hyperoxia versus hyperbaric pressure

# Chapter 3.0: Validation of experimental models



## 3.1 Introduction

In this chapter the validation of the retinal explant model and the experimental HBO chamber is presented. Endothelial cells are best studied in-situ because their constitutive phenotype is altered when explanted (Grant et al 1989). It is well accepted that single cell systems do not present the whole picture in mechanistic studies (Oberringer et al 2007). Hence, there is a need to examine single cell-based assay results in more complex systems. Realistic insights are best provided using animal models and human subjects. However, such studies have limitations that are met by using ex-vivo models (Oberringer et al 2007, reviewed in Jo et al 2013, Lai and Lo 2013, Matteucci et al 2015, and Costa and Andrade 2015). The primary determinants of retinal cell survival in cultured isolated retina are neither nutritive supply from the choroid, oxygen supply, or the provision of RPE, but the provision of a biomechanical milieu (Taylor et al 2014). In vivo, the retina resides in a highly biomechanical environment where adhesive tensile and hydrostatic forces come into play (Marmor et al 1994). Retinal biomechanical scaffolding and biochemical homeostasis is controlled by Mueller cells through their regulation of intermediate filaments such as glial fibrillary acidic protein (GFAP) and vimentin (reviewed in Taylor et al 2014). Absence of biomechanical support in retinal tissue culture results in pyknosis, an irreversible condensation of chromatin in the nucleus of a retinal cell undergoing necrosis or apoptosis (Taylor et al 2014). In addition, isolated adult retinal sheets cultured under standard condition display degeneration very early because of gliosis (Kaempfer et al 2008, Kobuch et al 2008, Fernandez-Bueno et al 2008, Taylor et al 2014). During gliosis, Mueller cells (the principal glial cell of the retina) become activated, losing their metabolic function and structural integrity in times of retinal injury and diseases. Also, the deaths of other neuronal cell types are accelerated in gliosis. Hence, retinal gliosis is the major limiting factor for retinal culture using standard conditions without a biomechanical support (Caffe et al 1989, and 2001, Taylor et al 2014). Furthermore, the rapid disintegration of explanted retinas cultured in media in serum-containing media has been reported. Therefore the exclusion of serum in media decreases the rate of retinal degeneration (Caffe et al 1989).

The culture of explanted retinas has been in existence since 1930s, with different approaches used by different workers to expedite retinal viability. Different biomechanical supports or platforms have been utilised. A retinal model of human retinal angiogenesis comprised of retinal tissue embedded within a fibrin-agar matrix was employed by Knott et al 1999. In addition, a porous polycarbonate culture membrane (0.4  $\mu\text{m}$ ) was used by Taylor et al 2014. In this study a biomechanical scaffold (matrix) was utilised in the culture of isolated porcine retina as described in the method section (2.3).

Agarose is porous (0.4-1  $\mu\text{m}$ ), inert, and biocompatible and forms a fine web-like matrix in combination with collagen fibres (Lake et al 2011). Here, porcine retinal tissues cultured as three-dimension (3D) explants were used to examine endothelial cell responses. Isolated whole retinal tissues were sandwiched within agarose-collagen bilayer matrices with the outer and inner retina in immediate contact with matrices. This method of retinal culture utilised is expected to delay retinal degeneration and provide extracellular cues with the provision of a biomechanical scaffold (agarose matrix) and an extracellular matrix protein, collagen (Caffe et al 1989, Lake et al 2011, Taylor et al 2015).

Hyperbaric oxygen therapy (HBOT) is a treatment modality involving the use of hyperbaric oxygen (HBO) which entails breathing in  $\geq 95\%$  oxygen ( $\text{O}_2$ ) breathing at a pressure greater than 1 absolute atmosphere (ATA) that is, greater than the atmospheric pressure at sea level (Löndahl 2013, HBOT Trust 2018). HBO protocol is modified in practice to suit local facilities and circumstances. Variations exist in the total number of sessions (30 - 60), pressure used (2.0 - 2.5 ATA), length of each session (60 - 120 minutes), frequency (once or twice a day), adoption of a 5-minute reprieve in every 30-minute interval for preventing oxygen toxicity and continued administration of pure oxygen during the decompression period (Bennett et al 2016, HBOT Trust 2018). HBO protocol as modelled in this study was closely aligned to clinical HBO therapy regimen in the United Kingdom (UK). Validations of the retinal explant and HBO chamber were carried out to ensure protocol and method robustness as these methods were developed during the course of this study.

The aim in this chapter is to demonstrate the suitability and robustness of the two models (retinal explants and experimental HBO model) utilized in this study. Here, the retinal explant model development, protocols and assays validated in relation to oxygen availability, retinal tissue integrity and vessel functionality are presented. In addition, validations of HBO protocol, method and model development in relation to pressure, temperature, oxygen and pH monitoring are also presented.

## 3.2. Methods

### 3.2.1 Retinal explants

Porcine ocular globes ( $n \geq 10$ ) donated from a local abattoir were cleaned and sterilised. Retinal tissues were extracted as described (Rzeczinski et al 2005 and Johnson and Martin 2008), and cultured within three dimension (3D) matrices (explants) made from 0.5% agarose (BIOLINE) and collagen (0.25mg/ml) (Gibco, Life Technology) in low (5.5 mM) or high (25 mM) D-glucose DMEM media (ThermoFisher Scientific). The total matrix depth was 7mm. Explants were incubated in media of low or high glucose 30 mins before treatment and harvested at 2 h and 24 h post treatment. Full details of methods utilised for validating the retinal explant model are reported in the general materials and methods chapter 2.0; explant culture (section 2.3.1), matrix oxygen measurement (section 2.3.2), measurement of contractile response (section 2.3.3), explant harvest (section 2.3.4), haematoxylin and eosin staining (section 2.3.5), and Gomori Trichrome stain for collagen (section 2.3.6). See section 3.3.1 for results of retinal explant validations.

### 3.2.2 Hyperbaric oxygen model

A Honeywell gauge gas pressure sensor was used to monitor and convert gas pressure to voltage (millivolts, mV) and logged with PicoLog data logger. To demonstrate the sensitivity of pressure (ATA) conversion to mV, initial control experiments,  $n = 6$  were performed to define the relationship between gas pressure and voltage (see section 3.3.2). The determination of pressure- voltage (mV) conversion was derived based on the equation below (equation 3.1) using a PicoLog software. External factors other than the applied gas pressure such as relative humidity and any substantial changes in the atmospheric pressures were accounted for with the equation of the relationship between gas pressure and voltage transmitted (mV). Thirty (30) mins prior to experiments, all units were switched on to acclimatize. The equation below (3.1) shows the relationship between pressure (ATA) and voltage (millivolts, mV).

$$Y = 0.0075X + 0.006 \text{ — — — — —}$$

**— Equation 3.1.**

Where Y equals the independent variable, voltage and X equals the dependent variable, Pressure.

The gas pressures within the chamber at normal atmospheric pressure (1 ATA) at 21% or at 95% oxygen were measured, converted to voltage and recorded as mV, and measurements were repeated with the pressure cylinder increased to +1.2 bar (2.2 ATA) and the corresponding mV values recorded. The average (n = 22) voltages (mV) which was an indicator of the average applied gas pressure within the chamber at 1 ATA and 2.2 ATA were plotted. Results of pressure-voltage (mV) validation are reported in section 3.3.2. Oxygen saturation in the chamber was measured with a Strathkelvin oxygen meter (v782). Electrodes were calibrated at high point (100% saturation) and zero-point (0% O<sub>2</sub>). For high point calibration, electrodes were placed in air-bubbled distilled water at 37°C. Zero-point was calibrated in 2% sodium sulphite solution at 37°C. Results of calibration are presented as plots of average O<sub>2</sub> saturation (%) from n = 3 independent calibration measurements (section 3.3.2). The HBO chamber was tightly secured and the chamber was flushed continuously with the relevant gas. The outlet tube at the posterior end of chamber was opened, and a Frith's stone fitted and placed into a beaker of water at 37°C containing an oxygen sensor meter. Oxygen saturation in the chamber was monitored in this way to establish oxygen saturation at normoxia (21% Air/Nitrogen) and hyperoxia (95% O<sub>2</sub>/5% CO<sub>2</sub>). In addition, time taken (in mins) to reach saturation was determined, to inform on the duration needed to reach saturation point with the relevant gas. Results are reported in section 3.3.2. The effect(s) of treatment on media buffering capacity was also verified. Moreover, since the gas mixture for normoxia (21% O<sub>2</sub>/Air/Nitrogen) contained less than 5% CO<sub>2</sub>, the effect of using normoxia gas with less than 5% CO<sub>2</sub> on media buffering capacity was ascertained. Hence, validation (n = 4) of media buffering capacity was undertaken.

The pH of HDMEC incubated media were measured with a pH meter (Denver Instruments) after 120 mins of incubation in the chamber in the presence of hyperoxia (at 1 ATA/ 2.2 ATA) or normoxia (2ATA) or controls. Equivalent controls were incubated within the bench top and a normal 5% CO<sub>2</sub> incubator. HDMEC are best maintained at 37°C. To ascertain any variations in temperature which might impact pH or oxygen dissolution since the hyperbaric chamber was placed within a bench top incubator during operation, validations (n = 5) were undertaken with control experiments to exclude variability in temperatures within the chamber.

To do this, a mercury thermometer was inserted within chamber (internal reading) and was compared with readings from an external thermometer on the bench top incubator (external).

## 3.3. Results

### 3.3.1. Retinal explant

Mean ( $n = 6$ ) oxygen concentration (%) in media (control) at 0.5 h and 24 h were  $14.8\% \pm 1.7$  and  $23\% \pm 0.0$  respectively relative to atmospheric air at 1 ATA. Oxygen saturation at 4mm depth of the matrix at 0.5 h and 24 h were  $14.3\% \pm 1.1$  and  $18.3\% \pm 1.5$  respectively relative to atmospheric air at 1 ATA. The observed mean matrix oxygen saturation of 14.3% and 18.3% corresponded to a partial pressure of oxygen ( $\text{PaO}_2$ ) of 57 mmHg and 76 mmHg respectively at sea level (1 ATA) (Hodges et al 2003). Based on a 1 way analysis of variance (ANOVA), there were significant differences between the means of all samples ( $p < 0.0003$ ,  $n = 4$ ). Based on Tukey's post hoc analysis, levels of oxygen within matrices (4mm depth) at 0.5 h and 24 h were not statistically different in comparison to their respective controls ( $p > 0.05$ ). Moreover mean oxygen saturation in matrices at 24 h was not significantly different relative to 0.5 h ( $p > 0.05$ ) suggesting explants at both these two time points were at comparable oxygen levels despite the prevailing atmospheric oxygen levels. Oxygen saturation in control (media) at 24 h was significantly higher in comparison to the control at 0.5 h ( $p < 0.0001$ ) and matrix at 0.5 h ( $p < 0.0001$ ). The differences in oxygen levels (controls) might be reflective of differences in the atmospheric oxygen levels at these times of measurement.

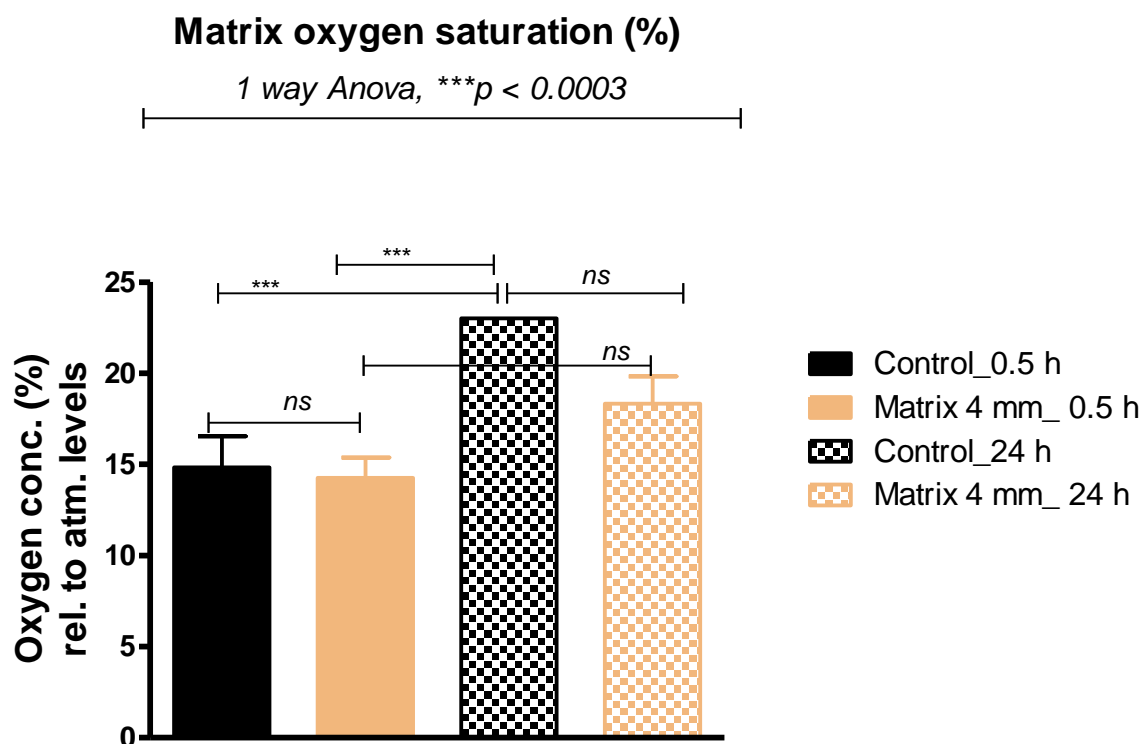


**Figure 3. 1 Oxygen saturation at 0.5 h and 24 h**

Mean oxygen saturation at 0.5 h and 24 h in media (control), were  $14.8\% \pm 1.7$  and  $23\% \pm 0.0$  respectively, and in the matrices,  $14.3\% \pm 1.1$  and  $18.3\% \pm 1.5$  respectively. Oxygen saturation in matrices at 0.5 h and 24 h were not significantly different versus their respective media control at 0.5 h and 24 h ( $p > 0.05$ ). There was no significant difference in oxygen levels in matrices at both times although oxygen saturation was higher at 24 h versus 0.5 h. Data is representative of the mean  $\pm$  SD of six independent measurements.

Visual inspection of retinal explants for signs of tissue degradation was undertaken with a light microscope on more than 15 independent occasions. Exemplar micrographs are presented in fig 3.2 below. In comparison to equivalent retinal tissues cultured as free-floating culture in 2D, explant tissues and vessels structure were better maintained for more than 48 h without signs of disintegration. But retinal tissues and vessels degradation was evident in 2D cultured retinas after 24 h and was further exaggerated after 48h.

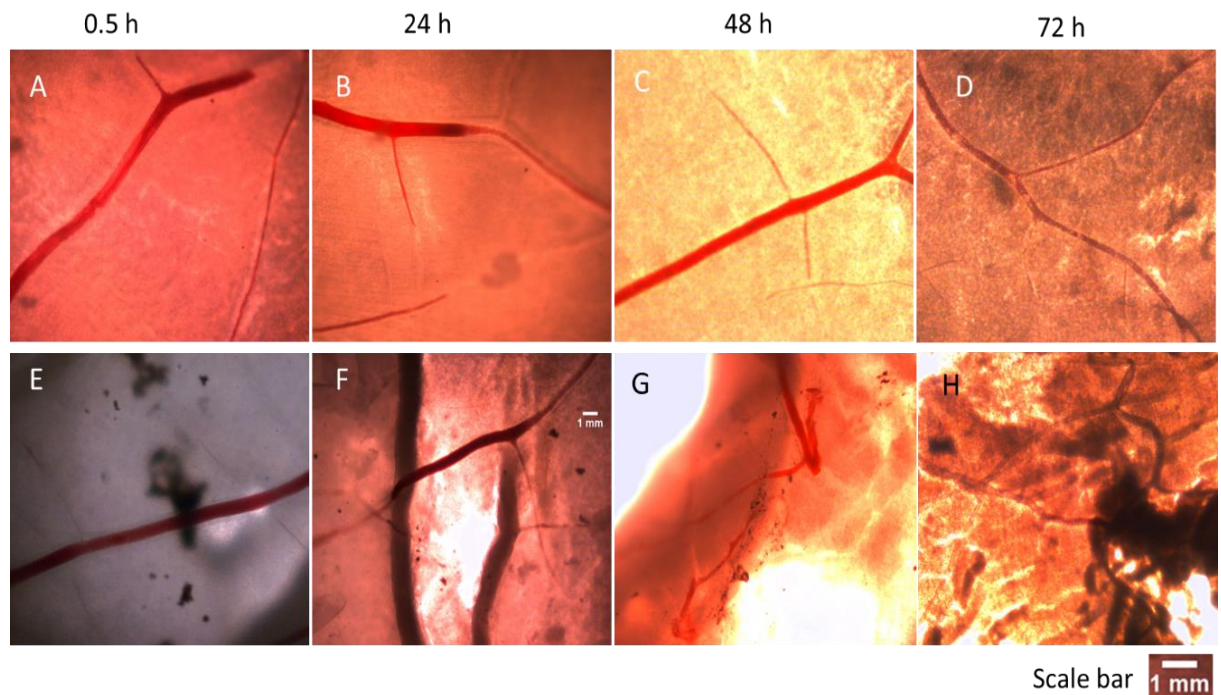


**Figure 3. 2 Representative images of explants and 2D control.**

Explant tissues and vessels showed vessel intactness and absence of degradation for up to 48 h without signs of tearing or degradation (A-D), with slight signs of disintegration seen at 72 h. Retinal tissue and vessel disruption and disintegration was evident within 24 h of culture in 2D plates, which was exaggerated after 24 h (E-H).

Morphological results (micrographs) were consolidated with histological examination. Results of retinal explants (fig 3.3) were consistent with typical retinal layers, nuclear bodies, and structures such as vascular networks (stained red), with erythrocytes (red) at 0.5 h (A) and 24 h (B) and were comparable to uncultured extracted retina (C), and uncultured non extracted retina fixed within the eye globe (D). Explants' photoreceptors at 24 h (B) showed dark/black spots which may be dead cell-bodies. Taken together, retinal layers demarcated by H and E stain were consistent with typical retinal structure and the major layers of the retina were clearly distinguishable confirming retinal tissue integrity.



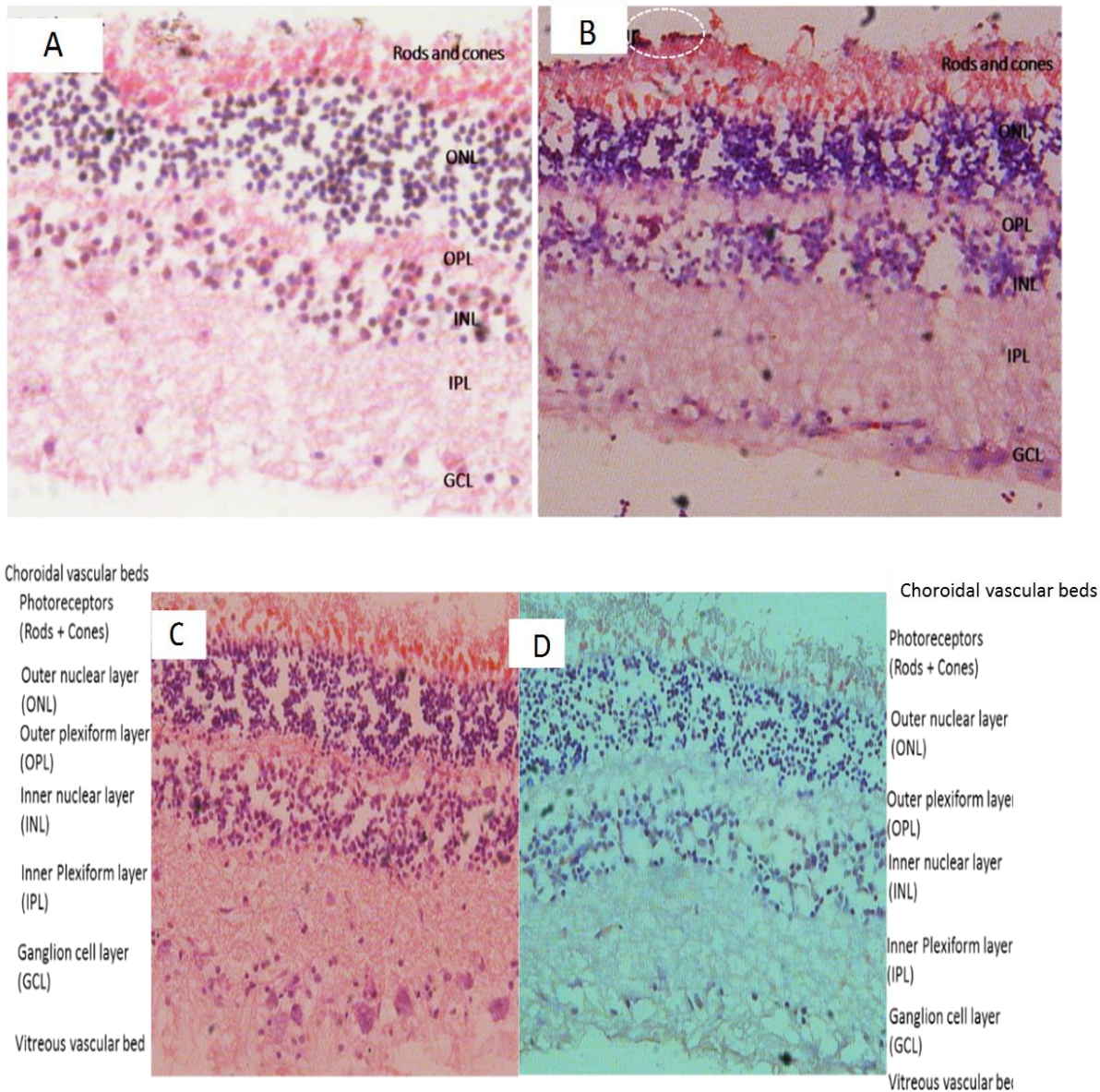


### Figure 3. 3 Representative Hand E results at 0.5 h and 24 h

Selected micrographs of retinal explant at 0.5 h (40X) and 24 h (20X) post culture. Retinal layers in explants were identified; photoreceptors, outer nuclear layer (ONL), outer plexiform layer (OPL), Inner nuclear layer (INL), Inner plexiform layer (IPL) and ganglion cell layer (GCL). Explant retinal tissues at 0.5 h (A) and 24 h (B) were comparable to uncultured controls (40X), (extracted retina, C), and retina fixed within globe (D) in regards to presence of retinal layers. Explants' photoreceptors (circled, white) at 24 h showed dark/black spots which may be due to an early photoreceptor injury or cell-death. Scale bar 500µm



The composition of Gomori assay employed in this study was modified green Gomori: Chromotrope 2R, Fast/light green and phosphotungstic acid with glacial acetic acid to give contrasting identification of collagen; cytoplasm (red), fibrin (pink), collagen (light or FCF green), and erythrocytes (red) (Garvey et al 1996). The dark stained (possibly green) contrasted from the pink/red (cytoplasmic/red blood cells) components of Gomori stain may indicate positivity of retinal explant section for collagen fibre (FCF/light green) at 0.5 h (B), 4 h (C) and 24 h (fig 3.4). Unstained tissue (A) counterstained with eosin alone (A) showed pink (eosin)cytoplasmic stain of the retinal outer nuclear layer (ONL), inner nuclear layer (INL) and the ganglion cell layer (GCL) without any Gomori stain. Retinal layers appear to have retained the green Gomori at 4 h in comparison to other time-points. In addition, based on the distribution of the dark Gomori stained (FCF green) which might be indicative of collagen fibre, the distribution of collagen (green/blue) appears to be localized to areas that corresponded with the outer nuclear layer (ONL), inner nuclear layer (INL), and ganglion cell layer (GCL). In addition to collagen, erythrocytes (red) were positively identified at all the time points (0.5 h, 4 h and 24 h), which may further add weight to the presence of viable red blood cells, thereby corroborating the presence of retinal vessel integrity (Garvey et al 1996). Sections were not counterstained with H & E in order not to mask any positivity for collagen but proper identification of Gomori positivity (green) may have been masked by poor image resolution.

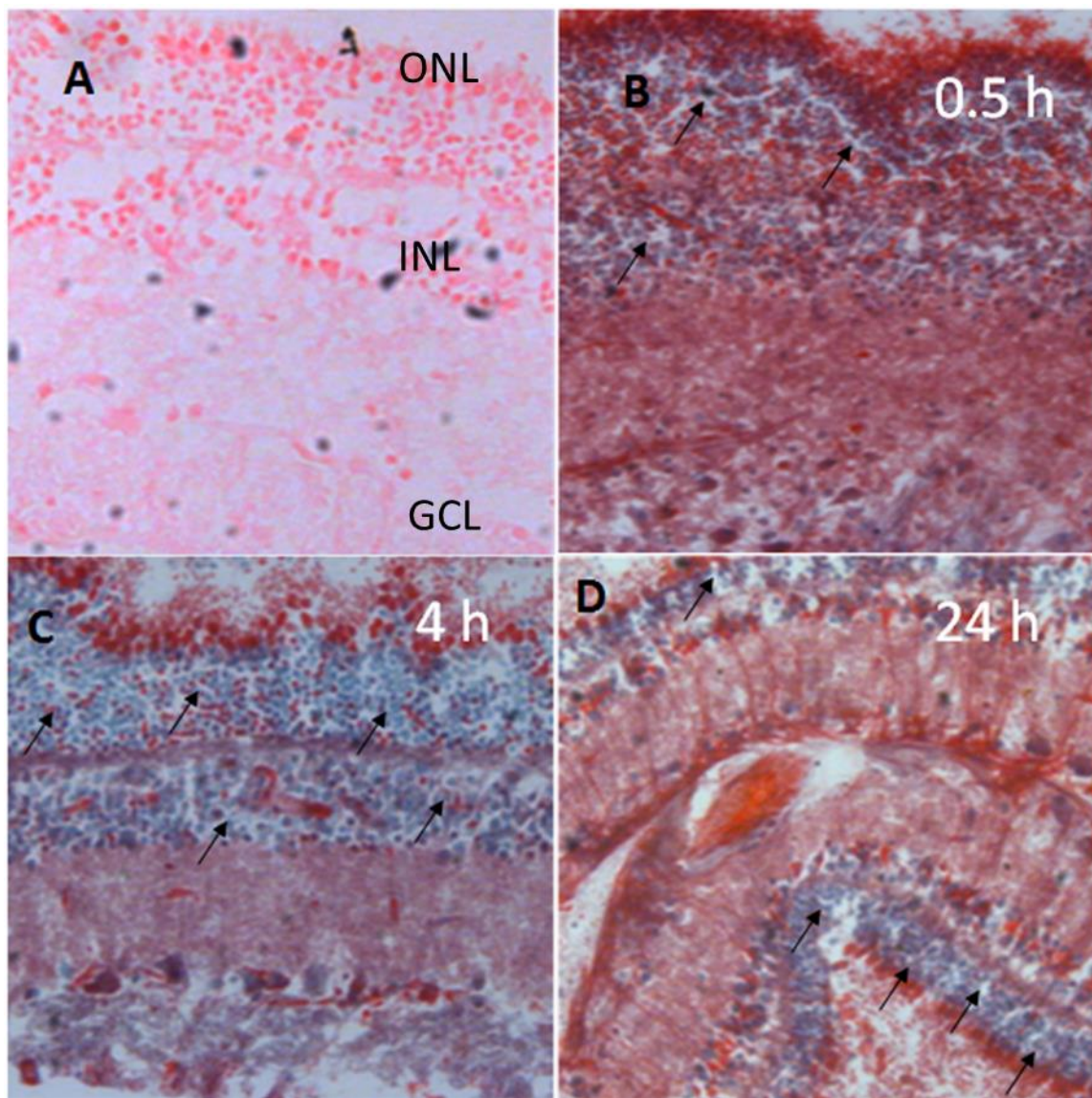


**Figure 3. 4 Representative modified Gomori results**

Selected micrograph of retinal explant sections at 0.5 h (B), 4 h (C) and 24 h (D) and unstained section (A) (control) counterstained with eosin to reveal cytoplasmic details. Dark stained Gomori may indicate structural collagen (FCF greenish) since sections were not counterstained with H & E in order not to mask any positivity for collagen, red blood cells (erythrocytes) (red), cytoplasm (red). Therefore the dark stained components of the Gomori sections might be indicative of collagen-fibre positivity but proper delineation of the FCF green stain may have been limited by the poor resolution of the images. Magnifications 400X. Scale bar 500µm

The functional viability of the explant vessels was demonstrated with contractile responses to KCl and Ang II. To illustrate the concept of contractile response, a selected retinal explant vessel at 24 h with a baseline diameter of 17  $\mu\text{m}$  before treatment with KCl, contracted to less than 16  $\mu\text{m}$  after KCl stimulation with 80 mM KCl (fig 3.5).

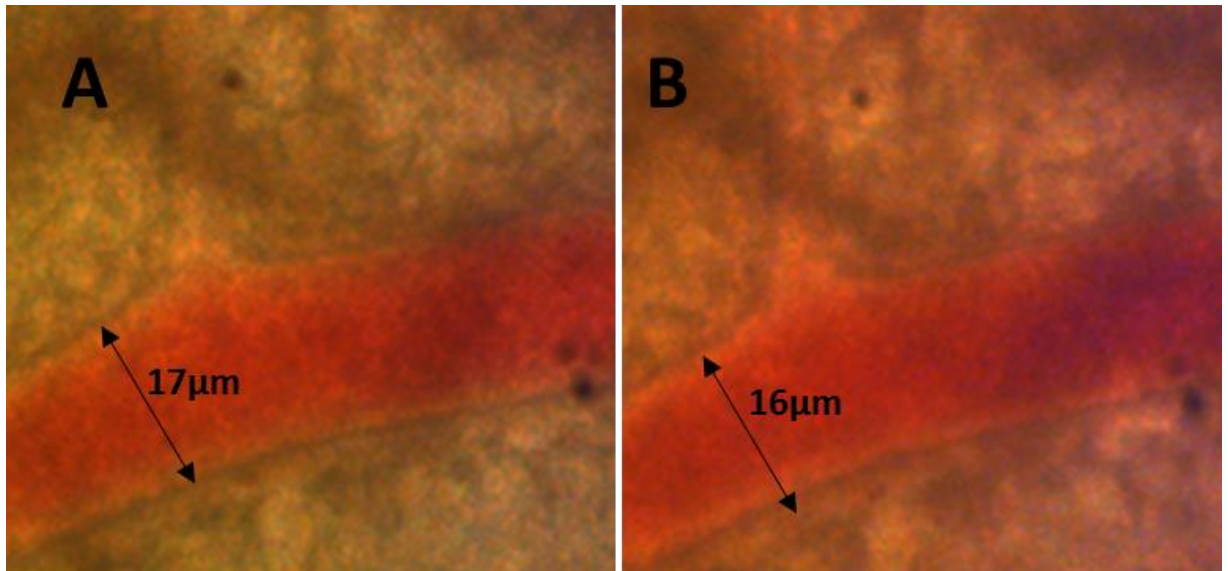


**Figure 3.5 Illustration of contractile response (KCl)**

Retinal explant vessel at 24 h responded to KCl evidenced by contractile response, which caused a reduction in the site measured from 17  $\mu\text{m}$  to less than 16  $\mu\text{m}$ . Final KCl concentration in the culture plate was 80 mM. Images were taken with a 10X objective lens.

Representative plot profiles of contractile responses to KCl (fig 3.6) and Ang II (fig 3.7) are presented to further illustrate contractile response. The y-axis is the Gray value which is the sum of all the pixels within the area measured and reflects the intensity, whilst the x-axis (distance in pixel) is a measure of the vessel diameter (in pixels which can be related to the actual diameter) by converting with a global scale at the magnification taken. For the purpose of illustration, the distance (in pixels) is used here, although the later results are analysed with diameter in microns. The profiles begin from the left (start) and end at the right ("End"). There was an inward shift in the distance (pixel) after stimulation with both KCl and Ang II versus their respective controls ("Before treatment") at 24 h. Bar plots of the plot profiles presented also demonstrates the vessel diameter decrease after KCl (fig 3.6C) or Ang II (fig 3.7 C) versus their respective controls (vessel dimension before treatment).

The plot profiles were automatically generated from Image J and the differences in the Y-axis scale might be reflective of the change in the vessel diameter post KCl addition as illustrated in the bar plot. In the Ang II result (fig 3.7), the scales remained the same because the effect of contractile effect (change in vessel diameter, less than 10 pixel units) was not as pronounced as the KCl effect (approximately 50 pixel units change). These representative plot profiles and their corresponding bar charts were further examples to illustrate contractile profiles, hence statistical analyses are not applied at this stage except that the mean and SD (error bar) were reported as shown.

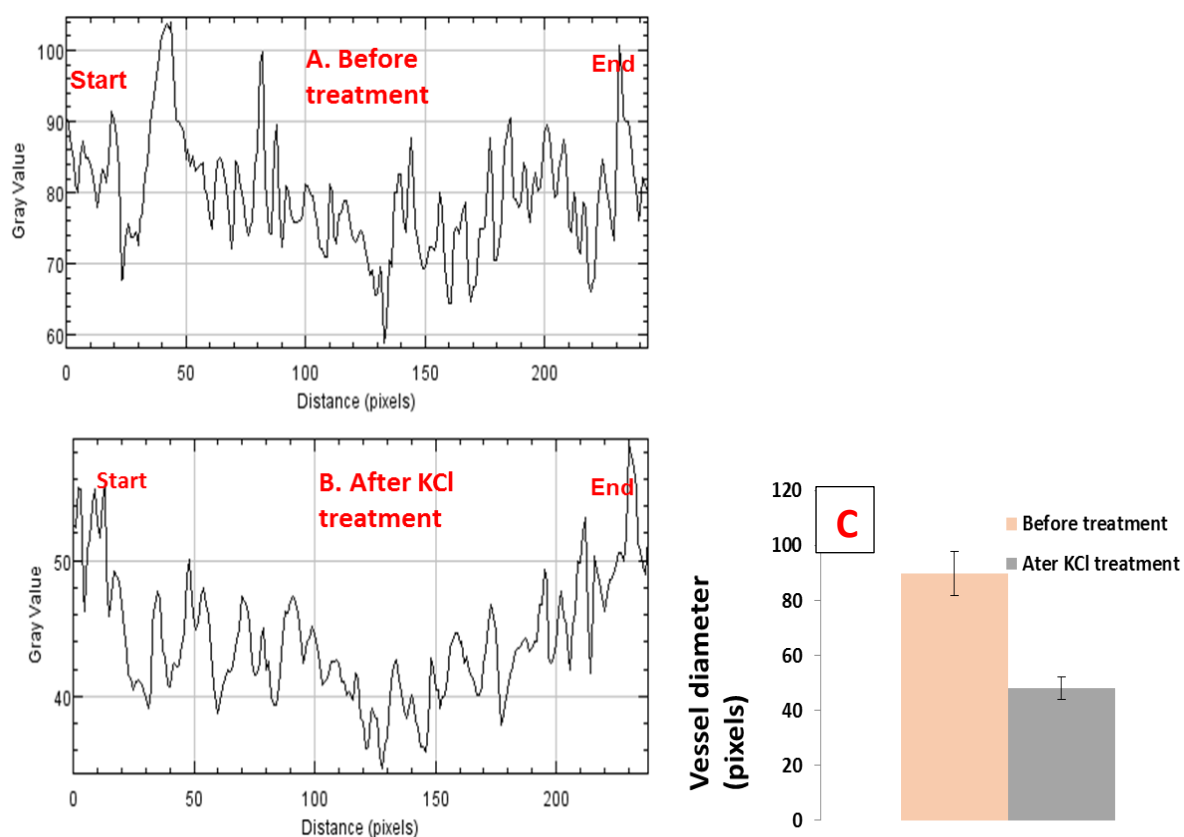


**Figure 3. 6 Representative plot profiles (KCl) at 24 h**

The distance in pixel (x-axis) showed an inward shift with the addition of KCL (B) in comparison to control (Before treatment) (A). Plot profile showing decrease in vessel diameter after KCl versus before and after treatment is shown with a sample bar chart, C. The plot profiles were automatically generated from Image J and the differences in the Y-axis scale might be reflective of the change in the vessel diameter (decrease) post KCl addition as shown with the bar plot. Representative bar chart is mean  $\pm$  SD.

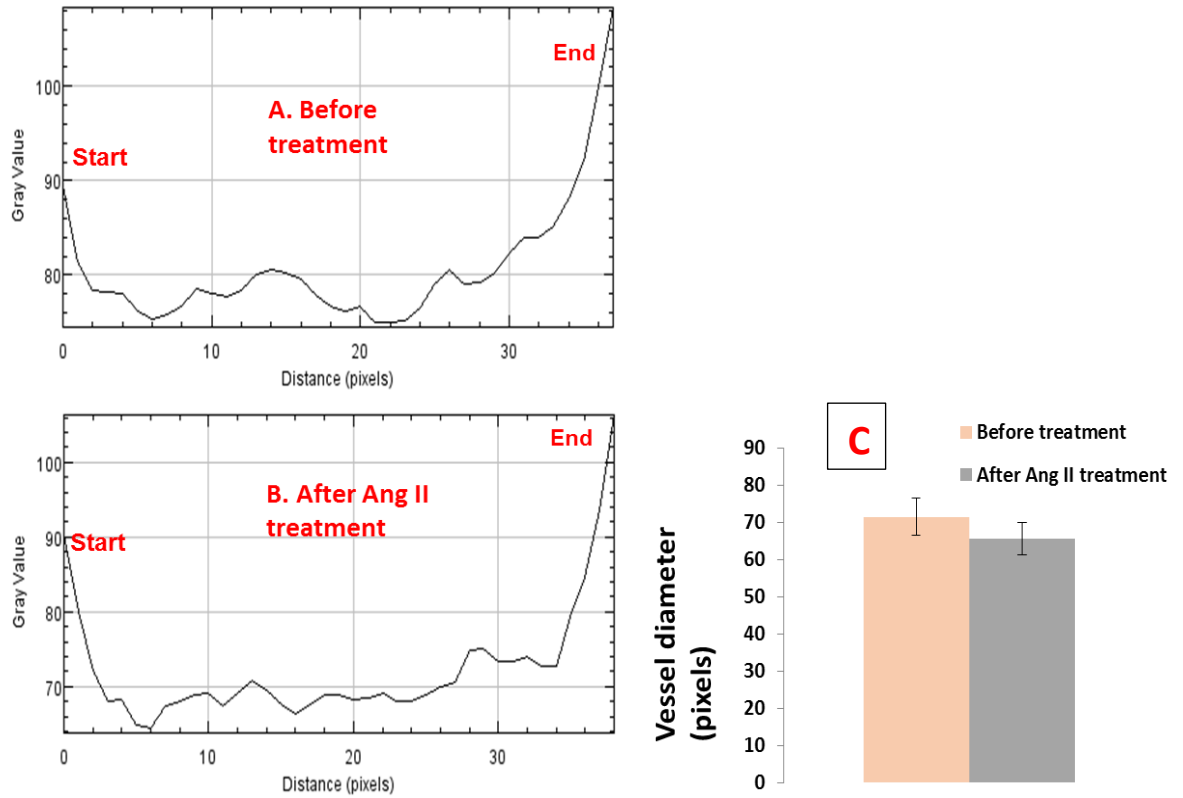


**Figure 3. 7 Representative plot profiles (Ang II) at 24 h**

The distance in pixel (x-axis) showed an inward shift with the addition of Ang II (B) in comparison to control (Before treatment) (A). Decrease in vessel diameter after Ang II versus before treatment is shown with the bar chart, C. In the example above, the Ang II effect (change in vessel diameter) did not appear as pronounced as the KCl effect. Representative bar chart is mean  $\pm$  SD.

A total of 24 retinal vessels were tested with KCl (n = 8) and Ang II (n = 16) in n = 8 independent experiments. Responses were characterised as decrease (contraction) or increase (dilation) in vessel sizes relative to baseline (i.e. control). Summary of retinal vessel functionality by contractile response is presented with fig 3.8. The data in fig 3.8 represents change in vessel diameter ( $\mu\text{m}$ ) (extent of contractile response or effect) measured from video recordings of selected vessels relative to the baseline (control) determined using equation 3.2. Original size at baseline (A) was subtracted from vessel size after treatment (KCl or Ang II) (B). The difference was divided by the original size (A) and expressed as a percentage (%).

$$\frac{\text{Size after treatment (B)} - \text{Original size (A)}}{\text{Original size (A)}} \times 100$$

-----Equation 3.2

The large SD associated with the data might be reflective of differences in pixel intensities across the selected vessel as well as variations associated with movements/agitations in the culture plates picked up during recordings. The average sizes for vessels used for KCl effect determination were  $35 \pm 19 \mu\text{m}$  (0.5 h) and  $27 \pm 15 \mu\text{m}$  (24 h), and for Ang II;  $72 \pm 18 \mu\text{m}$  (0.5 h) and  $69 \pm 7 \mu\text{m}$  (24 h). Thus, the high variability in responses may have been due to the use of vessels of various diameters. Moreover, distinction was not made of the type(s) of vessels or site (s) of treatment administration which could impact on the level or even the absence of response.

However, nearly 70% (16 out of 24) of vessels tested showed contraction in response to KCl and Ang II which suggests functional viability. A total of 8 vessels (33%) showed increase in size in diameter after treatment relative to the control. KCl appeared to elicit more pronounced effect versus Ang II, although the effect was not statistically significant ( $p > 0.05$ ) due to large standard deviations (SD). Since contractile response on Image J is measured by the differences in pixel intensities across a selected vessel, the large SD may be reflective of the differences in pixel intensities (grayscale) between adjacent ends of a vessel. Thus areas in the outer walls of a vessel may be lower in pixel intensity due to the lighter depth of red blood colour versus areas in the middle of the vessel. Data are reported as averages sizes  $\pm$  SD.

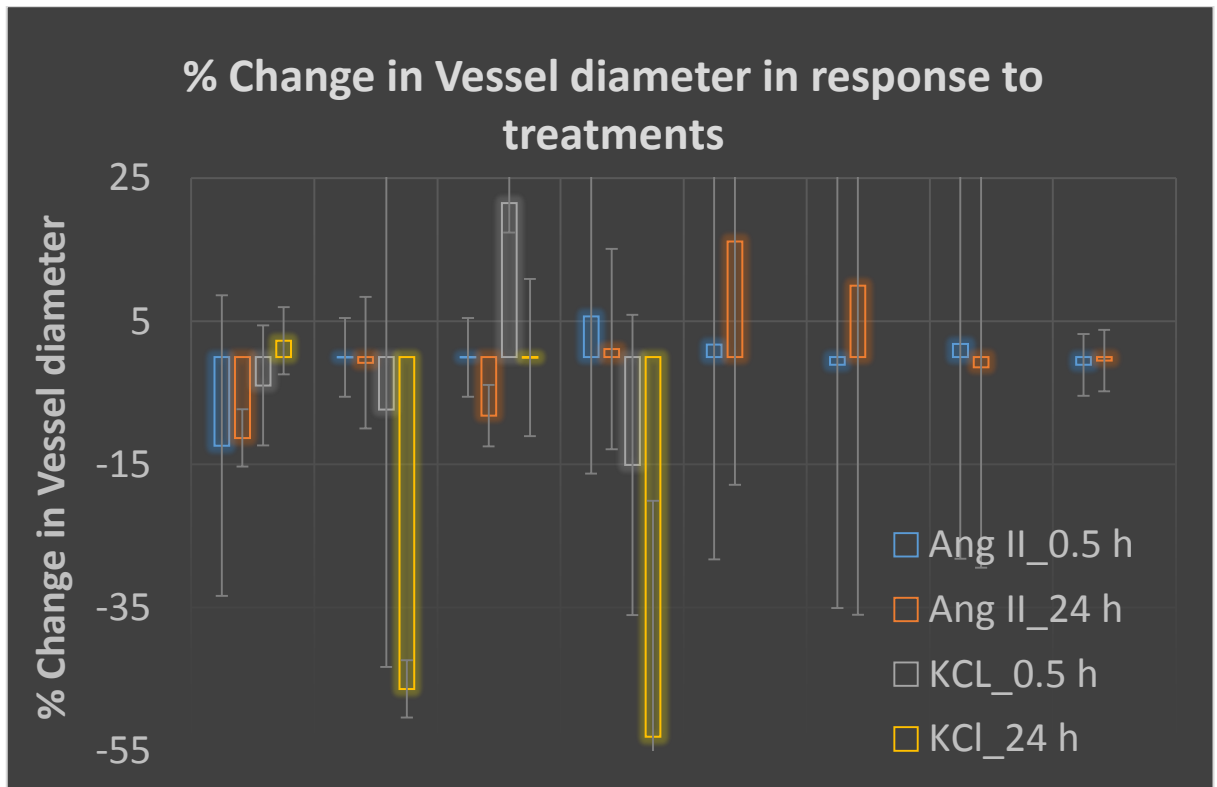


**Figure 3. 8 Functional viability (KCl/Ang II) at 0.5 h and 24 h**

Data representing video recording of change in vessel diameter following addition of Ang II or KCl. Large SD associated with responses might be due to differences in pixel intensities across the selected vessel as well as variations associated with movement/agitation picked up during recordings. Also the variability in responses may be due intrinsic due to the differences in the vessel sizes/types which may have impacted on the level/absence of responses. Nearly 70% of explant vessels showed contractile responses to KCl or Ang II at 0.5 h and 24 h relative to controls. From the plots, the effect with KCl appears to be more versus to Ang II. Profiles are representative of  $n = 8$  for KCl and  $n = 16$  for Ang II,  $n = 24$  independent occasion and is representative of  $\text{mean} \pm \text{SD}$ .

Taken together, explant vessel viability and functionality during the period of culture was satisfactorily demonstrated with contractile responses to KCl and Ang II.

### 3.3.2. Hyperbaric oxygen model

Gas pressure conversion to voltage (mV) was successful and sample traces of voltage in millivolts (mV) at 1 ATA and at 2.2 ATA are shown (fig 3.9, A) from which the pressure-voltage (mV) relationship (B) was derived. Average ( $n = 6$ ) voltage value at 1 ATA and 2.2 ATA were  $5.5 \text{ mV} \pm 0.0$  and  $15 \text{ mV} \pm 0.0$  respectively (B). To demonstrate consistency, measurements of  $n = 22$  were taken (fig 3.9, C). Average voltage (mV) at 1 ATA and 2.2 ATA were  $6 \text{ mV} \pm 0.0$  and  $15 \text{ mV} \pm 0.0$  which was consistent with the earlier validation with no significant variation seen between the two validations ( $p > 0.05$ ). HBO procedure required gas pressure cycling between normoxia and hyperoxia, and the sensitivity of the pressure sensor to gas pressure cycling was demonstrated (D).



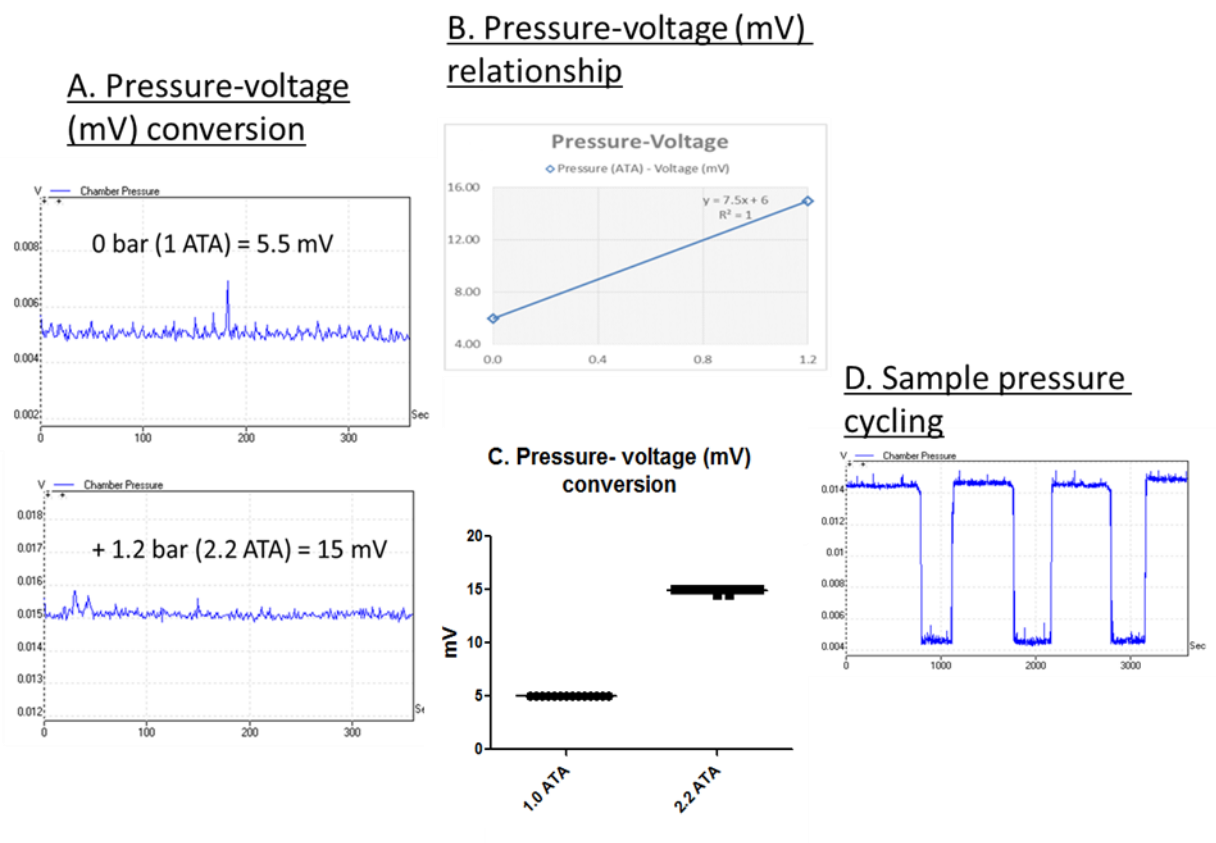


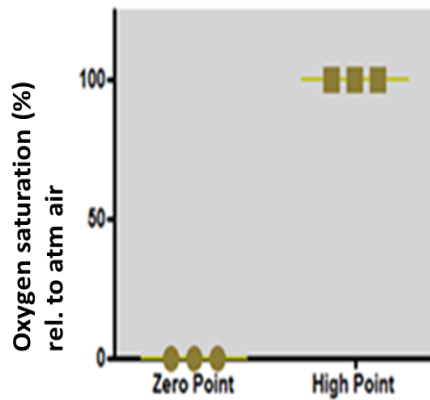
**Figure 3. 9 Pressure-Voltage conversion**

Gas pressure at 1 ATA and 2.2 ATA were converted to voltage (in millivolts) with a Honeywell gauge gas pressure sensor. Voltage (mV) measurements were assessed prior and during experiments to ensure consistency using the PicoLog voltage traces. Pressure to voltage conversion was not significantly different between initial validation and tests ( $p > 0.05$ ). Cycling of pressure was possible as shown in the figure (D). Initial pressure validation was undertaken on six independent occasions. Further pressure-voltage validations were repeated  $n = 22$ .

Electrodes for the oxygen meter were calibrated at high point (100%) and zero point (0%) (fig 3.10 A). Oxygen saturation (%) relative to atmospheric air as measured with a Strathkelvin oxygen meter (v782) in air bubbled distilled water were  $68\% \pm 1.3$  (control), and increased to 165% with the addition of 95% O<sub>2</sub>/5% CO<sub>2</sub> gas (hyperoxia) at 1 ATA, and increasing further to  $1200\% \pm 151$  ( $p < 0.0001$ ,  $n = 3$ ) when pressure was elevated to 2.2 ATA. These % saturation equates to 320mmHg (control), 780 mmHg (95% O<sub>2</sub> at 1 ATA) and 5700 mmHg (HBO) partial pressures of oxygen (Pao<sub>2</sub>) at sea level (Hodges et al 2003). Oxygen saturation was significantly higher in 95% O<sub>2</sub> bubbled distilled water at elevated pressure of 2.2 ATA versus 1 ATA ( $p < 0.001$ ), and air bubbled water at 1 ATA (control) ( $p < 0.0001$ ). In converse, oxygen saturation was not significantly higher ( $p > 0.05$ ) in 95% O<sub>2</sub> bubbled distilled water versus air (21% O<sub>2</sub>) bubbled water ( $p > 0.05$ ). This demonstrated that elevated pressure (2.2 ATA) increases oxygen dissolution versus 1 ATA at constant temperature of 37°C.

The average time ( $n = 3$ ) required to flush the chamber with relevant gas at 1 ATA or 2.2 ATA was 2.2 mins  $\pm 0.3$ , which was rounded up to 3 mins. This informed the time taken for the chamber to be saturated with the relevant gas for all experiments.

### A. Oxygen meter calibration



### B. Chamber oxygen saturation

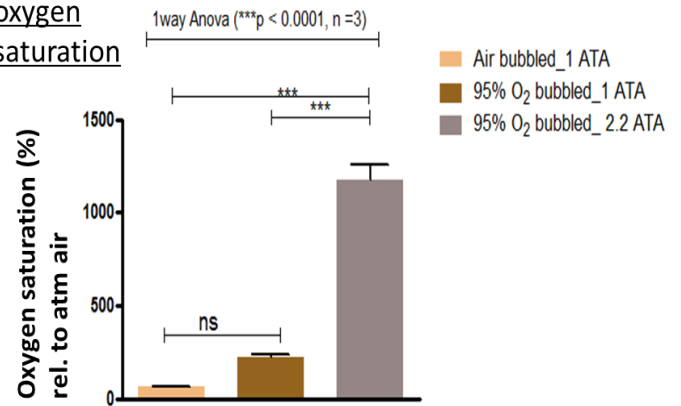


**Figure 3. 10 Oxygen meter calibration and saturation**

Oxygen meter (v782) was calibrated at zero (0%) and high point (100%) as recommended by manufacturer (Strathkelvin). Oxygen saturation in chamber was measured in three independent experiments. Oxygen saturation was significantly higher in 95%bubbled distilled water at 2.2 ATA in comparison to controls; 95% O<sub>2</sub> bubbled water at 1 ATA ( $p < 0.0001$ ) and air-bubbled water at 1 ATA ( $p < 0.001$ ). Data is representative of  $n = 3$  independent validations. Data is representative of mean oxygen saturation (%)  $\pm$  SD.

Average pH ( $n = 3$ ) of HDMEC incubated media harvested after 120 mins of incubation of HDMEC in hyperbaric conditions; HBO and hyperbaric pressure were  $7.3 \pm 0.1$  and  $7.4 \pm 0.1$  respectively versus controls; bench top incubator ( $7.4 \pm 0.1$ ) and a normal 5% CO<sub>2</sub> incubator ( $7.1 \pm 0.1$ ). The pH at all conditions; HBO, hyperbaric pressure and bench top incubator were higher in comparison to normal 5% CO<sub>2</sub> incubator, but these differences were not statistically significant ( $p > 0.05$ ,  $n = 5$ ) at 95% confidence level.

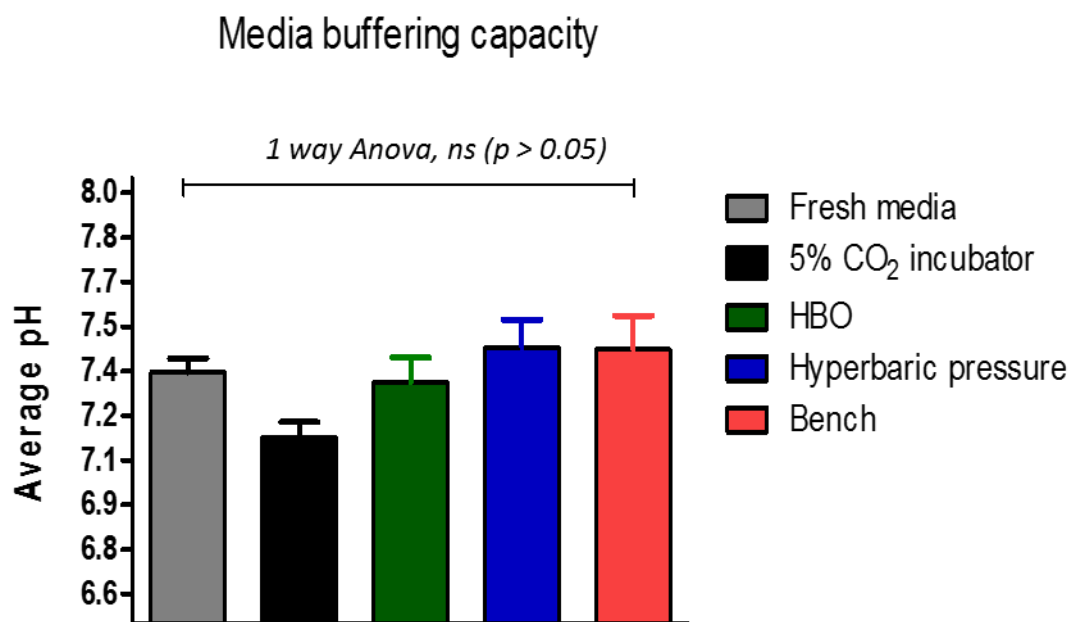


**Figure 3. 11 Media buffering capacity**

Media pH harvested from HDMEC incubated media after 120 mins of incubation in HBO, hyperbaric pressure, controls; bench top incubator and a normal 5% incubator were not significantly different ( $p > 0.05$ ) and although media pH of 5% incubator was lower versus the rest of the samples, it was not statistically different ( $p > 0.05$ ). Data is representative of  $n = 3$  independent validations and it is representative of mean  $\pm$  SD.

Average temperature for internal (inside chamber) and external (within the incubator housing the chamber,  $n = 5$ ) were  $37^{\circ}\text{C} \pm 0.0$ , and  $37^{\circ}\text{C} \pm 0.1$  respectively and no significant difference was seen ( $p > 0.05$ ).

### 3.4. Discussion

Anchorage is vital for retinal tissue and vessel viability (Discher et al 2005). Here, provision for a biomechanical scaffold (anchorage) to preserve retinal tissue and vessel integrity was made with agarose-collagen three-dimension (3D) bilayer matrices within which whole retinal tissues were embedded and cultured as explants. This method of culture was employed to reduce retinal degradation due to rapid gliosis which occurs in free floating retinal cultures (Taylor et al 2014, Kaempfer et al 2008, Kobuch et al 2008, and Fernandez-Bueno 2008).

Circulation and innervations ceases upon the separation of the ocular globe from the main retinal blood vessels and the optic nerve, which will impact on tissue/cellular oxygen availability (Ferrer-Martin et al 2014). Thus, oxygen availability to explants is a critical need in the absence of circulation. Oxygen availability within matrices was successfully validated. Based on the results obtained, matrix oxygen saturation (%) at 0.5 h and 24 h were comparable to their respective controls (media) ( $p > 0.05$ ). This showed the matrices did not pose a significant barrier/retardant to oxygen availability relative to the prevailing atmospheric oxygen levels. Matrix oxygen saturation (%) expressed as  $P_{aO_2}$ , at 0.5 h and 24 h were 57 mm Hg and 76 mmHg respectively. These values are higher than tissue and retinal compartments oxygen levels; inner segment of photoreceptors (0-5 mmHg), which goes to up to 20 mmHg in light and inner retinal oxygen is 20 mmHg (Yu and Cringle 2001, Wangsa-Wirawan and Linsenmeier 2003). Although the absence of circulation in the explant might impact global retinal circulation in explants and consequently circulating oxygen supply for vessels and tissues, the matrices are not likely to perturb in-vitro atmospheric oxygen availability to the retinal tissues based on the determined oxygen saturation (%) within matrices. Whilst matrix oxygen content was measured as part of the validation, matrix oxygen saturation was not measured during exposure to HBO treatments. However, since HBO is known to increase oxygen dissolution, it is likely that HBO will increase matrix oxygen content but this would have to be ascertained with further studies.

Morphological evidence showed retinal tissue preservation for more than 48 h in comparison to controls (2D) cultures. In 2D cultures, retinal tissues showed early (within 24 h) tissue and vessel disintegration which was exaggerated with time. This suggested the provision of a 3D environment enhanced retinal tissue preservation when compared to 2D culture which appears to be consistent (Knott et al 1999, Discher et al 2005, Taylor et al 2014). In future, it might be useful to delineate the mechanisms leading to dampened gliosis in retinal explants as a result of the agarose-collagen 3D matrix approach. Retinal explant cultures have been maintained for more than 2 weeks (Knott et al 1999, Caffé et al 2001). In these studies, the provision of a 3D environment was essential to the experimental design, which further illustrates the argument here of the beneficial role of the agarose collagen matrix, although the maintenance (48 h) of the matrix here pales in comparison to the aforementioned works. ECM proteins such as collagen are important for key endothelial cell functions such as proliferation, differentiation, adherence, and cell-cell communication (Stendahl et al 2009 and Ulrich et al 2010, and Taylor et al 2015). It is likely the inclusion of collagen in matrices contributed positively to the longer preservation of explants on 3D matrices versus 2D.

Gomori (dark/green) stained sections of retinal explants at 0.5 h, 4 h, and 24 h but more so at 4 h may indicate collagen incorporation from matrix into retinal tissues relative to control (unstained retinal section). In addition, Gomori stained collagen appeared to be associated with areas corresponding to the ONL, INL and GCL of the retina. Furthermore, erythrocyte (red) appeared to co-localise with the areas of the retina which stained positive for collagen, highlighting the likelihood of collagen uptake via vessel networks. It will be useful in any future studies to verify collagen uptake from matrices into retinal layers and to show any functional relevance of collagen uptake e.g. inclusion as ECM component by staining explant sections with primary antibodies such as vinculin to check for focal adhesions between matrix collagen and retinal cytoskeleton.

Routine Haematoxylin and eosin (H and E) histological stain is used for retinal layer identification (Knott et al 1999 and Caffé et al 2001). When stained with H and E, the retina is a layered structure; the outer nuclear layer (ONL) containing the cell bodies of photoreceptors (rods and cones), the inner nuclear layer (INL), and the ganglion cell layer (GCL). These three nuclear layers are separated by two synaptic (plexiform) layers; the outer plexiform layer (OPL) lies between the ONL and the INL and the inner plexiform layer (IPL) which separates the INL and GCL (Gregg et al 2013). Therefore, the results of Hand E stained retinal sections which revealed clearly defined retinal layers are consistent with the typical retinal layered structure previously described (Taylor et al 2013, Knott et al 1999, Kaempf et al 2008, Kobuch et al 2008, and Fernandez-Bueno et al 2008). This result further consolidated the earlier observation with a light microscope and strengthens the hypothesis that culturing retinal tissues as explants on agarose-collagen matrices preserves retinal tissue integrity. Early demise of the photoreceptors and physiological thinning of the ganglion cell layer (GCL) occur as a result of blood flow cessation and nerve connection severance post sacrifice (Gancharova et al 2013, Thangaraj et al 2011). Phenomenon such as thinning of the GCL was not seen within the time points under experiment in this study. However, observation was made of necrotic (dark-stained) cell-bodies associated with the area of the photoreceptor layer at 24 h in the vicinity of the photoreceptor – RPE (retinal epithelium) boundary. It is likely that trauma associated with excision of the retinal tissue from the RPE contributed to photoreceptor damage in the segment with necrotic like dark-stain cell bodies.

Explant vessel functionality was satisfactorily demonstrated with a depolarising agent, KCl and a receptor specific agonist, Ang II. Nearly 70% (16 out of the 24 vessels) tested contracted in response to KCl or Ang II, whilst a total of 8 vessels (33%) showed increase in vessel sizes after treatment relative to control. In addition, more than 33% of the contractile responders were of effect sizes  $\geq 10\% \pm \text{SD}$  which is regarded as substantial effect. In general, Ang II appeared to elicit a lesser effect in comparison to KCl. In addition, its effect was very variable and it is likely Ang II response is much more complex in comparison to KCl. In pigs, Ang II is found in the Muller cells, retinal vessel endothelial cells, ganglion cells, photoreceptor cells, sub retinal fluid, vitreous fluid and choroid (reviewed in Choudhary et al 2017). Hence, Ang II response could have been elicited in any of these cells within the porcine retina, although only vessel associated effects were examined in this instance.

Ang II elicits most of its well-known vascular effects including vasoconstriction through its well-known receptor, angiotensin receptor 1 (AT<sub>1</sub>R). On the other hand, AT receptor 2 (AT<sub>2</sub>R) is not well defined but it is proposed to oppose the actions of the AT<sub>1</sub>R contributing to vasodilatory effects rather than vasoconstriction (reviewed in Choudhary et al 2017). Therefore, theoretically vasoconstriction response by AT<sub>1</sub>R in explant vessels may have been blocked by AT<sub>2</sub>R. Although the distribution of AT<sub>1</sub>R and AT<sub>2</sub>R in pig retinal blood vessel is not well defined, in human retina, AT<sub>1</sub>R is more abundant and appears to be more associated with blood vessel responses than AT<sub>2</sub>R (Senanayake et al 2007, Choudhary et al 2017). Furthermore, Ang II effect is associated with the release of endothelial derived relaxing factors (EDRFs) such as NO which exhibits vasodilatation effect. Thus the possibility of Ang II associated EDRF release leading to vessel size increase as seen with some of the explant vessel is very likely. Moreover, the response of retinal vessels to Ang II is dependent on the site or type of vessel being stimulated (Kawamura et al 2004), with 3<sup>rd</sup> order (17-19µm), and the smallest arterioles, 7-12µm being described as responders, while larger (A2 and A1) arterioles with luminal diameter of  $79 \pm 8\mu\text{m}$  and  $126 \pm 6\mu\text{m}$  are non-responder (Kulkarni et al 1999). Therefore, variability in response may have also accrued from this possibility. More so, the relatively low effect of Ang II in comparison to KCl may be due to the sizes of the explant vessels utilised in this study since the average vessel diameters for Ang II assays; at 0.5 and 24 h;  $71.7 \pm 18\mu\text{m}$  and  $69.2 \pm 7\mu\text{m}$  respectively were larger than the sizes described for responders (Kulkarni et al 1999). Moreover, because distinction was not easily made on the type of vessel being stimulated, it is possible some of the vessels tested were lymphatic, which would not respond to Ang II. These underline the complexity of Ang II response and might explain the large variability.

Taken together, retinal vessel functionality by contractile response of explant vessel was sufficiently demonstrated with the outstanding (nearly 70%) effect with KCl and KCl which may indicate vessel viability and function at the times measured.



HBO therapy is a treatment carried out in diabetic patients with co-existing recalcitrant ulcers. HBO is also indicated for treatment of non-diabetic conditions such as poisoning, autism etc. There are set regimens for its administration and these can vary depending on the local guideline (HBOT Trust 2018, Ritchie et al 2008). Therefore, to replicate clinical HBO procedure in order to understand its mechanisms, validations were necessary to ensure appropriate pressure and oxygen levels were applied in addition to controlling external factors such as temperature and pH which affects oxygen dissolution. It was also important to demonstrate robust gas cycling (i.e. changing from hyperoxia to normoxia) in HBO procedure was achieved without losing hyperbaric pressure (i.e. pressure was maintained at 2.2 ATA).

Based on the results detailed previously in section 3.3.2, the conversion of gas pressure to a measurable and observable property, voltage (mV) was consistent without wide variations (SD 0.0, n = 22). This demonstrated the high sensitivity of the pressure-voltage converter that was used (Honeywell) as well as the relative constancy of the environment under which HBO experiments were undertaken. In vivo, pH and temperature can impact oxygen dissolution (Anaesthesia UK 2018). Therefore, constancy in pH and temperature in the HBO model setting was validated. The results showed no significant variation with respect to temperature and pH in samples (HDMEC) after 120 mins of exposure to treatments; HBO or its single component controls; hyperoxia and hyperbaric pressure versus controls in normal 5% CO<sub>2</sub> incubator (p > 0.05). In addition, the pH measured post HBO ( $7.3 \pm 0.1$ ) /hyperbaric pressure ( $7.4 \pm 0.1$ ) were within acceptable ranges for cell culture similar to the controls ( $7.1 \pm 0.1$ ) (Arora 2013). It likely, the treatments were associated with stress, which may have raised media pH immediately post treatments. However, treatments were not likely to affect media buffering capacity because such raises in pH post treatments relative to control were not significant (p > 0.05). There are studies that have reported on the impact of extracellular/intracellular pH on endothelial cell physiology (Capellini et al 2013). Based on the pH results, HDMEC physiology are not expected to be affected, since the validations established the pH post treatments were not statistically different from the controls.

With respect to validation of the HBO unit, a key observation was that HBO gave rise to significantly higher oxygen dissolution in water in comparison to hyperoxia alone ( $p < 0.0001$ ). While it is appreciated that distilled water posed no barrier to diffusion in comparison to the complex systems of diffusion transport in the human body, this observation highlights a key principle of HBO therapy which is its ability to increase oxygen dissolution (HBOT Trust 2018, Ritchie et al 2008, and Godman et al 2010). Plasma  $\text{PaO}_2$  of up to 1804 mmHg was achieved at 2.5 ATA, which was 10-fold higher than the normal  $\text{PaO}_2$  at sea level (1 ATA) (Hodges et al 2003). Likewise, in this study,  $\text{PaO}_2$  with HBO at 2.2 ATA (5700 mmHg) was significantly 18X higher than the control (air bubbled water) (320 mmHg) at 1 ATA and 7X higher than hyperoxia bubbled water in the absence of elevated pressure at 1 ATA (780 mmHg).

In summary, the retinal explant model was validated, and the integrity of the tissues and vessels were demonstrated. HBO was validated with respect to pressure, oxygen saturation, pH and temperature. Importantly, increased oxygenation with HBO was demonstrated which is consistent (Ritchie et al 2008, Thom 2011, HBOT Trust 2018).

Increased oxygenation is associated with increased production and signalling of reactive species such as ROS and RNS (Thom 2011). Both of these reactive species are implicated in the beneficial mechanisms of HBO (Godman et al 2008, Ritchie et al 2018, Thom 2011), but also are associated with endothelial deregulations as seen in diabetic perturbations (Cai and Harrison 2000, Tiganis 2011). In the next chapter, the effects of increased oxygen and pressure levels in high glucose concentration on the morphology (size) and metabolic activities of human dermal microvascular endothelial cells (HDMEC) were studied.

### 3.5. Limitations

There were wide variations in contractile response assays which may in part be indicative of the differences that are intrinsic, for example due to vessel specific variations; vessel size, vessel type, site of application etc. since the electrotonic responses of retinal vasculature differs based on these factors (Nakaizumi et al 2012). In addition, the method of video capture and limitations with the magnifications of the microscope used limited the possibility of differentiating what vessel types are selected for stimulation in order to elicit response since not all vascular beds are responsive to KCl and Ang II (e.g. lymph vessels), and Ang II associated responses are dependent on the vessel size (type) (Nakaizumi et al 2012). Confounding factors to Ang II induced contraction such as EDRFs or AT<sub>2</sub>R induced antagonism were not controlled or excluded prior to Ang II stimulation. In any future experimental design contractile assay could be performed only on designated vessel type, to reduce inherent variability in response. EDRF or AT<sub>2</sub>R blockade prior to Ang II stimulation might have helped to reduce the variability and complexity in order to appreciate true Ang II effects. The validation of matrix oxygen was not extended to measure oxygen content post HBO, or hyperoxia and hyperbaric pressure as conducted for HDMEC. It is likely this aspect would have provided an insight into the possible role of HBO (and its single constituents) on oxygen dissolution within matrices.

## Chapter 4.0: Endothelial cell size and metabolic activity

## 4.1 Hypothesis

The changing concentration of glucose, oxygen tension and pressure has an effect on human dermal microvascular endothelial cell morphology leading to changes in size and metabolic activity.

## 4.2 Introduction

In chapter 3.0, the protocol and method used for the HBO model development were confirmed to be robust and repeatable. Here, HDMEC were exposed to treatments in the validated HBO chamber in the context of high glucose. Post treatments, the impact of HBO, or its single components on HDMEC morphology or metabolic activity in the context of high glucose was assessed with analysis of HDMEC live images and metabolic activities (relative fluorescent units) (RFU) with Resazurin relative to controls.

The endothelium releases ROS and vasoactive molecules such as Ang II and endothelin -1 (ET-1) in response to mechanical stimuli (shear stress/stretch) (De Keulenaer et al 1998, Schramm et al 2012). Hyperoxia in the context of HBO administration enhances blood oxygenation and increased ROS production is a key mechanism in HBO associated beneficial effects (Thom 2011, HBOT Trust 2018). Therefore, it is imperative to understand the effect(s) of increased oxygenation on endothelial cells which are in immediate contact with increased levels of oxygen and the attendant mechano-associated stimuli (shear stress/elevated pressure).

The physiological functions of endothelial cells are dependent and reflective of their morphology. In static in-vitro culture, ECs exhibit a non-aligned polygonal cobblestone appearance (Phillips et al 1988; Malek and Izumo 1996 Chung et al 2000; Leung et al 2002 and Potter et al 2011). Depending on the stimulus, cultured endothelial cells exhibit cell-specific change in shape and size. In pulmonary vascular beds, size enlargement of endothelial cells occur in response to hyperoxia due to ROS elevation which is associated with an increase in endothelial  $[Ca^{2+}]$  levels and actin cytoskeleton rearrangements (Bowden and Adamson 1974, Crapo et al 1980, Phillips et al 1988, Brueckl et al 2006, Roan et al 2012 and Attaye et al 2017).

On the other hand, in renal and mesenteric microvascular beds, hyperoxia results in a decrease in EC size due to hyperoxia mediated decrease in endothelial nitric oxide (NO) and increase in vasoconstrictors such as cyclooxygenase (Attaye et al 2017). Moreover, hyperoxia-induced retinal vasoconstriction in the human retina occurs via hyperoxia-induced ET-1 upregulation (Dallinger et al 2000). Furthermore, hyperoxia is associated with cerebral vasoconstriction (Floyd et al 2003). The impact of hyperoxia on endothelial cells of dermal origin is not well reported. Therefore, an insight can be gained from this study on the effect of hyperoxia on HDMEC which is of a dermal origin.

The morphological shape of endothelial cells in-vivo is closely related to their location within the vessel lumen. Luminal endothelial cells in areas of high laminar shear stress are elongated and aligned while those in low shear stress areas are randomly orientated (Chung et al 2000, Potter et al 2011). Likewise, endothelial cells in static culture change their polygonal shape and adopt uniform alignment (retracted and smaller in size) in response to increased flow and shear stress, or elevated pressure which has a knock on effect on shear stress (Malek and Izumo 1996). Cell alignment in response to flow or shear stress is common to ECs of all vascular beds (Barbee et al 1994, Malek and Izumo 1996, Chung et al 2000). Increased intra-cellular calcium via tyrosine kinase activity and actin microtubule rearrangement independent of PKC activation is proposed as a mechanism (Malek and Izumo 1996).

Permeability factors including high glucose and inflammatory cytokines also exert influence on endothelial cell morphology (Himmel et al 1993, Malek and Izumo 1996, and Leung et al 2017). In cultured endothelial cells, high glucose induced whole phenotypic change in a glucose dependent mechanism involving PKC $\alpha$  activation (Hempel et al 1997). In vivo (db/db mice), high glucose induced endothelial cell shape to a mesenchymal (spindle) (Peng et al 2016). In addition, ultrastructural alterations in endothelial cells was induced by high glucose (25 mM) in human aortic EC (HAEC) cultured for 1–2 weeks and in (the vasculature of mice and golden Syrian hamsters at 6 weeks and 6 months, respectively after streptozotocin injection have been documented (Simionescu et al 1996, Popov and Simionescu 2006). High glucose associated changes in human vascular endothelial cell contraction and hyperpermeability is proposed to be due to cytoskeleton configuration as a result of hyperglycaemia induced AGE and RAGE/Rho signalling pathway (Hirose et al 2009).

Inflammatory cytokines and endothelium derived factors (EDRFs) such as Ang II and ET-1 are another class of permeability factors which are associated with 'rounding' i.e. retraction and contraction of endothelial cells leading to reduction in EC size (Himmel et al 1993, Malek and Izumo 1996 and Leung et al 2002).

Endothelial cells are quiescent with little change on their metabolic need, but they increase metabolic need when switching from quiescent to vascular sprouting (De Bock et al 2013, Doddaballapur et al 2015). There are not many studies that have investigated the direct effect of hyperbaric oxygen (HBO) on endothelial cell metabolic activity. A HBO associated protective effect on the metabolic activity of immortalized human microvascular endothelial cell (HMEC-1) was shown (Godman et al 2010), which suggested that HBO may be associated with the reversal/modulation of hyperoxia-associated metabolic activity decline in endothelial cells. The likelihood of HBO alleviation of metabolic decline in HDMEC will be tested in this study. In this chapter, the aim is to examine effect (s) of HBO and its single components on the morphology (size) and metabolic activity of human dermal microvascular endothelial cell (HDMEC) in the context of high glucose in comparison to control conditions.

## 4.3 Materials and Methods

HDMEC in low or high glucose HDMEC growth media (MV) were exposed to treatment as previously described in chapter 2 section 2.8. Post treatment, HDMECs were incubated in a normal 5% CO<sub>2</sub> incubator for 4 h and images of live HDMEC were captured and used for size analysis. Full detail of image capture and size measurements are covered in the materials and methods section in chapter 2.0 section 2.9. HDMEC in low or high glucose HDMEC growth media (MV) were also incubated with Resazurin post treatment for 24 h. Prior to carrying out Resazurin assay in experimental samples, control experiments were carried out to determine optimal seeding density and incubation duration. All Resazurin optimisation experiments were carried with HDMEC in control condition in low glucose. HDMEC were seeded in clear 96-well plates (surface area of 0.32cm<sup>2</sup>) at a density of 1 x 10<sup>3</sup>, 2 x 10<sup>3</sup>, 5 x 10<sup>3</sup>, 8 x 10<sup>3</sup>, and 10 x 10<sup>3</sup> per well in 100 µl of HDMEC growth media (MV) according to kit manufacturer's (Cell Signalling Technology, CST) seeding density and HDMEC supplier (PromoCell) recommendations. Blank (no cell) control with 100-µl of media was set up as control. Fluorescence from the no-cell control wells was subtracted from cell-incubated wells to obtain the relative fluorescence units (RFU), an indicator of metabolic activity expressed in x 10<sup>4</sup>. For initial validation to determine optimal cell density per well and incubation time, samples in triplicates were incubated at 37°C in a 5% CO<sub>2</sub> incubator and reached approximately 70% confluence after 48 h. HDMEC were treated with 10µl Resazurin (10X) solution (CST) per well in the dark. Fluorescence was measured at 0, 6, and 24 h using a Synergy HT microplate reader (Biotek) at 530-570nm excitation wavelength and 585-590nm emission wavelength. Results of Resazurin optimisation are presented first in the result section for Resazurin assay (4.4.2) before experimental assay results in the same section. More details of the Resazurin assay are described in chapter 2.0 sections 2.7. In all experiments non-confluent HDMEC were incubated with Resazurin for 24 h. Non confluent HDMEC at cell plating density of 5 x 10<sup>3</sup> were used for Resazurin assay since confluent cultures are associated with senescence.



To determine the effects of treatment on HDMEC sizes (P4-7), photomicrographs of live HDMEC were captured as described in chapter 2 section 2.9. A total of  $n = 40$  photomicrographs from four independent experiment (10 micrographs/experiment) were coded independently (blinded). Before actual measurements, trial measurements with Image J free-hand tool were undertaken and repeated several times on the same cell and/or with several samples until measurements with minimal standard deviations ( $<10\%$ ) were reached. Measurement of coded samples was undertaken by measuring the perimeter (size) around HDMEC with clearly defined borders as shown in fig 4.1 (A) by tracing around the cell with an Image J free-hand drawing tool, as shown in fig 4.1, B (circled for illustration). The identities were revealed post image analysis. Analysis was performed with 1way Anova and Tukey's post hoc test in Graph Pad Prism vs 5.0.

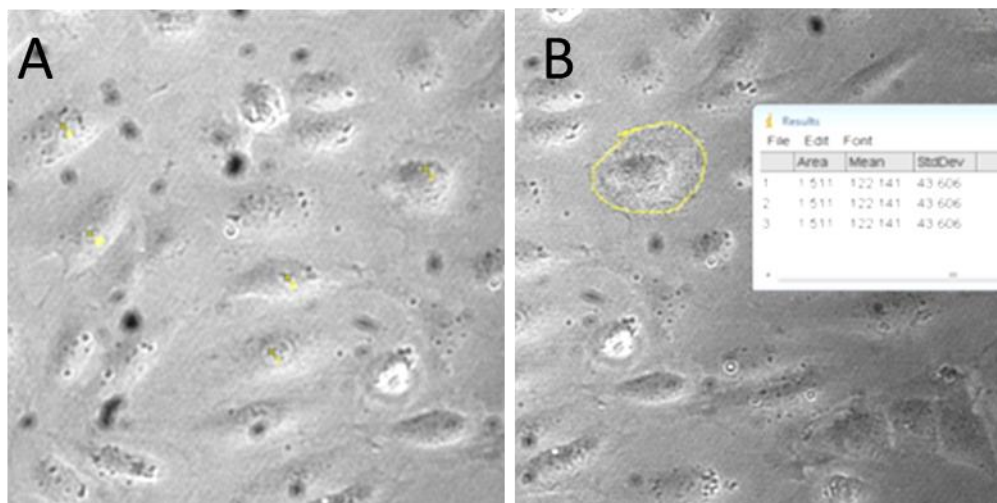


**Figure 4. 1 Illustration of HDMEC size measurement**

K8HDMEC sizes were measured with Image J free hand drawing tool. Marked cells, (A) with visible borders were traced around the perimeter with a free drawing tool (highlighted in yellow) (B). Therefore the values in the result section in microns ( $\mu\text{m}$ ) represents mean values ( $n = 40$ ) measured for cells (HDMEC) for controls and treatment conditions. The values represents the distance around cells rather the diameter or length.

## 4.4 Results

### 4.4.1 Effect of varying glucose concentrations, oxygen tension and pressure on HDMEC morphology and size.

Control HDMEC in low glucose showed typical cobblestone polygonal HDMEC morphology at 4 h (fig 4.2, A). HDMEC in high glucose showed no distinct difference in phenotype relative to low glucose samples. Likewise, HDMEC in HBO displayed typical cobblestone/polygonal morphology relative to controls (fig 4.2, C and D). When hyperbaric pressure alone was applied, HDMEC appeared stretched and retracted around the cell edges (Fig. 4.3, A and B) in comparison to control. However, although these cells in hyperbaric pressure condition exhibited retracted and stretched morphology, their mean sizes were not significantly different from the control samples ( $p > 0.05$ ). In converse, HDMECs in hyperoxia appeared engorged and spread out (fig 4.3, C and D). These morphological alteration post hyperoxia in low glucose was associated with a significant increase in HDMEC size relative to control ( $p < 0.05$ ) (fig 4.4). In the representative images (fig 4.2-4.3), close-up images of single cells have been inserted for all the conditions to better delineate any effect of treatment on HDMEC sizes. For instance, a representative cell in the control condition (insert) has a distance of approximately 1400  $\mu\text{m}$  around it i.e. perimeter/circumference rather diameter or length. This value relates to the size for the cell and reported as mean size ( $n = 40$ )  $\pm$  SEM from four independent experiment.

## HDMEC morphology at 4 h post control condition or HBO

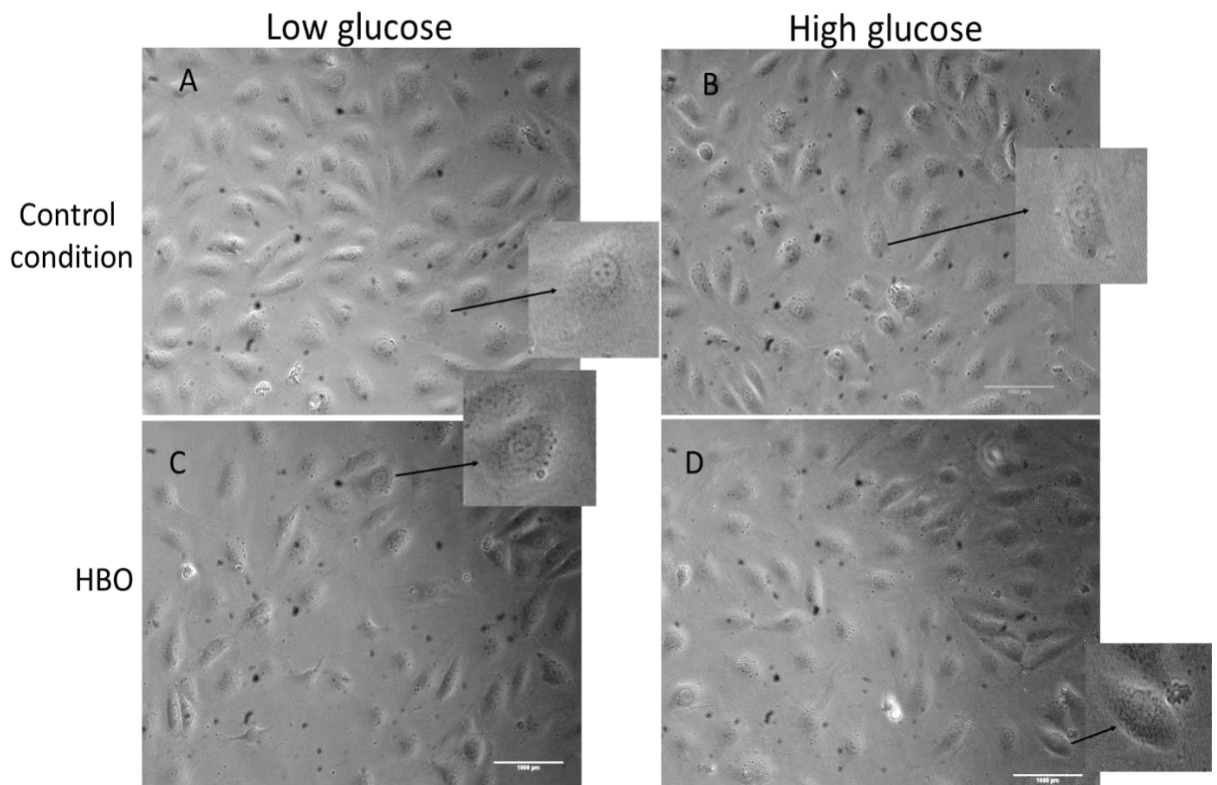


**Figure 4. 2 HDMEC morphology in control and HBO at 4 h**

Live cell image of HDMECs at 4 h post treatment in control condition in low (A) and high (B) glucose showed no distortions from typical HDMEC morphology (see fig 2.1). Similarly, HDMEC exposed to HBO treatment did not show any distortions and remained similar in characteristics (shape and size) to HDMECs in control condition. Representative cell (insert) with cross-sectional area (perimeter) of approximately 1400  $\mu\text{m}$  (this value is the distance around the selected cell which may be reflective of its perimeter/circumference). Images were reduced to 50% of their original size to fit the page. Result represents mean size ( $\mu\text{m}$ ) ( $n=40$ )  $\pm$  SEM from four independent experiments. Scale bar = 1000  $\mu\text{m}$ .

## HDMEC morphology at 4 h post hyperbaric pressure or hyperoxia

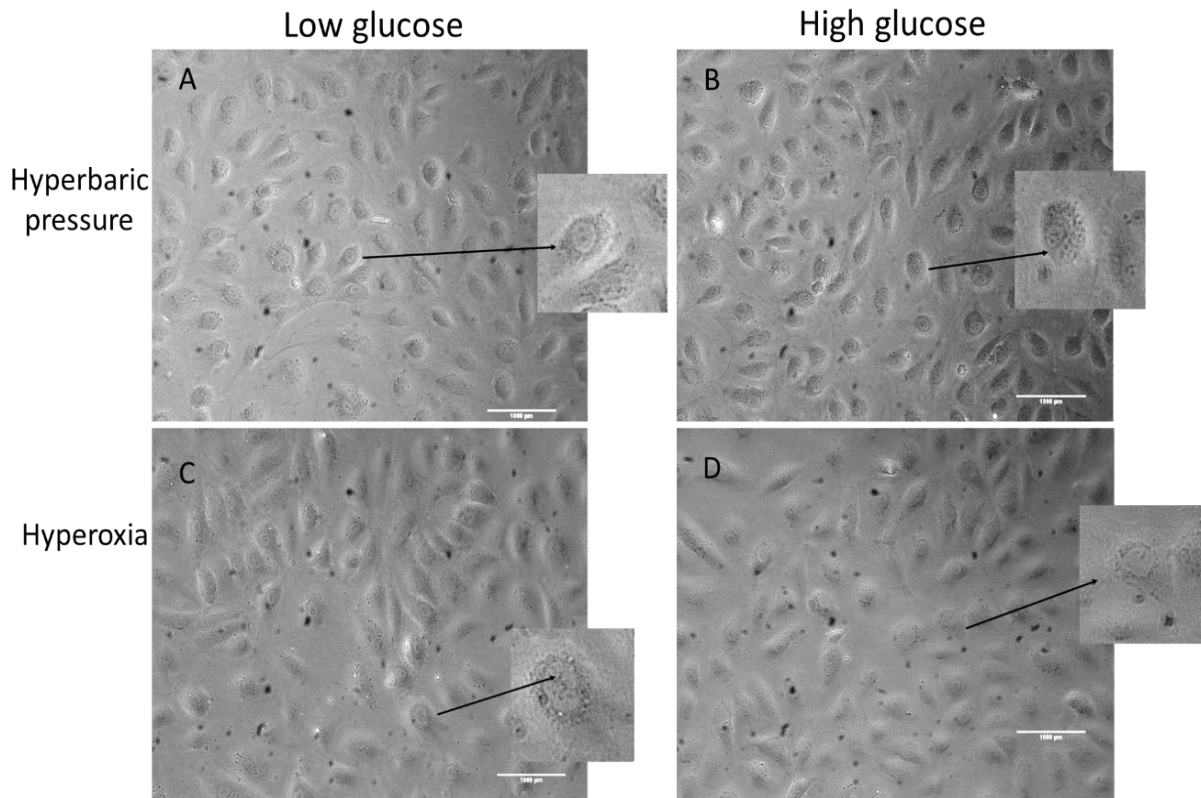


**Figure 4.3 HDMECs morphology in hyperbaric pressure and hyperoxia at 4 h**

Live cell photomicrographs of HDMEC taken 4 h after exposure to hyperbaric pressure in low (A) and high (B) glucose appeared stretched and more rounded in comparison to controls (see fig 4.1, A). On the other hand, HDMECs exposed to hyperoxia in low (C) and high (D) glucose appeared engorged and spread out in comparison to control. Images were reduced to 50% of their original size to fit the page. Result represents mean size ( $\mu\text{m}$ ) ( $n=40$ )  $\pm$  SEM from four independent experiments. Scale bar = 1000  $\mu\text{m}$ .

One-way analysis of variance indicated that mean ( $n = 40$ ) HDMEC sizes were significantly changed between samples ( $p < 0.0001$ ,  $n = 8$ ) (fig 4.4). This value (i.e. size) is the distance around a selected cell which is reflective of its perimeter/circumference, rather than the cell diameter or length expressed as mean sizes ( $n = 40$ ) (see fig 4.1 for illustration). Tukey's post hoc analysis showed the mean sizes of HDMEC in low glucose post hyperoxia were significantly higher in size in comparison to control ( $p < 0.05$ ). In addition, the mean sizes of HDMEC in hyperoxia were significantly higher in comparison to HBO ( $p < 0.05$ ) and hyperbaric pressure ( $p < 0.01$ ). Glucose effect on HDMEC sizes for control or treated samples was not significant ( $p > 0.01$ ), although a pattern of high glucose associated increase in sizes appeared imminent for HDMEC in control and HBO conditions ( $p > 0.05$ ). HDMEC in hyperbaric pressure showed a pattern of decreased sizes which may be reflective of the observed retracted morphology however their sizes were not significantly changed in comparison to control samples ( $p > 0.05$ ).

### Effect of changing glucose concentration, oxygen and pressure level on HDMECs morphology

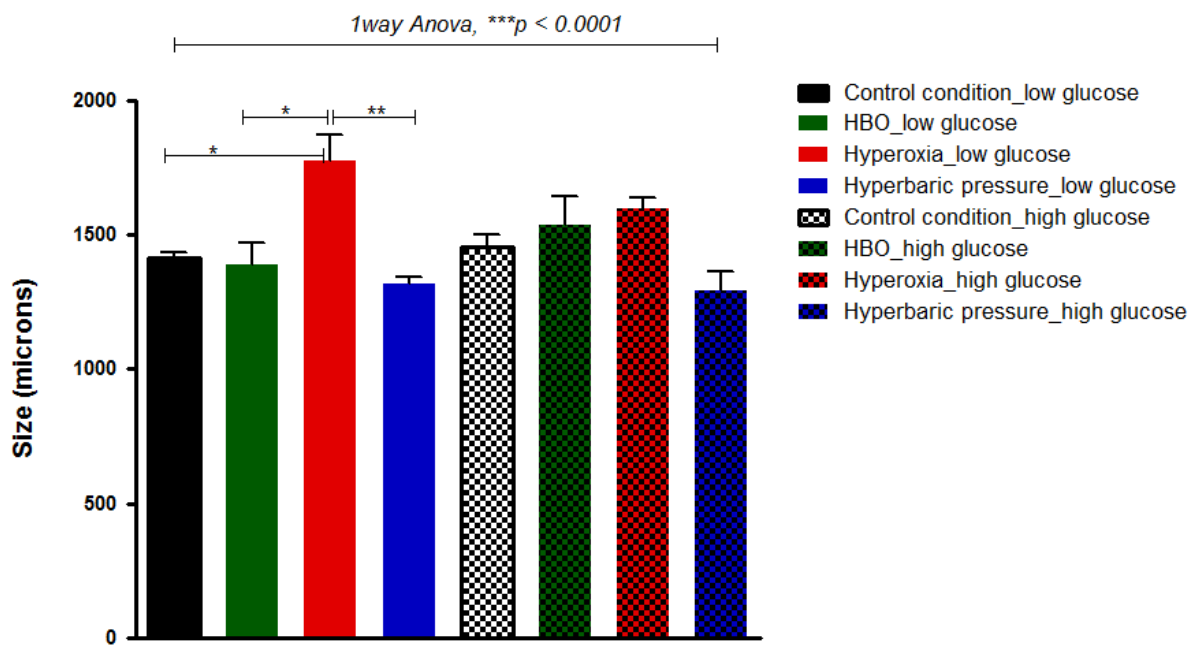


**Figure 4.4 Effect of treatments on HDMECs sizes**

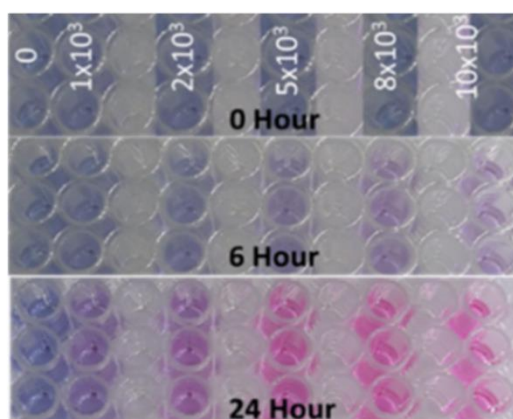
A 1way ANOVA determined significant differences (\*\*\* $p = 0.0001$ ,  $n = 8$ ) between the means of all sample.

HDMEC sizes did not change with respect to glucose concentration for HDMEC in control condition. Similarly following exposure to HBO, no glucose associated changes were seen. HDMEC in HBO and hyperbaric pressure were comparable in size to control condition samples ( $p > 0.05$ ). HDMEC in hyperoxia in low glucose had significantly higher sizes in comparison to control ( $p < 0.05$ ), HBO ( $p < 0.05$ ), and hyperbaric pressure ( $p < 0.01$ ). The values plotted are the mean  $\pm$  SEM distances around the selected cells ( $n = 40$  per sample) which may be reflective of its perimeter/circumference). Result represents mean size ( $\mu\text{m}$ ) ( $n = 40$ )  $\pm$  SEM from four independent experiments.

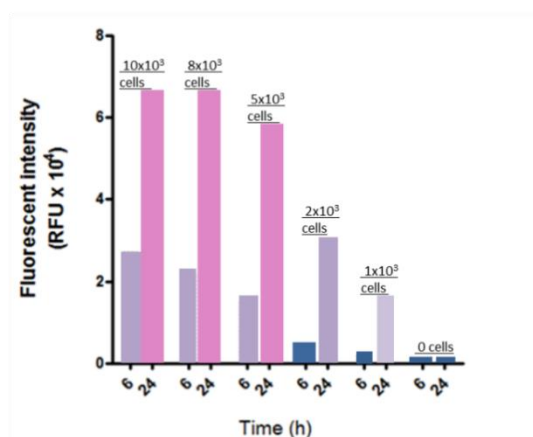
## 4.4.2 Resazurin metabolic activity assay

Results for Resazurin assay optimisation for the determination of optimal seeding density and optimal incubation time are shown in the figure fig 4.5. As shown from the figure, Resazurin detection was highest at 24 h (B) in comparison to 6 h. Maximum colour change was seen after 24 h, with seeding densities of  $5 \times 10^3$ ,  $8 \times 10^3$  and  $10 \times 10^3$  (A), which indicated showed the optimal incubation period was 24 h. These changes were quantified by determining the relative fluorescent units (RFU). Line plots shows a linear change in RFU with increasing plating density which is indicative of a linear conversion of Resazurin in relation to metabolic activity (Ahmed et al 1994), but higher plating densities of  $8 \times 10^3$  and  $10 \times 10^3$  per well were associated with a plateauing in RFU values (C and D), which suggests the conversion of blue Resazurin to pink resorufin at these cell densities was no longer directly proportional. Bar charts are coloured to reflect picture in A. Based on these optimisation, a cell concentration of  $5 \times 10^3$  cells (HDMECs) per well and incubation time of 24 h was used for Resazurin assay. In all validation and experiments including Resazurin experiments, non-confluent HDMEC were incubated with Resazurin for 24 h.

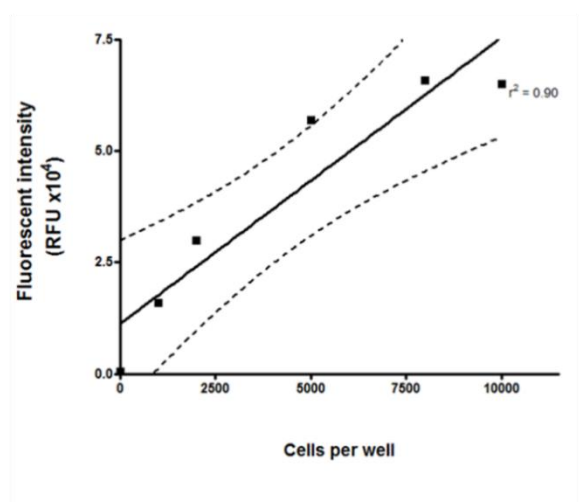
### A. Resazurin conversion



### B. Detection of Resazurin at 6 h & 24 h



### C. Linearity of Resazurin conversion at 24 h



### D. Cell plating density optimization

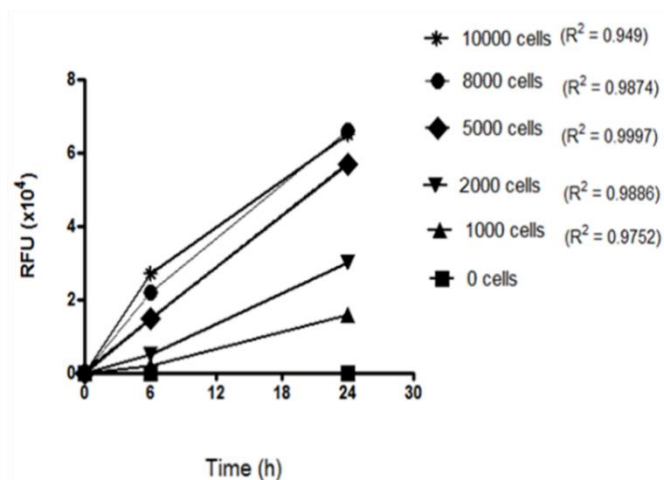


## Figure 4.5 Resazurin assay optimisation

Maximum Resazurin colour change was seen at 24 h (A and B), with a slight colour change at 6 h. Resazurin conversion was quantified as RFU, an indicator of metabolic activity. Plot (B), shows RFU values for different cell densities of HDMEC in control conditions at 6 h and 24 h. Bar charts are coloured to reflect picture in A. Resazurin conversion at 24 h showed linear Resazurin conversion in relation to cell density (C). Higher cell densities of  $\geq 8 \times 10^3$  were associated with Resazurin conversion plateau (D) where there was no longer linear conversion of Resazurin to resorufin. Plating cell density of  $5 \times 10^3$  showed linear conversion and was considered optimal plating density for Resazurin assay.



When data from Resazurin experiment were analysed there were significant inter-batch variations in RFU ( $p < 0.05$ ) between replicates warranting data normalisation. Samples in hyperoxia showed a pattern of decreased metabolic activity as a group in comparison to controls and the rest of the samples. Thus, HDMEC in hyperoxia with significantly larger sizes appeared to have the lowest metabolic activity. Post normalisation, 1way Anova identified differences in mean metabolic activities between samples ( $p < 0.05$ ). Using Tukey's post-hoc analysis, there were no significant differences in mean metabolic activities between all samples in comparison to the control ( $p > 0.05$ ). A Bonferroni's analysis indicated significant reduction in metabolic activities for HDMEC in hyperoxia (low glucose) in comparison to hyperbaric pressure ( $p < 0.05$ ) but it was not significant relative to control ( $p > 0.05$ ) (fig 4.6). Statistically significant glucose effect on metabolic activities was not evident ( $p > 0.05$ ) ( $p > 0.05$ )

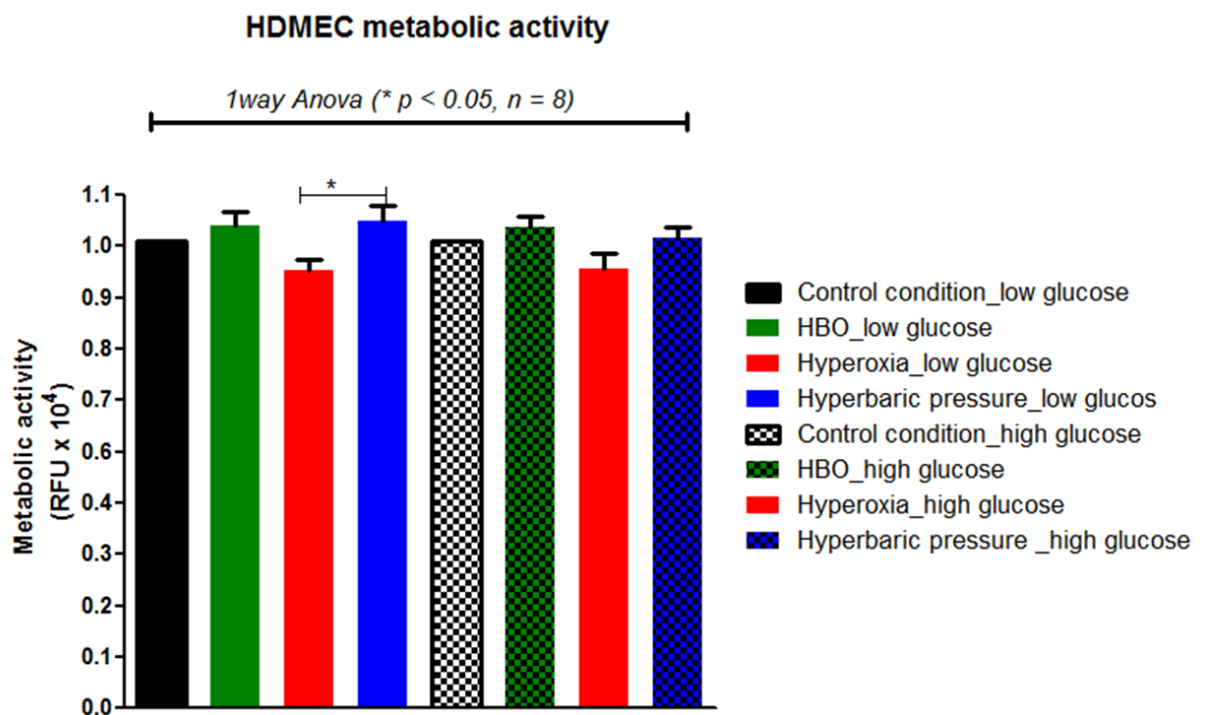


**Figure 4.6 Metabolic activity of HDMEC after normalisation**

HDMEC metabolic activity was changed between samples ( $p < 0.05$ ) based on 1way Anova. Tukey's post-hoc did not reveal significant differences in metabolic activity between samples ( $p > 0.05$ ) but a statistically less stringent Bonferroni's comparison showed significant decrease in metabolic activity for samples in hyperoxia (low glucose) in comparison to samples in hyperbaric pressure ( $p < 0.05$ ), but not to controls ( $p > 0.05$ ). Data is representative of mean (RFU) (5.5 mM: control, HBO, hyperbaric pressure,  $n = 30$ , hyperoxia,  $n = 18$ ) of sixplicates repeated on five (controls/HBO, hyperbaric pressure), or three (hyperoxia) independent occasions.

## 4.5 Discussion

HDMEC is made up of 87% human dermal lymphatic endothelial cells (HDLEC) and 13% blood endothelial cells (BEC). Therefore, the vast majority of HDMEC are of HDLEC origin. HDMEC are approximately 60-100  $\mu\text{m}$  in length and 27-54  $\mu\text{m}$  in diameter (width) (PromoCell). In this study, the total length around selected cells, i.e. perimeter or circumference ( $n = 40$ ) rather than length or diameter (width) were determined to ascertain the impact of treatment on HDMEC sizes (morphology). Hyperoxia (in low glucose) was associated with HDMEC that were significantly bigger in size in comparison to control and HBO ( $p < 0.05$ ), and hyperbaric pressure ( $p < 0.01$ ). In addition, HDMEC in hyperoxia showed a pattern of diminished metabolic activity relative to control ( $p > 0.05$ ). The metabolic activity of HDMEC in hyperoxia was significantly lower in comparison to hyperbaric pressure ( $p < 0.05$ ) but this analysis was based on Bonferroni's analysis, and the data requires more experimental repeats in order to establish a stronger link.

The results here showed sufficiently some previously reported alterations in endothelial cell morphology in response to hyperoxia and elevated pressure (Bowden and Adamson 1974, Crapo et al 1980, and Brueckl et al 2006, Phillips et al 1988; Malek and Izumo 1996 Chung et al 2000; Leung et al 2002 and Potter et al 2011). Hyperoxia associated change in HDMEC sizes appeared to corroborate their enlarged/engorged phenotype of HDMEC post hyperoxic treatment. Although, HDMEC in hyperbaric pressure appeared retracted and rounded morphologically, their altered phenotype was not associated with statistically significant change in their mean sizes relative to control. To further establish the implications of these results, it is important to have more robust experiments, with larger data sets and perhaps longer incubation periods with excellent cell analysis software e.g. CellProfiler<sup>TM</sup> in combination with Bioinformatics.

Theoretically HBO should result in higher ROS or oxygen associated signalling/effect in comparison to hyperoxia since HBO is associated with higher oxygenation (Thom 2011). Yet as seen from this study, hyperoxia and not HBO was associated with significant alterations in HDMEC morphology, with a pattern of dampened metabolic activity. This suggests the effects of hyperoxia alone and the compounded use hyperoxia and hyperbaric pressure (HBO) on HDMEC are distinct and poses pertinent question(s) as to the likely mechanism(s) elicited in hyperoxia in comparison to HBO and vice versa.

It is noteworthy that hyperoxia-associated endothelial cell size enlargement has predominantly been reported in studies of hyperoxia in pulmonary context owing to ROS mediation. Thus in this study, hyperoxia associated size increase in HDMEC is suggestive of ROS associated/mediated effect. But ROS blockade studies are necessary to accurately pin-point ROS involvement. In addition, it is needful to establish downstream mediators that were central to HDMEC size enlargement post hyperoxia. Fundamentally, since HDMEC are dermal in origin, this result represents a new insight on the possible role of hyperoxia on dermal endothelial cell and warrants further investigation to establish its exact effects and mechanisms.

The enzyme 6-phosphofructo-2-kinase/fructose-2, 6-bisphosphatase 3 (PFKFB3) offers a direct link between endothelial cell morphology and metabolic activities (Doddaballapur et al 2015). Decreased expression of PFKFB3 enzyme is associated with a stress-mediated modulation of endothelial cell phenotype (Doddaballapur et al 2015). Hence, inference could be made to the possibility of hyperoxic stress-mediated inhibition of PFKFB3 (decreased expression) and modulation of HDMEC phenotype (size). And because the modulation of HDMEC size post hyperoxia was significantly evident in low glucose, this strengthens the indication of a hyperoxia alone effect. Since PFKFB3 links stress and endothelial phenotype with metabolic activity, it would be worthwhile to examine further the expression levels of this enzyme post HBO or hyperoxia as it may also reveal further evidence.

Mechanical stimuli (shear stress/stretch) in the endothelium are associated with increased secretion of permeability mediators such as inflammatory cytokines and vasoconstrictors Ang II and increased ROS production (De Keulenaer et al 1998, Schramm et al 2012). HDMEC exposed to hyperbaric pressure showed phenotypic retraction and contraction, although their mean sizes were not significantly different relative to the control ( $p > 0.05$ ). Such phenotypic retraction in response to hyperbaric pressure is likely an adaptive response in response to elevated pressure acting on their cell surfaces. Phenotypic retraction and contraction is associated with the release of mediators such as cytokines (De Keulenaer et al 1998, Schramm et al 2012). Importantly, endothelial cells activate the expression of an endothelial specific mediator, the platelet endothelial cell adhesion molecule -1 (PECAM-1) in response to mechanical stresses/stimuli such as retraction and contraction (Conway and Schwartz 2014). Thus it is likely, these treatments will be associated with changes in the expression of mediators in comparison to control. However, this inference needs to be established with further experiments.

Glucose effect on HDMEC morphology was not statistically significant although a pattern of high glucose associated increase in HDMEC mean sizes appeared imminent in the control and HBO conditions ( $p > 0.05$ ). Human umbilical vein endothelial cells (HUVEC) exposed to 60 – 120 mM of glucose for up to 168 h exhibited endothelial – mesenchymal phenotype (polygonal – spindle) transition with manifest changes in sizes (Yu et al 2017). In addition, increased endothelial cell contraction and VE-cadherin junctional permeability was observed with glucose concentrations of 20 mM (Hempel et al 1997, Sandoval et al 2001). More so, ultrastructural alterations in human aortic EC (HAEC) cultured for 1–2 weeks in high glucose (25 mM), and mice/golden Syrian after streptozotocin injection are reported (Simionescu et al 1996, Popov and Simionescu 2006). In human vascular endothelial cell, high glucose associated contraction and hyperpermeability were caused by hyperglycaemia induced AGE and RAGE/Rho signalling pathway and AGE formation (Hirose et al 2009). Incidentally, AGE induction by hyperglycaemia requires long duration ( $\geq 2$  weeks). Hence, it is likely the glucose concentration used (20 mM) and duration of incubation (4 h) in this study was not sufficient to instigate substantially pronounced and observable phenotypic changes in HDMEC. As a caution, the absence of measurable phenotypic change does not completely negate the likelihood of glucose-mediated effect, which may have been obscured to light image microscopy. In retrospect, a confocal might have been advantageous in revealing these deeper structural details/deregulations.

Resazurin conversion to resorufin by dehydrogenase enzymes in viable cells is visually assessed by the colour change from blue to bright pink (Ahmed et al 1994). From the optimisation experiments, it was apparent the metabolic activities of HDMEC were not acutely (6 h) changed in control condition even at high plating densities  $\geq 8 \times 10^3$  per well. Also, although there was an observable colour change at 6 h which was indicative of metabolic activity, maximal colour change was seen only after 24 h which is suggestive of a slow metabolic phenotype in comparison to the aggressively fast metabolic phenotype of transformed cells or sprouting endothelial cells (Ahmed et al, 1994, Nakayama et al 1997, Zalata et al 1998, Perrot et al 2003, De Bock et al 2013 and Doddaballapur et al 2015).

In summary, a key observation in this chapter is the modulation of characteristics in HBO that were widely out of norm in hyperoxia (mean HDMEC size). The use of HBO or hyperbaric pressure alone was not associated with significant changes in HDMEC sizes or metabolic activity relative to the control samples. Morphologically, based on live cell images, HDMEC in hyperbaric pressure appeared retracted in comparison to cells in control condition although this morphological change was not linked with a significant change in their mean sizes relative to control. Furthermore, varying concentrations of glucose was not associated with a significant effect on HDMEC size or metabolic activity.

Cells mount inflammatory and redox response as a protective mechanism. Arguably HBO is associated with both stress and ROS activation (Thom, 2011). The pertinent question is why/how the changes associated with hyperoxia were not seen with HBO. There is likely a HBO stress/trauma response that is far more protective, and possibly more sustained and more extensive to give such balanced effect in the presence of perturbations that otherwise drove phenotypic and biochemical changes in hyperoxia. Therefore, in the next chapter, redox and pro-inflammatory responses are investigated.

## 4.6 Limitations

Live HDMEC imaging and size measurements were carried out using Image J analysis of photomicrographs captured with a light microscope. Cellular details were sometimes obscured, thus limiting the total number of HDMEC analysed per condition, because only cells with clearly defined edges were measured ( $n = 40$ ). Had larger number of cells been analysed, the power of the experiment and statistical outcome may have been more significant. Therefore, it is needful in any further studies to use better imaging and cell size analysis software such as CellProfiler<sup>TM</sup>. In retrospect, a cell plasma membrane stain such as CellMask Plasma Membrane Stains (Invitrogen, ThermoFisher) could have been used to stain and delineate HDMEC cell edges more precisely. Due to limitations with magnification of the imaging microscope, it was not possible to assess HDMEC cell-cell adhesion/junction in order to ascertain any glucose-mediated disruption of junctional networks. ROS elevation was not investigated in the study. Instead, inference to treatment mediated ROS elevation was made based on what is reported in relation to hyperoxia/hyperbaric pressure/HBO (Thom 2009 and 2011, De Keulenaer et al 1998, Schramm et al 2012). To rightly establish the role of ROS, ROS blockade ideally could have been incorporated in the experimental design. To circumvent this limitation, the expression of nrf2 is examined in the next chapter but a study could have been included to investigate the effects of ROS blockade on some of the experimental outcomes including HDMEC morphology and nrf2 expressions.

Although the premise of this study was the examination of the effects of conditions on HDMEC morphology, size and metabolic activity in the context of high glucose, significant high glucose related changes were not identified and although high-glucose associated trends were imminent ( $p > 0.05$ ). The time of incubation of HDMEC in high glucose prior to imaging may have been too short (4 h), and a longer incubation period would have been more revelatory. In experimental designs where a glucose concentration of 25 mM was utilised in HAEC, a longer duration of culture (1-2 weeks) was employed (Simionescu et al 1996, Popov and Simionescu 2006). Moreover it is possible the glucose concentration used was not optimal for inducing such rapid morphological changes since previous work in HUVEC using 60-120 mM glucose was associated with significant size changes in HUVECs (Yu et al 2017). Finally, microscopy with a confocal might have been advantageous in revealing deep structural details/deregulations due to high glucose.

## Chapter 5.0: Inflammatory and Redox Responses

## 5.1 Hypothesis

The changing concentration of glucose, oxygen tension and pressure has an effect on human dermal microvascular endothelial cell redox and immunological responses.

## 5.2 Introduction

In chapter 4.0, the morphology (size and shape) of HDMECs was significantly changed in hyperoxia (low glucose) in comparison to control. Under the duration of study (4 h), no significant glucose associated effects on HDMEC size was seen. Endothelial cells are sensitive to varying glucose concentration, oxygen levels and mechanical (shear/stretch) stimuli (Ruderman et al 1992, Brownlee et al 1989 and 2005, Akgu"et al 2014). Elevated glucose, hyperoxia and mechanical shear/stretch stress increase ROS production both in-vitro and in-vivo (Brownlee, 2005, Li et al 2011, Hsieh et al 2009, reviewed in Nguyen et al 2009), and in-vitro application of elevated pressures of  $\geq 2.2$  ATA has a knock on effect on mechanical stimuli (shear/stretch stress) on cultured endothelial cells (Godman et al 2010). Acute short-term ROS is beneficial in the right milieu. For instance HBO exerts some of its beneficial effects via ROS and reactive nitrogen species (RNS) (Thom 2011, Godman et al 2010, and HBOT Trust 2018). In addition, acute ROS generation is a defensive mechanism to forestall sustained oxidative damage. However, sustained elevated ROS level causes endothelial dysfunction (reviewed in Knott and Forrester 2003, Du et al 2003, reviewed in Falanga 2005, Brownlee 2005, and Adamis 2008).

The nuclear factor erythroid 2-related factor 2 (nrf2) is a key transcription factor that regulates the expression of genes involved in cytoprotection, cellular metabolism and ageing (reviewed in Nguyen et al 2009, Heiss et al 2013). It is likely present in the plasma membrane as part of the plasma membrane redox system (PMRS), a system associated with cell survival and membrane homeostasis under stress conditions such as high intracellular glucose (Hyun et al 2006, Leiser and Miller 2010, Saraswat and Rizvi 2017). Nrf2 is distributed in the cytosol and translocate to the nucleus when stabilised (reviewed in Nguyen et al 2009). Constitutive expression of nrf2 in the cytosol in unstressed conditions is not a regulated process (Nguyen et al 2009). However, the accumulation and activation of nrf2 is controlled in the basal steady state by Keap 1. Two aspects in nrf2 regulation are key; nrf2 degradation or accumulation. Mechanism(s) that reduces Keap 1 access to nrf2 or decreases GSK-3 $\beta$ -mediated phosphorylation of nrf2 increases nrf2 stabilization leading to its activation (Nguyen et al 2009, Siewart et al 2003).



Nrf2 is closely associated with insulin and glucose metabolism. The activation of nrf2 by insulin in cells results in increased cellular uptake of glucose (Heiss et al 2013). Nrf2 does not alter glycolysis or oxidative metabolism, however in high glucose; nrf2 mediates increased glucose uptake and shunting of glucose to the pentose phosphate pathway (PPP) for the production of NADPH and ribose-5-phosphate (Heiss et al 2013). Incidentally, several enzymes of the PPP including glucose-6 phosphate dehydrogenase (G6PD) are under the control of nrf2.

Nrf2 is involved in the modulation of several targets. The anti-oxidant response element (ARE) on target such as heme-oxygenase (HO-1) is modulated by nrf2 (Keum and Choi 2014). ROS is a signal for the nuclear factor kappa-light-chain-enhancer of activated B cells (NFkB) activation. In cells, the intersection of ROS-mediated activation of pro-death c-Jun N-terminal kinases (JNK) signalling and NFkB activation is modulated by nrf2 (Bellezza et al 2010). In endothelial cells, interleukin 6 (IL6) mRNA is constitutively expressed and important immunological responses are executed via IL-6 signalling. For instance, endothelial cells (EC) respond to ROS/stretch/ shear stress via IL-6 signalling in an NFkB dependent manner (Tanaka et al 2014). Hence, ROS/stimuli mediated activation of JNK/ NFkB culminates in nrf2 activation because the promoter sequence on NFE2/2 (Nrf2) gene contains a binding site for NFkB (Rushworth et al 2012 and Xiang et al 2014). Fundamentally, in cells, this intersection (cross-talk) between ROS/JNK and NFkB/nrf2 is pro-survival and demonstrates a critical link between pro-inflammatory and redox response (Bellezza et al 2010).

The aim of the study is to understand the role of varying glucose concentration, oxygen and pressure on redox and pro-inflammatory responses in HDMEC by examining the protein expressions of nrf2 and NFkB. In addition, the protein and mRNA expressions of HO -1, a target of nrf2, and IL-6, an activator of NFkB respectively are examined. This study will inform on HDMEC redox and pro-inflammatory responses post HBO in the context of high glucose. The contributions of the single components of HBO will also be deciphered.

## 5.3 Materials and method

Full details of materials and method are reported in the general material and methods section in chapter 2.0 sections; immunocytochemistry (ICC) (2.4), Western blot (WB) (2.5), mRNA (2.6). Details that are specific to the method used in this chapter are presented below.

### 5.3.1 Cell culture and assays

HDMECs cells were grown at a density of 35,000-38,000 cells/well according to the recommended seeding density (PromoCell) in 24-well plates in HDMEC growth media containing low (5.5 mM) or high glucose. For high glucose treatments, cells were incubated in HDMEC growth media supplemented with 14.5 mM D-glucose to give a final concentration of 20 mM. HDMEC were exposed to HBO (or hyperoxia or hyperbaric pressure with equivalent samples incubated in a normal 5% incubator in control conditions (control) (refer to chapter 2.0 section 2.8). At 4 h and 24 h post incubation, HDMEC were harvested for assays. Immunocytochemical (ICC) stained HDMECs were incubated overnight at 4°C with primary antibodies (1:50); anti-nrf2 (Santa Cruz), followed with incubation in goat anti-mouse IgG, DyLight 488 conjugated highly cross-adsorbed secondary antibody (1:500) (ThermoFisher Scientific). HDMEC were counterstained with DAPI and at 400X magnification. Results are presented as representative micrographs from 3 or more independent experiments. Western blot (WB) PVDF membranes were incubated with primary targets (1:100); anti-nrf2, anti-HO-1, and anti-NFκB (Santa Cruz) overnight, followed with anti-β-actin (St Johns Labs, UK) as loading control, and detected with goat anti-mouse IgG Horseradish peroxidase (HRP) conjugated secondary antibody diluted in 1.5% BSA/TBS, and visualised by chemiluminescence. Results are presented as micrographs of blots from n = 3 separate experiments relative to β-actin level.

WB results are preliminary because the protein expression and actin loading controls showed wide variations and therefore warrants further experimental investigations to obtain robust and repeatable results.

Polymerase chain reaction was performed with 0.25µM of validated forward and reverse primers for; human beta-2-microglobulin (B2M) primers; F: 5'-GGGCATTCCTGAAGCTGACA-3'; R: 5'-TGGAGTACGCTGGATAGCCT-3' and interleukin (IL)-6 primer; F: 5'-TCAATATTAGAGTCTCAACCCCCA-3'; R: 5'-TTCTCTTTCGTTCCCGGTGG-3' with 2X PowerUP SYBR Green Master Mix with ROX reference (catalogue # 4309155) (ThermoFisher Scientific) and a total of 10ng of cDNA from HDMECs in duplicate performed on three independent occasions. Post analysis check with melt curve was performed to discriminate between specific PCR products and non-specific primer-primer products. The fold change method was used for determination of IL-6 mRNA expression relative to β2m and study calibrator (untreated 5.5 mM sample in control condition) (Winer et al 1999 and Schmittgen et al 2000). Primer set efficiency determination and inspection of PCR product with melt curve were performed as initial validation. To ascertain primer efficiencies, serial dilutions of cDNA HDMEC with 0.25 µM of forward and reverse primers of β2m and IL-6 in duplicates were prepared. Amplification was performed as described in materials and method (chapter 2.0 section 2.6) and average cycle threshold (CT) calculated per sample. Average CTs were plotted against log10 of the serial cDNAs to generate a standard curve for β2m and IL-6. The efficiency of primers was calculated with equation 5.1 below. A melt curve was used as quality check for PCR product formed. Experimental PCR assay were set up in duplicates and were repeated in 3 separate experiments. Statistical analysis was performed as reported in chapter 2.0, section 2.11.

$$\% \text{ Efficiency} = (10^{-(1/\text{gradient})} - 1) \times 100$$

----- Equation 5.1

## 5.4 Results

### 5.4.1 Effect of glucose concentration, oxygen tension and pressure on redox response.

Redox responses were studied by examining the expressions of nrf2 protein expressions (levels). Nrf2 is rapidly cleared ( $t_{1/2}$  = 20 mins) after synthesis but, its half-life increases to 200 mins post stabilisation (Canning et al 2015). Based on n =2 independent experimental replicates of nuclear HDMECs lysates pooled from six identical wells per sample at 4 h post treatment, nuclear nrf2 expression at 4 h appeared elevated in response to treatment with HBO, hyperoxia and hyperbaric pressure in comparison to controls. Based on the available WB result, glucose effect on nrf2 expression was not evident (fig 5.1). The actin loading controls were variable and the blot contained some non-specific stains and poor image resolution which made it difficult to clearly delineate bands. Therefore, the presented WB blots are preliminary and further WB studies are needed for more robust and repeatable results. Immunocytochemical (ICC) staining of HDMEC samples at 4 h and 24 h was used to ascertain nrf2 expression and to have a preliminary indication of cellular distribution of nrf2 in response to glucose concentration, oxygen and/or pressure. Although, HDMEC WB results were highly variable, ICC stained data as shown in figs 5.2-5.5 showed satisfactory expression and cellular distribution of nrf2 (figs 5.2 – 5.5).

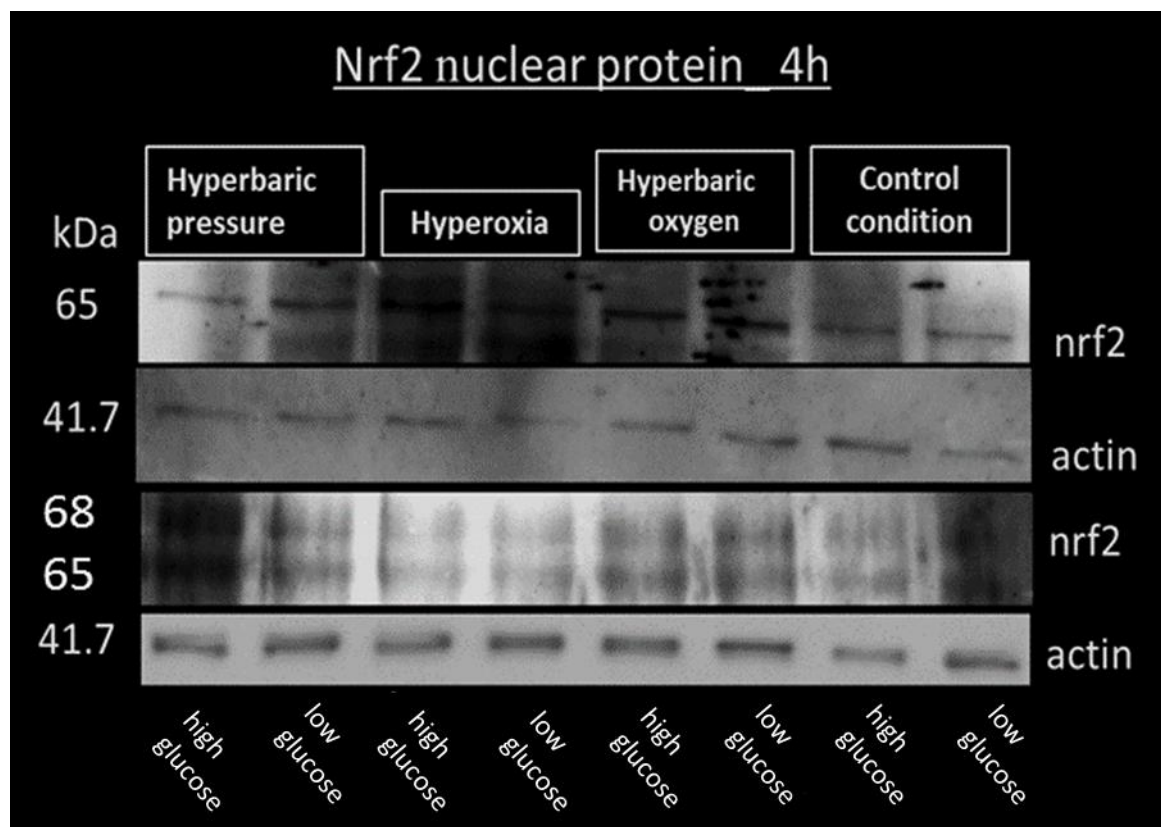


**Figure 5. 1 Western blots of nrf2 at 4 h**

Nuclear Evcimen nrf2 protein appeared elevated post HBO, hyperoxia and hyperbaric pressure in comparison to control at 4 h. The blot contains some non-specific stains and poor image resolution which made it difficult to delineate bands. In addition, actin loading controls were variable. Data is based on n =2 independent experimental replicates of nuclear HDMECs lysates pooled from six identical wells per sample at 4 h post treatment.

In the following paragraphs, exemplary ICC photomicrographs of anti-nrf2 stained HDMEC are presented. Distinction is made of non-specific staining (possibly debris) which are not cell/structure associated (false-positives) (exemplified by red circle). Where relevant, arrow heads were used to highlight details. In general, the intensity of nrf2 signal which is an indication of nrf2 levels (immunoreactivity/expression) appeared lower in control in comparison to treated samples (fig 5.2 vs 5.3 – 5.5). In addition, nrf2 intensity appeared lower in high glucose in comparison to low glucose for HDMECs in control conditions (fig 5.2, A vs B). Moreover, the distribution of nrf2 signal in HDMEC in control condition appeared predominantly cytoplasmic associated irrespective of glucose concentration or time.

## Nrf2 expression in control condition at 4 h and 24 h

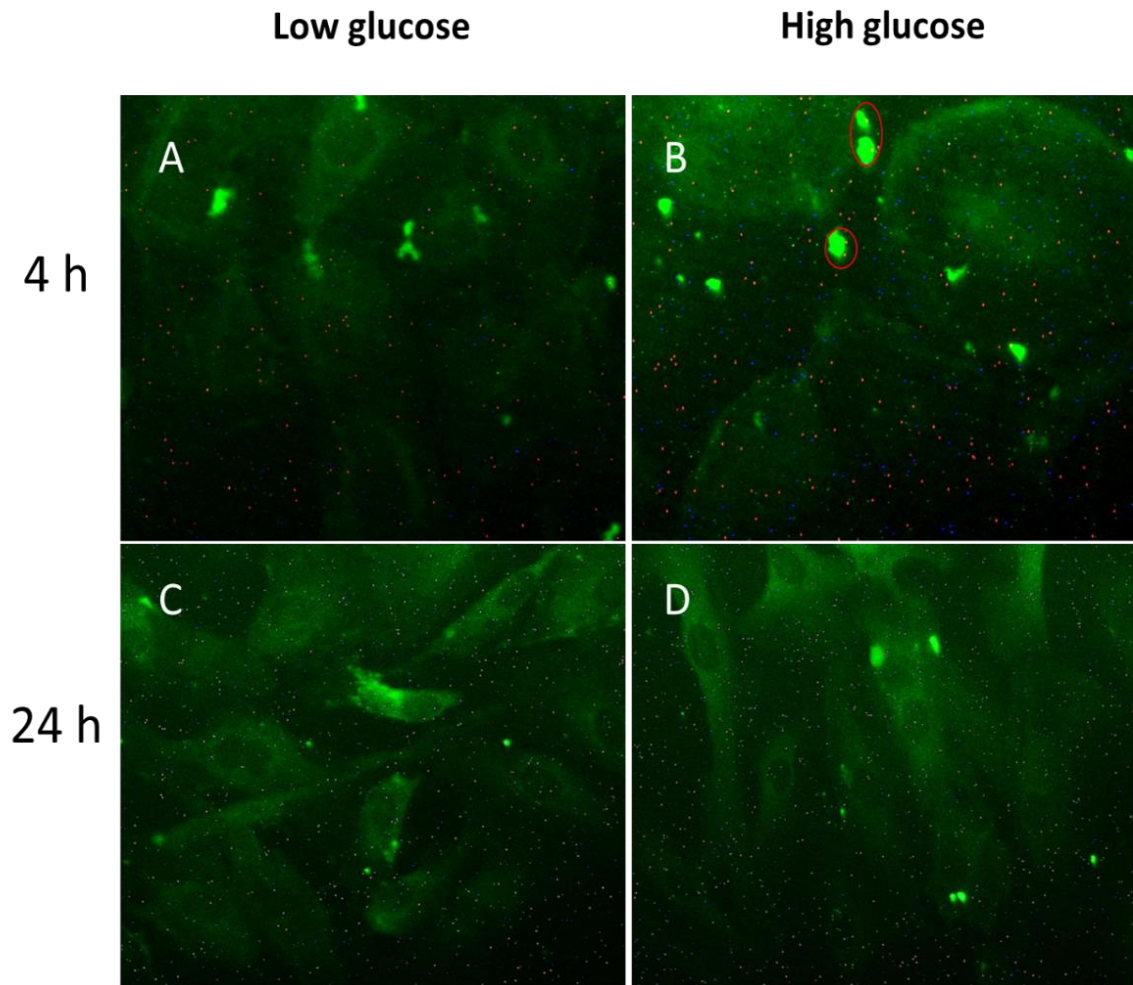


**Figure 5. 2 ICC of nrf2 in control condition at 4 h and 24 h**

The signal intensity of nrf2 in control sample was low which may suggest low basal levels. In addition, nrf2 signal intensity appeared lower in high glucose at 4 h (B) in comparison to low glucose (A). Moreover, the distribution of nrf2 appeared predominantly cytoplasmic associated. Selected images are representative of  $n = 3$  independent experimental replicates. Magnifications 400X. Scale bar 500 $\mu$ m

HBO treated HDMEC (fig 5.3) appeared consistent with stronger nrf2 signal intensity in comparison to control. In addition, nrf2 distribution in HBO treated HDMEC showed nuclear and plasma membrane association at 4 h and 24 h relative to control. Moreover, nrf2 level and distribution post HBO appeared unchanged irrespective of glucose concentration or time relative to control.

### Nrf2 expression in HBO at 4 h and 24 h

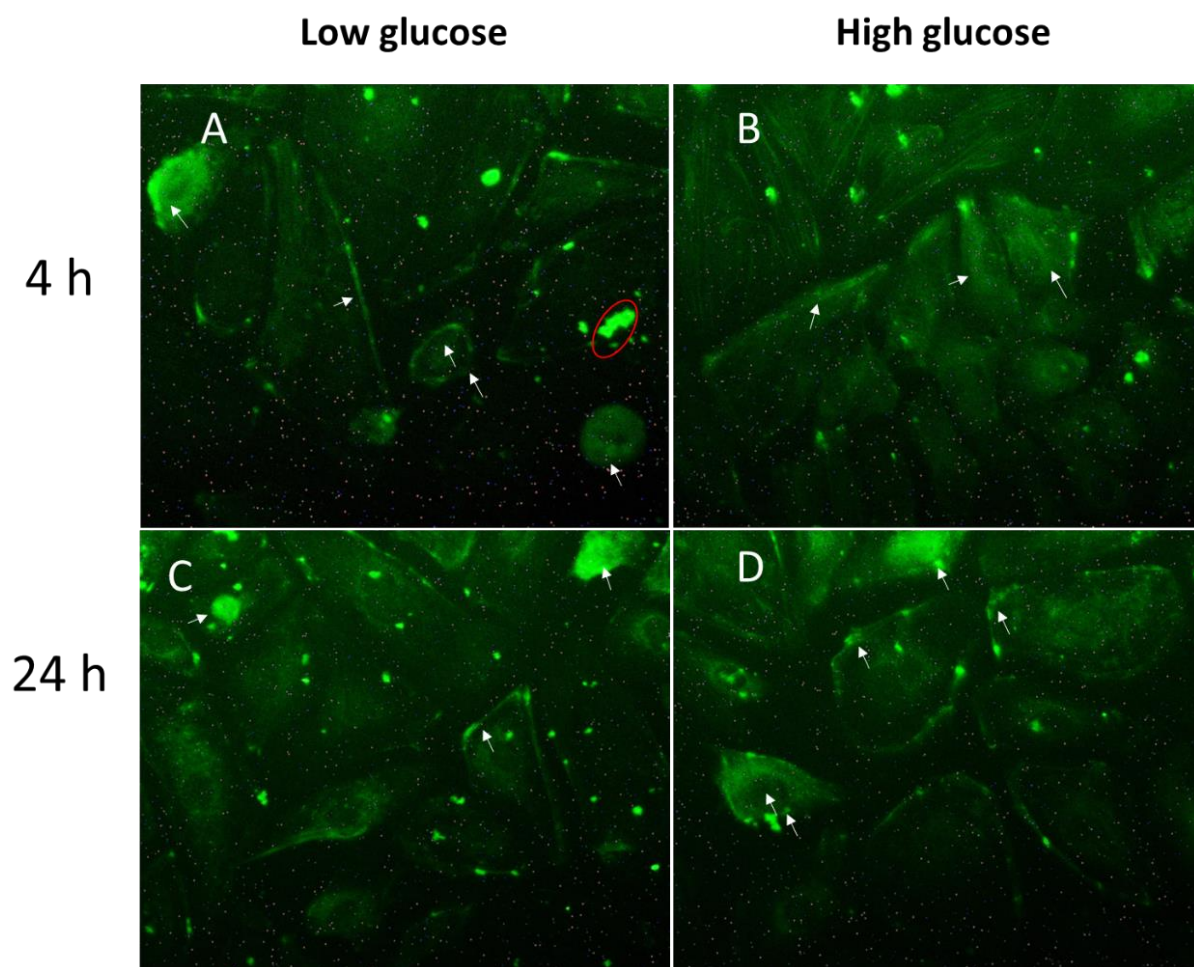


**Figure 5. 3 ICC of nrf2 in HBO at 4 h and 24 h**

Nrf2 signal in HDMEC which is indicative of its expression (immunoreactivity) appeared higher post HBO in comparison to control. In addition, nrf2 level or distribution did not appear to change with respect to glucose concentration or time post HBO in comparison to controls. Moreover, nrf2 distribution post HBO seemed consistent with nuclear (white arrowheads), and plasma membrane association (white arrowheads). Selected images are representative of n = 3 independent experimental replicates. Magnifications 400X. Scale bar 500µm



HDMEC treated with hyperoxia (fig 5.4) showed nrf2 accumulation at 4 h relative to control. Nrf2 distribution appeared consistent with perinuclear association post hyperoxia in comparison to control. Curiously, nrf2 signal post hyperoxia and more so in high glucose were decreased at 24 h relative to 4 h. Hyperoxia associated enlargement in HDMEC size and actin cytoskeleton striation were more apparent at 4 h relative to 24 h and more so in the low glucose samples in comparison to control.

## Nrf2 expression in hyperoxia at 4 h and 24 h

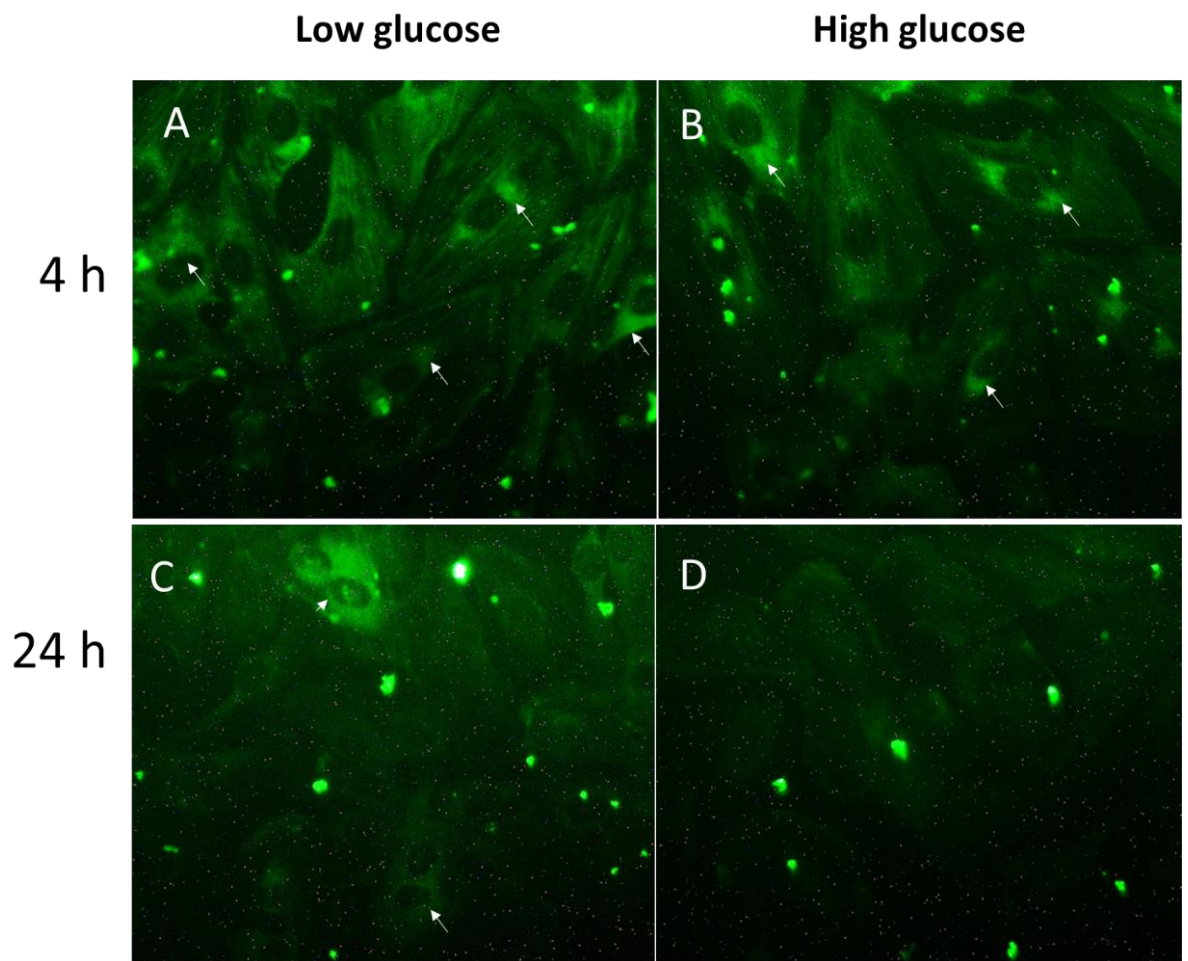


**Figure 5. 4 ICC of nrf2 protein in hyperoxia at 4 h and 24 h**

HDMEC exposed to hyperoxia showed nrf2 accumulation in perinuclear associated areas at 4 h. Hyperoxia associated nrf2 expression was diminished at 24 h and more so in high glucose in comparison to 4 h. Selected images are representative of n = 3 independent experimental replicates. Magnifications 400X. Scale bar 500µm

Hyperbaric pressure treated HDMEC were associated with higher nrf2 signal in comparison to control which may be indicative of nrf2 accumulation in hyperbaric pressure in comparison to control (fig 5.5). In converse to control, nrf2 signal post hyperbaric pressure did not seem affected by glucose concentration or time. Moreover, nrf2 distribution appeared consistent with nuclear and plasma membrane association, with some perinuclear association in comparison to control.

Nrf2 expression in hyperbaric pressure at 4 h and 24 h

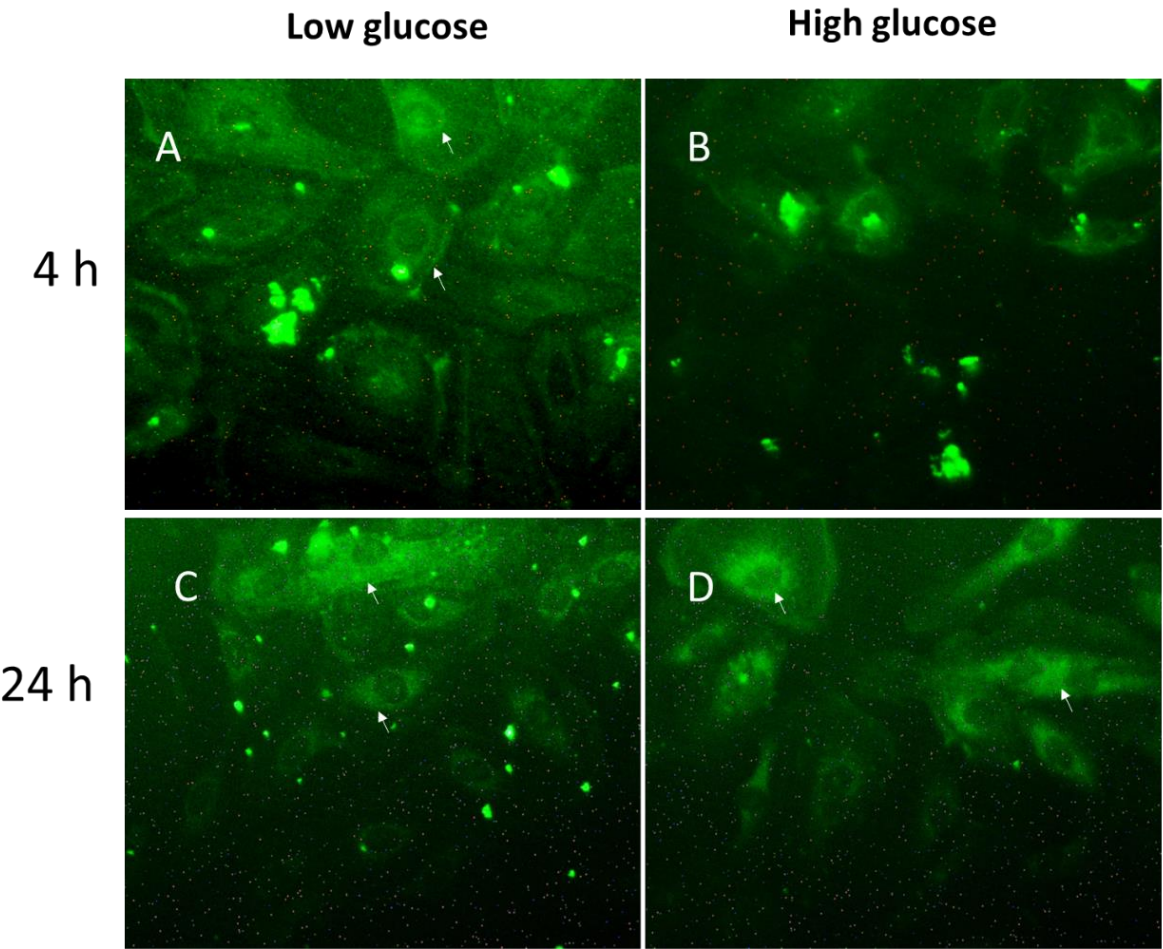


**Figure 5. 5 ICC of nrf2 protein in hyperbaric pressure at 4 h and 24 h**

Nrf2 accumulation appeared evident post hyperbaric pressure in comparison to control. Nrf2 accumulation post hyperbaric pressure appeared consistent with nuclear and plasma membrane association with some perinuclear association. Selected images are representative of n = 3 independent experimental replicates. Magnifications 400X. Scale bar 500µm

Nrf2 fluorescent signal intensities in HDMEC post treatments were quantified (fig 5.6). There was a net decrease in nrf2 intensity in response to high glucose in comparison to low glucose in the control condition ( $p < 0.05$ ). The earlier observations of nrf2 accumulation with ICC micrographs (figs 5.2 - 5.5) were further demonstrated. In low glucose, there were net increases in nrf2 intensities post HBO ( $p < 0.0001$ ), hyperoxia ( $p < 0.0001$ ) and hyperbaric pressure ( $p < 0.05$ ), and in high glucose, net increases post HBO ( $p < 0.0001$ ), hyperoxia ( $p < 0.0001$ ) and hyperbaric pressure ( $p < 0.05$ ) in comparison to controls at 4 h. In addition, nrf2 signal intensities in low glucose were significantly higher post HBO ( $p < 0.0001$ ), hyperoxia ( $p < 0.0001$ ) and hyperbaric pressure ( $p < 0.01$ ), and in high glucose, HBO ( $p < 0.0001$ ) and hyperbaric pressure ( $p < 0.01$ ) in comparison to controls at 24 h. Nrf2 signal intensity was dampened post hyperoxia (high glucose) but remained sustained post HBO irrespective of glucose concentration in comparison to controls ( $p < 0.001$ ) after 24 h.

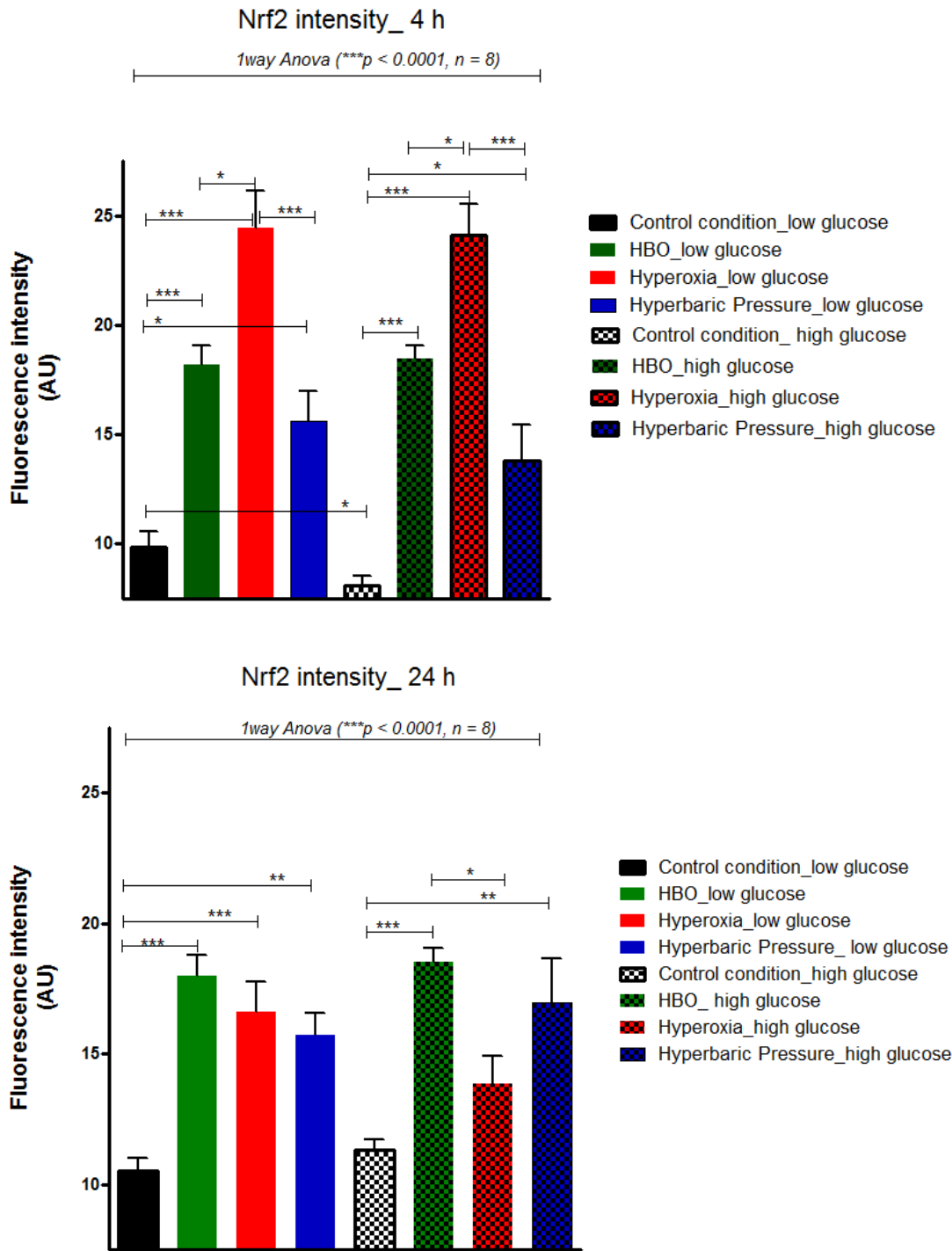


**Figure 5. 6 Fluorescence intensity of nrf2 signal at 4 h and 24 h**

Mean nrf2 signal intensities were significantly different between samples (\*\**p* < 0.0001, *n* = 8) and (\**p* < 0.0001, *n* = 8). At 4 h, nrf2 signal intensity was decreased in HDMEC in high glucose in comparison to low glucose in the control condition (*p* < 0.05). HDMEC in low or high glucose post HBO, hyperoxia or hyperbaric pressure were associated with significant increases in nrf2 intensities (accumulation) in comparison to controls; HBO (*p* < 0.0001), hyperoxia (*p* < 0.0001), hyperbaric pressure (*p* < 0.05). After 24 h, nrf2 level for HDMEC in low or high glucose in HBO, hyperoxia or hyperbaric pressure continued to be significantly higher in comparison to controls excluding HDMEC in hyperoxia in high glucose where signal intensity was no longer significantly higher in comparison to control (*p* > 0.05). Also at 24 h, nrf2 signal intensity for HDMEC in high glucose post hyperoxia was significantly lower in comparison to HBO (*p* < 0.05). Data is based on *n* = 9 replicates for all samples otherwise stated for 4 h; hyperoxia low/high glucose, *n* = 6 and 7 respectively), for 24 h, control condition low/high glucose (*n* = 9), HBO low/high glucose, *n* = 4 and 6 respectively, HBO low/high glucose (*n* = 4 and 6 respectively), hyperoxia low glucose (*n* = 7), hyperbaric pressure low/high glucose (*n* = 7).

Nrf2 protein stabilization and nuclear activation is associated with induction of the cytoprotective heme oxygenase (HO-1). To test the possibility of HO-1 induction, WB analysis of HDMEC extracts at 24 h were performed. But, WB results of HDMECs lysates blotted with anti-HO-1 and their actin loading controls were variable making it difficult to draw definite conclusions although some preliminary trends were apparent (fig 5.7). HO-1 levels appeared elevated in response to high glucose in comparison to low glucose samples for HDMEC in control condition. Similarly, HO-1 levels for HBO treated HDMEC appeared elevated in high glucose in comparison to their low glucose counterparts. On the other hand, it appears hyperoxia alone was sufficient to induce HO-1, and a concomitant hyperoxia and glucose effect on HO-1 induction was not easily discernible. Overall, HO-1 levels appeared elevated in response to treatments; HBO, hyperoxia and hyperbaric pressure in comparison to control. These results are considered to be preliminary and experiments would need to be repeated to confirm these data.

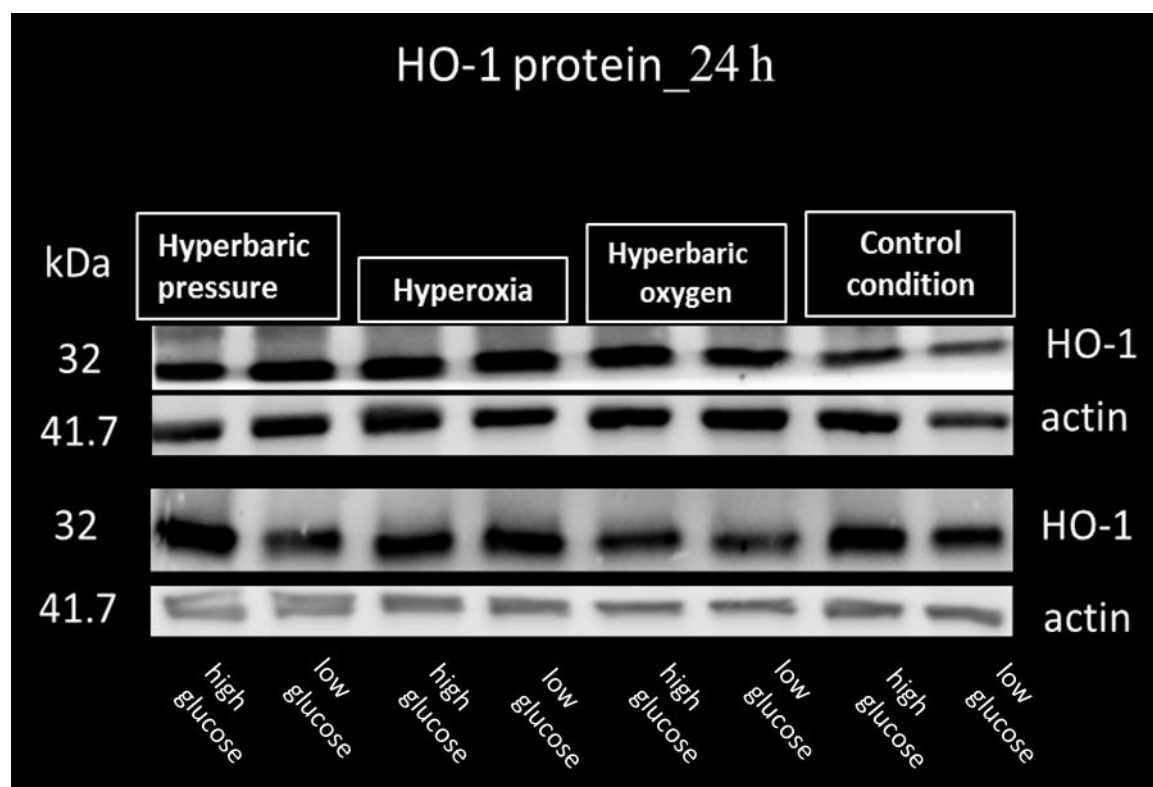


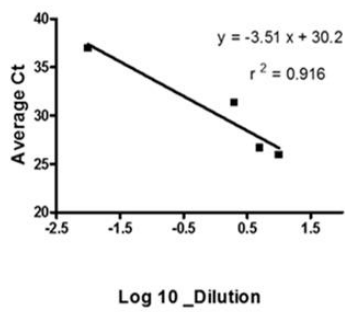
**Figure 5. 7 Western blots of HO-1 protein at 24 h**

HO-1 appeared elevated in control condition and HBO in response to glucose concentration, but a concomitant hyperoxia and high glucose effect on HO-1 elevation was not so apparent. In addition, HO-1 levels appeared elevated in response to treatments; HBO, hyperoxia and hyperbaric pressure in comparison to control (low glucose). Data is based on n =2 independent experimental replicates of cytosolic HDMECs lysates pooled from six identical wells per sample at 24 h post treatment. Results are preliminary due to inconsistencies in HO-1 expression and actin loading controls.

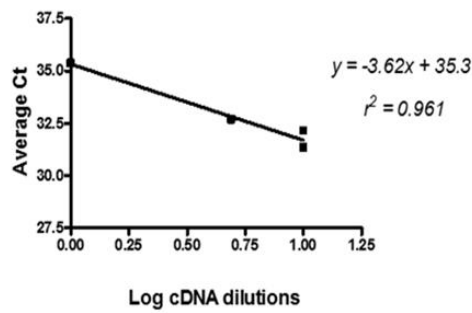
## 5.4.2 Effect of glucose concentration, oxygen tension and pressure on inflammatory response

Inflammatory responses were studied by examining the expression of IL-6 mRNA and NFκB protein in total lysates of HDMEC at 4 h. Beta-microglobulin (β2m) and IL-6 primer sets efficiencies were 105% and 90% (A and B), which were within efficient primer set range (90-110%) (Livak and Schmittgen 2001, Primer Design 2018). Amplification cycles were earlier than 35 cycles confirming the absence of genomic DNA (C and D) (Livak and Schmittgen). A melt curve analysis (E and F) showed good quality PCR product for β2m and IL-6 primers with true product peaks at melting temperatures within 80°C -90°C (Livak and Schmittgen, 2001). IL-6 melt curve had a primer dimer with T<sub>m</sub> (65-75°C) (Livak and Schmittgen) (Fig. 5.8).

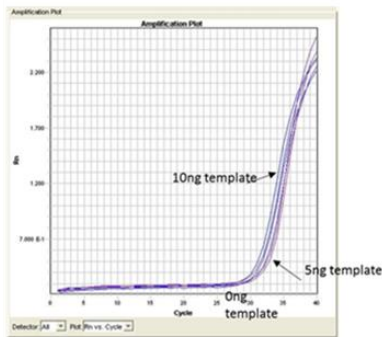
A Standard curve\_B2m



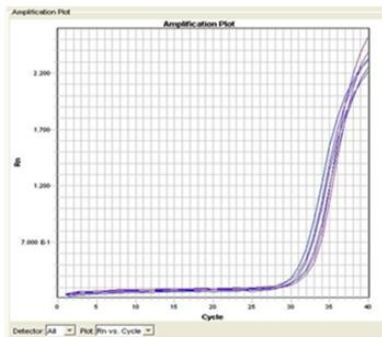
B Standard curve\_IL-6



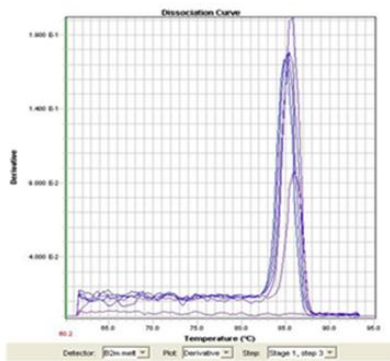
C Amplification plot\_B2m



D Amplification plot\_IL-6



E Melt curve\_B2m



F - Melt curve\_IL-6

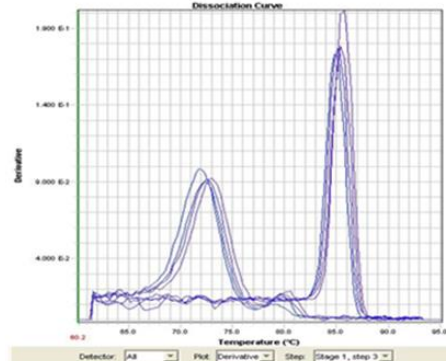


**Figure 5. 8 Primer set efficiency**

Efficiencies of B2m and IL-6 primer sets were 105 % and 90 % (A and B). Amplifications were earlier than 33 cycles. No primer dimer signal was seen in B2m and IL-6 amplification plots (C and D). Melt curve for B2m showed a distinct PCR product peak at  $T_m \geq 80^\circ\text{C}$  (E and F). IL-6 peak had an additional signal at  $T_m (65-75^\circ\text{C})$  which may be primer-dimer.



Endothelial cell (EC) responses to stimuli such as ROS and stretch and shear stress are transduced to a cellular pro-inflammatory response by IL-6 via sequential activation of IKKs and NF $\kappa$ B in a ROS dependent manner (Kobayashi et al 2003). To test the possibility of immunological response in HDMEC post treatments, the expression of IL-6 mRNA was examined with real-time qPCR. The average threshold values (CT) of samples post normalisation and fold determination with  $\beta$ 2m were expressed relative to control (calibrator). Therefore, the bar plot (fig 5.9) represents the extent of change (downregulation/suppression) (fold change) of IL-mRNA relative to  $\beta$ 2m/calibrator.

Analysis of the qPCR data with 1way ANOVA with Tukey's post hoc tests showed IL-6 mRNA expression changed significantly between the means of all samples ( $p < 0.0001$ ,  $n = 8$ ) (fig 5.9). HDMEC in control condition showed no significant glucose-dependent change in IL-6 mRNA level ( $p > 0.05$ ). Post exposure to treatments, there were significant suppression of IL-6 mRNA for HDMEC in low glucose; HBO (5.2-fold,  $p < 0.0001$ ), hyperoxia (2-fold ( $p < 0.0001$ ), hyperbaric pressure (2-fold;  $p < 0.0001$ ) and in high glucose; HBO (4.9-fold,  $p < 0.0001$ ), hyperoxia (3-fold,  $p < 0.0001$ ) and hyperbaric pressure (2-fold,  $p < 0.0001$ ) relative to  $\beta$ 2m/calibrator. In HBO, a significant high glucose associated decrease in IL-6 mRNA suppression relative to the low glucose counterpart was seen ( $p < 0.01$ ). In hyperoxia, high glucose resulted in increased IL-6 mRNA suppression relative to the low glucose counterpart ( $p < 0.0001$ ). No significant glucose associated change was evident for samples in hyperbaric pressure ( $p > 0.05$ ).

Taken together, IL-6 mRNA was significantly suppressed (downregulated) following treatments; HBO, hyperoxia and hyperbaric pressure but more so post HBO relative to controls. In addition, IL-6 mRNA was less suppressed in high glucose post HBO, whilst more suppressed post hyperoxia in comparison to low the glucose counterpart.

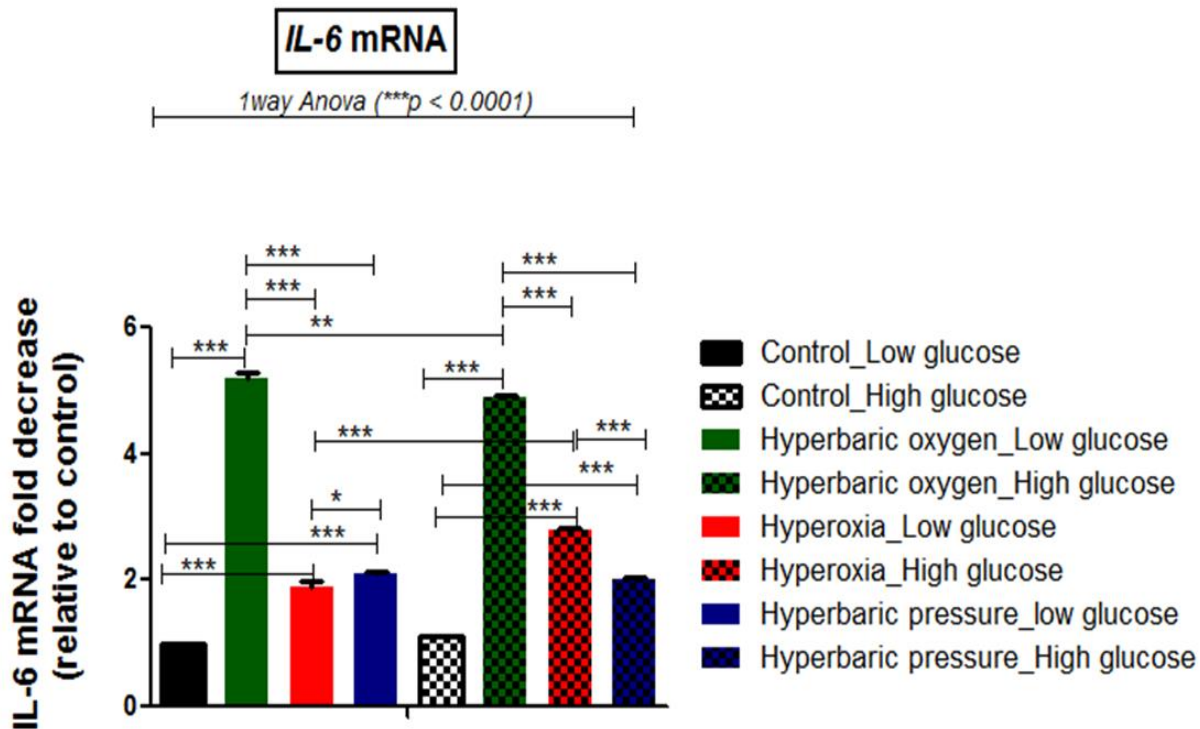


**Figure 5. 9 IL-6 mRNA at 4 h**

Mean IL-6 mRNA in HDMEC changed significantly between samples at 4 h ( $p < 0.0001$ ,  $n = 8$ ). Bar chart represents fold change in IL-6 mRNA (downregulation) relative to  $\beta 2m$ /calibrator. For HDMEC in low glucose, IL-6 mRNA was significantly downregulated post HBO (5.2-fold ( $p < 0.0001$ ), hyperoxia (2-fold) ( $p < 0.0001$ ), hyperbaric pressure (2-fold) ( $p < 0.0001$ ), and in high glucose a significant decrease post HBO (4.9-fold) ( $p < 0.0001$ ), hyperoxia (3-fold) ( $p < 0.0001$ ), and hyperbaric pressure (2-fold) ( $p < 0.001$ ) relative to  $\beta 2m$ /calibrator. In HBO, a significant high glucose associated decrease in IL-6 mRNA suppression relative to the low glucose counterpart was present ( $p < 0.01$ ). In hyperoxia, high glucose resulted in an increase in IL-6 mRNA suppression relative to the low glucose sample ( $p < 0.0001$ ). No significant glucose associated change was evident for samples in hyperbaric pressure ( $p > 0.05$ ). Experiments were repeated in  $n = 3$  independent occasions and the reported data is representative of fold change in IL-6 mRNA post normalisation and relative to  $\beta 2m$  (reference) /calibrator (untreated control). Control LG ( $n = 6$ ), control HG ( $n = 5$ ), HBO, LG 5.5 mM ( $n = 4$ ), HBO, HG 20 mM ( $n = 4$ ), hyperoxia LG ( $n = 4$ ), hyperoxia HG ( $n = 6$ ), hyperbaric pressure LG ( $n = 6$ ), and hyperbaric pressure HG ( $n = 3$ ). LG = low glucose, HG = high glucose.

NFκB is activated by IL-6 and cross-talks with ROS/JNK dependent nrf2 redox pathway activation in a pro-survival cellular response (Tanaka et al 2014, Bellezza et al 2010, Rushworth et al 2012 and Xiang et al 2014, reviewed in Evcimen and King 2007). Activated NFκB (p65) expression was examined with WB but replicates of NFκB WB data and their actin loading controls were variable. Preliminary WB results show NFκB (p65) detection in HDMEC (fig 5.10). NFκB appeared unchanged in response to high glucose in the control condition and HBO relative to control which may be indicative of basal NFκB levels. NFκB appeared elevated post hyperoxia and hyperbaric pressure but more so post hyperoxia relative to control. Variability in actin loading may have made it impossible to clearly delineate glucose effect in the different conditions.

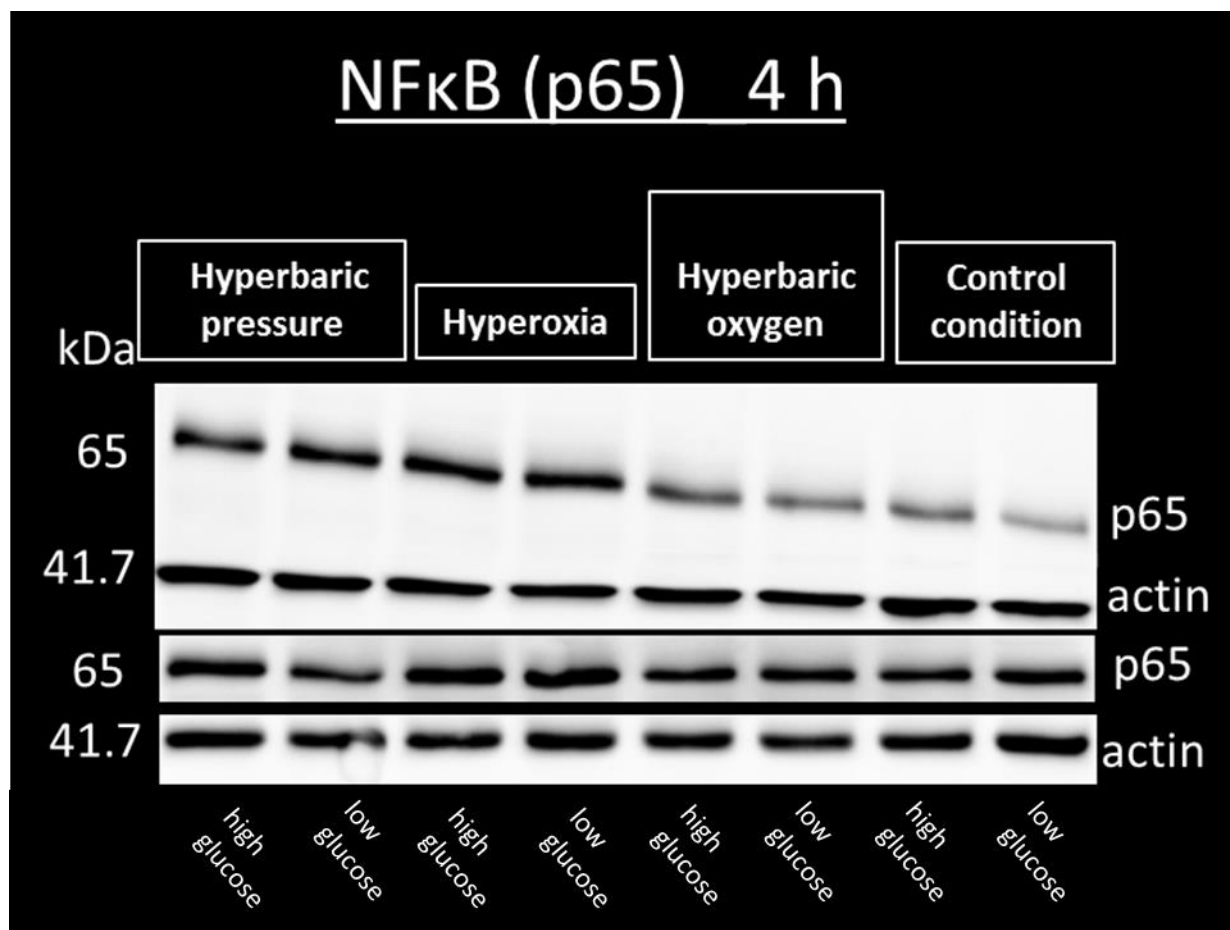


**Figure 5. 10 Western blots of NFκB protein in HDMEC at 4 h**

NFκB levels in control condition appeared unchanged in response to high glucose in comparison to low glucose. In addition NFκB levels appeared basal post HBO relative to control. NFκB appeared elevated post hyperoxia and hyperbaric pressure but more so post hyperoxia relative to control. There were variabilities in NFκB expression between replicates and actin loading controls necessitating further studies for robust WB results. Also, glucose associated effects did not appear evident but variability in actin loading may have contributed to the lack of distinction of glucose effects. Data is based on n =2 independent experimental replicates of total HDMECs lysates pooled from six identical wells per sample at 4 h post treatment.

## 5.5 Discussion

In this study, varying glucose concentrations, oxygen and pressure resulted in redox and pro-inflammatory responses in HDMEC. Nrf2 is rapidly cleared after synthesis with a  $t_{1/2}$  of 20 mins which increases to 200 mins post stabilisation (Canning et al 2015). For that reason, nrf2 detection and accumulation at 4 h (HBO, hyperoxia and hyperbaric pressure) and at 24 h (more so in HBO and hyperbaric pressure) are indicative of nrf2 stabilisation post treatments relative to control. HBO associated nrf2 activation/stabilisation is consistent with previous study in human microvascular endothelial cells (HMEC-1) (Godman et al 2010). Profoundly, this study has revealed nrf2 stabilisation post HBO, hyperbaric pressure and hyperoxia in HDMEC.

During homeostasis (e.g. control condition), the majority of nrf2 are rapidly ( $t_{1/2} = 20$  mins) are degraded in the cytoplasm (Canning et al 2015), which might explain the basal levels of nrf2 in the control sample. In response to oxidative stress, nrf2 dissociates from Keap 1 complex, translocates and activates the expression of cytoprotective proteins in the nucleus and restores redox equilibrium (Katsuoka et al 2005, reviewed in Hayes and Dinkova-Kostova 2014). Thus, the treatments; HBO, hyperbaric pressure and hyperoxia, but more so HBO and hyperbaric pressure are expected to be associated with increased expression of cytoprotective genes/proteins.

Nrf2 activity is tightly regulated with three subcellular populations of nrf2 identified; cytoplasmic, transcriptionally active population in the nucleus and a third population that localises to the outer mitochondrial membrane (reviewed in Plafker and Plafker 2015). A fourth redox protective plasma membrane distribution is hypothesised (HPA 2018, Hyun et al 2006). Keap 1 system serves to isolate nrf2 in the cytoplasm, whilst Gsk-3 $\beta$  promotes nuclear nrf2 extrusion and degradation (Biswas et al 2014). Emerging evidence suggests the Ub-conjugating enzyme (UBE2E3) and its nuclear import receptor importin 11 (Imp-11) regulates (promotes) nrf2 activity by restricting nrf2 partitioning into the mitochondria as well as limiting nuclear Keap 1 mediated repression of nrf2 (Plafker and Plafker 2015).

In this study, distinct patterns of nrf2 distribution post treatments in comparison to control were observed. Post HBO and to a lesser extent hyperbaric pressure, nrf2 accumulation showed predominant nuclear and plasma membrane association relative to control which suggests nuclear nrf2 activation and plasma redox system (PMRS) activity. Therefore, the prospect of nuclear nrf2 activation and PMRS activity post HBO and hyperbaric pressure represents a more efficient cell protective mechanism which may have been less functional in hyperoxia and possibly inactivated in the control sample. On the other hand, nrf2 distribution showed predominant perinuclear association post hyperoxia relative to the control. Perinuclear nrf2 partitioning in oxidatively stressed human choriocarcinoma cells is due to mitochondrial dysfunction and precedes cell membrane disruption and cell death (Hallmann et al 2004, Plafker and Plafker 2015). Likewise, here, the prospect of mitochondrial dysfunction in HDMEC post hyperoxia, and to a smaller extent hyperbaric pressure is inferred based on the observed nrf2 perinuclear partitioning. Owing to these differences in nrf2 distribution post treatments, further studies are required to accurately pin-point the effects of HBO, hyperoxia and hyperbaric pressure on nrf2 distribution in HDMEC. In addition, due to the limitations of using an ordinary fluorescent microscope such as the possibility of overlapped cellular structures, these preliminary cellular distribution data require further studies with confocal imaging to accurately pin-point nrf2 distribution.

HO-1 possesses a complex role in angiogenesis, in addition to exhibiting antioxidant, antiapoptotic, and anti-inflammatory roles (Bussolati et al 2006). Based on preliminary WB data, HO-1 appeared elevated in response to treatments; HBO, hyperoxia and hyperbaric pressure relative to control, which may have been nrf2 mediated. In addition, HO-1 protein appeared elevated in control condition and HBO in response to high glucose versus low glucose which suggests HO-1 induction to arrest high glucose associated cellular insult. In hyperoxia, HO-1 level seemed consistent in low and high glucose, suggesting a hyperoxia alone associated effect. Fundamentally, HO-1 exerts a positive feedback control on the synthesis and activity of VEGF, thus highlighting an essential role for HO-1 in VEGF mediated angiogenesis (Bussolati et al 2006). Therefore, it is likely HO-1 induction in response to these treatments might result in HO-1 mediated mechanisms e.g. angiogenesis, anti-oxidation, anti-apoptosis and anti-inflammation but further studies are required to qualify this. Due to variabilities in HO-1 expression between replicates and actin loading controls, these results are preliminary and warrant further studies to obtain robust results and to further piece together the relevant mechanisms.

IL-6 mRNA levels in HDMEC post HBO, hyperoxia and hyperbaric pressure but more so HBO were significantly suppressed relative to control. In addition, IL-6 mRNA downregulation showed glucose dependency post HBO and hyperoxia. IL-6 mRNA downregulation in HBO is consistent with previous studies (Benson et al 2003, Al-Waili 2006). In addition, the glucose dependent raise in IL-6 mRNA (i.e. less suppression) in response to high glucose is consistent with a previous study (Piconi et al 2004). Incidentally, unlike HBO, hyperoxia was associated with further suppression of IL-6 mRNA in response to high glucose. Enhanced IL-6 levels is protective in hyperoxic lung injury, hyperoxia-induced cell death, and DNA fragmentation via IL-6 induced expression of the B-lymphoma 2 (Bcl-2) apoptotic regulator gene (Waxman and Kolliputi 2009). Therefore, these glucose-associated responses in IL-6 mRNA post HBO or hyperoxia are likely to have pertinent and distinct cellular effects.

Since IL-6 is regulated mainly at the mRNA level, these changes represent specific regulatory response(s)/mechanisms. It is possible the treatments were associated with decreased synthesis of IL-6 mRNA reflected as a downregulation in IL-6 mRNA levels, which would be in agreement with Benson et al 2003 and Al-Waili 2006. In addition, the likelihood of IL-6 mRNA destabilisation post treatment is not excluded. Possibly, the treatments may have been associated with activation of non-coding micro-RNA (miRNA) mediated destabilisation of IL-6 mRNA (Chen et al 2012, Zilahi et al 2012). Alternatively, the treatments may have been associated with increased IL-6 mRNA translation to IL-6 protein (resulting in the lower levels of IL-6 mRNA) relative to controls. Therefore, more studies are still needed to rightly pin-point the mechanism(s) behind the significant changes in IL-6 mRNA levels post treatments.

HBO is not expected to affect circulating levels of IL-6 in normal individuals (i.e. in unstressed condition) (Thom 2009). But links between high altitude environment (a condition associated with increased cellular stress and adaptation) and increased serum IL-6 exist (Kubo et al 1996, reviewed in Grocott et al 2007). Thus, owing to the observed changes in IL-6 mRNA in response to treatments, the likelihood of cellular stress and adaptation responses post treatments are predicted. Essentially, this suggests the glycemic status of patients undergoing HBO might influence their immunological (IL-6) responses and vice versa.

The probable (preliminary WB) elevation of NFκB post hyperoxia and hyperbaric pressure may be indicative of an acute endothelial cell activation and pro-inflammatory response relative to control (Kobayashi et al 2003). Ironically, NFκB levels post HBO appeared consistently low relative to control which may indicate of a basal NFκB level that is necessary for normal endothelial cell function such as cell growth and the regulation of inflammatory gene targets (Barkett and Gilmore 1999, Dolcet et al 2005). Since nrf2 distribution post HBO was predominantly nuclear, the possibility of an enhanced nuclear nrf2/ NFκB cross-talks leading to amelioration of NFκB accumulation/activation in HBO cannot be excluded (Grottelli et al 2016, Li et al 2008, Kim et al 2013, and Minelli et al 2012). In addition, elevated nuclear nrf2 levels post HBO might have resulted in an increase in nrf2 mediated anti-inflammatory target signalling which might have dampened any NFκB activation and pro-inflammatory responses (Bellezza et al 2018, Grottelli et al 2016, Li et al 2008, and Minelli et al 2012). Exposure of human aortic endothelial cells (HAEC), high glucose (10 mM and 20 mM) resulted in increased activation of NFκB leading to the inhibition of endothelial cell migration, a phenotype associated with impaired wound healing (Hamuro et al 2002). In this study, whilst NFκB activation was observed post hyperoxia and hyperbaric pressure, the effect of glucose on NFκB activation was not evident. However, it is likely variability in actin loading controls may have confounded the discernment of any glucose associated effect.

To summarize this chapter, redox (nrf2) and pro-inflammatory responses in HDMEC were affected by varying glucose concentration, oxygen and pressure. Redox and pro-inflammatory are associated with cellular responses to high glucose (hyperglycaemia). In the following chapter, the role of HIF1α as a converging point is examined. In addition, the expression of vascular endothelial growth factor (VEGF) is examined. Lastly, an endothelial cell proliferation marker (PECAM-1) is used to examine the effect(s) of treatments on HDMEC. These studies are carried out using both single cell system (HDMECs) and a retinal explant model.



## 5.6 Limitations

There were variabilities in NFκB expression between replicates as well as their actin loading controls making it difficult to draw conclusions on the expression of nrf2, HO-1 and NFκB based on WB assay alone. Due to these inconsistencies, the WB data are seen as initial preliminary data which require further experimental designs and optimisations for robust WB data. Throughout the study, HDMEC between passages P4-7 were used. So, it is likely the variabilities in target expressions are as a result of cells being in different cell cycle stages. In future design, prior validation experiments should be undertaken to identify optimal passage number(s) for the expression of targets of interest. Secondly, HDMEC is a mixture of HDLEC and BECs, and the variability may be a reflection of having two cell populations, albeit since HDLEC are in majority, it is possible they exhibited dominant characteristics. The use of an ordinary fluorescent microscope for ICC imaging of nrf2 expression produced satisfactory results for ascertaining nrf2 accumulation as well as giving preliminary indication to nrf2 cellular distribution. However, exact cellular distribution and association of nrf2 under the different conditions could not be confirmed. In future experimental design, confocal microscopy would be desirable.

Lastly, measurement of IL-6 content of media was not undertaken in order to postulate any functional implication of IL-6 mRNA downregulation post treatments. In future, the experimental design would need to be adapted to include the measurement of IL-6 protein in the media using an ELISA technique in order to confirm a functional effect of IL-6 mRNA downregulation.

## Chapter 6.0: HIF-1 $\alpha$ , VEGF and PECAM-1 expression

## 6.1 Hypothesis

The changing concentration of glucose, oxygen tension and pressure has an effect on human dermal microvascular endothelial cell HIF-1 $\alpha$  expression leading to angiogenesis and cell proliferation

## 6.2 Introduction

Endothelial cell phenotype, metabolic activity and key endothelial cell functions such as migration and angiogenesis are linked (Doddaballapur et al 2015). From the previous chapters, HDMEC sizes were significantly changed in response to hyperoxia relative to control. Based on ICC fluorescence intensity, nrf2 level was significantly decreased in response to high glucose in the control condition whilst HBO, hyperoxia and hyperbaric pressure were associated with nrf2 stabilisation and accumulation relative to control. In addition, nrf2 distribution was distinct post HBO and hyperbaric pressure, and hyperoxia relative to control. Consequently, based on preliminary WB, nrf2 stabilisation and accumulation post treatments appeared to have resulted in HO-1 induction relative to control. Moreover, high glucose associated effect on HO-1 induction appeared imminent for HDMEC in control condition and HBO, but HO-1 induction post hyperoxia seemed independent of glucose concentration. Immunological response (IL-6) was significantly impacted following treatments and IL-6 mRNA levels showed pertinent glucose dependent response in HBO. More so, HDMEC activation and pro-inflammatory response appeared likely post hyperoxia and hyperbaric pressure, whilst remaining basal post HBO relative to control. Caution is to be exercised in the interpretation and conclusions of results from WB data since there were variabilities in targets (HO-1 and NF $\kappa$ B) expression between replicates and actin loading controls.

In this chapter, the effects of high glucose in isolation or in combination with HBO, hyperoxia and hyperbaric pressure on HIF-1 $\alpha$ , VEGF and PECAM-1 are examined. Acute or prolonged hyperglycaemia leads to increased ROS, AGEs and RAGE resulting in the activation of PKC and overstimulation of the hexosamine pathway (Brownlee 2005). These hyperglycaemia induced responses result in damaging oxidative stress which sets up damaging glucotoxicity pathways: PKC, hexosamine and polyol and AGE, in addition to NF $\kappa$ B driven expression of pro-inflammatory cytokines (Knott and Forrester 2003, Obrosova et al 2005, Brownlee 2001 and 2005, Adamis 2002). In the diabetic endothelium, glucotoxicity associated insults impair endothelial function leading to macro and microvascular complications including DR and impaired wound healing (reviewed in Sena et al 2013).

Importantly, hyperglycaemia is the primary initiating factor in DR affecting all the three parts of retinal vessels (reviewed in Knott and Forrester 2003). Chronic hyperglycaemia complexly affects both HIF-1 $\alpha$  stability and activation, resulting in the suppression of HIF-1 target genes that are essential for wound healing (Sunkari et al 2015). HIF-1 $\alpha$  is regulated by oxygen-dependent and non-oxygen dependent stimuli such as growth factors, ROS, and mechanical stress (Wang et al 1995, Semenza, 1998, Zhong et al 1998, Haddad et al 2001 and 2002). Several of the non-oxygen dependent activators of HIF-1 $\alpha$  primarily trigger HIF-1 signalling through their action on HIF-1 $\alpha$  translation, which is different from the classic hypoxic stimuli on HIF-1 because hypoxia classically exerts its effect on HIF-1 $\alpha$  protein (reviewed in Ziello et al 2007).

ROS increase during inflammation causes HIF-1 $\alpha$  accumulation and activation (Haddad et al 2001 and 2002). In addition, HIF-1 $\alpha$  activation during inflammation and upregulation of classical target genes like VEGF, GLUT1 and metalloproteinase, as well as HIF-1 targeting of immune functions such as  $\beta$ 2 integrins and chemokines receptors activation are documented (reviewed in Ziello et al 2007). Hyperglycemia activates signalling pathways such as the PKC pathway and drives HIF-1 signalling even in normoxia. Moreover, the PKC pathway also stimulates the expression of the S6 ribosomal proteins which specifically recognizes and drives HIF-1 $\alpha$  mRNA translation. Hence, in normoxia prolyl hydroxylases (PHD) driven proteasomal degradation of HIF-1 $\alpha$  can be countered via high glucose associated PKC driven increased S6 phosphorylation which is associated with increased HIF-1 $\alpha$  mRNA translation into HIF-1 $\alpha$  protein, and consequently increased HIF-1 signalling (Ziello et al 2007).

Arguments that support HIF-1 $\alpha$  destabilisation, proteasomal degradation as well as inhibition of HIF-1 $\alpha$  transactivation in hyperglycaemia under normoxia exist which may reflect specific cell-type responses (reviewed in Xiao et al 2013). These cell-specific HIF-1 $\alpha$  responses in hyperglycaemia under normoxia as reviewed in Xiao et al (2013) is summarised in the following paragraphs. In HDMEC and human dermal fibroblasts (HDF), hyperglycaemia induced osmolality results in HIF-1 $\alpha$  destabilisation. In addition, hyperglycaemia promotes the formation of methylglyoxal (MGO) which covalently modifies HIF-1 $\alpha$  and p300/CBP co-activator. Covalent modification of HIF-1 $\alpha$  leads to decreased HIF-1 $\alpha$  and HIF-1 $\beta$  dimerization, culminating in decreased HIF-1 and HRE binding. More so, HIF-1 $\alpha$  modification by MGO increases its association with heat shock protein (HSP) 40/70, which recruits the carboxyl terminus of the Hsc70-interacting protein (CHIP) and promotes HIF-1 $\alpha$  proteasomal degradation. Furthermore, covalent modification of p300 by MGO leads to a reduction in HIF-1 $\alpha$  transactivational capacity because p300 modification inhibits the interaction of the C-terminal transactivation domain (CTAD) of HIF-1 $\alpha$  and p300.

In retinal epithelial (RPE) cells, MGO formed as a result of hyperglycaemia increases the sensitivity of the hydroxyl groups on HIF-1 $\alpha$  to VHL machinery. Moreover, hyperglycaemia suppresses the N-terminal (NTAD) and C-terminal (CTAD) transactivation domains on HIF-1 $\alpha$ . Ironically, hyperglycaemia induced ROS can result in HIF-1 $\alpha$  impairment although ROS is classically expected to increase HIF-1 $\alpha$  (Brownlee 2005, Nishikawa et al 2000). In addition, ROS produce  $O^{2-}$  which reacts with NO leading to NO unavailability leading to decreased HIF-1 $\alpha$  accumulation and activation because NO is required for HIF-1 $\alpha$  activation. More so, ROS inhibits HIF-1 $\alpha$  expression via ROS induced repression of Ras-related C3 botulinum toxin substrate 1 (Rac1) expression because Rac1 contributes to HIF-1 $\alpha$  transactivation. Moreover ROS impairs HIF-1 $\alpha$  by activating PHD ubiquitin-proteasome activity.

Growth factors are oxygen independent mediators of HIF-1 $\alpha$  regulation. Growth factors drive HIF-1 signalling via the PI3K, a serine/threonine kinase AKT (protein kinase B), and FKBP-rapamycin associated protein signalling (FRAP) (Zhong et al 1998). The PI3K/AKT/mTOR pathway is involved in HIF-1 signalling and angiogenesis in endothelial cells and in normal or cancerous tissues, thus providing a link between HIF-1 signalling in physiological and diseased states (Karar and Maity 2011). Taken together, HIF-1 $\alpha$  impairment/ destabilisation by hyperglycaemia is a cell-type specific/dependent response (Xiao et al 2013).

Angiogenesis is under the control of HIF-1 activity via HIF-1 mediated regulation of VEGF, the primary cytokine in angiogenesis (Lin et al 2004). HO-1 is also involved in VEGF-induced endothelial activation and angiogenesis (Bussolati et al 2006). In addition, VEGF molecule is involved in migration and in the transduction of mechano-stimuli in endothelial cells (Fujiwara 2006, Tzima et al 2005). In diabetic wounds, HIF-1 $\alpha$  and VEGF are suppressed, with decreased angiogenesis and wound healing, which is reversed with HBO (Sunkari et al 2014, Lin et al 2017). Incidentally, wound healing and clinical outcomes with HBO vary and a lack of tight glycemic control might play a role, since hyperglycaemia exerts suppresses HIF mediated VEGF expression in dermal endothelial cells. Contrarily, in diabetic retinopathy (DR), there is over-production of VEGF which causes the progression of proliferative DR and diabetic macular oedema (DME) even in the face of a hyperglycaemic milieu (Simo and Hernandez 2009, Antonetti et al 1999). This again illustrates a cell/tissue-type specific and dependent response to hyperglycaemia.

The platelet endothelial cell adhesion marker (PECAM-1) is expressed by endothelial cells of all vascular beds and it plays a critical role in the maintenance of endothelial cell to cell contact and junctional integrity needed for normal endothelial cell growth (Podgrabinska et al 2010, Privratsky and Newman 2014). In addition, PECAM-1 presence in endothelial cells is associated with absence of endothelial-mesenchymal transition (EMT) and MMP-2 expression (Enciso et al 2003). Thus, the absence/downregulation of PECAM-1 may be indicative of endothelial cell activation. PECAM-1 undergoes phosphorylation on tyrosine residues (activation) in response to mechanical and biochemical stimuli such as shear/stretch stress and high glucose respectively (reviewed in Ilan et al 2000, Fleming et al 2005, Fujiwara 2006, and Tzima et al 2005). Moreover, high glucose is associated with the downregulation of junctional proteins in endothelial cells (Yan et al 2012). Hence, mechanical stimuli and high glucose are expected to influence PECAM-1 expression in HDMEC.

HBOT is a treatment modality involving the use of hyperbaric oxygen (HBO). Its exact mechanisms are still being studied and there are questions about the contribution of its components (HBOT Trust 2018, Thom 2011, Godman et al 2010, Löndahl et al 2013, and Akgu"et al 2014). HBO is known to elicit beneficial ROS response (Thom 2011, Zhao et al 2017). Hyperoxia when used as a single component is associated with cell death, inflammation, induction of stress responses, and modulation of cell growth. In addition, hyperoxia elicits its mechanisms majorly via the mitogen-activated protein kinases (MAPK; ERK, JNK and p38), activator protein -1 (AP-1) and NFkB and these pathways converge, in the expression of a range of stress response genes, cytokines, and growth factors (Lee and Choi 2003).

HBO has a complex effect on HIF-1 $\alpha$  stability and transactivation (Sunkari et al 2015). HBO-mediated HIF-1 $\alpha$  stabilisation is not a direct consequence of high oxygen levels but HBO-induced mechanisms including ROS increase (Thom 2009). Paradoxically, ROS is not the direct effector of HIF-1 $\alpha$  stability post HBO because ROS stabilises HIF-1 $\alpha$  through VHL mediated prolyl hydroxylase (PHD) inhibition, whilst HBO-mediated HIF-1 $\alpha$  stability is VHL/PHD-independent (Sunkari et al 2015). Likely mechanisms for HBO mediated HIF-1 $\alpha$  stabilisation have been proposed. ROS mediated increases in heat shock protein (HSP90) post HBO is proposed to result in HIF-1 $\alpha$  stabilisation (Isaacs et al 2002, Cabigas et al 2006). Other HBO induced mechanisms are suggested to occur via; the receptor for activated C kinase 1 (RACK1), mouse double minute 2 Mdm2, fork head box O4 (FOXO4), Jun activation domain-binding protein-1 (Jab1) and glycogen synthase kinase 3 (GSK3) (Liu et al 2007, Carroll and Ashcroft 2008, Tang and Lasky 2003, and Flugel et al 2007).

There is on-going debate on the safety of HBO in DR based on a theoretical risk of increased neovascularisation, but available data have so far suggested otherwise. For instance, based on a recent report, HBO administration caused increased oxygenation and choroidal blood supply as well as decreased fluid retention (oedema) in the retina (Murphy-Lavoie et al 2017). As a caution, more studies are still required to understand HBO and its long-term effects in retinal complications in diabetes for safer clinical use as a treatment option.

The aim of this chapter is to understand the role of varying glucose concentration, oxygen and pressure on the expression of HIF-1 $\alpha$  and VEGF. In addition, the effect (s) of treatment on PECAM-1 expression is examined. The understanding of this concept will help inform further on the mechanisms of HBO in the context of high glucose, as well as decipher the contribution of the single components of HBO.

## 6.3 Materials and Method

Sample when used in this section may refer to cells (HDMECs), or retinal explants. Where needed, the sample is mentioned specifically. Non-confluent HDMECs cells grown in HDMEC growth media (MV) (PromoCell) at a density of 35,000-38,000 cells/well in 24-well plates in low (5.5 mM). For high glucose treatment, HDMEC growth media (containing 5.5 mM glucose) was supplemented with 14.5 mM D-glucose to give a final concentration of 20mM. Samples were set up in duplicates (immunocytochemistry) or sixplicates (western blot, WB). Retinal tissues from adult pigs weighing 70-80kg of both sexes were derived under aseptic conditions. Retinal tissues were cultured in low (1g/L i.e. 5.5 mM) or high (4.5g/L i.e. 25 mM) glucose within a three-dimension (3D) bilayer matrix with retinal tissue sandwiched (explants) in duplicates. Full details of HDMEC and retinal explant culture are reported in chapter 2 sections 2.2 and 2.3 respectively. Samples were exposed to; HBO, hyperoxia, or hyperbaric pressure alone with equivalent samples in control condition (controls). Post treatment, samples were incubated for 2 h (explants) or 4 h (HDMECs) and 24 h, and harvested for assays.

HDMEC were stained for immunocytochemical analysis by incubating overnight at 4°C with primary antibodies (1:50); anti-HIF-1 $\alpha$  (ThermoFisher Scientific), anti-VEGF (Santa Cruz), and anti-CD31 (Sigma-Aldrich), followed by incubation with goat anti-mouse IgG, DyLight 488 conjugated highly cross-adsorbed secondary antibodies (1:500) (see table 2.1 for full list of antibodies and supplier details). HDMEC were counterstained with DAPI (1 $\mu$ g/ml) and images were visualised with a fluorescent microscope; Leica DMIL microscope with attached camera (Leica DC200) at 400X magnification. Serial retinal explant sections (20  $\mu$ m) on Superfrost Plus slides were stained according to standard Immunohistochemical protocol with validated primary monoclonal mouse anti-Hif1 $\alpha$  (1:20), and anti-cd31 (1:20) diluted in 1x TBS. Antigen detection was completed with fluorescently labelled DyLight 488 Goat anti-mouse IgG (H+L) Highly crossed adsorbed secondary antibody (1:200) (ThermoFisher Scientific) according to the manufacturer's instructions. Sections were counterstained with 1  $\mu$ g/ml of DAPI for nuclear delineation and visualized with an inverted fluorescent microscope at 200X magnification and documented as micrographs. Blotted PVDF membranes were incubated with primary targets (1:100); anti-HIF-1 $\alpha$  (ThermoFisher Scientific), anti-VEGF (Santa Cruz) overnight with anti- $\beta$ -actin (St John's Labs, UK) as loading control. Blotted targets were detected with Goat anti-mouse IgG\_ Horseradish peroxidase (HRP) conjugated secondary antibody diluted in 1.5% BSA/TBS and visualised by chemiluminescence. WB results are presented as sample blots in the relevant sections. WB results are preliminary results due to variabilities in the target (HIF-1 $\alpha$  and VEGF) expression and actin loading controls.



## 6.4 Results

### 6.4.1 Effect of glucose concentration, oxygen tension and pressure on HIF-1 $\alpha$ , VEGF and PECAM-1 protein expression

The expressions of HIF-1 $\alpha$  and VEGF between replicates and their actin loading controls were variable and the presented WB blots are preliminary. Variability of HIF-1 $\alpha$  expression may be indicative of HIF-1 $\alpha$  destabilisation via PHDs in normoxia post treatment, which highlights a potential need for PHD blockade in future studies. Although, HBO-mediated HIF-1 $\alpha$  stabilisation is VHL/PHD independent (Sunkari et al 2015), the likelihood of HIF-1 $\alpha$  destabilisation during incubation under control condition post treatment cannot be excluded.

Based on preliminary representative WB data, nuclear HIF-1 $\alpha$  appeared elevated at 4 h post HBO, hyperoxia and hyperbaric pressure in comparison to control (fig 6.1, A). Cytosolic HIF-1 $\alpha$  levels appeared consistent in all samples which may be indicative of basal HIF-1 $\alpha$  level (fig 6.1, B). In both nuclear and cytosolic fraction, glucose associated effects on HIF-1 $\alpha$  expression did not appear evident.

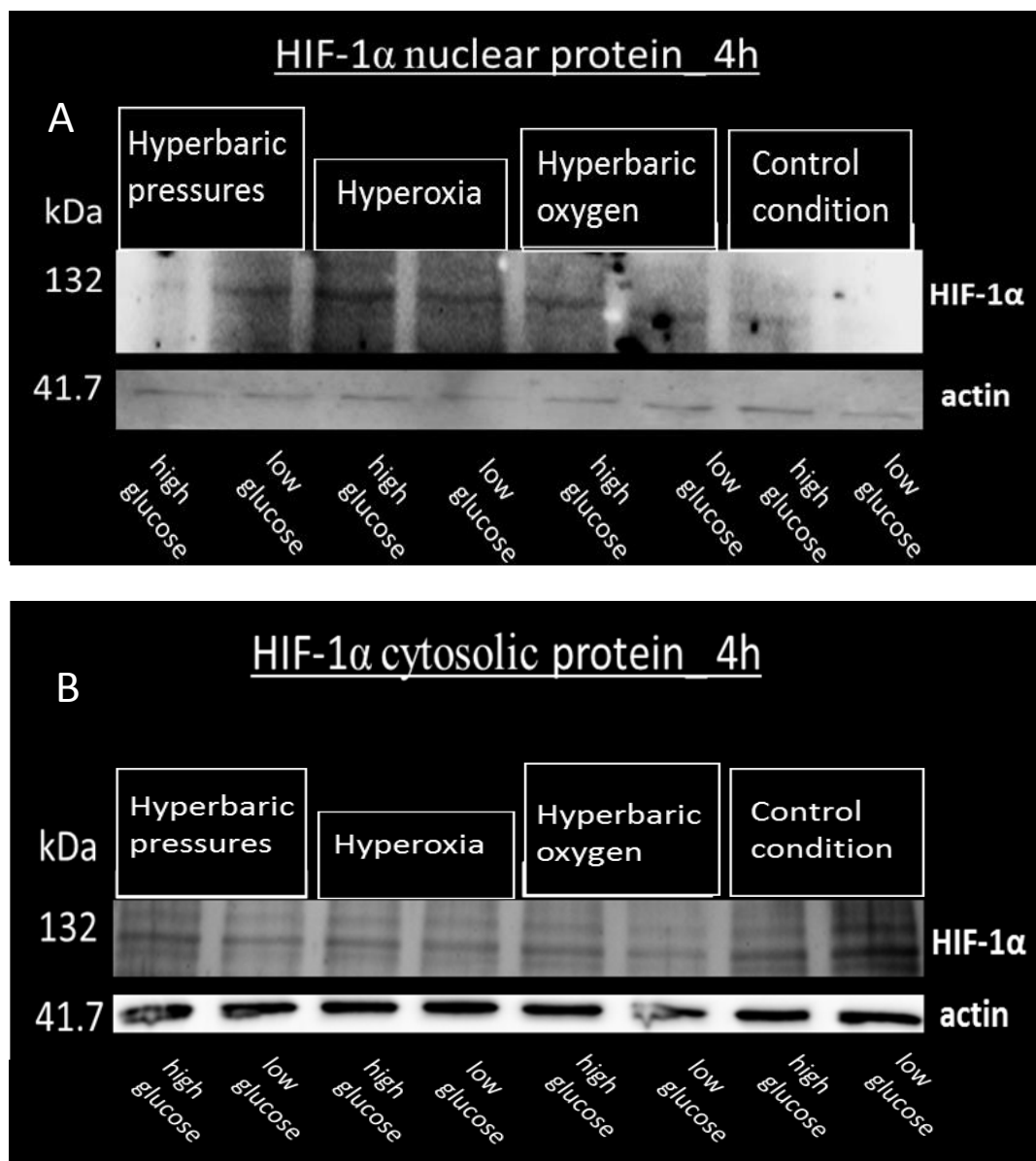


**Figure 6. 1 Western blots of HIF-1 $\alpha$  at 4 h**

Representative nuclear blot may indicate increased HIF-1 $\alpha$  protein following HBO, hyperoxia and hyperbaric pressure in comparison to control. Cytosolic HIF-1 $\alpha$  levels appeared unchanged in all the conditions relative to control which may be indicative of basal cytosolic levels. WB data of nuclear and cytosolic expression of HIF-1 $\alpha$  at 4 h and the actin loading were variable. Therefore, the presented blots are preliminary. WB analysis of nuclear HIF-1 $\alpha$  was performed in more than three independent experiments which were variable and only result of one replicate is presented. Lysates were harvested from HDMEC pooled from six identical wells per sample at 4 h post treatment.

Based on preliminary results, nuclear HIF-1 $\alpha$  appeared elevated post HBO (low glucose) when compared to control, which might be indicative of HBO associated nuclear HIF-1 $\alpha$  increase (fig 6.2, A). HIF-1 $\alpha$  levels in high glucose post HBO appeared diminished relative to low glucose sample, which may be suggestive of high glucose mediated HIF-1 $\alpha$  suppression in HDMEC. Cytosolic HIF-1 $\alpha$  protein appeared elevated post hyperoxia relative to control (fig 6.2, B).

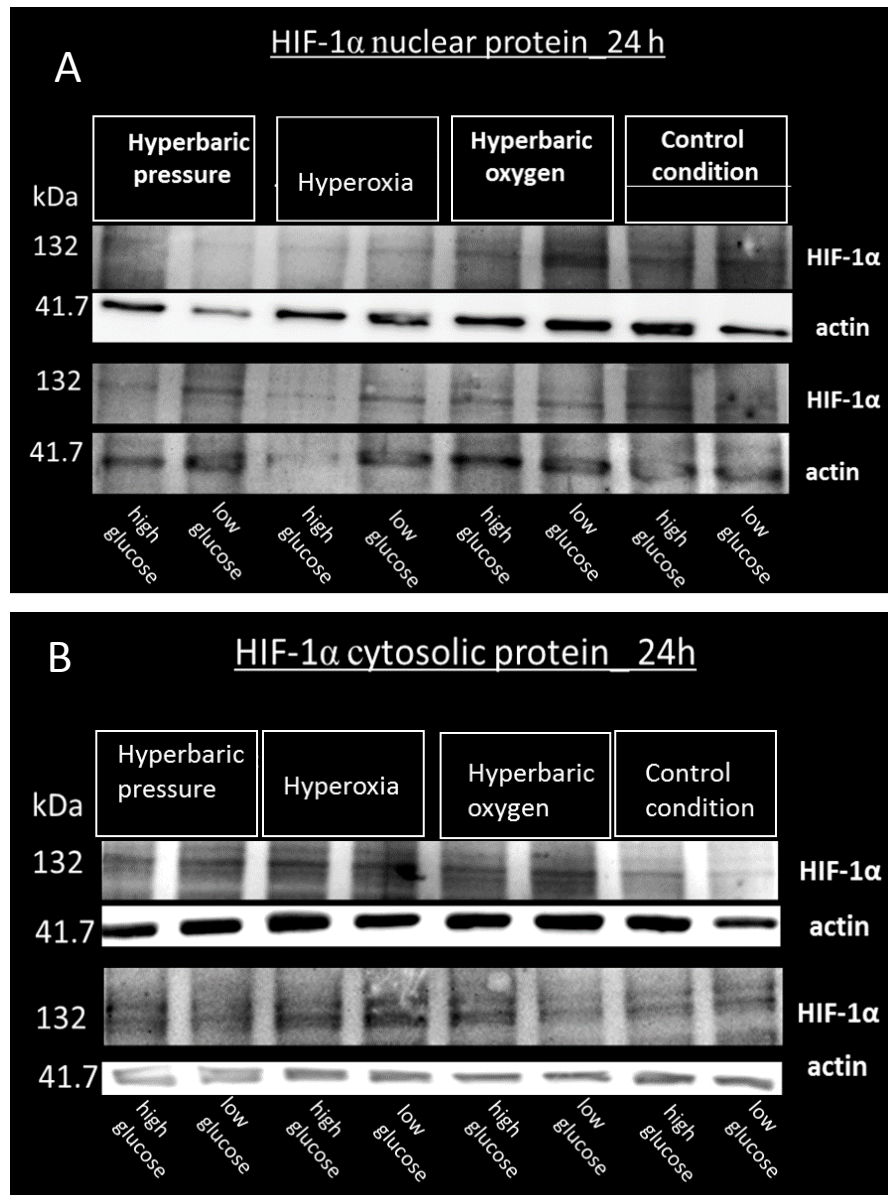


**Figure 6. 2 Western blots of HIF-1 $\alpha$  at 24 h**

Representative nuclear blots may indicate increased nuclear HIF-1 $\alpha$  post HBO (low glucose) relative to control (A). In addition, nuclear HIF-1 $\alpha$  post HBO appeared diminished in high glucose relative to low glucose. Cytosolic HIF-1 $\alpha$  appeared elevated in hyperoxia relative to control. Blots are representative of n = 2 independent experiments. WB results and actin loading were variable and would need to be repeated further for a more reproducible result. Lysates were harvested from HDMEC pooled from six identical wells per sample at 24 h post treatment.

Preliminary WB data of VEGF expression appeared to indicate increased VEGF levels post hyperoxia (high glucose) in comparison to control. VEGF accumulation may coincide with an earlier observed increase in HO-1 following hyperoxia which may suggest a VEGF mediated HO-1 induction in hyperoxia but further studies are needed.

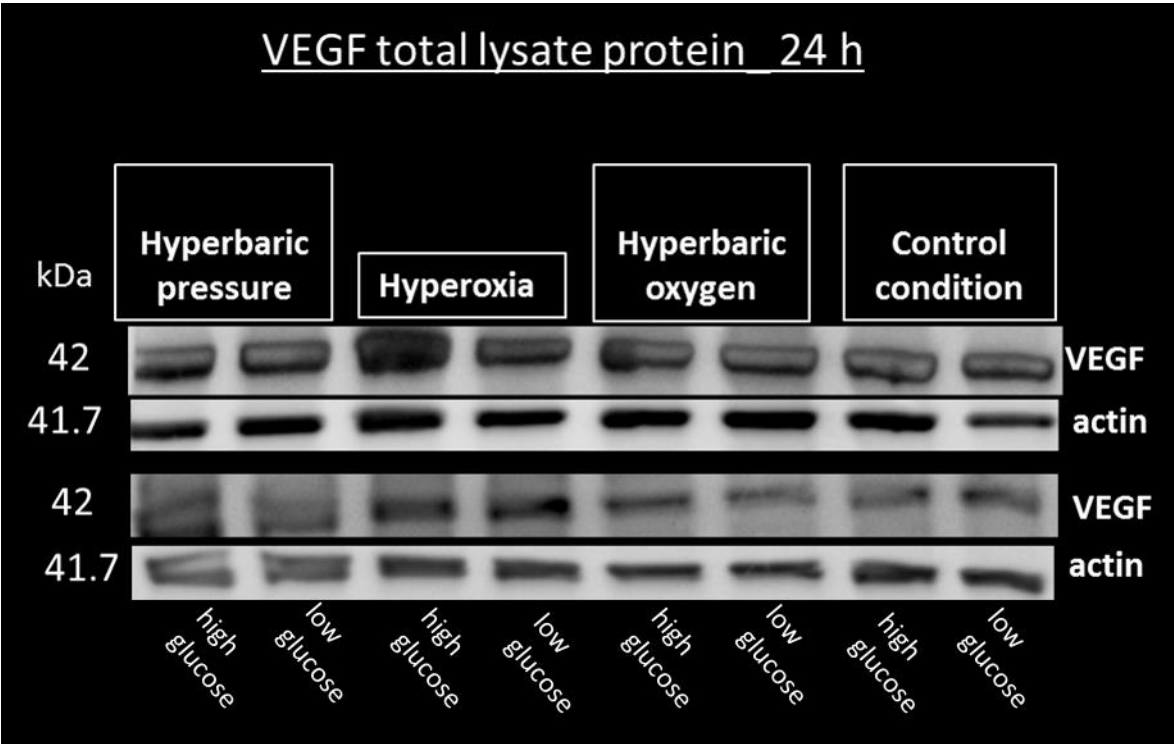


**Figure 6. 3 Western blots of VEGF at 24 h**

VEGF level appeared elevated in response to concomitant hyperoxia and high glucose relative to control. Blots are representative of n = 2 Independent experiments. Owing to the variability in WB results and corresponding variation of actin loading control, these preliminary data would need to be further examined to obtain more reliable data.

Immunocytochemical (ICC) staining was used to ascertain HIF-1 $\alpha$ , VEGF, and PECAM-1 expression in HDMEC at 4 h and 24 h post treatments. But HIF-1 and VEGF detection with ICC were not satisfactory (results not included). Representative ICC micrographs of PECAM-1 of  $n \geq 4$  independent experimental replicates are presented.

In control samples, high glucose was associated with an acute (4 h) downregulation of PECAM-1 in comparison to low glucose (fig 6.4A vs B). High glucose associated downregulation of PECAM-1 may not have been sustained as the effect was no longer apparent after 24 h (fig 6.4D vs B). Increased deposition of PECAM-1 within likely endothelial junctions with stress fibres visible seemed apparent (fig 6.4D, white arrowheads). HBO was not associated with PECAM-1 downregulation in response to high glucose and PECAM-1 appeared unchanged irrespective of time in culture relative to control (fig 6.5). Hyperoxia alone (fig 6.6) was associated with PECAM-1 upregulation (increase) relative to control. Concomitant hyperoxia and high glucose further augmented PECAM-1 upregulation (increase) relative to control, which may indicate an acute (4 h) PECAM-1 upregulation to counter concomitant hyperoxic and high glucose insult. Within 24 h, PECAM-1 expression post hyperoxia appeared suppressed and seemed worsened in concomitant hyperoxia and high glucose relative to control (fig 6.6 C and D). HDMEC exposure to hyperbaric pressure was associated with PECAM-1 upregulation relative to control. PECAM-1 expression in hyperbaric pressure did not change in response to glucose concentration or time in culture relative to control (fig 6.7).

## ICC detected PECAM-1 in HDMEC in control condition

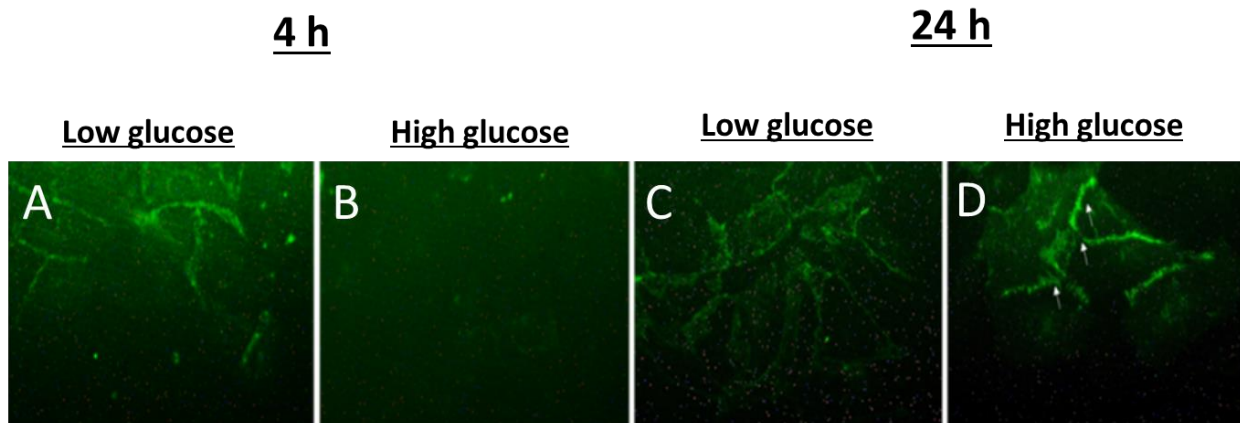


**Figure 6.4 ICC detection of PECAM-1 in HDMEC at 4 h and 24 h in control condition**

HIF-1 $\alpha$  and VEGF protein were not at a level detectable with ICC for HDMEC in control condition. Acute (4 h) high glucose associated downregulation of PECAM-1 appeared imminent, but the effect was no longer apparent at 24 h. Increased deposition of PECAM-1 within likely endothelial junctions with stress fibres visible appeared imminent (white arrowheads). Selected micrographs are representative of  $n \geq 4$  independent experiments. Magnification = 400X, scale bar = 500  $\mu$ m.

## ICC detected PECAM-1 in HDMEC in HBO

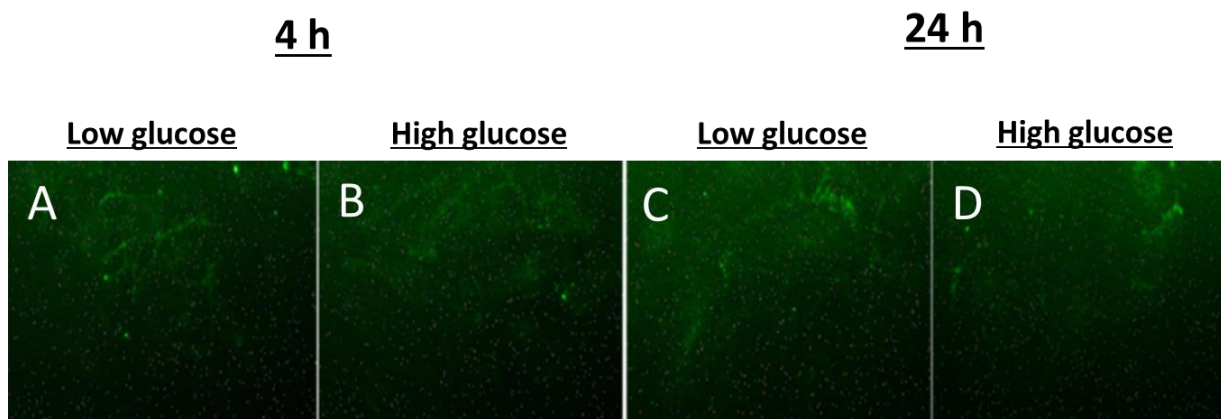


**Figure 6. 5 ICC detection of PECAM-1 in HDMEC at 4 h and 24 h in HBO**

HIF-1 $\alpha$  and VEGF protein were not at a level detectable with ICC for HDMEC in HBO. HBO was not associated with PECAM-1 downregulation/change irrespective of glucose concentration or time in incubation. Selected micrographs are representative of  $n \geq 4$  independent experiments. Magnification = 400X, scale bar = 500  $\mu$ m.

## ICC detected PECAM-1 in HDMEC in Hyperoxia

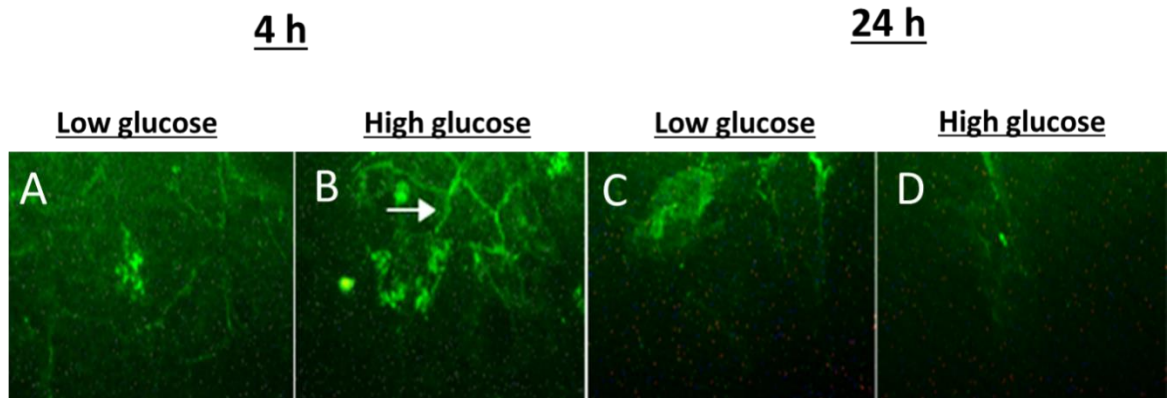


**Figure 6. 6 ICC detection of PECAM-1 in HDMEC at 4 h and 24 h in hyperoxia**

HIF-1 $\alpha$  and VEGF protein were not at a level detectable with ICC for HDMEC in hyperoxia. Acute (4 h) PECAM-1 upregulation in hyperoxia appeared to be present relative to control. Concomitant hyperoxia and high glucose appeared to further augment PECAM-1 expression at 4 h relative to control with increased PECAM-1 deposition along endothelial junctions seen (white arrow). PECAM-1 levels at 24 h was decreased in hyperoxia and further suppressed in concomitant hyperoxia and high glucose relative to control. Selected micrographs are representative of  $n \geq 4$  independent experiments. Magnification = 400X, scale bar = 500  $\mu\text{m}$ .

## ICC detected PECAM-1 in HDMEC in Hyperbaric pressure

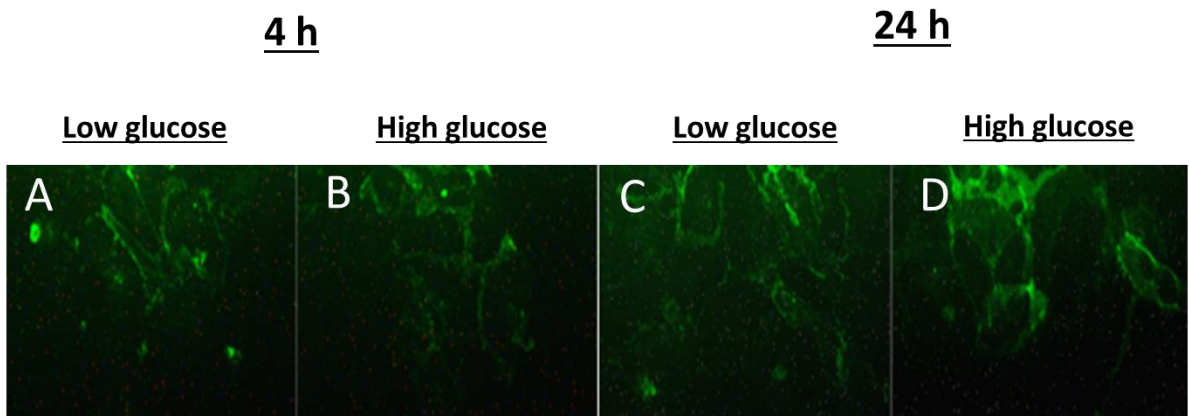


**Figure 6. 7 ICC detection of PECAM-1 in HDMEC at 4 h and 24 h in hyperbaric pressure**

HIF-1 $\alpha$  and VEGF protein were not at a level detectable with ICC for HDMEC in hyperbaric pressure. Hyperbaric pressure appeared to be associated with increased PECAM-1 deposition relative to control. PECAM-1 accumulation post hyperbaric pressure did not appear to be affected by glucose concentration of time in culture. Selected micrographs are representative of  $n \geq 4$  independent experiments. Magnification = 400X, scale bar = 500  $\mu\text{m}$ .

Owing to the lack of HIF-1 $\alpha$  detection with WB or ICC in single endothelial cell model (HDMEC), HIF-1 $\alpha$  expression was studied using immunohistochemistry (IHC) methods in a retinal explant model, which represents a higher complex model with the added benefit of intra- and intercellular cross-talk which might enhance HIF-1 $\alpha$  detection (Matteucci et al 2015). Serial sections were blotted with anti-HIF1 $\alpha$  and anti-PECAM-1. Co-localisation of HIF-1 $\alpha$  and PECAM-1 immunoreactivity served as guide to pin-point endothelial cell associated/specific HIF-1 $\alpha$  expression. HIF-1 $\alpha$  immunoreactivity with punctate (strong and sharp) distribution were tentatively associated with endothelial or leukocyte specific nuclear expression, whilst diffused HIF-1 $\alpha$  immunoreactivity within vessel-like structures which were PECAM-1 positive were associated with HIF-1 $\alpha$  expression within microvessels of the retina. Due to limitations with the quality of the images, it was not possible to accurately pin-point cell-specific HIF-1 $\alpha$  association and distinctions could not be made regarding endothelial or leukocyte specific HIF-1 $\alpha$  associations. The results here therefore provide preliminary data that provide a basis for further investigations. Furthermore, although HIF-1 $\alpha$  expression was linked with their expression in the different layers of the retina and vascular cells (endothelial cells or leukocytes), it is possible that non-vascular cells such as neuronal cells (rods and cones), Muller cells etc. might be expressing HIF-1 $\alpha$ . Hence, the study was further limited in accurately delineating specific HIF-1 $\alpha$  associated cells, and further clarification with confocal is necessary.



Retinal explants in control condition (control) at 2 h and 24 h post treatments showed increased HIF-1 $\alpha$  in high glucose relative to low glucose explants (fig 6.8). Based on the location of the HIF-1 $\alpha$  immunoreactivity, HIF-1 $\alpha$  reactivity appeared limited to the outer retinal layer (ONL) at 2 h (C and D). Remarkably, HIF-1 $\alpha$  immunoreactivity was dampened at 24 h in the low glucose explants but HIF-1 $\alpha$  immunoreactivity appeared elevated and invasive through retinal layers in high glucose explants. HIF-1 $\alpha$  immunoreactivity may be endothelial specific since HIF-1 $\alpha$  reactivity was localised within vessel-like structures which stained positive for PECAM-1 (G and H). This seemed to echo the previous ICC result of increased PECAM-1 expression in response to high glucose for HDMEC in control condition. In retrospect, HIF-1 $\alpha$  upregulation in response to high glucose in the explants was in converse to the absence/lack of HIF-1 $\alpha$  expression in HDMEC highlighting a potential cell-type difference between endothelial cells from retinal origin and dermal origin. In addition, it appears to highlight differences between single versus complex study models.

## IHC detected targets in Retinal explants in control condition

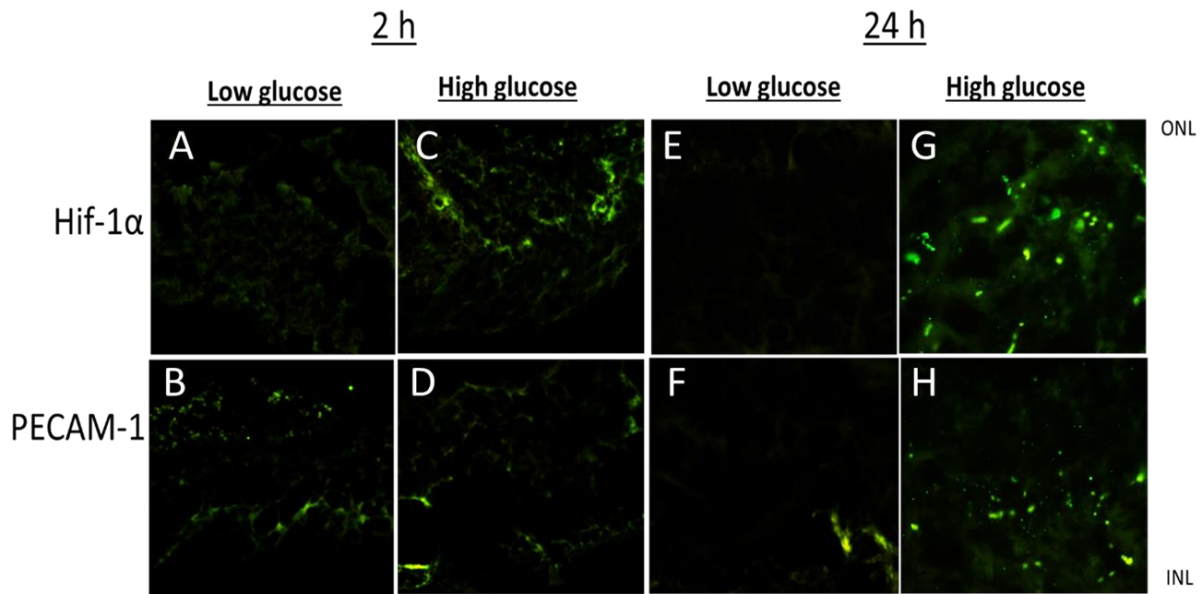


**Figure 6. 8 IHC detection of HIF-1 $\alpha$  in retinal explants at 2 h and 24 h in control condition**

HIF-1 $\alpha$  reactivity appeared elevated in retinal explants in high glucose relative to low glucose at 2 h and 24 h. In addition, HIF-1 $\alpha$  expression at 24 h in response to high glucose appeared to co-localise with PECAM-1 within vessel-like structures which is suggestive of a vessel associated and endothelial or leukocyte associated HIF-1 $\alpha$  expression/activation. Micrographs are representative of  $n \geq 4$  independent experiments. Magnification = 400X, scale bar = 500  $\mu$ m.

Explants in HBO exhibited HIF-1 $\alpha$  immunoreactivity in all retinal layers going from the outer nuclear layer (ONL) (including the photoreceptors) to the inner nuclear layer (INL) and retinal vascular bed (fig 6.9). The majority of HIF-1 $\alpha$  reactive cells appeared to be endothelial based on their elongated shape and co-localisation with PECAM-1. In addition, HIF-1 $\alpha$  reactivity post HBO was both time and glucose concentration independent in comparison to control. More so, several of the HIF-1 $\alpha$  labelled signals were punctate in nature suggesting nuclear associated HIF-1 $\alpha$  expression. Furthermore, HBO was associated with HIF-1 $\alpha$  immunoreactivity within large, moderate and small vessel-like structures identified as retinal vessels based on positive immunoreactivity to PECAM-1 (fig 6.9 G, white arrow (large vessel)). Curiously, large vessel associated HIF-1 $\alpha$  immunoreactivity was not seen in the control explants, which may be indicative of superior oxygenation and HIF-1 $\alpha$  stabilisation, and potentially higher HIF-1 signalling in retinal explant vessel post HBO relative to control.

## IHC detected targets in Retinal explants in HBO

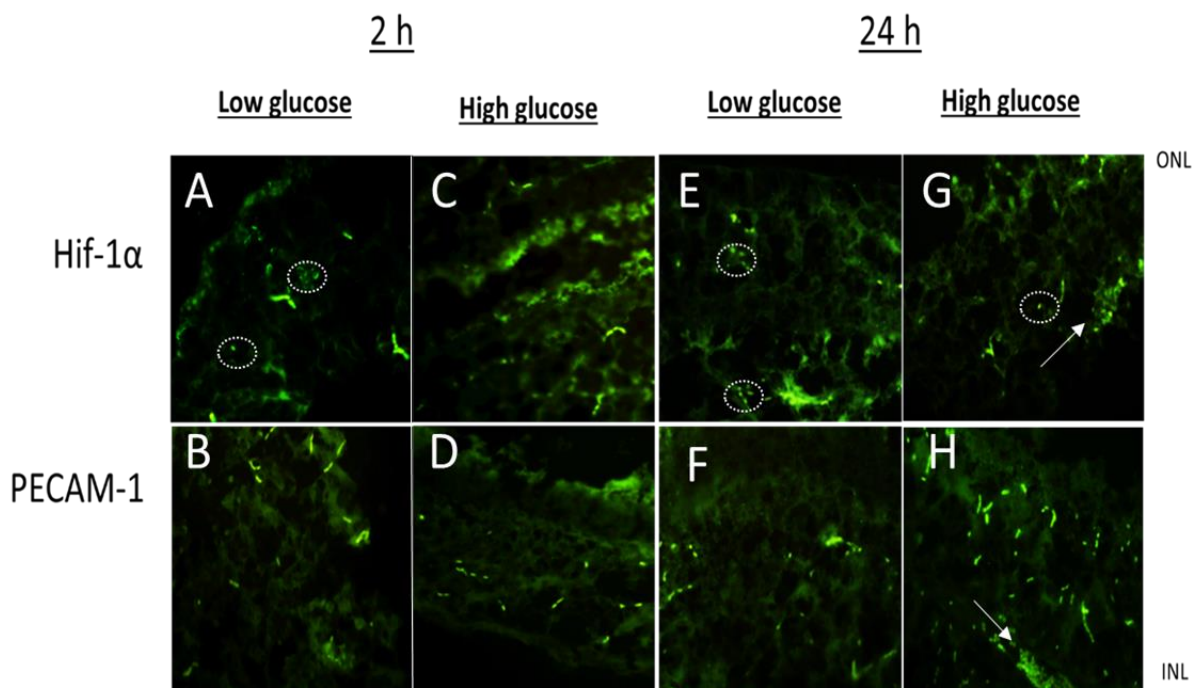


**Figure 6. 9 IHC detection of HIF-1α in retinal explants at 2 h and 24 h in HBO**


HIF-α expression was seen in all retinal layers. HIF-1α levels appeared elevated relative to control. In addition, HIF-1α immunoreactivity was independent of time and glucose concentration. Moreover, the majority of HIF-1α reactive cells were elongated and stained positive for PECAM-1 suggesting they were likely of endothelial lineage. More so, HIF-1α signals were punctate in nature which may be indicative of nuclear HIF-1α association. HIF-1α immunoreactivity in large retinal vessel was seen (white arrow) (G), in addition to moderate and smaller vessel-like structures which were PECAM-1 positive. Micrographs are representative of  $n \geq 4$  independent experiments. Magnification = 400X, scale bar = 500  $\mu$ m.

Explants in hyperoxia (fig 6.10) and hyperbaric pressure (fig 6.11) showed increased HIF-1 $\alpha$  reactivity associated with all retinal layers in comparison to control. In addition, based on the compact/punctate nature of the HIF-1 $\alpha$  labelled signals; hyperoxia and hyperbaric pressure were associated with more nuclear HIF-1 $\alpha$  reactivity relative to control. Vessel associated HIF-1 $\alpha$  immunoreactivity was not pronounced post hyperoxia but explants in hyperbaric pressure showed pronounced HIF-1 $\alpha$  immunoreactivity in moderate sized vessel-like structures relative to control. Hyperoxia was associated with strong HIF-1 $\alpha$  immunolabelling in the ganglion cell layer (GCL) at 2 h. In addition, similar to the pattern of hyperoxia associated PECAM-1 downregulation in HDMEC at 24 h, retinal explants in hyperoxia exhibited dampened PECAM-1 immunoreactivity at 24 h, which was further suppressed in concomitant high glucose and hyperoxia. HIF-1 $\alpha$  immunoreactivity in hyperbaric pressure treated explants was dampened at 24 h similar to control, and unlike HBO explants which highlight a difference in HIF-1 $\alpha$  stabilisation between HBO and hyperbaric pressure.

## IHC detected targets in Retinal explants in hyperoxia

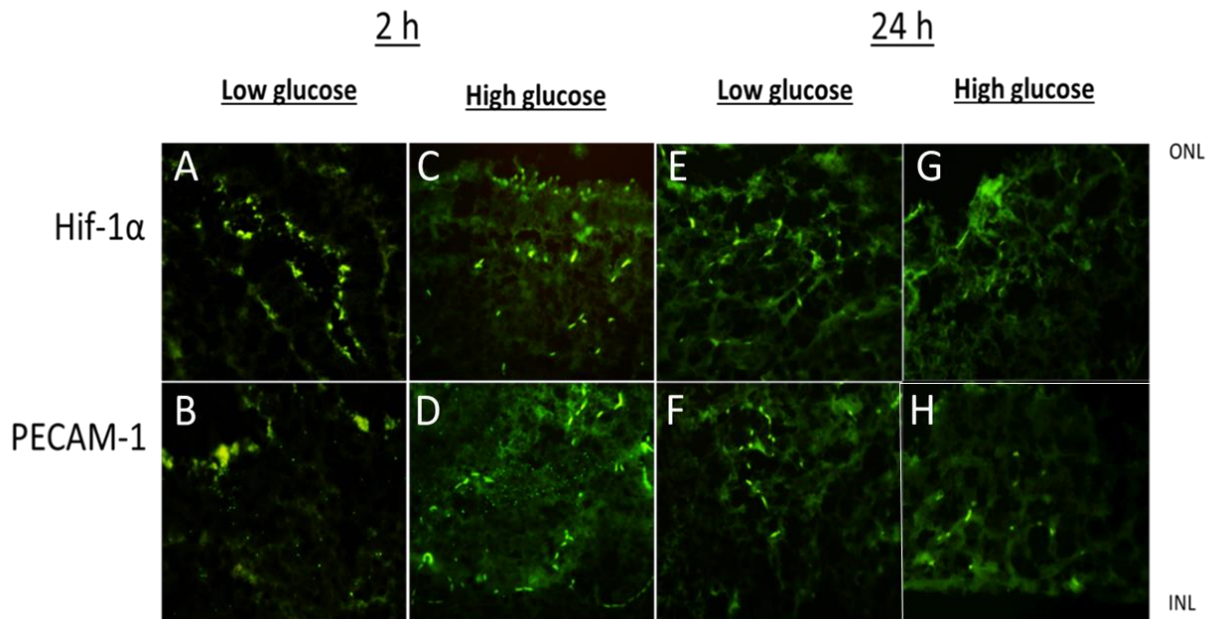


**Figure 6. 10 IHC detection of HIF-1 $\alpha$  in retinal explants at 2 h and 24 h in hyperoxia**

HIF-1 $\alpha$  was detected in explants following hyperoxia in both low glucose and high glucose explants. HIF-1 $\alpha$  immunoreactivity was associated with the outer and inner retinal layer with sparse expression in the middle retinal layer. Strong HIF-1 $\alpha$  labelling in retinal ganglion cell layer was evident in low glucose post hyperoxia. HIF-1 $\alpha$  activation and PECAM-1 expression appeared lessened at 24 h. Micrographs are representative of  $n \geq 4$  independent experiments. Magnification = 400X, scale bar = 500  $\mu$ m. 

## IHC detected targets in Retinal explants in hyperbaric pressure

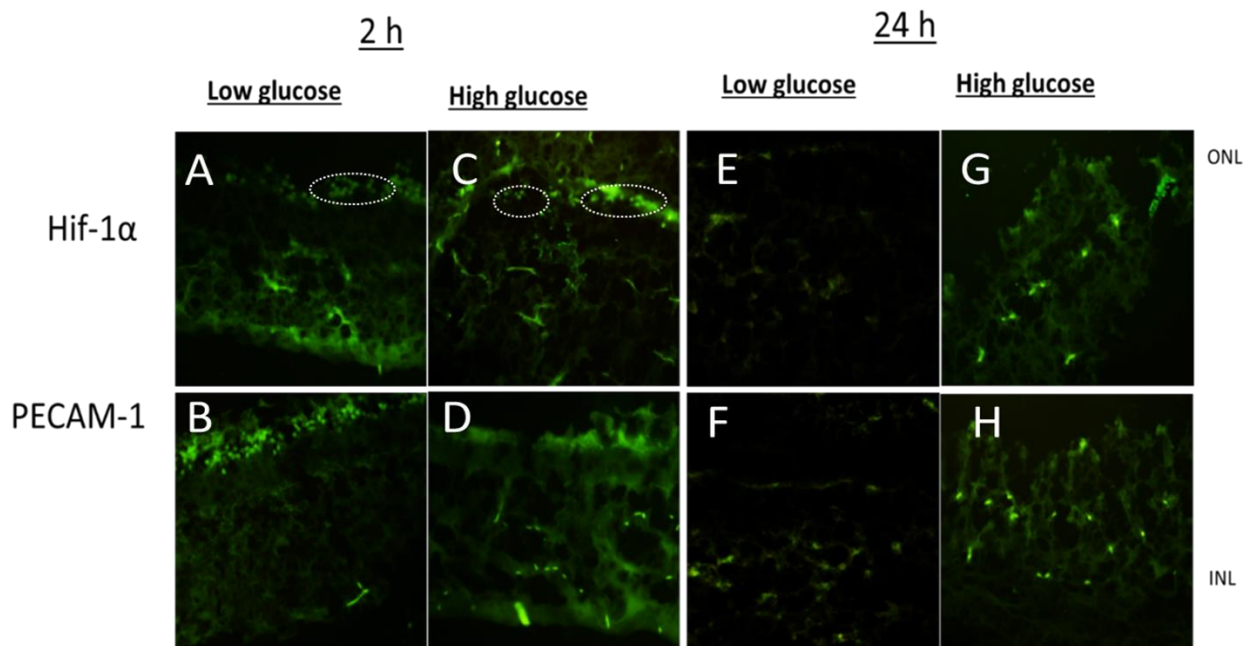


**Figure 6. 11 IHC detection of HIF-1 $\alpha$  in retinal explants at 2 h and 24 h in hyperbaric pressure**

HIF-1 $\alpha$  immunoreactivity appeared elevated at 2h post hyperbaric pressure relative to control. HIF-1 $\alpha$  immunoreactivity post hyperbaric pressure was associated with all retinal layers, moderate and small vessel-like structures (co-localised with PECAM-1). HIF-1 $\alpha$  immunoreactivity was dampened (low glucose) at 24 h. Micrographs are representative of  $n \geq 4$  independent experiments. Circled- highlights photoreceptor reactivity. Magnification = 400X, scale bar = 500  $\mu$ m.



## 6.5 Discussion

Western blot (blot) data of HIF-1 $\alpha$  and VEGF expressions between replicates and their actin loading controls were variable. In addition, ICC study of HIF-1 $\alpha$  and VEGF expressions was not successful. Based on preliminary WB data, HIF-1 $\alpha$  was basal in control condition which may be reflective of low endogenous levels in HDMEC. Curiously, the treatments did not elicit modest HIF-1 $\alpha$  elevation relative to control unlike other HIF-1 $\alpha$  inducers such as dimethyloxallylglycine (DMOG) or cobalt (Ayrapetov et al 2011).

Classically HIF-1 $\alpha$  is degraded in normoxia (Wang et al 1995). Therefore, if normoxia (proline hydroxylation) was exclusively associated with HIF-1 $\alpha$  degradation in this study, then PHD blockade could have been optimal in the experimental design (Wang et al 1995, Baek et al 2005). Hyperglycaemia impairs hypoxia-dependent HIF-1 $\alpha$  protein stability and function (Botusan et al 2008). Here, high glucose appeared to suppress HIF-1 $\alpha$  relative to low glucose in HDMEC. Fundamentally, this demonstrates the impact of glycemic status on HBO outcome, in this instance on HIF-1 $\alpha$  stabilisation. Since all samples were incubated in normoxia for 4 h and 24 h post treatment, it is hard to distinguish between normoxia associated (proline hydroxylation) and hyperglycaemia mediated HIF-1 $\alpha$  degradation, although both can act in concert (Botusan et al 2004). In HDMEC, high glucose (hyperglycaemia) in normoxia causes increased HSP40/70 mediated HIF-1 $\alpha$  ubiquitination and degradation (reviewed in Xiao et al 2013). Hence, HIF-1 $\alpha$  degradation in HDMEC (high glucose) post HBO/treatments stabilisation due to HSP40/70 activity in normoxia is likely. In addition, high glucose induced ROS causes HIF-1 $\alpha$  destabilisation via ROS mediated RAC1 suppression and PHD activation (reviewed in Xiao et al 2013). Thus, ROS mediated PHD activation leading to augmented HIF-1 $\alpha$  degradation in normoxia is expected. This possibility is made more conceivable because nrf2, a ROS regulator, as seen from previous result chapter was induced in response to HBO/treatments. Therefore, low/basal levels of HIF-1 $\alpha$  in HDMEC in general and, in particular in high glucose poses a complex scenario and the exact mechanism(s) remains to be ascertained and these preliminary data warrant further studies.



A clearer picture of HIF-1 $\alpha$  stabilisation/ expression was apparent using the retinal explant model. HIF-1 $\alpha$  was notably increased in response to high glucose relative to low glucose for explants in control condition. Interestingly, explants in control condition did not evidence HIF-1 $\alpha$  immunoreactivity in all retinal layers, although HIF-1 $\alpha$  is expressed in all layers of the retina (Thiersch et al 2009). On the other hand, HBO/hyperoxia/hyperbaric pressure explants showed elevated HIF-1 $\alpha$  immunoreactivity in all retinal layers. In addition, HIF-1 $\alpha$  immunoreactivity post HBO was associated with large, moderate and small retinal vessels (PECAM-1 positive), which appeared consistent with the concept of superior oxygenation and HIF-1 $\alpha$  stabilisation with HBO (Murphy-Lavoie et al 2012). HIF-1 $\alpha$  is stabilised by HBO (Thom 2011, Sunkari et al 2015), in a PHD/VHL independent manner which may involve mechanisms such as increased HSP90 induction, RACK1, Mdm2, FOXO4, Jab1 and GSK3 (Liu et al 2007, Carroll and Ashcroft 2008, Tang and Lasky 2003, and Flugel et al 2007). Therefore, the elevation of HIF-1 $\alpha$  in retinal explants which is indicative of its stabilisation relative to control is expected to have come about via several of these mechanism but further studies are necessary to pin-point the exact mechanism(s).

VEGF exhibits intertwined functions with HO-1 in angiogenesis (Bussolati et al 2004). In human endothelial cells, VEGF induced prolonged HO-1 expression and activity, and inhibition of HO-1 abrogated VEGF-driven angiogenesis (Bussolati et al 2004). Here, preliminary WB suggested VEGF accumulation post hyperoxia relative to control, which may have been oxidant mediated (Sheikh et al 2010). In addition, it is likely the effect (VEGF elevation) accrued from concomitant high glucose and hyperoxia which may be indicative of a hyperglycaemia (PKC mediated) and oxidant mediated VEGF accumulation. Consequently, the likelihood of VEGF mediated HO-1 induction post hyperoxia (high glucose) is a strong possibility since HO-1 levels appeared consistent relative to VEGF. On the other hand, although HO-1 appeared elevated in response to other treatments/high glucose (e.g. in HBO), no corresponding elevation in VEGF levels was seen.

Paradoxically, VEGF expression is also induced via HIF-1 mediated signalling (Botusan et al 2008). Therefore, the low levels of HIF-1 $\alpha$  and consequently decreased HIF-1 signalling as seen with HDMEC samples may be connected to the absence of distinct VEGF upregulation post treatments, the exception being hyperoxia sample (high glucose) where the prevalent mechanisms could not have been HIF-1 $\alpha$  mediated. Interestingly, although HDMEC samples in HBO for instance did not display discernible VEGF upregulation, glucose dependent response in HO-1 induction seemed apparent. Perhaps, the glucose associated HO-1 inductions in these conditions were due to the predominant nuclear nrf2 elevation in HBO and hyperbaric pressure. Based on the variability in VEGF and HO-1 expression, caution is exercised in the over interpretation of these data because further studies are still required to accurately pin-point the exact mechanism.

Long-term (14 days) culture of HUVEC in 30 mM glucose was associated with significant downregulation of PECAM-1 expression in HUVEC cells (Baumgartner-Parzer et al 1995). Likewise here, PECAM-1 expression in HDMEC and retinal explants changed in response to treatment and high glucose was associated with acute (4 h) PECAM-1 downregulation in control condition. In addition, hyperoxia and/or high glucose were associated with PECAM-1 downregulation at 24 h. High glucose phosphorylates VE-cad in endothelial adherens junction causing junctional disruptions in endothelial cells (Haidari et al 2014). Therefore, it is conceivable that high glucose and/or hyperoxia associated downregulation of PECAM-1 in HDMEC might result in disruption of endothelial adherens junctions and consequently loss of endothelial barrier integrity. PECAM-1 downregulation is associated with endothelial cell activation and loss of PECAM-1 protective effect. Thus, hyperoxia and/or high glucose might impact negatively on HDMEC barrier integrity or functions, whilst HBO and hyperbaric pressure are likely to be associated with maintenance of endothelial integrity and PECAM-1 cell-mediated activities (Wang et al 2009, Podgrabinska et al 2010, Privratsky and Newman 2014, Enciso et al 2003, Yan et al 2012).

## 6.6 Limitation

Targets (VEGF and HIF-1 $\alpha$ ) expressions in HDMEC (P4-7) and actin loading control were variable due to differences in passages of HDMEC used. Prior validation of target expression to establish an optimal passage number would have been optimal. In addition, the loading control may not have been optimal. Although, the study deciphered HIF-1 $\alpha$  stabilisation and increased expression in the explants, the mechanisms behind HIF-1 $\alpha$  stabilisation were not determined. In addition, the possibility of HIF-1 $\alpha$  transactivation was not explored, which could have been addressed with HRE reporter gene assay. Instead, efforts were made to answer this question by examining VEGF in HDMEC, a known target of HIF-1. However, HIF-1 $\alpha$  associated VEGF up-regulation was not identified possibly due to HIF-1 $\alpha$  destabilisation in normoxia/hyperglycaemia in HDMEC. Based on preliminary results, the possibility of oxidant and hyperglycaemia associated VEGF elevation appeared likely but the exact mechanisms were not clearly ascertained. Moreover, the variability in VEGF and HO-1 WB expressions further complicated the observations made. More so, corresponding ICC examinations for HIF and VEGF did not give any meaningful results which opens up more questions to address HIF-1 $\alpha$ , VEGF and HO-1 regulations in future studies.

# Chapter 7.0: Limitations, overall discussion and future work

## 7.1 Over all study limitations

Several limitations were encountered in the course of this study. In the western blot (WB) assay, target expressions were varied. In biological experimental systems, the exact same cell (sample) cannot be collected between replicates since protein synthesis, cell size/cycle, or apoptotic ability may be changed at each stage. Thus, it is likely some of the variabilities in target expressions arose from the use of HDMEC at different passage numbers (P4-7), in addition to HDMEC being a mixture of two cell populations (HDLEC and BEC). Actin (loading control) expressions were also highly variable. Being a house-keeping protein (HKP), actin is constitutively expressed and performs essential tasks in cytoskeleton microfilaments in all cellular compartments making it an ideal loading control (Moritz 2017). However, actin exhibits loading and biological variation leading to inaccuracies in loading control, and consequently in accurate determination of target expression. In retrospect, an initial study could have been conducted to determine an optimal loading control well-suited for the experimental conditions in this study. In addition, total protein loading staining (TPS) which are superior to HKP could have been more optimal in comparison to actin (Moritz 2017). Based on these variabilities, WB data of target expressions were preliminary, necessitating further experiments.

Another limitation encountered was image acquisition. Throughout the study, light/fluorescent microscopes were used. Whilst, these forms of microscopy serve well certain purposes, some of the readouts; HDMEC size measurement, the role of glucose on HDMEC, confirmation of nrf2 sub-cellular localisation, and identification of cell-specific HIF-1 $\alpha$  expressions in explants for instance were not sufficiently addressed with light/fluorescent microscopes. In hind-sight, the combinations of light/fluorescent and confocal microscopy could have been optimal.

In terms of experimental design, the durations (4/24 h) of high glucose incubation were too short for discerning glucose-related effects on HDMEC morphology. In addition, studies were not undertaken to address pertinent questions that had arisen from some of the results. This includes establishing the involvement of ROS in nrf2 activation and stabilisation, the functional implication of IL-6 mRNA downregulation including assessment of IL-6 protein, confirmation of HIF-1 signalling post HIF-1 $\alpha$  stabilisation in explants. These aspects have been discussed in all relevant result sections and further studies (section 7.3).

## 7.2 Result summary

A summary of relevant results is presented and illustrated with a simplified diagram (fig 7.1), with detailed discussion and conclusion in section 7.3. Early degeneration of retinal tissue is apparent within minutes in free floating retinal culture, stemming from gliosis in the absence of anchorage. In 3.0, retinal tissues and vessels cultured as explants based on a novel retinal explant model developed in this study were maintained intact and viable for more than 24 h. In addition, a hyperbaric model closely aligned to UK clinical protocol for HBOT was successfully validated.

In chapter 4.0, mean sizes of HDMEC ( $n = 40$ ) were changed significantly post treatments ( $***p < 0.0001$ ,  $n = 8$ ). HDMEC in hyperoxia (low glucose) were significantly bigger in comparison to control and HBO ( $*p < 0.05$ ), or hyperbaric pressure ( $**p < 0.01$ ) based on Tukey's post hoc analysis. In addition, the metabolic activity of HDMEC post treatment was changed ( $*p < 0.05$ ,  $n = 8$ ) with HDMEC in hyperoxia exhibiting a pattern of decreased metabolic activity relative to control but the effect did not reach statistical significance ( $p > 0.05$ ). HBO was not associated with significant changes in HDMEC size, shape or metabolic activity relative to control ( $p > 0.05$ ).

In chapter 5.0, nrf2 was basal (control) but showed an acute (4 h) glucose associated suppression in redox response (nrf2) ( $p < 0.05$ ) in high glucose relative to low glucose. Nrf2 stabilisation and accumulation at 4 h and 24 h post treatments (HBO, hyperoxia and hyperbaric pressure) relative to control was determined. In addition, the cellular distributions of nrf2 were distinct post treatments relative to control. The distribution of nrf2 in the control sample was predominantly cytoplasmic as expected under basal homeostatic conditions. On the other hand, post HBO and hyperbaric pressure, nrf2 protein was accumulated in areas associated with nuclear and plasma membrane relative to control. Curiously, nrf2 distribution in hyperoxia and to a lesser extent hyperbaric pressure appeared predominantly perinuclear associated. Nrf2 stabilisation and accumulation is consistent with nrf2 activation and nuclear expression of targets including heme-oxygenase -1 (HO-1). Therefore, it is conceivable that nrf2 stabilisation/accumulation may have resulted in HO-1 induction since HO-1 protein appeared raised post treatments relative to control. Moreover, HO-1 appeared raised in response to high glucose relative to low glucose for HDMEC in control condition and HBO but HO-1 levels post hyperoxia appeared to be glucose-independent.

Immunological responses were varied depending on glucose concentration, oxygen and pressure levels. IL-6 mRNA levels were significantly downregulated (suppressed) at 4 h post treatments ( $p < 0.0001$ ,  $n = 8$ ); HBO, hyperoxia and hyperbaric pressure, but more so post HBO relative to  $\beta 2m$ /calibrator. IL-6 mRNA was significantly less suppressed in high glucose post HBO ( $p < 0.01$ ), whilst more suppressed following hyperoxia ( $p < 0.0001$ ) relative to  $\beta 2m$ /calibrator in comparison to low glucose. Based on preliminary WB data, activated NF $\kappa$ B (p65) protein at 4 h appeared elevated post hyperoxia and hyperbaric pressure, whilst basal post HBO relative to control.

In chapter 6.0, preliminary WB data of nuclear HIF-1 $\alpha$  protein in HDMEC at 4 h appeared raised post treatments in comparison to control. In addition, HIF-1 $\alpha$  appeared suppressed in high glucose relative to low glucose post HBO at 24 h. Hyperoxia may have resulted in increased cytosolic HIF-1 $\alpha$  protein at 24 h relative to control. Furthermore, it is likely hyperoxia was associated with increased VEGF levels relative to control which may be suggestive of an oxidant mediated VEGF increase in HDMEC. Moreover, it is plausible hyperoxia associated VEGF increase and HO-1 induction post hyperoxia are connected, i.e. VEGF increase may have resulted in HO-1 induction (Bussolati et al 2004), although other mechanisms could be at play. PECAM-1 expression showed an acute (4 h) downregulation (in high glucose) in the control sample. Likewise, PECAM-1 expression post hyperoxia showed a hyperoxia associated downregulation, which was further exaggerated in concomitant hyperoxia and high glucose. Interestingly, PECAM-1 expression post HBO and hyperbaric pressure appeared unaffected by glucose concentration relative to control. Whilst HIF-1 $\alpha$  inductions post treatments in HDMEC were hardly pronounced, HIF-1 $\alpha$  inductions was distinctly evoked post treatments, and particularly post HBO relative to control. In addition, although HDMEC based study of HIF-1 $\alpha$  (all conditions) and PECAM-1 (control and hyperoxia) showed high glucose associated variations (decrease), glucose treatment was associated with heightened HIF-1 $\alpha$  with corresponding elevated PECAM-1 expression in retinal explants. This might be reflective of cell-origin differences (dermal versus retinal). In addition, it may be indicative of inter-cellular cross-talk obtainable in complex systems such as retinal tissue in comparison to a single cell type (HDMEC) (Matteucci et al 2015).

In general WB expression and actin loading for the study of targets; HO-1, NF $\kappa$ B, HIF-1 $\alpha$  and VEGF were highly variable. Hence, caution is exercised in the interpretation of preliminary WB data which requires future studies for further clarification.

Glucose effect was a key aim in this study because HBO is utilised in diabetic settings in the treatment of recalcitrant diabetic ulcers. HBO is also utilised for non-diabetic conditions such as autism, gas poisoning, decompression illness etc. The role of glycemic status on HBO outcome in these diabetic/non-diabetic indications is not yet well understood.

In general, glucose dependent effects in HDMEC were not ubiquitous in this study as expected. The incubation period (4 /24 h) were perhaps too short for significant glucose dependent effect particularly on morphology in HDMEC as discussed in section 7.1 (Overall study limitation). On the other hand, the absence of robust HIF-1 $\alpha$  induction is conceivably a cell-dependent response in HDMEC since HIF-1 $\alpha$  reactivity was pronounced in retinal explants at shorter incubation periods (2 h). In the control condition, nrf2 showed an acute (4 h) glucose associated impairment in high glucose relative to low glucose ( $p < 0.05$ ). High glucose associated impairment of nrf2 expression was not present in HBO or its components ( $p > 0.05$ ). Based on preliminary WB results, HO-1 appeared raised in response to high glucose relative to low glucose and may have been a cell-mediated response to override high glucose associated effect, which is consistent with previous studies (Castilho et al 2012, He et al 2015). Curiously, HO-1 appeared raised to a similar extent in low and high glucose relative to control in hyperoxia, which may be suggestive of a hyperoxia alone effect.

Immunological responses showed glucose dependence. IL-6 mRNA in HBO was significantly less suppressed ( $p < 0.01$ ), whilst more suppressed post hyperoxia ( $p < 0.0001$ ) in high glucose relative to low glucose in HDMEC. This highlights a potential role of glycemic status on HBO associated immunological (IL-6) responses. Similarly, glycemic status might have a role on HBO associated benefit in HIF-1 $\alpha$  stabilisation because nuclear HIF-1 $\alpha$  in HDMEC was suppressed at 24 h in high glucose relative to low glucose. Ironically, VEGF appeared elevated post hyperoxia in high glucose relative to low glucose although HIF-1 $\alpha$  induction was not evident which may highlight a HIF-1 independent VEGF upregulation, possibly oxidant mediated (Sheikh et al 2000). As mentioned previously, whilst HIF-1 $\alpha$  (all samples) and PECAM-1 (control and hyperoxia) were downregulated in HDMEC, high glucose was associated with heightened HIF-1 $\alpha$ /PECAM-1 immunoreactivity in all samples relative to control in retinal explants. These HIF-1 $\alpha$  specific differences between HDMEC and retinal explants may highlight differences in endothelial cells of different origin (retinal versus dermal) (Yuen et al 2009). It may also reflect differences between a single cell type response and complex intercellular cross-talk and responses in the retina (Matteucci et al 2015).



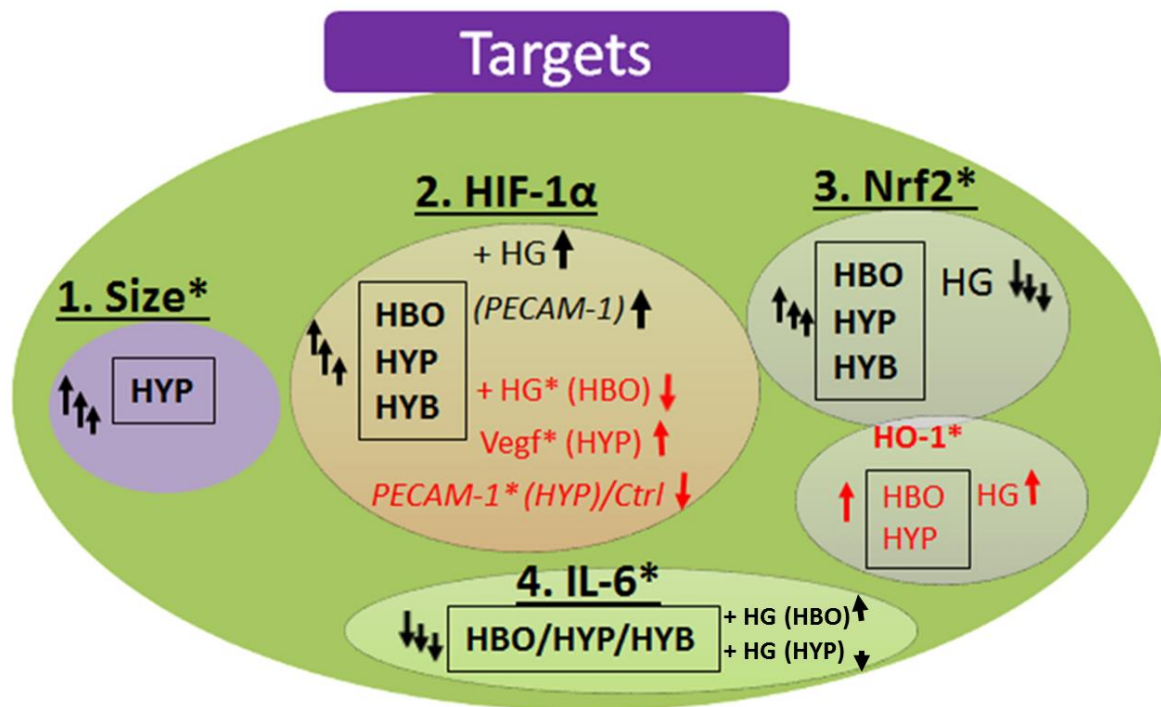


**Figure 7.1 Summary of relevant study results**

The diagram above shows a summary of study result which may be a preliminary mechanism (s) in the investigation of the molecular mechanisms in HDMEC (\*) and a novel retinal explant model of endothelial cell responses to varying glucose concentration, oxygen and pressure (HBO) using a bespoke hyperbaric unit simulated according to HBOT procedures. 1. HDMEC size was significantly increased following exposure to hyperoxia (HYP) relative to control. 2. HIF-1α expression in retinal explants in control condition (control) was increased in response to high glucose (HG). HIF-1α expression was exaggerated in response to treatments; hyperbaric oxygen (HBO), hyperoxia (HYP), and hyperbaric pressure (HYB), which showed further increase in the presence of HG and associated with a corresponding increase in PECAM-1 immunoreactivity in retinal explants in response to HG. In HDMEC high glucose (+ HG\*) was associated with decreased HIF-1α protein relative to low glucose (LG) in HBO. In addition, in HDMEC (\*), VEGF appeared elevated in response to HYP (HG). Moreover, in HDMEC, PECAM-1 appeared downregulated in response to HG in HYP and control (Ctrl). 3. In HDMEC, nrf2 was significantly increased in response to treatments; HBO, HYP and HYB relative to control. Nrf2 showed a statistically significant acute (4 h) impairment in nrf2 induction in HG relative to LG for HDMEC in control condition. HO-1 protein appeared raised in HG relative to LG for HDMEC (control condition and HBO), and in response to treatments; HBO and HYP relative to control. IL-6 mRNA was significantly suppressed in response to treatments; HBO, HYP and HYB relative to control. IL-6 mRNA suppression was lessened (i.e. higher IL-6 mRNA) in HG relative to LG in HBO, but more suppressed in HYP (i.e. lower IL-6 mRNA) in HG relative to LG.

Key: HBO (hyperbaric oxygen), HYP (hyperoxia), HYB (hyperbaric pressure), HG (high glucose), LG (low glucose), Ctrl (control), arrowhead up (increase), arrowhead down (decrease). The number of arrows is used as an indication of the level of expression and three arrows are used for results with statistical significance or obvious predominant expression was seen. Red labels indicate results based on western blots (WB) which are subject to further examination for more robust results. Results relating to HDMEC are indicated with (\*).

## 7.3 Overall Discussion and Conclusion

In the following paragraphs, study findings are discussed in the context current literature, in addition to discussions in the relevant result chapters. Firstly, the role of high glucose is discussed. In normal, physiological condition, endothelial cells (ECs) are exposed to tightly regulated circulating blood glucose range of approximately 3.6–5.8 mM (physiological basal levels). When exposed to high glucose, defined as exposure of vascular ECs to glucose levels over 10 mM (in vitro or in vivo), cellular homeostasis and biochemistry are perturbed. As a consequence, EC lose their typical quiescent phenotypes and endothelial dysfunction ensues. Physiologically, EC dysfunction is characterised by deficiency in NO availability, reduction in endothelial-derived vasorelaxation, impaired fibrinolytic ability, altered expression of growth factors, adhesion molecules and inflammatory genes leading to oxidative stress and enhanced permeability of cell layer (reviewed in Popov 2010). In addition to these direct effects of high glucose, high glucose can also lead to accelerated formation of diacylglycerol (DAG), methylglyoxal (MGO), AGEs, ROS and nitrosylated species which further amplify the imbalance. Fundamentally, it is well agreed that endothelial dysfunction precedes the development of vascular structural changes in diabetes, which underlines the importance of examining high glucose effects in HDMEC.

Upregulation of aryl hydrocarbon receptor transcription factor, p300 and the chicken ovalbumin upstream promoter-transcription factor II (COUP-TFII) is associated with enhanced glucose metabolism (Dabir et al 2008, Chen et al 2010). In HUVEC, high glucose increased p300 upregulation short term (60-240 min), whilst decreased longer term (48 h) (Chen et al 2010). However, in this study, based on Resazurin assay, incubations of HDMEC in high glucose for 4 h post treatments were associated with significant change (increase/decrease) in HDMEC metabolic activity, although a pattern of high glucose associated increase was seen for HDMEC in control and HBO conditions ( $p > 0.05$ ). This suggests a distinctive cell dependent response and it is likely HDMEC have a slow metabolic phenotype (Ahmed et al, 1994, Nakayama et al 1997, Zalata et al 1998, Perrot et al 2003, De Bock et al 2013 and Doddaballapur et al 2015). As regards morphological changes, high glucose did not elicit evident structural/significant size changes in HDMEC ( $p > 0.05$ ). High glucose is associated with disorganisation of tight junction structures in diabetic retina and cerebral microvessels as a result of diabetic hyperpermeability (Antonetti et al 1999). In addition, high glucose induced actin stress fibre formation in endothelial cells (Salameh et al 1997). More so microvascular leakage in the retinal microvasculature is enhanced in STZ-induced diabetic rats due to high glucose dependent modulation of cytoskeletal contraction (Yu et al 2005).

Furthermore, in human vascular endothelial cell, hyperglycaemia induced AGE and RAGE/Rho signalling was associated with cell contraction (Hirose et al 2009). Incidentally, it takes up to 2 weeks of high glucose exposure for AGE formation to occur in endothelial cells (Catrina et al 2004, reviewed in Cheng et al 2011). Thus, the absence of evident high glucose associated structural or significant size alterations in HDMEC might be alluded to a non-optimal incubation period because glucose mediated changes in phenotype require durations longer than 4 h (De Nigris et al 2015). Moreover, the use of an ordinary microscope rather than confocal imaging may have contributed to the lack of identification of early structural/micro-level deregulations.

Nrf2 is not essential for survival but, activation of nrf2-ARE pathway is fundamental for the maintenance of the intracellular glutathione (GSH) and the induction of antioxidant defense enzymes. Nrf2 counteracts high-glucose induced damage and downstream inflammatory responses in diabetes. High glucose induced ROS and AGE rather than a direct high glucose effect is the mechanism for nrf2 activation/accumulation in high glucose (He et al 2010). In human endothelial cells, high glucose concentration of 30 mM (6 h) did not elicit nrf2-pathway (Xue et al 2008). However, nrf2 activators increase hyperglycaemia-induced ROS generation leading to nrf2 activation (Xue et al 2008). So, although high glucose does not directly evoke nrf2 activation, high glucose associated increase in ROS production can precipitate nrf2 and nrf2-dependent HO-1 expression (He et al 2010). In this study, high glucose (20 mM, 4 h) was associated with acutely lower levels of nrf2 relative to low glucose for HDMEC in control condition ( $p < 0.05$ ), which suggested a lack of acute high glucose associated ROS dependent induction of nrf2. Interestingly, this phenomenon appeared lacking for HDMEC in HBO and hyperbaric pressure. Evidently, increased ROS (as a result of increased partial pressures of oxygen and associated stress) post HBO, hyperoxia and hyperbaric pressure would have augmented nrf2 activation in concert (or in the absence) of high glucose associated ROS dependent nrf2 induction.

Remarkably high glucose associated impairment in nrf2 induction for HDMEC in control condition was no longer evident at 24 h, suggesting a cell mediated response. On the other hand, HDMEC in hyperoxia demonstrated a delayed (24 h) high glucose associated trend of nrf2 decline ( $p > 0.05$ ). In diabetic condition, nrf2 activation and HO-1 accumulation is an adaptive response against oxidative stress (Jiang et al 2010). So it is notable that total protein HO-1 levels as determined with preliminary WB data appeared elevated in response to high glucose relative to low for HDMEC in control and HBO conditions at 24 h. Ironically, HDMEC in hyperoxia did not appear to show the same glucose associated response, which may further strengthen the previous observation of nrf2 decline at 24 h in concomitant hyperoxia and high glucose. In addition, it suggests the apparent elevation in HO-1 protein elevation may have been due to hyperoxia effect alone. Since diminished nrf2 activity may render endothelial cells vulnerable to oxidative stress (reviewed in Cheng et al 2011), the consequence of continued concomitant hyperoxia and high glucose on nrf2 and consequently adaptive responses is worth examining in further studies because of the likely implications on cellular oxidative stress.

High glucose is associated with pro-inflammatory changes in vascular endothelial cells (reviewed in Popov 2010). Likewise in this study, IL-6 mRNA level was significantly higher in high glucose post HBO ( $p < 0.01$ ), whilst decreased post hyperoxia ( $p < 0.0001$ ). A high glucose effect on NF $\kappa$ B expression was not evident (all samples) due to inconsistencies in actin loading control, although NF $\kappa$ B elevation post hyperoxia and hyperbaric pressure but not HBO relative to control was apparent. This apparent NF $\kappa$ B modulation post HBO may have subject to nrf2 mediated amelioration. Nrf2 is associated with shear stress response, inflammation resolution and suppression of endothelial dysfunction, which is consistent with the nrf2/ NF $\kappa$ B cross-talk postulation (Zakkar et al 2009, Bellezza et al 2018). Therefore, the seeming abrogation of NF $\kappa$ B activation judging from its basal levels in HBO relative to control suggests a likely functional nrf2/NF $\kappa$ B cross-talk, a concept which is prospective and requires further investigation.

Based on preliminary WB results, nuclear HIF-1 $\alpha$  protein appeared diminished in high glucose relative to low glucose in HDMEC, which seems consistent with previous reports (Catrina et al 2004, reviewed in Xiao et al 2013). In addition, high glucose associated decline in HIF-1 $\alpha$  protein appeared imminent for HDMEC in HBO. Essentially, this appears to demonstrate the impact of glycaemic status on HBO outcome in regards to HIF-1 $\alpha$  stabilisation. It is plausible HDMEC incubation in normoxia post HBO may have resulted in prolyl hydroxylases (PHD) mediated HIF-1 $\alpha$  degradation of any HBO-stabilised HIF-1 $\alpha$ , which raises the question of how long HIF-1 $\alpha$  can be stabilised post HBO. Another reasonable consideration is the role of cell-type (HDMEC) dependent response. This last rationale becomes more acceptable when considering the outcome of HIF-1 $\alpha$  expression in retinal explants where HIF-1 $\alpha$  expression was abundantly elicited in response to high glucose relative to low glucose, which fitted with the concept of high glucose mediated HIF-1 $\alpha$  protein stabilisation and accumulation via PKC activation in retinal cells (Suzuma et al 2002, Geraldles et al 2009). Thus, HIF-1 $\alpha$  regulation in high glucose and/or HBO is complex and intrinsic cell-type differences between dermal (HDMEC) and retinal (explants) endothelial cells might play a role in these complexities. Moreover, heightened HIF-1 $\alpha$  expression in response to high glucose may also reflect cross-talks between different cell types in the retina which is otherwise absent in single cell systems such as HDMEC (Matteucci et al 2015).

High glucose (20 mM, 4 h) was associated with PECAM-1 suppression in control condition, but concomitant high glucose and hyperoxia resulted in PECAM-1 upregulation. Acute PECAM-1 upregulation in concomitant high glucose and hyperoxia may have been an early intervention to activate early inflammatory cascade which is crucial to forestall cellular damage (Piedboeuf et al 1998). Therefore, it seems congruent that NF $\kappa$ B appeared elevated post concomitant high glucose and hyperoxia. Ironically, although early (4 h) PECAM-1 upregulation in concomitant high glucose and hyperoxia was seen, it was suppressed at 24 h. Thus, continued concomitant high glucose and hyperoxia would likely result in loss of endothelial cell integrity via PECAM-1 downregulation.

VEGF and HO-1 show complex inter-dependent functions in angiogenesis. In retinal endothelial cells, high glucose induced apoptosis stimulates recruitment of endothelial progenitor cells and VEGF (Bhatwadekar et al 2009). On the other hand, hyperglycaemia induced VEGF suppression via HIF-1 inactivation impairs wound healing in diabetes. In this study, preliminary WB data suggested VEGF accumulation in HDMEC at 24 h in concomitant hyperoxia and high glucose. Incidentally, the same samples showed a likely HO-1 upregulation relative to control. Thus, more studies are required to examine further the role(s) of hyperoxia and high glucose on VEGF expression in HDMEC.

The remaining section focuses on the roles of the treatment alone or in concert with high glucose.

Nrf2 stabilisation/accumulation and cellular distributions in HDMEC post treatments were distinct relative to control. Post HBO and to a lesser extent hyperbaric pressure, nrf2 stabilisation/accumulation was apparent for up to 24 h with nuclear and plasma membrane associated distributions relative to control. This distinct nrf2 distribution in HBO relative to control is likely a protective mechanism. Ironically, in hyperoxia nrf2 appeared diminished (24 h) and its distribution appeared predominantly perinuclear associated relative to control. HBO is associated with the activation of the PKC/JNK pathways (Hsieh et al 2010), and this occurs via PKC phosphorylation of the serine residue (Ser40) in Neh2 domain of nrf2, a Keap 1 interaction domain (Steinberg 2015). So, it is likely HBO promoted nrf2 dissociation from Keap 1 and consequently increased stabilisation via increased HBO associated PKC phosphorylation of ser40 residue of Keap 1 (Neh2) interaction domain. In addition, HBO associated stimulation of the PI3K (Akt), MAPK, ERK and PKC signalling may have resulted in increased inhibition of GSK-3 $\beta$  mediated nrf2 nuclear export and proteasomal degradation (Biswas et al 2014).

Nrf2 stabilisation/activation is stimulated by increased NADPH bioavailability mediated via increased cellular glucose uptake and pentose phosphate pathway (PPP) activity (Heiss et al 2013). In patients, HBO administrations is consistent with increased glucose metabolism possibly via oxygen mediated increased oxidative phosphorylation (Löndahl et al 2013). HBO mediated increase in glucose metabolism would arguably be preceded by a corresponding increase in cellular glucose uptake and possibly increased PPP furnishing of NADPH. Hence, it is plausible nrf2 was stabilised post HBO (and to a lesser extent hyperbaric pressure) via mechanisms in these conditions that resulted in increased glucose uptake, PPP activity and NADPH bioavailability relative to control. Therefore, such HBO associated increase in NADPH might further relieve Keap 1 mediated suppression of nrf2 (Yates et al 2009). In converse, hyperoxia mediated activation of nrf2 via ROS dependent means are immediate (acute) and short-lived (Nguyen et al 2009). Likewise in this study, nrf2 stabilisation in hyperoxia appeared potent acutely (4 h) ( $p < 0.0001$ ) but seemed diminished at 24 h ( $p > 0.05$ ) relative to control. In addition, hyperoxia causes the impairment of the glycolytic and mitochondrial oxidative metabolism, and inactivation of the ETC system (Das 2013). Essentially, hyperoxia shuts down glucose metabolism, consequently limiting NADPH bioavailability. Moreover, in concomitant high glucose and hyperoxia, these scenario might be exacerbated because of the build-up of metabolic intermediates which downregulates oxidative metabolism (Yates et al 2009). Whilst, no significant hyperoxia associated downregulation of metabolic activity was identified in this study, HDMEC in hyperoxia appeared consistent with a lower metabolic profile relative to control ( $p > 0.05$ ). Taken together, nrf2 appears to exhibit peculiar characteristics in hyperoxia distinct from compounded hyperoxia and pressure (HBO). Therefore, more studies are needed to rightly discern these mechanistic details to further inform on the anti-oxidant contributions of HBO which can make a difference in patient outcome.

Immunological responses in HDMEC were different under the conditions tested, consistent with previous reports (Thom 2011). Fundamentally, the glucose dependent changes in IL-6 mRNA levels post HBO (increased IL-6 mRNA) relative to control might be of clinical relevance. It is worth weighing the differences in IL-6 mRNA regulation/response in high glucose post HBO and hyperoxia. IL-6 release triggers the activation of the Janus kinase / signal transducer and activator of transcription (JAK/STAT) and MAPK cascades (Heinrich et al 2003). In cells, JAK/STAT signalling is mediated primarily by NFκB and regulates apoptotic, proliferation, immune and inflammatory responses (O'Shea and Plenge 2012, Tanaka et al 2014). Thus, the apparent elevation of NFκB post hyperoxia may be demonstrating a hyperoxia associated JAK/STAT NFκB activation in HDMEC. On the other, since NFκB remained basal relative to control post HBO, it is probable HBO is not associated with IL-6 mediated activation of JAK/STAT mediated NFκB activation. Fundamentally, judging from the sustained profile of nrf2 post HBO, it is plausible HBO resulted in the activation of the nrf2/NFκB cross-talk and this may have played a key role in the abrogation of the IL-6 associated NFκB activation in HDMEC.

As mentioned previously, HIF-1α induction in the retinal explants, is indicative of a distinct retinal cell response as well as demonstrates the importance of intercellular-cross-talks in complex systems (retinal tissue) which is absent in single cell systems. Essentially, HIF-1α induction and stabilisation in retinal explants post treatments and in particular post HBO is critical and might be of clinical relevance when considering the role of some HIF-1α target genes such as EPO, HO-1, and Glut-1 which promote neurogenesis, in addition to being neuroprotective. This prospect of HIF-1α stabilisation and retinal neurogenesis presents another insight into the role of HIF-1α and HBO in ocular diseases, and warrants further studies. In retrospect, judging from the low and variable expression of HIF-1α in HDMEC which is suggestive of low endogenous levels, the incorporation of 2-oxoglutarate analogue dimethyloxalylglycine (DMOG), a PHD blocker might have contributed to greater HIF-1α stabilisation (Hirota and Semenza 2005). It is reasoned, this might have given a better insight into the effect of treatments on HIF-1α induction.



Oxidants stimulate VEGF accumulation in endothelial cells (Sheikh et al 2000, Terraneo et al 2014). In addition, hyperoxia induces VEGF accumulation in a redox dependent manner (Terraneo et al 2014). Likewise in this study, hyperoxia (high glucose) was associated with an apparent increase in VEGF in concert with elevated HO-1 and nrf2, which appear consistent with Terraneo et al. Both HBO and hyperoxia lead to the generation of oxidants (ROS), which are known to stabilise HIF-1 $\alpha$  (Thom 2011, Lee and Choi 2003). Paradoxically, high glucose induced ROS results in HIF-1 $\alpha$  impairment via increased ROS impairment of NO and ROS repression of Rac1, in addition to ROS induction of PHD activities (reviewed in Xiao et al 2013). Thus, ROS mediated HIF-1 $\alpha$  impairment and degradation might represent another avenue for increased HIF-1 $\alpha$  degradation and low levels in HDMEC. In essence, it is plausible that hyperoxia associated VEGF elevation was independent of HIF-1 $\alpha$  since nuclear HIF-1 $\alpha$  was low and variable in hyperoxia and in all HDMEC as a whole. Fundamentally, hyperoxia associated VEGF elevation appears more consistent with an oxidant mediated mechanism rather than a HIF-1 $\alpha$  mediated mechanism. VEGF upregulation in diabetic wounds is mediated via HIF-1 mediated mechanism (Thom 2009, Sunkari et al 2015). Ironically HBO mediated HIF-1 $\alpha$  stabilisation and consequently HIF-1 signalling activities are not a direct result of increased oxygen levels or ROS. This is because ROS stabilises HIF-1 $\alpha$  through VHL mediated prolyl hydroxylase (PHD) inhibition, whilst HBO-mediated HIF-1 $\alpha$  stability is VHL/PHD-independent (Sunkari et al 2015). Therefore, the absence of modest HIF-1 $\alpha$  induction post HBO beggars the question of what factors might have contributed to low HIF-1 $\alpha$  and consequently decreased HIF-1 signalling mediated VEGF upregulation. As previously noted, it is possible HDMEC in general exhibit low endogenous HIF-1 $\alpha$  levels. Secondly, although HBO mediated HIF-1 $\alpha$  stabilisation is PHD/VHL independent, the likelihood of PHD mediated HIF-1 $\alpha$  degradation, and consequently low HIF-1 signalling mediated VEGF induction in normoxia during incubation cannot be excluded.

Antioxidants and oxidant scavengers are associated with mitigation of oxidant induced VEGF production. Therefore, sustained levels of antioxidants or oxidant scavengers would result in the amelioration/abrogation of oxidant mediated VEGF accumulation. The implication of this is that sustained nrf2 or other oxidant scavengers mitigates VEGF elevation, which appears consistent with a possible nrf2 mitigation of hyperoxia associated VEGF accumulation in HBO since nrf2 was sustained in HBO. On the other hand, nrf2 reduction in hyperoxia after the initial surge possibly resulted in the enhancement of VEGF elevation. Interestingly, hyperoxia induced VEGF fraction is biologically active, which presents a prospective beneficial role for hyperoxia mediated VEGF upregulation (Sheikh et al 2010). Hyperoxia induced VEGF upregulation may come at a cost to cells because of hyperoxia associated signalling in cell death, stress, inflammation, JAK/ STAT, MAPK, NFkB and the AP-1 pathways, which orchestrate the expression of a range of stress response genes, cytokines, and growth factors (O' Shea and Plenge 2012), therefore further studies are needed to rightly discern key mechanistic details. Caution is to be exercised in the interpretation of VEGF upregulation based on WB data alone due to inconsistencies VEGF expression in this study and further studies are needed for more robust data.

Endothelial cells respond to extracellular forces by modulating tension across junctional proteins and PECAM-1 is the primary e-cadherin utilised by endothelial cells to bear mechanical tension. PECAM-1 induction in response to mechanical stress causes increased expression of weight bearing intermediate cytoskeletal filament such as vimentin (Conway and Schwartz 2014). Therefore, increased expression of PECAM-1 post hyperbaric pressure may have facilitated HDMEC retraction from increased extracellular pressure acting on its surface (Woodfin et al 2007). As previously noted, PECAM-1 expression is critical for the maintenance of endothelial cell phenotype and integrity. Therefore, it is conceivable that acute (4 h) PECAM-1 upregulation in concomitant hyperoxia and high glucose is an initial HDMEC specific response for cell survival and maintenance of cellular integrity (Newman and Newman 2013). Fundamentally, the downregulation of PECAM-1 downregulation at a later time point (24 h) in concomitant hyperoxia and high glucose suggests the absence of appropriate cell response for maintenance of HDMEC integrity and survival. Interestingly, HDMEC in HBO showed no apparent changes in PECAM-1 which suggests a likely favourable modulation of homeostasis for HDMEC in HBO, but these would need to be ascertained in further experiments.

## 7.3 Further studies

Firstly, hyperoxia associated VEGF accumulation in a HIF-1 $\alpha$  independent manner warrants further studies to clarify the key pathways including the role(s) of HIF-1 isoforms owing to its potential implication in diabetic wounds. The possibility of HIF-1 $\alpha$  in retinal explants in high glucose via a likely ROS/PKC mediated mechanism ought to be addressed in future studies. HBO associated nrf2 activation/stabilisation in HDMEC is predicted to have had an effect on amelioration of NF $\kappa$ B activation possibly via a cross-talk between NF $\kappa$ B and the ROS/JNK pathway HDMEC and this warrants further examination. In addition, cellular distribution of nrf2 post HBO which may be associated with greater cellular protection against cellular oxidative stress requires further examination. Furthermore, it is needful to explore the possibility of HBO-induced nrf2 stabilisation and accumulation on endothelial progenitor cells (EPCs). In these studies, in-vitro approaches with HDMEC primary culture/retinal explants in conjunction with animal models of oxidative stress will be essential. The investigation might also include a clinical approach involving the analysis of blood samples of patients that are undergoing HBO, as well as those that have undergone HBO, after a significant time interval to verify any immediate and sustained nrf2 stabilization and activation. Moreover, PECAM-1 downregulation in high glucose, and hyperoxia and upregulation post hyperbaric pressure require further attention, to delineate the difference in mechanistic pathways post HBO, hyperoxia and hyperbaric pressure. The role of hyperbaric pressure on PECAM-1 upregulation in HDMEC is very critical because of the correlation between elevated pressure and increased haemodynamic pressure on endothelial expression of PECAM-1 and the likely consequence of PECAM-1 upregulation in the vasculature. To do this, in-vitro studies can be designed with the same HDMEC model as well as in-vivo animal model to correlate findings.

## Chapter 8.0: References

## A

**Adamis A** (2002) Is DR an inflammatory disease. *British Journal of Ophthalmology*, 86, 363-285.

**Adler AI, Stevens RJ, Manley SE et al** (2003) Development and progression of nephropathy in type 2 diabetes: the United Kingdom Prospective Diabetes Study (UKPDS 64). *Kidney International*, 63, 225 - 232.

**ADVANCE Collaborative Group, Patel A, MacMahon S et al** (2008) Intensive blood glucose control and vascular outcomes in patients with type 2 diabetes. *New England Journal of Medicine*, 358, 2560-2572.

**Ahmed SA, Gogal (Jr) RM, and Walsh JE** (1994) A new rapid and simple non-radioactive assay to monitor and determine the proliferation of lymphocytes: an alternative to [3H] thymidine incorporation assay. *Journal of Immunological Methods*, 170, 211-224

**Ahn JD, Morishita R, Kaneda Y** (2001) Transcription factor decoy for activator protein-1 (AP-1) inhibits high glucose- and angiotensin II-induced type 1 plasminogen activator inhibitor (PAI-1) gene expression in cultured human vascular smooth muscle cells. *Diabetologia*, 44, 713-720.

**Aiello LP** (2005) Angiogenic pathways in DR. *New England Journal of Medicine*, 353, 839–841.

**Aiello LP, Pierce EA, Foley ED et al** (1995) Suppression of retinal neovascularization in vivo by inhibition of vascular endothelial growth factor (VEGF) using soluble VEGF-receptor chimeric proteins. *Proceedings of the National Academy of Sciences*, 92, 10457-10461.

**Akg  IE, Karakaya J and Aydin S.** (2014) Role of Comorbidities as limiting factor to the effect of oxygen in diabetic foot patients: A retrospective analysis. *Diabetes Therapy*, 10, 1-10.

**Alam J, Stewart D, Touchard C et al** (1999) Nrf2, a Cap'n'Collar transcription factor, regulates induction of the heme oxygenase-1 gene. *Journal of Biological Chemistry*, 274, 26071–26078.

**Alien D, Maguire J, Mahdavian M et al** (1997) Wound hypoxia and acidosis limit neutrophil bacterial killing mechanisms. *Archives of Surgery*, 132, 991-996.

**Al-Waili NS and Butler GJ** (2006) Effects of Hyperbaric Oxygen on Inflammatory Response to Wound and Trauma: Possible Mechanism of Action. *The Scientific World Journal*, 6, 425–441.

**Amadeu TP, Coulomb B, and Desmouliere A et al** (2003) Cutaneous wound healing: myofibroblastic differentiation and *in vitro* models. *International Journal of Low Extremity Wounds*, Wounds 2, 60–68.

**American Diabetes Association (ADA)** (2014) Diagnosis and Classification of Diabetes Mellitus. *Diabetes Care*, 37 (Supplement 1): S81-S90.

**Anaesthesia UK** (2018). <http://www.frca.co.uk/article.aspx?articleid=100345>. Date/time of access: 30<sup>th</sup> September 2018 @ 17.03 GMT.

**Antonetti DA, Lieth E, Barber AJ et al** (1999) Molecular mechanisms of vascular permeability in diabetic retinopathy. *Seminars in Ophthalmology*, 14, 240– 248.

**Aoki N, Siegfried M, Lefer AM** (1989) Anti-EDRF effect of tumour necrosis factor in isolated, perfused cat carotid arteries. *American Journal of Physiology*, 256, H1509–H1512.

**Aoki M, Morishita R, Nata T et al (2001).** Endothelial apoptosis induced by oxidative stress through activation of NF-kappa B: antiapoptotic effect of antioxidant agents on endothelial cells. *Hypertension*, 38, 48-55.

**Arora MK and Singh K (2013)** Molecular mechanisms in the pathogenesis of diabetic nephropathy: An update. *Vascular Pharmacology*, 58, 259-271

**Arora M (2013)** Cell Culture Media: A Review. *MATER METHODS*, 3, 75

**Ayo SH, Radnik RA, Glass WF et al (1990)** Increased extracellular matrix synthesis and mRNA in mesangial cells grown in high-glucose medium. *American Journal of Physiology*, 260, F185-191.

**Ayo R, Radnik JA, Garoni DA et al (1991)** High glucose increases diacylglycerol mass and activates protein kinase C in mesangial cells. *American Journal of Physiology*, 261, F571-577.

**Ataie-Kachoie P, Pourgholami MH, Richardson DR et al (2014)** Gene of the month: Interleukin 6 (IL-6). *Journal of Clinical Pathology*. <http://dx.doi.org/10.1136/jclinpath-2014-202493>

**Attaye I, Smulders YM, De Waard MC (2017)** The effects of hyperoxia on microvascular endothelial cell proliferation and production of vaso-active substances. *Intensive Care Experimental Medicine*, 5. <https://doi.org/10.1186/s40635-017-0135-4>

**Ayrappetov MK, Xu C, Sun Y et al (2011)** Activation of Hif1 $\alpha$  by the prolyl hydroxylase inhibitor dimethyloxalylglycine decreases radiosensitivity. *PLoS One*, 6, e26064. doi:0.1371/journal.pone.0026064

## B

**Badrichani AZ, Stroka DM, Bilbao G et al (1999)** Bcl-2 and Bcl-XL serve an anti-inflammatory function in endothelial cells through inhibition of NF $\kappa$ B. *Journal of Clinical Investigation*, **103**, 543-553.

**Baek JH, Mahon PC, Oh J (2005)** OS-9 interacts with hypoxia-inducible factor 1 $\alpha$  and prolyl hydroxylases to promote oxygen-dependent degradation of HIF-1 $\alpha$ . *Molecular Cell*, 17, 503-512.

**Bai X, Chen Y, Hou X et al (2016)** Emerging role of Nrf2 in chemoresistance by regulating drug-metabolizing enzymes and efflux transporters, *Drug. Metabolic Reviews*, 48, 541-567.

**Balla G, Jacob HS, Balla J et al (1992)** Ferritin: a cytoprotective antioxidant stratagem of endothelium. *Journal of Biological Chemistry*, 267, 18148–18153.

**Barbee K A, Davies PF, Lal R (1994).** Shear stress-induced reorganization of the surface topography of living endothelial cells imaged by atomic force microscopy. *Circulation Research*, 74, 163-171.

**Barkett and Gilmore (1999)** Control of apoptosis by Rel/NF-kappa B transcription factors. *Oncogene*, 18, 6910-6924.

**Barnes TC, Anderson ME, Moots RJ (2011)** The Many Faces of Interleukin-6: The Role of IL-6 in Inflammation, Vasculopathy, and Fibrosis in Systemic Sclerosis. *International Journal of Rheumatology*, 2011, 1-6.

- Barnett T** (1998) Epidemiology, complications and costs of diabetes mellitus. In: Barnett Tony., editor. The insulin treatment of diabetes: a practical guide. London: E-map healthcare, 6–9.
- Bartel DP** (2004) MicroRNAs: genomics, biogenesis, mechanism, and function. *Cell*, 116, 281–297.
- Barr-Nea L** and Barishak RY (1970) Tissue culture studies of the embryonal chicken retina. *Investigative ophthalmology*, 9, 447–457.
- Baumgartner-Parzer SM**, Wagner L et al (1995) Modulation by high glucose of adhesion molecule expression in cultured endothelial cells. *Diabetologia*, 38, 367-1370.
- Beckman JA**, Creager MA, Libby P (2002) Diabetes and atherosclerosis: epidemiology, pathophysiology, and management. *Journal of American Medical Association*, 287, 2570-2581.
- Bellezza I**, Mierla AL, Minelli A (2010) Nrf2 and NFκB and their concerted modulation in cancer pathogenesis and progression, *Cancer*, 2, 483–497.
- Bellezza I**, Tucci A, Galli F (2012) Inhibition of NFκB nuclear translocation via HO-1 activation underlies α-tocopheryl succinate toxicity, *Journal of Nutritional Biochemistry*, 23, 1583–1591.
- Bellezza I**, Giambanco I, Minelli A et al (2018) Nrf2-Keap1 signalling in oxidative and reductive stress. *Biochimica et Biophysica Acta (BBA) - Molecular Cell Research*, 1865, 721-733.
- Bennett MH**, Feldmeier J, Hampson NB et al (2016) Hyperbaric oxygen therapy for late radiation tissue injury. *Cochrane Database Systemic Reviews*, 28; 4:CD005005.
- Benson RM**, Minter LM, Osborne BA et al (2003) Hyperbaric oxygen inhibits stimulus-induced proinflammatory cytokine synthesis by human blood-derived monocyte-macrophages. *Clinical and Experimental Immunology*, 134, 57-62.
- Ben-Yosef Y**, Lahat N, Shapiro Set al (2002) Regulation of endothelial matrix metalloproteinase-2 by hypoxia/reoxygenation. *Circulation Research* 90, 784-791
- Berrone E**, Beltramo E, Solimine C et al (2006) Regulation of intracellular glucose and polyol pathway by thiamine and benfotiamine in vascular cells cultured in high glucose. *Journal of Biological Chemistry*, 281, 9307-9313.
- Bhatwadekar AD**, Glenn JV, Curtis TM et al (2009) Retinal endothelial cell apoptosis stimulates recruitment of endothelial progenitor cells. *Investigative Ophthalmology and Visual Science*, 50, 4967-4973.
- Bierhaus A**, Hofmann MA, Ziegler R et al (1998) AGEs and their interaction with AGE receptors in vascular disease and diabetes mellitus. Part I. The AGE concept. *Cardiovascular Research*, 37, 586-600.
- Bierhaus A**, Chevion A, Chevion M et al (1997) AGEs (AGEs) induced activation of NFκB is suppressed by α-lipoic acid in cultured endothelial cells. *Diabetes*, 46, 1481-1490.
- Biswas C**, Shah S, Muthu M et al (2014). Nuclear heme oxygenase-1 (HO-1) modulates sub-cellular distribution and activation of Nrf2 impacting metabolic and anti-oxidant defences. *Journal of Biological Chemistry*, 289, 26882–26894.

**Botusan** IR, Sunkari VG, Savu O (2008) Stabilization of HIF-1 $\alpha$  is critical to improve wound healing in diabetic mice. PNAS, 105, 19426–19431.

**Boykin** JV and Baylis C (2007) Hyperbaric oxygen therapy mediates increased nitric oxide production associated with wound healing: a preliminary study. Advances in Skin and Wound Care, 20, 382-388

**Boyle** PJ (2007) Diabetes mellitus and macrovascular disease: mechanisms and mediators. American Journal of Medicine, 120, S12-S17.

**Bowden** DH and **Adamson** IY (1974) Endothelial regeneration as a marker of the differential vascular responses in oxygen-induced pulmonary oedema. Lab Investigation, 30, 350-357

**Brownlee** M, Cerami A, Vlassara H (1988) Advanced glycosylation end products in tissue and the biochemical basis of diabetic complications. New England Journal of Medicine, 318, 1315-1321.

**Brownlee** M, Cerami A, Viassara H (1989) AGEs in tissues and the biochemical basis of diabetic complications. New England Journal of Medicine, 318, 1315.

**Brownlee** M, Aiello LP, Cooper ME et al (2016) In: Chapter 33 - Complications of Diabetes Mellitus. In: Williams Textbook of Endocrinology, chapter 33, 1484-1581.

**Brownlee** M (2001) Biochemistry and molecular cell biology of diabetic complication. Nature, 414, 813-820.

**Brownlee** M (2005) The pathobiology of diabetic complications. Diabetes, 54, 1615-1625.

**Brueckl** C, Kaestle S, Kerem A et al (2006) Hyperoxia-induced ROS formation in pulmonary capillary endothelial cells in situ. American Journal of Cell Molecular Biology, 34, 453-463

**Bull** N, Johnson T, Martin K (2011) Organotypic explant culture of adult rat retina for in vitro investigations of neurodegeneration, neuroprotection and cell transplantation. Protocol Exchange. doi:10.1038/protex.2011.215

**Buse** JB, Ginsberg HN, Bakris GL et al (2007) Primary prevention of cardiovascular diseases in people with diabetes mellitus: a scientific statement from the American Heart Association and the American Diabetes Association. Diabetes Care, 30, 162-172.

**Bussolati** B, Ahmed A, Pemberton H (2004) Bifunctional role for VEGF-induced heme oxygenase-1 in vivo: induction of angiogenesis and inhibition of leukocytic infiltration. Blood, 1, 761-766.



## C

**Cabigas BP, Su J, Hutchings W et al (2006)** Hyperoxia and hyperbaric-induced cardioprotection: role of nitric oxide synthase 3. *Cardiovascular Research*, 72, 143-151.

**(CADTH)** Canadian Agency for Drugs and Technologies in Health. Adjunctive hyperbaric oxygen therapy for diabetic foot ulcer: an economic analysis. 2007 [cited 2018 August 28<sup>th</sup>]; Available from: [http://www.cadth.ca/media/pdf/274\\_HBOT\\_tr\\_e.pdf](http://www.cadth.ca/media/pdf/274_HBOT_tr_e.pdf)

**Caffe AR, Visser H, Jansen HG et al (1989)** Histotypic differentiation of neonatal mouse retina in organ culture” *Current Eye Research*, 8, 1083–1092.

**Caffe AR, Ahuja P, Holmqvist B et al (2001)** “Mouse retina explants after long-term culture in serum free medium” *Journal of Chemical Neuroanatomy*, 22, 263–273.

**Cai H, Harrison DG (2000)** Endothelial dysfunction in cardiovascular diseases: the role of oxidant stress. *Circulation Research*, 87, 840-844.

**Cameron NE and Cotter MA (1999)** Effects of antioxidants on nerve and vascular dysfunction in experimental diabetes. *Diabetes Research and Clinical Practice*, 45, 137–146.

**Canning P, Sorrell FJ, Bullock AN (2015)** Structural basis of KEAP1 interactions with Nrf2. *Free Radical Biology and Medicine*, <http://dx.doi.org/10.1016/j.freeradbiomed.2015.05.034>

**Capellini VK, Restini CB, Bendhack LM et al (2013)** The Effect of Extracellular pH Changes on Intracellular pH and Nitric Oxide Concentration in Endothelial and Smooth Muscle Cells from Rat Aorta. *PLOS One*, <https://doi.org/10.1371/journal.pone.0062887>.

**Carmeliet P (2000)** Mechanisms of angiogenesis and arteriogenesis. *Nature Medicine*, 6, 389–395.

**Carreau A, El Hafny-Rahbi B, Matejuk A (2011)** Why is the partial oxygen pressure of human tissues a crucial parameter? Small molecules and hypoxia. *Journal of Cellular and Molecular Medicine*, 15, 1239–1253.

**Catrina SB, Okamoto K, Pereira T et al (2004)** Hyperglycaemia regulates hypoxia-inducible factor-1α protein stability and function. *Diabetes*, 53, 3226–3232.

**Castell JV, Geiger T, Gross V et al (1988)** Plasma clearance, organ distribution and target cells of interleukin-6/hepatocyte-stimulating factor in the rat. *European Journal of Biochemistry*, 177, 357–361.

**Castilho AF, Aveleira CA, Leal EC et al (2012)** Heme Oxygenase-1 Protects Retinal Endothelial Cells against High Glucose- and Oxidative/Nitrosative Stress-Induced Toxicity. *PLOS One*, <https://doi.org/10.1371/journal.pone.0042428>

**Ceriello A (2010)** Point: Postprandial Glucose Levels Are a Clinically Important Treatment Target. *Diabetes Care*, 33, 1905-1907.

**Chakravarthy U, Hayes RG, Stitt AW et al (1998)** Constitutive nitric oxide synthase expression in retinal vascular endothelial cells is suppressed by high glucose and AGEs. *Diabetes*, 47, 945-952.

- Chance** B, Sies H, Boveris A (1979) Hydroperoxide metabolism in mammalian organs. *Physiology Reviews*, 59, 527-605.
- Chang** YH, Chen PL, Tai M C et al (2006) Hyperbaric oxygen therapy ameliorates the blood-retinal barrier breakdown in DR. *Clinical Experimental Ophthalmology*, **34**, 584-589.
- Chatterjee** S, Khunti K, Davies M (2017) Type 2 diabetes. *Lancet*, 389, 2239-2251.
- Chen** HH, Chen YT, Huang YW et al (2012) 4-Ketopinoresinol, a novel naturally occurring ARE activator, induces the Nrf2/HO-1 axis and protects against oxidative stress-induced cell injury via activation of PI3K/AKT signalling. *Free Radical Biology and Medicine*, 52, 1054- 1066.
- Chen** S, Feng B, George B et al (2010) Transcriptional coactivator p300 regulates glucose-induced gene expression in endothelial cells. *American Journal of Physiology- Endocrinology and Metabolism*, 298, E127-E137.
- Chen** C, Pore N, Behrooz A et al (2001) Regulation of glut1 mRNA by hypoxia-inducible factor-1. Interaction between H-ras and hypoxia. *Journal of Biological Chemistry*, 276, 9519-9525.
- Cheng** L, Yu H, Yan N et al (2017) Hypoxia-Inducible Factor-1 $\alpha$  Target Genes Contribute to Retinal Neuroprotection. *Frontiers in Cellular Neuroscience*, 11, 20, doi: 10.3389/fncel.2017.00020.
- Cheng** X, Siow RC, Mann GE (2011) Impaired redox signaling and antioxidant gene expression in endothelial cells in diabetes: a role for mitochondria and the nuclear factor-E2-related factor 2-Kelch-like ECH-associated protein 1 defense pathway. *Antioxidants and Redox Signalling*, 14, 469-487.
- Cheung** N, Wong IY, Wong TY (2014) Ocular Anti-VEGF Therapy for DR: Overview of Clinical Efficacy and Evolving Applications. *Diabetes Care*, 37, 900-905.
- Chien** S, Li S, Shyy JY (1998) Effects of Mechanical Forces on Signal Transduction and Gene Expression in Endothelial Cells. *Hypertension*, 31, 162-169.
- Choi** AM and Alam J (1996) Heme oxygenase-1: function, regulation, and implication of a novel stress-inducible protein in oxidant-induced lung injury. *American Journal of Respiratory Cell and Molecular Biology*, 15, 9-19.
- Cholkar** K, Dasari SR, Pal D (2013) Eye: anatomy, physiology and barriers to drug delivery. Woodhead Publishing Series in Biomedicine, 1-36.
- Chomczynski** P and **Sacchi** N (1987) Single-step method of RNA isolation by acid guanidinium thiocyanate-phenol-chloroform extraction. *Analytical Biochemistry*, 162, 156-159.
- Chung** C, Chang JK, Min BG et al (2000) Streamlined shape of endothelial cells. *KSME International Journal*, 14, 861-866.
- Costa** A and Andrade F (2015) Tissue based in vitro and ex vivo models for permeability studies. *Concepts and Models for Drug Permeability Studies*, 2015, 255–272.
- Costagliola** C, Romano V, De Tollis M (2013) TNF-Alpha Levels in Tears: A Novel Biomarker to Assess the Degree of DR. *Mediators of Inflammation*, 2013, Article ID 629529, 1-6.
- Chung** C, Chang JK, Min BG, Han DC (2000) Streamlined shape of endothelial cells. *KSME International Journal*, 14, 861-866.

**Cines** DB, Pollak ES, Clayton A (1998) Endothelial Cells in Physiology and in the Pathophysiology of Vascular Disorders. *Blood*, 91, 3527-3561.

**Clark** RJ, McDonough PM, Swanson E et al (2003) Diabetes and the accompanying hyperglycaemia impairs cardiomyocyte calcium cycling through increased nuclear O-GlcNAcylation. *Journal of Biological Chemistry*, 278, 44230–44237.

**Cnop** M, Welsh N, Jonas J et al (2005) Mechanisms of pancreatic beta-cell death in type 1 and type 2 diabetes: many differences, few similarities. *Diabetes*, 54, S97-107.

**Cogan** DG, Toussaint D, Kuwabara T (1961) Retinal vascular patterns. IV. DR. *Archives of Ophthalmology*, 66, 366–78.

**Crapo** JD, Barry BE, Foscue HA et al (1980) Structural and biochemical changes in rat lungs occurring during exposures to lethal and adaptive doses of oxygen. *The American Review of Respiratory Disease*, 122,123-143.

**Craven** P, Studer R, Felder J et al (1997) Nitric oxide inhibition of transforming growth factor-beta and collagen synthesis in mesangial cells. *Diabetes*, 46, 671–681.

**Ctercteko** GC, Dhanendran M, Hutton WC et al (1981) Vertical forces acting on the feet of diabetic patients with neuropathic ulceration. *British Journal of Surgeons* 1981; **68**: 608–14.

**Cuadrado** A, Martin-Moldes Z, Ye J et al (2014) Transcription factors NRF2 and NF-kappa B are coordinated effectors of the Rho family, GTP-binding protein RAC1 during inflammation. *Journal of Biological Chemistry*, 289, 15244–15258.

## D

**Dabir** P, Marinic TE, Krukovets I et al (2008) Aryl Hydrocarbon Receptor is activated by glucose and regulates the thrombospondin-1 gene promoter in endothelial cells. *Circulation Research*, 102, 1558-1565.

**Das** A, Frank RN, Zhang NL et al (1990) Increases in collagen type IV and laminin in galactose-induced retinal capillary basement membrane thickening – prevention by an AR inhibitor. *Experimental Eye Research*, 50, 269–80.

**Daffu** G, del Pozo CH, O'Shea KM et al (2013) Radical roles for RAGE in the pathogenesis of oxidative stress in cardiovascular diseases and beyond. *International Journal of Molecular Sciences*, 14, 19891–19910.

**Dallinger** S, Dorner GT, Wenzel R (2000) Endothelin-1 Contributes to Hyperoxia-Induced Vasoconstriction in the Human Retina. *Investigative Ophthalmology and Visual Science*, 41, 864-869.

**De Bock** K, Georgiadou M, Carmeliet P (2013) Role of Endothelial Cell Metabolism in Vessel Sprouting. *Cell Metabolism* 18, 634-647.

**Deckert** T, Poulsen JE, Larsen M (1978) Prognosis of diabetics with early onset diabetes before the age of thirty-one. *Diabetologia*, 14, 366- 377.

**Degenhardt T**, Thorpe S, Baynes J (1998) Chemical modification of proteins by methylglyoxal. *Cell and Molecular Biology*, 44, 1139–1145.

**Dejana E** (1996) Endothelial adherens junctions: Implications in the control of vascular permeability and angiogenesis. *Journal of Clinical Investigations*, 98, 1949.

**De Keulenaer GW**, Chappell DC, Ishizaka N et al (1998) Oscillatory and steady laminar shear stress differentially affect human endothelial redox state: role of a superoxide-producing NADH oxidase. *Circulation Research*, 82, 1094-1101.

**De Nigris**, Pujadas G, La Sala L (2015) Short-term high glucose exposure impairs insulin signalling in endothelial cells. *Cardiovascular Diabetology*, 14, 114.

**Dennery PA** (2013) Signalling function of heme oxygenase proteins. *Antioxidants and redox Signalling*, 20, 1743–1753

**Devling TW**, Lindsay, CD, McLellan et al (2005) Utility of siRNA against Keap1 as a strategy to stimulate a cancer chemo preventive phenotype. *Proceedings of National Academy of Science U S A*, 102, 7280-7285A.

**Diabetes Control and Complications Trial (DCCT) Research Group**: Nathan DM, Genuth S, Lachin et al (1993) The effect of intensive treatment of diabetes on the development and progression of long-term complications in insulin-dependent diabetes mellitus. *New England Journal of Medicine*, 329, 977-986-a.

**Diabetes Control and Complications Trial/Epidemiology of Diabetes Interventions and Complications (DCCT/EDIC) Study Research Group** (2005) Intensive Diabetes Treatment and Cardiovascular Disease in Patients with Type 1 Diabetes. *New England Journal of Medicine*, 353, 2643-53.

**Didion SP**, Kinzenbaw DA, Faraci FM (2005) Critical role for CuZn-superoxide dismutase in preventing angiotensin II-induced endothelial dysfunction. *Hypertension*, 46, 1147–1153.

**Ding M**, Cui S, Li C et al (2006) Loss of the tumour suppressor Vhlh leads to upregulation of Cxcr4 and rapidly progressive glomerulonephritis in mice. *Nature Medicine*, 12, 1081-1087.

**Dinh T** and Veves A (2005) Microcirculation of the diabetic foot. *Current Pharmaceutical Design*, 11 (2005), pp. 2301-2309

**Discher D**, Janmey D, Wang L (2005) Tissue cells feel and respond to the stiffness of their substrate. *Science*, 310, 113-1143.

**Doddaballapur A**, Michalik KM, Manavski Y et al (2015). Laminar Shear Stress Inhibits Endothelial Cell Metabolism via KLF2-Mediated Repression of PFKFB3. *Arteriosclerosis, Thrombosis, and Vascular Biology*, 35, 137-145.

**Doctor N**, Pandya S, Supe A et al (1992) Hyperbaric oxygen therapy in diabetic foot. *Journal of Postgraduate Medicine*, 38, 112-114.

**Dolcet X**, Llobet D, Pallares J et al (2005) NF- $\kappa$ B in development and progression of human cancer. *Virchows Archiv*, 446, 475-482.

**Du** XL, Sui GZ, Stockklauser-Färber K et al (1998) .Induction of apoptosis by high proinsulin and glucose in cultured human umbilical vein endothelial cells mediated by ROS. *Diabetologia*, 41, 249-256.

**Du** X, Matsumura T, Edelstein D et al (2003) Inhibition of GAPDH activity by poly (ADP-ribose) polymerase activates three major pathways of hyperglycaemic damage in endothelial cells. *Journal of Clinical Investigation*, 112, 1049–1057.

**Du** Y, Veenstra A, Palczewski K et al (2013) Photoreceptor cells are major contributors to diabetes-induced oxidative stress and local inflammation in the retina. *Proceedings of the National Academy of Sciences of the United States of America*, 110, 16586–16591.

**Duckworth** W, Abraira C, Moritz T et al (2009).Glucose control and vascular complications in veterans with type 2 diabetes. *New England Journal of Medicine*, 360, 129-139.

**Duzgun** AP, Satir HZ, Ozozan O et al (2008) Effect of hyperbaric oxygen therapy on healing of diabetic foot ulcers [J]. *Journal of Foot and Ankle Surgery*, 515-519

## E

**EDIC/DCCT)** The Diabetes Control and Complications Trial/Epidemiology of Diabetes Interventions and Complications (DCCT/EDIC) Study Research Group (2005) Intensive Diabetes Treatment and Cardiovascular Disease in Patients with Type 1 Diabetes. *New England Journal of Medicine*, 353, 2643-53.

**Elbirt** K and Bonkovsky H (1999) Heme oxygenase: recent advances in understanding its regulation and role. *Proceedings of Associations of American Physicians banner*, 1999, 438-447.

**Enciso** J, Camenisch T, Gratzinger D et al (2003) Elevated glucose inhibits VEGF-A-mediated endocardial cushion formation: Modulation by PECAM-1 and MMP-2. *Journal of Biological Chemistry*, 160, 605-615.

**Engel** WK and **Cunningham** GG (1963) Rapid examination of muscle tissue: An improved trichrome method for fresh-frozen biopsy sections. *Neurobiology* 13, 919.

**Evcimen** ND and **King** GL (2007) The role of protein kinase C activation and the vascular complications of diabetes. *Pharmacological Research*, 55, 498-510.

## F

**Fadini GP, Sartore S, Schiavon M et al (2006)** Diabetes impairs progenitor cell mobilisation after hind limb ischaemia-reperfusion injury in rats. *Diabetologia*, 49, 3075–3084.

**Falanga V (2005)** Wound healing and its impairment in diabetic foot. *Lancet*, 366, 1736-1743.

**Falanga V (2004)** The chronic wound: impaired healing and solutions in the context of wound bed preparation. *Blood Cells, Molecules and Diseases*, 32, 88-94.

**Falanga V (2002)** Physiology and pathophysiology of wound healing. In Veves A, Giurini JM, LoGerfo FW (Eds.), *The diabetic foot: medical and surgical management*, Human Press, Totowa, hedges NJ, pp. 59-73.

**Federici M, Menghini R, Mauriello A et al (2002)** Insulin-dependent activation of endothelial nitric oxide synthase is impaired by O-linked glycosylation modification of signalling proteins in human coronary endothelial cells. *Circulation*, 106, 466–472.

**Feng S, Yu H, Yu Y (2018)** Levels of Inflammatory Cytokines IL-1 $\beta$ , IL-6, IL-8, IL-17A, and TNF- $\alpha$  in Aqueous Humour of Patients with DR. *Journal of Diabetes Research*, 2018, Article ID 8546423, 1-6.

**Fernandez-Bueno I, Pastor JC et al (2008)** Müller and macrophage-like cell interactions in an organotypic culture of porcine neuroretina. *Molecular Vision*, 14, 2148–2156.

**Ferrara N, Gerber HP, LeCouter J (2003)** The biology of VEGF and its receptors *Nature Medicine*, 9, 669-676.

**Ferrara N (2004)** Vascular endothelial growth factor: basic science and clinical progress. *Endocrine Reviews*, 25, 581-611.

**Ferrer-Martin RM, Martin-Oliva D, Sierra A et al (2014)** Microglial cells in organotypic cultures of developing and adult mouse retina and their relationship with cell death. *Experimental Eye Research*, 121, 42–57

**Fife CE, Buyukcikir C, Otto G (2007)** Factors influencing the outcome of lower extremity diabetic ulcers treated with hyperbaric oxygen therapy. *Wound Repair Regeneration*, 15, 22-31.

**Fishman AP (1982)** Endothelium: a distributed organ of diverse capabilities. *Annals of the New York Academy of Sciences*, 40, 1-8.

**Fleming I, Fisslthaler B, Dixit M et al (2005)** Role of PECAM-1 in the shear-stress-induced activation of Akt and the endothelial nitric oxide synthase (eNOS) in endothelial cells. *Journal of Cell Science*, 118, 4103-4111.

**Floyd TF, Clark JM, Gelfand R (2003)**.Independent cerebral vasoconstrictive effects of hyperoxia and accompanying arterial hypocapnia at 1 ATA. *The American Physiological Society*, 95, 2453-2461.

**Fong DS, Aiello LP, Ferris FL 3<sup>rd</sup> et al (2004)** DR. *Diabetes Care*, 27, 2540 -2553.

**Förster R, Davalos-Misslitz AC, Rot A (2008)** CCR7 and its ligands: balancing immunity and tolerance. *Nature Reviews. Immunology*, 8, 362-371.

**Fotino C, Ricordi C, Lauriola V et al (2010)** Bone marrow-derived stem cell transplantation for the treatment of insulin-dependent diabetes. *Reviews on Diabetes Studies*, 7, 144-157.

**Fowler MJ** (2008) Microvascular and Macrovascular Complications of Diabetes. *Clinical Diabetes*, 26, 77-82.

**Frank RN**, Keirn RJ, Kennedy A et al (1983) Galactose-induced retinal capillary basement membrane thickening: prevention by Sorbinil. *Investigative Ophthalmology and Visual Science*, 24, 1519–24.

**Freedman**, BI, Wuerth JP, Cartwright K (1999) Design and baseline characteristics for the aminoguanidine clinical trial in overt type 2 diabetic nephropathy (ACTION II)(Article). *Controlled clinical trials*, 20, 493-510.

**Fujiwara K** (2006) Platelet endothelial cell adhesion molecule-1 and mechanotransduction in vascular endothelial cells. *Journal of Internal Medicine*, 259, 373-380.

**Funatsu H**, Yamashita H, Ikeda T et al (2003) Vitreous levels of interleukin-6 and vascular endothelial growth factors are related to diabetic macular oedema. *Ophthalmology*, 110, 1690-1696.

**Furlani RE**, Richardson, MA, Poddell BK (2015) Second generation 2-aminoimidazole based AGEs inhibitors and breakers. *Bioorganic and Medicinal Chemistry Letters* , 21, 4820-4823

**Fuse Y** and Kobayashi M (2017) Conservation of the Keap1-Nrf2 System: An Evolutionary Journey through Stressful Space and Time. *Molecules*, 22.

## G

**Gabbay KH** (1975) Hyperglycaemia, polyol metabolism, and complications of diabetes mellitus. *Annual Reviews of Medicine*, 26, 521 -536.

**Gabbay KH** (2004) AR inhibition in the treatment of DN: where are we in 2004? *Current Diabetes Reports*, 4, 405 -408.

**Gabbay** (2006) Interleukin-6 and chronic inflammation. *Arthritis Research and Therapy*, 8, S3.  
<https://doi.org/10.1186/ar1917>

**Gadad P**, Matthews K, Knott R (2013) Role of HIF1 alpha and PKC beta in mediating the effect of oxygen and glucose in a novel wound assay. *Journal of Microvascular Research*, 88, 61-69.

**Gaddini L**, Villa M, Matteucci A et al (2009) Early effects of high glucose in retinal tissue cultures: Renin–Angiotensin system-dependent and -independent signalling. *Neurobiology of Disease* 35, 278–285

**Gallagher KA**, Goldstein LJ, Thom S R et al (2006) Hyperbaric oxygen and bone marrow-derived endothelial progenitor cells in diabetic wound healing. *Vascular*, 14, 328-337.

**Galley HF** and Webster NR (2004) Physiology of the endothelium. *British Journal of Anaesthesia*, 93, 105-113.

**Galli-Resta L**, Leoneb P, Bottaria D et al (2008) The genesis of retinal architecture: An emerging role for mechanical interactions? *Progress in Retinal and Eye Research*, 27, 260-283.

**Gallin J** and Snyderman R (1999) Overview. In: Gallin J and Snyderman R. (3rd Ed.) *Inflammation*. Lippincott Williams and Wilkins, Philadelphia, 1–4.

**Gancharova OS**, ManskikhVN, Zamyatnin AA et al (2013) Organotypic culture of neural retina as a research model of neurodegeneration of ganglion cells. *Biochemistry*, 78, 1280–1286.

**Ganz M** and Seftel A (2000) Glucose-induced changes in protein kinase C and nitric oxide are prevented by vitamin E. *American Journal of Physiology*, 278, E146–E152.

**Gao W**, Ferguson G, Connell P et al (2006) High glucose concentrations alter hypoxia-induced control of vascular smooth muscle cell growth via a HIF-1 $\alpha$ -dependent pathway. *Journal of Molecular and Cellular Cardiology*, 42, 609–619.

**Garvey W**, Bigelow F, Fathi A et al (1996) Modified Gomori Trichrome Stain for Frozen Skeletal Muscle and Paraffin Embedded Sections. *Journal of Histotechnology*, 4.

**Geraldes P**, Hiraoka-Yamamoto J, Matsumoto M, et al (2009). Activation of PKC- $\delta$  and SHP-1 by hyperglycaemia causes vascular cell apoptosis and DR. *Nature Medicine*, 15, 1298–1306.

**Gerber HP**, Dixit V, Ferrara N (1998) Vascular endothelial growth factor induces expression of the antiapoptotic proteins Bcl-2 and A1 in vascular endothelial cells. *Journal of Biological Chemistry*, 273, 13313–13316.

**Giardino I**, Edelstein D, Brownlee M (1994) Nonenzymatic glycosylation in vitro and in bovine endothelial cells alters basic fibroblast growth factor activity: a model for intracellular glycosylation in diabetes. *Journal of Clinical Investigation*, 94, 110 –117.

**Gillies MC**, Su T, Stayt J (1997) Effect of high glucose on permeability of retinal capillary endothelium in vitro. *Investigative Ophthalmology and Visual Science*, 38, 635–642.

**Gillies MC** and Su T (1993) High glucose inhibits retinal capillary pericyte contractility in vitro. *Investigative Ophthalmology and Visual Science*, 34, 3396–3401.

**Girard JO**, Moussion C, Förster R (2012) HEVs, lymphatics and homeostatic immune cell trafficking in lymph nodes. *Nature Reviews. Immunology*, 12, 762–773.

**Godman CA**, Chheda KP, Hightower LE et al (2010) Hyperbaric oxygen induces a cytoprotective and angiogenic response in human microvascular endothelial cells. *Journal of Cell Stress and Chaperones*, 15, 431–442.

**Goldberg MA**, Dunning SP, Bunn HF (1988) Regulation of the erythropoietin gene: evidence that the oxygen sensor is a heme protein. *Science*, 242 1412–1415.

**Gomori G** (1950) Gomori's Trichrome Staining Protocol for Connective Tissues. *American Journal of Clinical Pathology*, 20, 665.

**Grant DS**, Tashiro KI, Segui-Real B (1989) Two different laminin domains mediate the differentiation of human endothelial cells into capillary-like structures in vitro. *Cell*, 58, 933.

**Grarup N**, Sandholt CH, Hansen T et al (2014) Genetic susceptibility to type 2 diabetes and obesity: from genome-wide association studies to rare variants and beyond. *Diabetologia*, 57, 1528–1541.



- Grocott M**, Montgomery H, Vercueilven A (2007) High-altitude physiology and pathophysiology: implications and relevance for intensive care medicine. *Critical Care*, 11, 203.
- Graven KK**, Yu Q, Pan D et al (1999) Identification of an oxygen responsive enhancer element in the glyceraldehyde-3-phosphate dehydrogenase gene. *Biochimica Biophysica Acta* 1447, 208-218.
- Gregg RG**, McCall MA, Massey SC (2013) Function and Anatomy of the Mammalian Retina in Anatomy and Physiology. *Retina*, 5<sup>th</sup> Ed., Vol1, pp 360-400.
- Griendling KK**, Ushio-Fukai M, Lassegue B et al (1997) Angiotensin II signalling in vascular smooth muscle. New concepts. *Hypertension*, 29, 366-373.
- Gross JL**, de Azevedo MJ, and Silveiro SP et al (2005) Diabetic nephropathy: diagnosis, prevention, and treatment. *Diabetes Care*, 28, 164-176.
- Grottelli S**, Ferrari I, Pietrini G et al (2016) The role of Cyclo (His-Pro) in neurodegeneration, *International Journal of Molecular Science*, 17, (pii E1332).
- Guo S** and Dipietro LA (2010) Factors affecting wound healing. *Journal of Biological Chemistry*, 285, 14217-14228.

## H

- Haddad JJ** and Land SC (2001) A non-hypoxic, ROS-sensitive pathway mediates TNF- $\alpha$ -dependent regulation of HIF-1 $\alpha$ . *FEBS Letters*, 505, 269-274.
- Haddad JJ** (2002). Oxygen-sensing mechanisms and the regulation of redox-responsive transcription factors in development and pathophysiology. *Respiratory Research*, 22, 3:1-26.
- Hadagali MD** and Chua LS (2014) The anti-inflammatory and wound healing properties of honey. *European Food Research and Technology*, 239, 1003–1014.
- Haffner SM**, Lehto S, Ronnemaa T et al (1998) Mortality from coronary heart disease in subjects with type 2 diabetes and in nondiabetic subjects with and without prior myocardial infarction. *New England Journal of Medicine*, 339, 229-234.
- Haidari M**, Zhang W, Willerson et al (2014) Disruption of endothelial adherens junctions by high glucose is mediated by protein kinase C- $\beta$ -dependent vascular endothelial cadherin tyrosine phosphorylation. *Cardiovascular Diabetology*, 13, 105.
- Hallmann A**, Milczarek R, Lipiński M et al (2004) Fast perinuclear clustering of mitochondria in oxidatively stressed human choriocarcinoma cells. *Folia Morphologica*, 63, 407-412.
- Hammes HP**, Feng Y, and Pfister F (2011) DR: Targeting Vasoregression. *Diabetes*, 60, 9-16.
- Hammes HP**, Du X, Edelstein D et al (2003) Benfotiamine blocks three major pathways of hyperglycaemic damage and prevents experimental DR. *Nature Medicine*, 9, 294-299.
- Hamuro M**, Polan J, Natarajan M et al (2002) High glucose induced nuclear factor kappa B mediated inhibition of endothelial cell migration. *Atherosclerosis*, 162, 277-287.

**Haneda M**, Koya D, Isono M et al (2003). Overview of glucose signalling in mesangial cells in diabetic nephropathy. *Journal of American Society of Nephrology*, 14, 1374-1382.

**Hayden MS**, Ghosh S (2004) Signalling to NF-kappa B. *Genes Development*, 18, 2195-2224.

**Hayden MS** and Ghosh S (2008) Shared principles in NF-kappa B signalling. *Cell*, 132, 344-362.

**Hayes JD** and **Dinkova-Kostova AT** (2014) The Nrf2 regulatory network provides an interface between redox and intermediary metabolism *Trends in Biochemical Sciences*, 39, 199-218.

**Hauser S**, Jung F, Pietzsch J (2017) Human endothelial cells in biomaterial research. *Trends in Biotechnology*, 35, 265-277.

**He M**, Nitti M, Piras S et al (2015) Heme oxygenase-1-derived bilirubin protects endothelial cells against high glucose-induced damage. *Free Radical Biology and Medicine*, 89, 91-98.

**He M**, Pan H, Xiao C, Pu M (2013) Roles for redox signalling by NADPH oxidase in hyperglycaemia-induced heme oxygenase-1 expression in the diabetic retina. *Investigative Ophthalmology and Visual Science*, 54, 4092-4101.

**He M**, Siow RC, Sugden D et al (2011) Induction of HO-1 and redox signaling in endothelial cells by advanced glycation end products: a role for Nrf2 in vascular protection in diabetes. *Nutrition, Metabolism Cardiovascular Disease*, 21, 277-285.

**Heinrich PC**, Castell JV, Andus T (1990) Interleukin-6 and the acute phase response. *Biochemistry Journal*, 265, 621-636.

**Heinrich PC**, Behrmann I, Haan S (2003) Principles of interleukin (IL)-6-type cytokine signalling and its regulation. *Biochemistry Journal*, 374, 1-20.

**Heiss EH**, Schachner D, Zimmermann K et al (2013) Glucose availability is a decisive factor for Nrf2-mediated gene expression. *Redox Biology*, 1, 359-365.

**Hempel A**, Maasch C, Heintze U et al (1997) High Glucose Concentrations Increase Endothelial Cell Permeability via Activation of Protein Kinase C $\alpha$ . *Circulation Research*, 81, 363-371.

**Herman WH** (1999) Glycemic control in diabetes. *British Medical Journal (BMJ)*, 319, 104. Doi: <https://doi.org/10.1136/bmj.319.7202.104>

**Himmel HM**, Whorton AR, Strauss HC (1993) Intracellular calcium, currents, and stimulus-response coupling in endothelial cells. *Hypertension*, 21, 112- 127.

**Hirano T**, Yasukawa K, Harada H et al (1986) Complementary DNA for a novel human interleukin (BSF-2) that induces B lymphocytes to produce immunoglobulin, *Nature*, 324, 73-76.

**Hirota K** and Semenza GL (2006) Regulation of angiogenesis by hypoxia-inducible factor 1. *Critical Reviews Oncology and Haematology*, 59, 15-26.

**Hoekstra KA**, Godin DV, Cheng KM (2004) Protective role of heme oxygenase in the blood vessel wall during atherogenesis. *Biochemistry and Cell Biology*, 82, 351-359.

**Hodges** AN, Delaney S, Lecomte JM (2003) Effect of hyperbaric oxygen on oxygen uptake and measurements in the blood and tissues in a normobaric environment. *British Journal of Sports Medicine*, 37, 516-520.

**Hombrebueno** JR, Chen M, Penalva RG et al (2014) Loss of synaptic connectivity, particularly in second order neurons is a key feature of diabetic retinal neuropathy in the Ins2Akita mouse *PLoS ONE*, 9, Article ID e97970.

**Hsieh** CP, Chiou YL, Lin CY (2010) Hyperbaric oxygen-stimulated proliferation and growth of osteoblasts may be mediated through the FGF-2/MEK/ERK 1/2/NFκB and PKC/JNK pathways. *Journal of Connective Tissue Research*, 51. <https://doi.org/10.3109/03008201003746679>

**Hu** C, Eggler AL, Mesecar AD et al (2011) Modification of keap1 cysteine residues by sulforaphane. *Chemical Research in Toxicology*, 24, 515–521.

**Hu** J, Discher DJ, Bishopric NH (1998) Hypoxia regulates expression of the endothelin-1 gene through a proximal hypoxia-inducible factor-1 binding site on the antisense strand. *Biochemical and Biophysical Research Communications*, 245: 894-899

**Huang** J, Zhao Q, Mooney SM (2002) Sequence determinants in hypoxia-inducible factor-1α for hydroxylation by the prolyl hydroxylases PHD1, PHD2, and PHD3. *Journal of Biological Chemistry*, 277, 39792-39800.

**Hughes** C, Postovit L, and Lajoie G (2010) Matrigel: A complex protein mixture required for optimal growth of cell culture. *Proteomics*, 10, 1886-1890.

**Human Protein Atlas**. <https://www.proteinatlas.org/ENSG00000116044-NFE2L2/cell> Time/date of access: 06:30am/13<sup>th</sup> September 2018.

**Hunt** T and Pai M (1972) The effect of varying ambient oxygen tensions on wound metabolism and collagen synthesis. *Surgery, Gynaecology and Obstetrics*, 135, 561-567.

**Hunt** TK, Linsey M, Grislis G et al (1974) The effect of differing ambient oxygen tensions on wound infection. *Annals of Surgery*, 181, 35-39.

**Hyperbaric** oxygen Treatment Trust (HBOT) <https://www.hyperbaricoxygentherapy.org.uk/what-is-hbot> Time/date of access: 09:01am 18/09/2018

**Hyun** DH, Hernandez JO, Mattson MP (2006) The plasma membrane redox system in aging. *Ageing Research Reviews*, 5, 209-220.

## I

**Ilan N, Cheung L, Pinter E et al (2000)** Platelet-Endothelial Cell Adhesion Molecule-1 (CD31), a Scaffolding Molecule for Selected Catenin Family Members Whose Binding Is Mediated by Different Tyrosine and Serine/Threonine Phosphorylation. *Journal of Biological Chemistry*, 275, 21435-21443.

**International Diabetes Federation.** <http://www.idf.org/types-diabetes> (2018)\_a. Time of access GMT 17.35pm 13/08/2018 <https://www.idf.org/aboutdiabetes/what-is-diabetes/types-of-diabetes.html>

**International Diabetes Federation.** <http://www.idf.org/World-diabetes-day> (2017)\_b. Time of access GMT 17.57pm 13/08/2018 <https://www.idf.org/news/94:new-idf-figures-show-continued-increase-in-diabetes-across-the-globe,-reiterating-the-need-for-urgent-action.html>

**Isaacs JS, Jung YJ, Mimnaugh EG et al (2002)** Hsp90 regulates a von Hippel Lindau-independent Hypoxia-inducible factor-1 alpha-degradative pathway. *Journal of Biological Chemistry*, 277, 29936–29944.

**Ishii H, Jirousek MR, Koya D (1996) et al** Amelioration of vascular dysfunctions in diabetic rats by an oral PKC beta inhibitor. *Science*, 272, 728-731.

**Ishizaki E, Fukumoto M, Puro DG (2009)** Functional K<sub>ATP</sub> channels in the rat retinal microvasculature: topographical distribution, redox regulation, spermine modulation and diabetic alteration. *Journal of Physiology*, 587, 2233–2253.

**Isoe T, Makino Y, Mizumoto K (2010)** High glucose activates HIF-1-mediated signal transduction in glomerular mesangial cells through a carbohydrate response element binding protein. *Kidney International*, 78, 48-59.

**Iversen PO, Nicolaysen A, Kvernebo K et al (1999)** Human cytokines modulate arterial vascular tone via endothelial receptors. *European Journal of Physiology*, 439, 93–100.

## J

**Jackson JR, Seed MP, Kircher CH et al (1997)** The co- dependence of angiogenesis and chronic inflammation. *FASEB Journal*, 11, 457–465.

**Jensen JC, Pogrebniak HW, Pass HI et al (1992)** Role of tumour necrosis factor in oxygen toxicity. *American Physiological Society*, 1902-1907.

**Jezek P, Hlavata L (2005)** Mitochondria in homeostasis of ROS in cell, tissues, and organism. *International Journal of Biochemistry and Cell Biology*, 37, 2478-2503.

**Jiang T, Huang Z, Lin Y et al (2010)** The protective role of Nrf2 in STZ-induced diabetic nephropathy. *Diabetes*, 59, 850–860.

**Jo D, Cho C, Kim J et al (2013)** Animal models of DR: doors to investigate pathogenesis and potential therapeutics. *Journal of Biomedical Sciences*, 20, 1-13.

**Johnson** DR, Douglas I, Jahnke A et al (1996). A sustained reduction in kappa B-beta may contribute to persistent NF-kappa B activation in human endothelial cells. *Journal of Biological Chemistry*, 271, 16317–16322.

**Johnson** T and Martin K (2008) Development and characterization of an adult retinal explant organotypic tissue culture system as an in-vitro intraocular stem cell transplantation model. *Investigative Ophthalmology and Visual Sciences*, 49, 3503 -3512.

**Joussen** AM, Poulaki V, Mitsiades N et al (2002) Nonsteroidal anti-inflammatory drugs prevent early DR via TNF-alpha suppression. *FASEB Journal*, 16, 438-440.

**Joussen** A, Poulaki V, Le M et al (2004) A central role for inflammation in the pathogenesis of DR. *The FASEB Journal*, 18, 1450-1452.

**Jung** NH, Kim HP, Kim BR (2003) Evidence for heme oxygenase-1 association with caveolin-1 and -2 in mouse mesangial cells. *International Union of Biochemistry and Molecular Biology Life*, 55, 525-532.

## K

**Kaempfer** S, Walter P, Salz AK, et al (2008) Novel organotypic culture model of adult mammalian neurosensory retina in co-culture with retinal pigment epithelium. *Journal of Neuroscience Methods*, 17, 47–58.

**Klagsbrun** M and Soker S (1993) VEGF/VPF: the angiogenesis factor found? *Angiogenesis*, 3, 699.

**Kaidanovich**-Beilin O Woodgett JR (2011) GSK-3: Functional Insights from Cell Biology and

**Kalani** M, Jorneskog G, Naderi N et al (2002) Hyperbaric oxygen (HBO) therapy in treatment of diabetic foot ulcers. Long-term follow-up [J]. *Journal of Diabetes Complications*, 16, 153-158.

**Kallio** PJ, Pongratz I, Gradin K et al (1997) Activation of hypoxia-inducible factor 1alpha: posttranscriptional regulation and conformational change by recruitment of the Arnt transcription factor. *Proceedings of National Academy of Sciences USA*, 94, 5667-567.

**Kannel** WB, McGee DL (1979) Diabetes and cardiovascular disease: the Framingham study. *Journal of American Medical Association*, 241, 2035 -2038.

**Karadurmus** N, Sahin M, Tasci C et al (2010) Potential benefits of hyperbaric oxygen therapy on atherosclerosis and glycaemic control in patients with diabetic foot. *Polish Journal of Endocrinology*, 51, 275-279.

**Karin** M and Ben-Neriah Y (2000) Phosphorylation meets ubiquitination: the control of NF-[kappa]B activity. *Annual Reviews of Immunology*, 18, 621-663.

**Kansanen** E, Kuosmanen SM, Leinonen H et al (2013) The Keap1-Nrf2 pathway: mechanisms of activation and dysregulation in cancer. *Redox Biology*, 1, 45–49

**Karar** J and Maity A (2011) PI3K/AKT/mTOR pathway in angiogenesis. *Frontiers in Molecular Neuroscience*, 4, 1-8.

**Kastelan** S, Tomic M, Antunica AG (2013) Inflammation and Pharmacological Treatment in DR. Mediators of Inflammation, doi: 10.1155/2013/213130

**Kato** M, Castro NE, Natarajan R (2013) MicroRNAs: potential mediators and biomarkers of diabetic complications. Free Radical Biology and Medicine, 64, 85-94.

**Kato** S, Madachi-Yamamoto S, Hayashi Y et al (1983) Effect of sodium fluorescein on neurite outgrowth from the retinal explant culture: an in vitro model for retinal toxicity. Brain Research, 313, 143–147.

**Katsuoka** F, Motohashi H, Ishii T et al (2005) Genetic evidence that small maf proteins are essential for the activation of antioxidant response element-dependent genes. *Molecular Cellular Biology*, 25, 8044-8051.

**Kay** AM, Simpson CL, Stewart JA (Jr) (2016) The Role of AGE/RAGE Signalling in Diabetes-Mediated Vascular Calcification. Journal of Diabetes Research, 2016. <http://dx.doi.org/10.1155/2016/6809703>

**Kawamura** H, Kobayashi M, Li Q (2004) Effects of angiotensin II on the pericyte-containing microvasculature of the rat retina. Journal of Physiology, 561, 671-683.

**Ke** Q and Costa M (2006) Hypoxia-Inducible Factor-1 (HIF-1). Molecular Pharmacology, 70, 1469–1480.

**Keck** PJ, Hauser SD, Krivi G, et al (1989) Vascular permeability factor, an endothelial cell mitogen related to PDGF. Science, 246, 1309–1312.

**Kelly** BD, Hackett SF, Hirota K et al (2003) Cell type-specific regulation of angiogenic growth factor gene expression and induction of angiogenesis in non-ischemic tissue by a constitutively active form of hypoxia-inducible factor 1. Circulation Research, 93, 1074–1081.

**Keenan** HA, Costacou T, Sun JK, et al (1995) Clinical factors associated with resistance to microvascular complications in diabetic patients of extreme disease duration: the 50-year medallist study. Diabetes Care, 30, 1995-1997.

**Keough** R, Dunlop M, Larkins R (1997) Effect of inhibition of AR on glucose flux, diacylglycerol formation, protein kinase C, and phospholipase A2 activation. Metabolism, 46, 41–47.

**Keum** YS and Choi BY (2014) Molecular and chemical regulation of the Keap1-Nrf2 signalling pathway. Molecules, 19, 10074–10089.

**Kietzmann** T, Roth U, Jungermann K (1999) Induction of the plasminogen activator inhibitor-1 gene expression by mild hypoxia via a hypoxia response element binding the hypoxia-inducible factor-1 in rat hepatocytes. Blood 94: 4177-4185.

**Kim** BS, Chen J, Weinstein T et al (2002) VEGF Expression in Hypoxia and Hyperglycaemia: Reciprocal Effect on Branching Angiogenesis in Epithelial-Endothelial Co-Cultures. Journal of American Society of Nephrology, 13, 2027-2036

**Kim** SW, Lee HK, Shin JH et al (2013) Up-down regulation of HO-1 and iNOS gene expressions by ethyl pyruvate via recruiting p300 to Nrf2 and depriving It from p65, Free Radical Biology and Medicine, 65 468–476.

- Kim J**, Montagnani M, Koh KK et al (2006) Reciprocal relationships between insulin resistance and endothelial dysfunction: molecular and pathophysiological mechanisms. *Circulation*, 113, 1888-1904.
- Khachigian LM**, Resnick N, Gimbrone MA et al (1995) Nuclear factor-kappa B interacts functionally with the platelet-derived growth factor B-chain shear-stress response element in vascular endothelial cells exposed to fluid shear stress. *Journal of Clinical Investigations*, 96, 1169-1175.
- Kharazmi A**, Jepsen S, Andersen BJ (1987) Generation of reactive oxygen radicals by human phagocytic cells activated by *Plasmodium falciparum*. *Scandinavian Journal of Immunology*, 25, 335-41.
- Klein R**, Klein B, Moss S (1989) The Wisconsin epidemiological study of DR: a review. *Diabetes/Metabolism Reviews*, 5, 559-570.
- Knighton D**, Halliday B, Hunt T (1984) Oxygen as an antibiotic. The effect of inspired oxygen on infection. *Archives of Surgery*, 119, 199-204.
- Kobuch K**, Herrmann WA, Framme C et al (2008) Maintenance of adult porcine retina and retinal pigment epithelium in perfusion culture: characterisation of an organotypic in vitro model. *Experimental Eye Research*, 86, 661–668.
- Knott RM**, Robertson M, Muckersie E (1999) A model system for the study of human retinal angiogenesis: activation of monocytes and endothelial cells and the association with the expression of the monocarboxylate transporter type 1 (MCT-1). *Diabetologia*, 42, 870 – 877.
- Knott RM**, Forrester JV (2003) Pathogenesis of diabetic eye disease. In: Pickup JC and Gareth W eds. *Textbook of diabetes*. 3<sup>rd</sup> ed. Oxford: Blackwell Sciences. Pp. 48, 1-48.17.
- Kobayashi M**, Yamamoto M (2006) Nrf2-Keap1 regulation of cellular defence mechanisms against electrophiles and ROS. *Advanced Enzyme Regulation*, 46, 113–140.
- Kobayashi K**, Tanaka M, Nebuya S (2012) Temporal change in IL-6 mRNA and protein expression produced by cyclic stretching of human pulmonary artery endothelial cells. *International Journal of Molecular Medicine*, 1023, 509-513.
- Kobayashi S**, Nagino M, Komatsu S (2003) Stretch-induced IL-6 secretion from endothelial cells requires NFκB activation. *Biochemical and Biophysical Research Communications*, 308, 306-312.
- Kolm-Litty V**, Sauer U, and Nerlich A et al (1998) High glucose-induced transforming growth factor β1 production is mediated by the hexosamine pathway in porcine glomerular mesangial cells. *Journal of Clinical Investigation*, 101, 160-169.
- Krajka-Kuźniak V**, Paluszczak J, Baer-Dubowska W (2017) The Nrf2-ARE signalling pathway: an update on its regulation and possible role in cancer prevention and treatment. *Pharmacological Reports*, 69 393–402.
- Kranke P**, Bennett MH, Martyn-St James M et al (2015) Hyperbaric oxygen therapy for chronic wounds. *Cochrane Database Systematic Reviews*, (6), CD004123.
- Kriehuber E**, Breiteneder-Geleff S, Groeger M et al (2001) Isolation and characterization of dermal lymphatic and blood endothelial cells reveal stable and functionally specialized cell lineages. *Journal of Experimental Medicine* 194, 797–808.

**Krischak** GD, Augat P, Claes L et al (2013) The effects of non-steroidal anti-inflammatory drug application on incisional wound healing in rats. *Journal of Wound Care*, 16.

**Kroll** J and Waltenberger J (1999) A novel function of VEGF receptor-2 (KDR): rapid release of nitric oxide in response to VEGF-A stimulation in endothelial cells. *Biochemistry and Biophysics. Research Communication*, 265, 636-699.

**Kubo** K, Hanaoka M, Yamaguchi Set al (1996) Cytokines in bronchoalveolar lavage fluid in patients with high altitude pulmonary edema at moderate altitude in Japan. *Thorax*, 51, 739–742.

**Kuboki** K, Jiang Z, Takahara N et al (2000) Regulation of endothelial constitutive nitric oxide synthase gene expression in endothelial cells and in vivo a specific vascular action of insulin. *Circulation*, 101, 676–681.

**Kulkarni** PS, Hamid H, Barati M (1999) Angiotensin II-induced constrictions are masked by bovine retinal vessels. *Investigative Ophthalmology and Visual Sciences*, 40, 721-728.

**Kunisaki** M, Bursell SE, Clermont AC et al (1995) Vitamin E prevents diabetes-induced abnormal retinal blood flow via the diacylglycerol-protein kinase C pathway. *American Journal of Physiology*, 269, E239 -E246.

**Kuwabara** T, Cogan DG (1960) Studies of retinal vascular patterns. I. Normal architecture, *Archives of Ophthalmology* 1960; 64, 904–11.

**Kuwabara** T, Cogan DG (1963) Retinal vascular patterns. VI. Mural cells of the retinal capillaries. *Archives of Ophthalmology* 1963, 69, 492–502.

**Kowluru** RA (2005) Effect of AGEs on accelerated apoptosis of retinal capillary cells under in vitro conditions. *Life Sciences*, 76, 1051-1060.

**Kwak** MK, Itoh K, Yamamoto M et al (2002) Enhanced expression of the transcription factor Nrf2 by cancer chemo preventive agents: role of antioxidant response element-like sequences in the nrf2 promoter. *Molecular and Cellular Biology*, 22, 2883-2892.



## L

- Lai** AK and Lo AC (2013) Animal Models of DR: Summary and Comparison. *Journal of Diabetes Research*, 2013, 1-29.
- Lake** S, Hald E, Barocas V (2011). Collagen-agarose co-gels as a model for collagen-matrix interaction in soft tissues subjected to indentation. *Journal of Biomedical Materials Research*, 99A, 507-515.
- Lando** D, Peet DJ, Whelan DA (2002) Asparagine hydroxylation of the HIF transactivation domain: a hypoxic switch. *Science*, 295, 858-861.
- Landler** HL, Tauras JM, Ogiste JS et al (1997) Activation of the receptor for AGEs trigger a MAP kinase pathway regulated by oxidant stress. *Journal of Biological Chemistry*, 272, 17810.
- Larkins** RG and Dunlop ME (1992) The link between hyperglycaemia and diabetic nephropathy. *Diabetologia*, 35, 499-504.
- Lawrence** T (2009) The nuclear factor NF-kappa B pathway in inflammation. *Cold Spring Harbor Perspectives in Biology*, 1, a001651.
- LeCouter** J, Kowalski J, Foster J (2001) Identification of an angiogenic mitogen selective for endocrine gland endothelium. *Nature (London)* 412: 877-884.
- Lee** HB and Ha H (2005) Plasminogen activator inhibitor-1 and diabetic nephropathy. *Nephrology*, 10, S11-S13.
- Lee** PJ, Jiang BH, Chin BY (1997) Hypoxia-inducible factor-1 mediates transcriptional activation of the heme oxygenase-1 gene in response to hypoxia. *Journal of Biological Chemistry*, 272, 5375-5381
- Leiser** SF and Miller RA (2010) Nrf2 Signalling, a Mechanism for Cellular Stress Resistance in Long-Lived Mice. *Molecular and Cellular Biology*, 30, 871–884.
- Leung** YM, Kwan TK, Kwan CY et al. (2002) Calyculin A-induced endothelial cell shape changes are independent of  $[Ca^{++}]$  elevation and may involve actin polymerization. *Biochimica et Biophysica Acta*, 1589 93-103.
- Levy** AP, Levy NS, and Wegner S (1995) Transcriptional regulation of the rat vascular endothelial growth factor gene by hypoxia. *Journal of Biological Chemistry*, 270, 13333-13340.
- Li** W, Khor TO, Xu C et al (2008) Activation of Nrf2-antioxidant signalling attenuates NF Kappa B-inflammatory response and elicits apoptosis. *Biochemical Pharmacology Journal*, 76, 1485–1489.
- Li W, Li Y, Guan S et al (2007) Extracellular heat shock protein-90alpha: linking hypoxia to skin cell motility and wound healing. *EMBO Journal* 26:1221–1233.
- Liang** X (2015) Activation of Prolyl Hydroxylase (PHD) 2 prevents high glucose-induced blood-retina barrier breakdown in DR. *Investigative Ophthalmology and Visual Science*, 56, 5188.
- Lim** LS, Mitchell P, Seddon JM et al (2012) Age-related macular degeneration. *Lancet*, 379, 1728–1738

**Limb** GA, Chignell AH, Green W et al (1996) Distribution of TNF alpha and its reactive vascular adhesion molecules in fibrovascular membranes of proliferative DR. *British Journal of Ophthalmology*, 80, 168-173.

**Lin** Q, Weis S, Yang G (2007) Heme oxygenase-1 protein localizes to the nucleus and activates transcription factors important in oxidative stress. *Journal of Biological Chemistry*, 282, 20621-20633.

**Lin** C, McGough R, Aswad B et al (2004) Hypoxia induces HIF- 1 alpha and VEGF expression in chondrosarcoma cells and chondrocytes. *Journal of Orthopaedic Research*, 22, 1175-1181.

**Lin** C, Yin, G, Ou M et al (2017) The effects of HIF-1 $\alpha$  and VEGF on wound healing in diabetic mice. *Biomedical Research*, 28, 8121-8124.

**Liu** R, Li L, Yang M et al (2013) Systematic review of the effectiveness of hyperbaric oxygenation therapy in the management of chronic diabetic foot ulcers. *Mayo Clinic Proceedings*, 88, 166-175.

**Livak** K and Schmittgen TD (2001) Analysis of Relative Gene Expression Data Using Real-Time Quantitative PCR and the 2- $\Delta\Delta$ CT Method. *Methods*, 4, 402-408.

**Loboda** A, Jozkowicz A, Dulak J (2015) HO-1/CO system in tumour growth, angiogenesis and metabolism — Targeting HO-1 as an anti-tumour therapy. *Vascular Pharmacology*, 74, 11-22.

**Loboda** A, Jazwa A, Grochot-Przeczek A et al (2008) Heme oxygenase-1 and the vascular bed: from molecular mechanisms to therapeutic opportunities. *Antioxidants and Redox Signalling*, 10, 1767–1812.

**LoGerfo** FW and Coffman JD (1984) Current concepts. Vascular and microvascular disease of the foot in diabetes. Implications for foot care. *New England Journal of Medicine*, 311, 1615-1619.

**Löndahl** M, Katzman P, Nilsson A et al (2010) Hyperbaric oxygen therapy facilitates healing of chronic foot ulcers in patients with diabetes. *Diabetes Care*, 33, 998-1003.

**Löndahl** M (2013) Hyperbaric oxygen therapy as adjunctive treatment for diabetic ulcers. *Journal of Lower Extremity Wounds*, 12, 152-158.

**Loots** MA, Lamme EN, Zeegelaar J et al (1998) Differences in cellular infiltrate and extracellular matrix of chronic diabetic and venous ulcers versus acute wounds. *Journal of Investigative Dermatology*, 111, 850-857.

**Loots** MA, Kenter SB, Au FL et al (2002) Fibroblasts derived from chronic diabetic ulcers differ in their response to stimulation with EGF, IGF-I, bFGF and PDGF-AB compared to controls. *European Journal of Cell Biology*, 81, 153-160.

**Love** A, Cotter MA, Cameron NE (1996) Nerve function and regeneration in diabetic and galactosaemic rats: antioxidant and metal chelator effects. *European Journal of Pharmacology*, 314, 33-39.

**Lu** L, Lu Q, Chen W (2018) Vitamin D3 Protects against DR by Inhibiting High-Glucose-Induced Activation of the ROS/TXNIP/NLRP3 Inflammasome Pathway. *Journal of Diabetes*, 2018. <https://doi.org/10.1155/2018/8193523>

**Lu** M, Kuroki M, Amano S et al (1998) AGEs increase retinal vascular endothelial growth factor expression. *Journal of Clinical Investigation*, 101, 1219–1224.

**Lush** CW, Cepinskas G, Kvietys PR (2000) LPS tolerance in human endothelial cells: reduced PMN adhesion, E-selectin expression, and NF-kappa B mobilization. *American Journal of Physiology and Heart Circulation Physiology*, 278, H853-H861.

## M

**Malek** AM and **Izumo** S (1996) Mechanism of endothelial cell shape change and cytoskeletal remodelling in response to fluid shear stress. *Journal of Cell Science* 109, 713-726

**Mackay** CR (2001) Chemokines: immunology's high impact factors. *Nature Immunology*, 2, 95–101.

**Mahajan** KD, Nabar GM, Xue W (2017) Mechanotransduction Effects on Endothelial Cell Proliferation via CD31 and VEGFR2: Implications for Immunomagnetic Separation. *Bioseparation*, 12, 1600750.

**Mäkinen** T, Veikkola T, Mustjoki S et al. (2001) Isolated lymphatic endothelial cells transduce growth, survival and migratory signals via the VEGF-C/D receptor VEGFR-3. *EMBO Journal*, 20, 4762–4773.

**Marfella** R, D'Amico M, Di Filippo C et al (2002) Myocardial infarction in diabetic rats: role of hyperglycaemia on infarct size and early expression of hypoxia-inducible factor 1. *Diabetologia*, 45, 1172-1181.

**Marmor** MF, Yao XY, Hangeman GS (1994) Retinal adhesiveness in surgically enucleated human eyes. *Retina*, 14, 181–186

**Martin** A, Komada MR, Sane DC (2003) Abnormal angiogenesis in diabetes mellitus. *Medicinal Research Reviews*, 23, 117–145.

**Martin** P (1997) Wound healing—aiming for perfect skin regeneration. *Science*, 276, 75-81.

**Martinez** I, Nedredal GI, Øie CI et al (2008). The influence of oxygen tension on the structure and function of isolated liver sinusoidal endothelial cells. *Comparative Hepatology*, 7, 4.

**Masson** N, William C, Maxwell PH (2001) Independent function of two destruction domains in hypoxia-inducible factor- $\alpha$  chains activated by prolyl hydroxylation(Article). *EMBO Journal*, 20, Issue 18, 5197-5206.

**Mathupala** SP, Rempel A, Pedersen PL (2001) Glucose catabolism in cancer cells: identification and characterization of a marked activation response of the type II hexokinase gene to hypoxic conditions. *Journal of Biological Chemistry*, 276, 43407-43412.

**Matsuo** J, Oku H, Kanbara Y et al (2009) Involvement of NADPH oxidase and protein kinase C in endothelin-1 induced superoxide production in retinal microvessels. *Experimental Eye Research*, 89, 693-699.

**Matteucci** A, Varano M, Mallozzi C et al (2015) Primary retinal cultures as a tool for modelling DR: An Overview. *Biomedical Research International*, 2015 (364924), 1-16.

**McKimmie** CS, Singh MD, Hewit K et al (2013) An analysis of the function and expression of D6 on lymphatic endothelial cells. *Blood*, 121, 3768-3777.

**McSweeney** SR, Warabi E, Siow RCM. (2016) Nrf2 as an Endothelial Mechanosensitive Transcription Factor: Going With the Flow. *Hypertension*, 67, 20-29.

**Melillo** G, Musso T, Sica A et al (1995) A hypoxia-responsive element mediates a novel pathway of activation of the inducible nitric oxide synthase promoter. *Journal of Experimental Medicine*, 182, 1683-1693.

**Metzen** E, Berchner-Pfannschmidt U, Stengel P et al (2003a) Intracellular localization of human HIF-1  $\alpha$  hydroxylases: implications for oxygen sensing. *Journal of Cell Science*, 116, 1319-1326.

**Minelli** A, Conte C, Grottelli S et al (2009) Cyclo (His-Pro) up-regulates heme oxygenase 1 via activation of Nrf2-ARE signalling. *Journal of Neurochemistry*, 111, 956–966.

**Minelli** A, Grottelli S, Mierla A et al (2012) Cyclo(His-Pro) exerts anti-inflammatory effects by modulating NF $\kappa$ B and Nrf2 signalling. *International Journal of Biochemistry*, 44, 525–535.

**Mitsuishi** Y, Motohashi H, Yamamoto M (2012) The Keap1-Nrf2 system in cancers: stress response and anabolic metabolism. *Frontiers in Oncology*, 2, 200.

**Mocan** MC, Kadayifcilar S, Eldem B (2006) Elevated intravitreal interleukin-6 levels in patients with proliferative DR. *Canadian Journal of Ophthalmology*, 41, 747-752.

**Moore** SF, van den Bosch MT, Hunter R (2013) Dual Regulation of Glycogen Synthase Kinase 3 (GSK3) $\alpha/\beta$  by Protein Kinase C (PKC) $\alpha$  and Akt Promotes Thrombin-mediated Integrin  $\alpha_{IIb}\beta_3$  Activation and Granule Secretion in Platelets. *The Journal of Biological Chemistry*, 288, 3918-3928.

**Morgan** MJ and **Liu** ZG (2011). Crosstalk of ROS and NF $\kappa$ B signalling. *Cell Research*, 21, 103-115.

**Motohashi** H, Katsuoka F, Shavit JA et al (2000) Positive or negative MARE-dependent transcriptional regulation is determined by the abundance of small Maf proteins. *Cell*, 103, 865-75

**Mulder** GD, Patt LM, Sanders L et al (1994) Enhanced healing of ulcers in patients with diabetes by topical treatment with glycyl-L-histidyl-L-lysine copper. *Wound Repair Regen*, 2, 259–269.

**Muniyappa** R and **Sowers** JR (2013) Roles of insulin resistance in endothelial dysfunction. *Reviews in Endocrine and Metabolic Disorders*, 14, 5-12.

**Murphy-Lavoie** H, LeGros T, Butler FK (2017) HBO Therapy and Ophthalmology. HBO Therapy and Ophthalmology. In: *Textbook of Hyperbaric Medicine*. Springer, Cham.

## N

- Naghibi M**, Smith RP, Baltch AL et al. (1987) The effect of diabetes mellitus on chemotactic and bactericidal activity of human polymorphonuclear leukocytes. *Diabetes Research and Clinical Practice*, 4, 27–35.
- Naldini A**, Pucci A, Bernini C et al (2003) Regulation of angiogenesis by Th1- and Th2-type cytokines. *Current Pharmaceutical Design*, 9, 511–519.
- Nangaku M**, Inagi R, Miyata T et al (2009) .Hypoxia and hypoxia-inducible factor in renal disease *Nephron Experimental Nephrology*, 110, e1-e7.
- Nakaizumi A**, Zhang T, Puro DG (2012) The electrotonic architecture of the retinal microvasculature: Diabetes-induced alteration. *Neurochemistry International*, 61, 948-953.
- Nakayama GR**, Caton MC Nova MP et al (1997) Assessment of the Alamar Blue assay for cellular growth and viability in vitro. *Journal of Immunological Methods*, 204, 205–208.
- Namani A**, Li Y, Wang XJ et al (2014) Modulation of Nrf2 signalling pathway by nuclear receptors: implications for cancer, *Biochimica et Biophysica Acta*, 1843, 1875–1885.
- National Diabetes Data Group (NDDG)**. Diabetes in America: diabetes data compiled 1984. Bethesda, Md: National Institute for Health, 1985. (NIH publication no 85-1468).
- NCBI** (2018) <https://www.ncbi.nlm.nih.gov/> Time/date of access 30<sup>th</sup> September @ 03:58am
- Nesto RW** (Correlation between cardiovascular disease and diabetes mellitus: current concepts. *The American Journal of Medicine*, 116, 11-22.
- National Institute of Health and Clinical Excellence (NICE)** (2018) DR - Ruboxistaurin [ID382]. <https://www.nice.org.uk/guidance/indevelopment/gid-tag386>. Time/date of access: 18:46pm GMT, 11<sup>th</sup> September 2018.
- National Institute of Health and Clinical Excellence (NICE)** (2015) Dexamethasone intravitreal implant for treating diabetic macular oedema (TA349). <https://www.nice.org.uk/guidance/ta349>Time/date of access: 20:57pm GMT, 11<sup>th</sup> September 2018.
- National Institute of Health and Clinical Excellence (NICE)** (2013) Fluocinolone acetonide intravitreal implant for treating chronic diabetic macular oedema after an inadequate response to prior therapy (TA301) <https://www.nice.org.uk/guidance/ta301>Time/date of access: 20:59pm GMT, 11<sup>th</sup> September 2018
- Negi G**, Kumar A, Sharma S (2011) Nrf2 and NFκB modulation by sulforaphane counteracts multiple manifestations of DN in rats and high glucose-induced changes. *Current Neurovascular Research*, 8, 1-11.
- Neufeld S**, Planas-Paz L, Lammert E (2014) Blood and lymphatic vascular tube formation in mouse. *Seminars in Cell and Developmental Biology*, 31, 115-123.
- Newman P** and Newman B (Signal Transduction Pathways Mediated by PECAM-1\_New Roles for an Old Molecule in Platelet and Vascular Cell Biology. *Arteriosclerosis, Thrombosis, and Vascular Biology*, 23, 953–964.

**Nguyen T**, Pickett CB, Nioi P (2009) The Nrf2-Antioxidant Response Element Signalling Pathway and Its Activation by Oxidative Stress. *Journal of Biological Chemistry*, 284, 13291-13295.

**Niinikoski J**, Hunt TK, Dunphy JE (1972) Oxygen supply in healing tissue. *American Journal of Surgery*, 123, 247-252.

**Nishikawa T**, Edelstein D, Du XL et al (2000) Normalizing mitochondrial superoxide production blocks three pathways of hyperglycaemic damage. *Nature*, 404, 787-790.

**Niu, CC**, Lin SS, Yuan LJ et al (2013) Hyperbaric oxygen treatment suppresses MAPK signalling and mitochondrial apoptotic pathways in degenerated human intervertebral disc cells. *Journal of Orthopaedic research*, 31, 204-209.

**Nussenbaum F** and Herman IM (2010) Tumour Angiogenesis: Insights and Innovations. *Journal of Oncology*, 2010, Article ID 132641, 1-24.

## O

**Oberringer M**, Meins C, Bubel M (2007) A new *in vitro* wound model based on the co-culture of human dermal microvascular endothelial cells and human dermal fibroblasts. *Biology of the Cell*, 99, 197-207.

**Obrosova IG**, Pacher P, Szabo C et al (2005) AR inhibition counteracts oxidative-nitrosative stress and poly(ADP-ribose) polymerase activation in tissue sites for diabetes complications. *Diabetes*, 54, 234-242.

**Oguz H** and Sobaci G (2008) The use of hyperbaric oxygen in ophthalmology. *Survey of Ophthalmology*, 53, 112-120.

**Ohkubo Y**, Kishikawa H, Araki E et al (1995) Intensive insulin therapy prevents the progression of diabetic microvascular complications in Japanese patients with non-insulin-dependent diabetes mellitus: a randomized prospective 6-year study. *Diabetes Research and Clinical Practice*, 28, 103-117.

**Oram RA**, Patel K, Hill A (2016) OA Type 1 Diabetes Genetic Risk Score Can Aid Discrimination Between Type 1 and Type 2 Diabetes in Young Adults. *Diabetes Care*, 39, 337-344.

**O'Shea JJ** and Plenge R (2012) JAK and STAT signalling molecules in immunoregulation and immune-mediated disease. *Immunity*, 36, 542-550.

**Osterby R** (1992) Glomerular structural changes in type 1 (insulin-dependent) diabetes mellitus: causes, consequences, and prevention. *Diabetologia*, 35, 803-819.

**Osterby R**, Gall MA, Schmitz A et al (1993) Glomerular structure and function in proteinuric type 2 (non-insulin-dependent) diabetic patients. *Diabetologia*, 36, 1064-1070.

**Otterbein, L**, Mantell, L. and Choi, AM (1999) Carbon monoxide provides protection against hyperoxic lung injury. *American Journal of Physiology*, 276, 688-694.

## P

- Perrella** MA and **Yet** SF (2003) Role of heme oxygenase-1 in cardiovascular function. *Current Pharmaceutical Designs*, 9, 2479-2487.
- Park** JY, Takahara N, Gabrielle A et al (2000) Induction of endothelin -1 expression by glucose: an effect of protein kinase C activation. *Diabetes*, 49, 1239-1248.
- Pascal** MM, Knott RM, Forrester JV (1996) Glucose mediated regulation of transforming growth factor beta in human retinal endothelial cells. *Biochemical Society Transactions*, 24, 228S.
- Paschoud** S, Gogar AM, Kuntz C et al (2006) Destabilization of Interleukin-6 mRNA requires a Putative RNA Stem-Loop Structure, an AU-Rich Element, and the RNA-Binding Protein AUF1. *Molecular and Cellular Biology*, 26, 8228–8241.
- Patel** V, Chivukala I, and Roy S et al (2005) Oxygen: from the benefits of inducing VEGF expression to managing the risk of hyperbaric stress. *Antioxidants Redox Signalling*, 7, 1377-1387.
- Peng** H, Li Y, Wang C et al (2016) ROCK1 induces endothelial-to-mesenchymal transition in glomeruli to aggravate albuminuria in diabetic nephropathy. *Science Reports*, 6, 1-10.
- Perrot** S, Duterte-Catella H, Martin C et al (2003) Resazurin metabolism assay is a new sensitive alternative test in isolated pig cornea. *Toxicological Sciences*, 72, 122–129
- Petrova** TV, Mäkinen T, Mäkelä TP (2002) Lymphatic endothelial reprogramming of vascular endothelial cells by the Prox-1 homeobox transcription factor. *EMBO Journal*, 21, 4593-4599.
- Piconi** L, Quagliaro L, Da Ros R et al (2004) Intermittent high glucose enhances ICAM-1, VCAM-1, E-selectin and interleukin-6 expression in human umbilical endothelial cells in culture: the role of poly(ADP-ribose) polymerase. *Journal of Thrombosis and Haemostasis*, 2, 1453-1459.
- Piedboeuf** B, Gamache M, Frenette J et al (1998) Increased endothelial cell expression of platelet-endothelial cell adhesion molecule-1 during hyperoxic lung injury. *American Journal of Respiratory Cell and Molecular Biology*, 19, 543-553.
- Pflicke** H and Sixt M (2009) Preformed portals facilitate dendritic cell entry into afferent lymphatic vessels. *Journal of Experimental Medicine*, 206, 2925-2935.
- Phillips** PG, Higgins PJ, Malik AB et al (1988) Effect of Hyperoxia on the Cytoarchitecture of Cultured Endothelial Cells. *American Journal of Pathology*, 132, 59-72.
- Pieper** G and Riaz-ul-Haq J (1997) Activation of nuclear factor-kappa B in cultured endothelial cells by increased glucose concentration: prevention by calphostin C. *Journal of Cardiovascular Pharmacology*, 30, 528–532.
- Plafker** KS and **Plafker** SM (2015) The ubiquitin-conjugating enzyme UBE2E3 and its import receptor importin-11 regulate the localization and activity of the antioxidant transcription factor NRF2. *Molecular Biology of the Cell*, 26, 327–338.
- Pober** JS (1999) Immunobiology of human vascular endothelium. *Immunology Research*, 19, 225–232.

**Podgrabinska S**, Braun P, Velasco et al (2002) Molecular characterization of lymphatic endothelial cells. *PNAS*, 99, 16069–16074.

**Polydefkis M**, Griffin JW, McArthur J (2003) New insights into diabetic polyneuropathy. *Journal of American Medical Association*, 290, 1371-1376.

**Popov D** and **Simionescu M** (2006) Cellular mechanisms and signaling pathways activated by high glucose and AGE-albumin in the aortic endothelium. *Archives Physiology Biochemistry*, 112, 265-273.

**Portilla D**, Dai G, Peters J et al (2000) Etomoxir-induced PPAR alpha-modulated enzymes protect during acute renal failure. *American Journal of Physiology- Renal Physiology*, 278, F667–F675

**Potter CM**, Lundberg MH, and Harrington LS et al (2011) Role of shear stress in endothelial cell morphology and expression of cyclooxygenase isoforms. *Arteriosclerosis, Thrombosis, and Vascular Biology*, 31, 384-391

**Privratsky JR** and Newman PJ (2014) PECAM-1: regulator of endothelial junctional integrity. *Cell Tissue Research*, 355: 607.

**Pugh CW**, O'Rourke JF, Nagao M (1997) Activation of hypoxia-inducible factor-1; definition of regulatory domains within the  $\alpha$  subunit. *Journal of Biological Chemistry*, 272, 11205–11214.

## Q

**Quehenberger P**, Bierhaus A, Fasching P et al (2000) Endothelin 1 transcription is controlled by nuclear factor-kappa B in AGE-stimulated cultured endothelial cells. *Diabetes*, 49, 1561-1570.

## R

**Rada P**, Rojo AI, Chowdhry S et al (2011) SCF/ {beta}-TrCP promotes glycogen synthase kinase 3-dependent degradation of the Nrf2 transcription factor in a Keap1-independent manner. *Molecular Cellular Biology*, 31, 1121-33.

**Rada P**, Rojo AI, Evrard-Todeschi et al (2012) Structural and functional characterization of Nrf2 degradation by the glycogen synthase kinase 3/beta-TrCP axis. *Molecular Cellular Biology*, 32, 3486-99.

**Rafii S** and Lyden D (2003) Therapeutic stem and progenitor cell transplantation for organ vascularization and regeneration. *Nature Medicine*, 9, 702-712.

**Ray R** and Shah AM (2005) NADPH oxidase and endothelial cell function. *Clinical Science (London)*, 109 217-226.

**Rask-Madsen C** and King GL (2013) Vascular Complications of Diabetes: Mechanisms of Injury and Protective Factors. *Cell Metabolism*, 17, 20-33.



- Ramakers BP**, de Goeij M, van der Hoeven G et al (2009) Inflammation-induced hepatotoxicity in humans. *Shock*, 31, 151-156.
- Ratcliffe PJ** (2006) Understanding hypoxia signalling in cells—a new therapeutic opportunity? *Clinical Medicine* 6, 573–578.
- Reed JA** (1954) Aretaeus, the Cappadocian. *Diabetes*, 3, 419–421.
- Reichard P**, Nilsson BY, Rosenqvist U (1999). The effect of long-term intensified insulin treatment on the development of microvascular complications of diabetes mellitus. *New England Journal of Medicine*, 329, 304-309.
- Ritchie K**, Baxter S, Craig J et al (2008) The clinical and cost effectiveness of hyperbaric oxygen therapy- HTA programme: Systematic Review 2 - July 2008. NHS Quality improvement Scotland.
- Roan E**, Wilhelm K, Bada A et al (2012) Hyperoxia alters the mechanical properties of alveolar epithelial cells. *American Journal of Physiology- Lung Cellular Molecular and Physiology*, 302, 1235–1241.
- Robichaux JL**, Tanno E, Rappleye JW (2010) Lymphatic/Blood Endothelial Cell Connections at the Capillary Level in Adult Rat Mesentery. *The Anatomical Record*, 293, 1629-1638.
- Robison Jr WG**, Kador PF, Kinoshita JH (1983) Retinal capillaries: basement membrane thickening by galactosemia prevented with AR inhibitor. *Science*, 221, 1177–9.
- Robison Jr, WG**, Kador PF, Akagi Y et al (1986) Prevention of basement membrane thickening in retinal capillaries by a novel inhibitor of AR, tolrestat. *Diabetes*, 35295–3599.
- Roeckl-Wiedmann I**, Bennett M, Kranke P (2005) Systematic review of hyperbaric oxygen in the management of chronic wounds. *British Journal of Surgery*, 92, 24-32.
- Romano M**, Sironi M, Toniatti C, et al (1997) Role of IL-6 and its soluble receptor in induction of chemokines and leukocyte recruitment. *Immunity*, , 315-325.
- Ruas JL**, Poellinger L, Pereira T (2004) Role of CBP in regulating HIF-1-mediated activation of transcription. *Journal of Cell Science*, 118, 302-310.
- Ruderman A**, Williamson N, Brownlee M (1992) Glucose and diabetic vascular disease. *FASEB Journal*, 6, 2905.
- Rushworth SA**, Zaitseva L, Murray MY (2012) The high Nrf2 expression in human acute myeloid leukaemia is driven by NF-kappa B and underlies its chemo-resistance. *Blood*, 120, 5188-5198.
- Rzeczinski S**, Victorov IV, Lyjin AA et al (2006). Roller culture of free-floating retinal slices: A new system of organotypic cultures of adult rat retina. *Ophthalmic Research*, 38,263-269.

## S

**Sacca P**, Meiss R, Casas G (2007) Nuclear translocation of heme oxygenase-1 is associated to prostate cancer. *Br J Cancer* 97, 1683-1689

**Sada K**, Nishikawa T, Kukidome D et al (2016) Hyperglycaemia Induces Cellular Hypoxia through Production of Mitochondrial ROS Followed by Suppression of Aquaporin-1. *PLoS One*, 11, e0158619.

**Salameh A**, Zinn M, Dhein S (1997) High d-glucose induces alterations of endothelial cell structure in a cell-culture model. *Journal of Cardiovascular Pharmacology*, 30, 182– 190.

**Santoro MM** and **Gaudino G** (2005) Cellular and molecular facets of keratinocyte reepithelization during wound healing. *Experimental Cell Research*, 304, 274-286.

**Saraswat K** and Rizvi SI (2017) Novel strategies for anti-aging drug discovery. *Expert Opinion on Drug Discovery*, 12, 9. <https://doi.org/10.1080/17460441.2017.1349750>

**Saitoh T**, Kokue E, Shimoda M (2000) The impact of acute phase response on the plasma clearance of antipyrine, theophylline, phenytoin and nifedipine in rabbits. *Journal of Veterinary Pharmacology and Therapeutics*, 23, 153-158.

**Salgado A**, Boveda JL, Monasterio J, et al (1994) Inflammatory mediators and their influence on haemostasis. *Haemostasis*, 24, 132–8.

**Sanchez I**, Martin R, Ussa F et al (2011) The parameters of the porcine eyeball Graefe's Archive for Clinical and Experimental Ophthalmology, 249,475–482

**Sandoval R**, Malik AB, Minshall RD et al (2001) Ca<sup>2+</sup> signalling and PKC $\alpha$  activate increased endothelial permeability by disassembly of VE-cadherin junctions. *Journal of Physiology*, 533, 433-445.

**Sato A**, Kamekura R, Kawata K (2016) Novel Mechanisms of Compromised Lymphatic Endothelial Cell Homeostasis in Obesity: The Role of Leptin in Lymphatic Endothelial Cell Tube Formation and Proliferation. *PLOS One*. <https://doi.org/10.1371/journal.pone.0158408>

**Sayeski PP** and Kudlow JE (1996) Glucose metabolism to glucosamine is necessary for glucose stimulation of transforming growth factor-alpha gene transcription. *Journal of Biological Chemistry*, 271, 15237–15243.

**Schaper and Rose-John S** (2015) Interleukin-6: Biology, signalling and strategies of blockade. *Cytokine and Growth Factors Reviews*, 26, 475-487.

**Scheid A**, Wenger RH, Schaffer Let al. (2002) Physiologically low oxygen concentrations in fetal skin regulates hypoxia-inducible factor 1 and transforming growth factor-beta3. *FASEB J* 16: 411-413

**Schleicher and Nerlich A** (1996) The role of hyperglycaemia in the development of diabetic complications *Hormone and Metabolic Research*, 28, 367-373.

**Schleicher ED** (1999) Biochemical aspects of diabetic nephropathy. In Mogensen CE (Ed.) *The kidney in hypertension and diabetes mellitus*, Kluwer, Dordrecht, 269-279.

**Schmidt AM**, Yan SD JL et al (1999) Activation of receptors for AGEs. A mechanism for chronic vascular dysfunction in diabetic vasculopathy and atherosclerosis. *Circulation Research*, 84, 489-497.

**Schmidt** AM, Vianna M, Gerlach M et al (1992) Isolation and characterization of binding proteins for AGEs from lung tissue which are present on the endothelial cell surface. *Journal of Biological Chemistry*, 267, 14987.

**Schmidt** AM, Hori O, Brett J (1994) Cellular receptors for AGEs: Implications for induction of oxidant stress and cellular dysfunction in the pathogenesis of vascular lesions. *Arteriosclerosis and Thrombosis*, 1521, 1528.

**Schmittgen** TD, Zakrajsek BA, Mills AG et al (2000). Quantitative Reverse Transcription-Polymerase Chain Reaction to Study mRNA Decay: Comparison of Endpoint and Real-Time Methods. *Analytical Biochemistry* **285**, 194-204.

**Schramm** A, Matusik P, Osmenda G et al (2012) Targeting NADPH oxidases in vascular pharmacology. *Vascular Pharmacology*, 56, 216-231.

**Semenza** GL (1998) Hypoxia-inducible factor 1: Master regulator of O<sub>2</sub> homeostasis. *Current Opinion in Genetics and Development*, 8, 588-594.

**Semenza** G L, Neifelt M K, Chi SM (1991). Hypoxia-inducible nuclear factors bind to an enhancer element located 3' to the human erythropoietin gene. *Proceedings of the National Academy of Sciences*, 88, 5680-5684.

**Semenza** GL, Jiang BH, Leung SW et al (1996) Hypoxia response elements in the aldolase A, enolase 1, and lactate dehydrogenase A gene promoters contain essential binding sites for hypoxia-inducible factor 1. *Journal of Biological Chemistry*, 271, 32529-32537.

**Semenza** GL, Roth PH, Fang HM et al (1994) Transcriptional regulation of genes encoding glycolytic enzymes by hypoxia-inducible factor 1. *Journal of Biological Chemistry*, 269, 23757-23763.

**Semenza** GL (2008) A new weapon for attacking tumour blood vessels. *New England Journal of Medicine*, 358, 2066-2067.

**Sena** CM, Pereira AM, Seica R (2013) Endothelial dysfunction — A major mediator of diabetic vascular disease. *Biochimica et Biophysica Acta (BBA) - Molecular Basis of Disease*, 1832, 2216-2231.

**Senanayake** PD, Drazba J, Shadrach K et al (2007) Angiotensin II and Its Receptor Subtypes in the Human Retina, *Investigative Ophthalmology and Visual Science*, 48, 3301-3311.

**Shaw** JE and **Zimmet** PZ (1999) The epidemiology of DN. *Diabetes Reviews*, 7, 245-252.

**Shepro** D and **Morel** NM (1993) Pericyte physiology. *The FASEB Journal*, 7, 1031–1038.

**Sheehan** P, Jones P, Caselli A *et al* (2003) .Percent change in wound area of diabetic foot ulcers over a 4-week period is a robust predictor of complete healing in a 12-week prospective trial [J]. *Diabetes Care*, 26, 1879-1882.

**Sheikh** AY, Gibson JJ, Rollins MD (2000) Effect of Hyperoxia on Vascular Endothelial Growth Factor Levels in a Wound Model. *Archives of Surgery*, 135, 1293-1297.

**Shinohara** M, Thornalley P, Giardino I et al (1998) Overexpression of glyoxalase-I in bovine endothelial cells inhibits intracellular AGE formation and prevents hyperglycaemia-induced increases in macromolecular endocytosis. *Journal of Clinical Investigation*, 101, 1142–1147.

- Siewart S**, Gonzalez I, Santillan L et al (2013) Downregulation of Nrf2 and HO-1 expression contributes to oxidative stress in type 2 diabetes mellitus: A study in Juana Koslay City, San Luis, Argentina. *Journal of Diabetes Mellitus*, 3, 71-78.
- Siddiqui A**, Galiano R, Gonnors D et al (1996) Differential effects of oxygen on human dermal fibroblasts: acute versus chronic hypoxia. *Wound Repair and Regeneration*, 4, 211-218.
- Sima AA** and **Sugimoto K** (1999) Experimental DN: an update. *Diabetologia*, 42, 773-788
- Singer AJ** and **Clark RA** (1999) Cutaneous wound healing. *New England Journal of Medicine*, 341, 738-746.
- Simionescu M**, Popov D, Sima A et al (1996) Pathobiochemistry of combined diabetes and atherosclerosis studied on a novel animal model: the hyperlipemic hyperglycemic hamster. *American Journal of Pathology*, 148, 997-1014.
- Simo R** and **Hernandez** (2009) Advances in the Medical Treatment of Diabetic Retinopathy. *Diabetes Care*, 32, 1556–1562.
- Slebos DJ**, Ryter SW, van der Toorn M (2007) Mitochondrial localization and function of heme oxygenase-1 in cigarette smoke-induced cell death. *American journal of respiratory cell and molecular biology* 36, 409-417
- Smith DR**, Kobrine AI, Rizzoli HV (1977) Absence of autoregulation in peripheral nerve blood flow. *Journal of Neurological Sciences*, 33, 347–352.
- Soares A**, Gomes NL, Mendoca L et al (2017) The efficacy of hyperbaric oxygen therapy in the treatment of central retinal artery occlusion. *British Medical Journal Case Reports*, 10.1136/bcr-2017-220113.
- Soccio M**, Toniato E, Evangelista V et al (2005) Oxidative stress and cardiovascular risk: the role of vascular NAD (P)H oxidase and its genetic variants. *European Journal of Clinical Investigation*, 35, 305-314.
- Solari M**, Srinivasan S, Boumaza I et al (2009) Marginal mass islet transplantation with autologous mesenchymal stem cells promotes long-term islet allograft survival and sustained normoglycaemia. *Autoimmunity*, 32, 116-24.
- Srinivas V**, Zhang LP, Zhu XH (1999) Characterization of an oxygen/redox-dependent degradation domain of hypoxia-inducible factor alpha (HIF-alpha) proteins. *Biochemical and Biophysical Research Communications*, 260, 557-561.
- Stavniichuk R**, Drel VR, Shevalye H (2011) Baicalcein inhibits diabetic peripheral neuropathy through inhibition of oxidative nitrosative stress and p38 MAPK activation. *Experimental Neurology*, 230, 106–113.
- Steinberg SF** (2015) Mechanisms for redox-regulation of protein kinase C. *Front Pharmacology*, 6, 128.
- Stendahl J**, Kaufman D, Stupp I (2009) Extracellular matrix in pancreatic islets: Relevance to scaffold design and transplantation. *Journal of Cell Transplant*, 18, 1–12.
- Studer R**, Craven P, DeRubertis F (1993) Role for protein kinase C in the mediation of increased fibronectin accumulation by mesangial cells grown in high-glucose medium. *Diabetes*, 42, 118–126.

**Sumner** CJ, Sheth S, Griffin JW et al (2003) The spectrum of neuropathy in diabetes and impaired glucose tolerance. *Neurology*, 60, 108-111.

**Sunkari** VG, Lind F, Botusan IR et al (2015) Hyperbaric oxygen therapy activates hypoxia-inducible factor 1 (HIF-1), which contributes to improved wound healing in diabetic mice. *Journal of Wound Repair Regeneration*, 23, 98-103.

**Sureda** A, Batle JM, Martorell M et al (2016) Antioxidant response of chronic wounds to hyperbaric oxygen therapy. *PLoS One*, 11, e0163371.

**Sutterwala** FS, Haasken S, Cassel SL (2014) Mechanism of NLRP3 inflammasome activation. *Annals of the New York Academy of Sciences*, 1319, 89-95.

**Suzuki** H, Swei A, Zweifach BW et al (1995) In vivo evidence for microvascular oxidative stress in spontaneously hypertensive rats. Hydroethidine microfluorography. *Hypertension*, 25, 1083-1089.

**Suzuma** K, Takahara N, Suzuma I et al (2002) Characterization of protein kinase C beta isoform's action on retinoblastoma protein phosphorylation, vascular endothelial growth factor-induced endothelial cell proliferation, and retinal neovascularization. *Proceedings of National Academy of Sciences USA*, 99, 721–726.

## T

**Taguchi** T and Brownlee M (2003) The biochemical mechanisms of diabetic tissue damage. In: Pickup JC and Gareth W, eds. *Textbooks of Diabetes*. 3<sup>rd</sup> eds. Oxford: Blackwell Science. Pp. 47.1-47.15.

**Takahashi** Y, Takahashi S, Shiga Y et al (2000) Hypoxic induction of prolyl 4-hydroxylase  $\alpha$  (I) in cultured cells. *Journal of Biological Chemistry*, 275, 14139-14146.

**Tak** PP and **Firestein** GS (2001) NF-kappa B: a key role in inflammatory diseases. *Journal of Clinical Investigation*, 107, 7-11.

**Takata** K, Hirano H, Kasahara M (1997) Transport of glucose across the blood-tissue barriers. *International Review of Cytology*, 172, 1-53.

**Tang** Y, Zhang MJ, Hellmann J (2013) Pro-resolution Therapy for the Treatment of Delayed Healing of Diabetic Wounds. *Diabetes*, 62, 618-627.

**Tanaka** T, Narazaki M, Kishimoto T (2014) IL-6 in Inflammation, Immunity, and Disease. *Perspectives in Biology*, Cold Spring Harbour, doi: 10.1101/cshperspect.a016295

**Tansley** K (1933) Formation of rosettes in the rat retina. *British Journal of Ophthalmology*, 17: 321–336.

**Tartour** E, Pere H, Maillere B et al (2011) Angiogenesis and immunity: a bidirectional link potentially relevant for the monitoring of antiangiogenic therapy and the development of novel therapeutic combination with immunotherapy. *Cancer Metastasis Reviews*, 30, 83–95.

**Terraneo** L, Virgili E, Caretti A et al (2014) In vivo hyperoxia induces hypoxia-inducible factor-1 $\alpha$  overexpression in LNCaP tumours without affecting the tumour growth rate. *The International Journal of Biochemistry and Cell Biology*, 51, 65-74.

**Taylor L, Arnér K, Holmgren T et al (2014)** Feet on the Ground: Physical Support of the Inner Retina Is a Strong Determinant for Cell Survival and Structural Preservation in Vitro. *Investigative Ophthalmology and Visual Science*, 55, 2200-2213.

**Taylor L, Arnér K, Engelsberg K et al (2015).** Scaffolding the retina: The interstitial extracellular matrix during rat retinal development. *International Journal of Developmental Neuroscience*, 42, 46-58.

**Tenhunen T, Marver H, Schmid, R (1968).** The enzymatic conversion of heme to bilirubin by microsomal heme oxygenase. *Proceedings of the National Academy of Science (USA)*, 61, 748-755.

**Thanabalasingham G, Pal A, Selwood MP et al (2012)** Systematic assessment of etiology in adults with a clinical diagnosis of young-onset type 2 diabetes is a successful strategy for identifying maturity-onset diabetes of the young. *Diabetes Care*, 35, 1206-1212.

**Thangaraj G, Greif A, Layer PG (2011)** “Simple explant culture of the embryonic chicken retina with long-term preservation of photoreceptors,” *Experimental Eye Research*, 93, 556–564.

**Thiersch M, Lange C, Joly S (2009)** Retinal neuroprotection by hypoxic preconditioning is independent of hypoxia-inducible factor-1 $\alpha$  expression in photoreceptors. *European Journal of Neuroscience*, 29, 2291-2302.

**Thom SR (2011)** Hyperbaric oxygen – its mechanisms and efficacy. *Plastic and Reconstructive Surgery*, 127, 131S-141S.

**Thom SR (2009)** Oxidative stress is fundamental to hyperbaric oxygen therapy. *Journal of Applied Physiology*, 106, 988–995.

**Thomas DD, Ridnour LA, Espey MG et al (2006)** Superoxide fluxes limit nitric oxide-induced signalling. *Journal of Biological Chemistry*, 281, 25984-25993.

**Thornalley P (1990)** The glyoxalase system: new developments towards functional characterization of a metabolic pathway fundamental to biological life. *Biochemistry Journal*, 269, 1–11.

**Thrainsdottir S, Malik RA, Dahlin LB et al (2003)** Endoneurial capillary abnormalities presage deterioration of glucose tolerance and accompany peripheral neuropathy in man. *Diabetes*, 52, 2615-2622.

**Tibbitt M and Anseth K (2009)** Hydrogels as Extracellular Matrix Mimics for 3D Cell Culture. *Biotechnology and Bioengineering*, 103, 655-663.

**Tiganis T (2011)** ROS and insulin resistance: the good, the bad and the ugly. *Trends in Pharmacological Sciences*, 32, 82–89.

**Tjarnstrom J, Holmdahl L, Arnell P et al (1999)** Treatment with hyperbaric oxygen affects endothelial cell fibrinolysis. *European Journal of Surgery*, 165, 834–838.

**Tomlinson DR (1999)** Mitogen-activated protein kinases as glucose transducers for diabetic complications. *Diabetologia*, 42, 1271-1281.

**Tong Land Tergaonkar V (2014)** Rho protein GTPases and their interactions with NF $\kappa$ B: crossroads of inflammation and matrix biology. *Bioscience Reports*, 2014, 34.

**Turrens JF** (2003) Mitochondrial formation of ROS. *Journal of Physiology*, 552, 335-344.

**Tzima E**, Irani-Tehrani M, Kiosses WB et al (2005) A mechanosensory complex that mediates the endothelial cell response to fluid shear stresses. *Nature*, 437, 426–431.

## U

**UK Prospective Diabetes Study (UKPDS) Group** (1991) UK prospective diabetes study VIII. Study design, progress and performance. *Diabetologia*, 34, 877–890.

**UK Prospective Diabetes Study (UKPDS) Group** (1998a) Intensive blood-glucose control with sulphonylureas or insulin compared with conventional treatment and risk of complications in patients with type 2 diabetes (UKPDS 33). *Lancet* 352, 837–853.

**UK Prospective Diabetes Study Group** (1998b) Tight blood pressure control and risk of macrovascular and microvascular complications in type 2 diabetes: UKPDS 38 (1998b). *British Medical Journal*, 317, 703–713.

**Ulrich T**, Jain A, Tanner K et al (2010) Probing cellular mechanobiology in three-dimensional culture with collagen–agarose matrices. *Biomaterials*, 31, 1875-1884

**Unfirer S**, Kibel A, Drenjancevic-Peric I (2008) The effect of hyperbaric oxygen therapy on blood vessel function in diabetes mellitus. *Journal of Medical Hypotheses*, 71, 776-780.

## V

**Velichkova M** and **Hasson T** (2005) Keap1 regulates the oxidation-sensitive shuttling of Nrf2 into and out of the nucleus via a Crm1-dependent nuclear export mechanism, *Molecular and Cellular Biology*, 25, 4501–4513.

## W

**Wakabayashi N**, Itoh K, Wakabayashi J et al (2003) Keap1-null mutation leads to postnatal lethality due to constitutive Nrf2 activation. *Nature Genetics*, 35, 238-245.

**Wakabayashi N**, Shin S, Slocum SL et al (2010) Regulation of notch1 signalling by nrf2: implications for tissue regeneration. *Science Signalling*, 3, ra52.

**Wang RY**, Liu LH, Liu H (2018) Nrf2 protects against diabetic dysfunction of endothelial progenitor cells via regulating cell senescence. *International Journal of Molecular Medicine*, 42, 1327-1340. <https://doi.org/10.3892/ijmm.2018.3727>

**Wang GL**, Jiang BH, Semenza GL (1995\_a) Effect of altered redox states on expression and DNA-binding activity of hypoxia-inducible factor 1. *Biochemical and Biophysical Research Communications*, 212, 550-556.

**Wang** GL, Jiang BH, Rue EA, Semenza GL (1995\_b) Hypoxia-inducible factor 1 is a basic-helix-loop-helix-PAS heterodimer regulated by cellular O<sub>2</sub> tension. *Proceedings of the National Academy of Science U S A*, 6, 5510-5514.

**Wang** GL, and **Semenza** GL (1993) Desferrioxamine induces erythropoietin gene expression and hypoxia-inducible factor 1 DNA-binding activity: implications for models of hypoxia signal transduction. *Blood*, 82, 3610-3615.

**Wang** XL, Fu A, Spiro C et al (2009) Proteomic Analysis of Vascular Endothelial Cells-Effects of Laminar Shear Stress and High Glucose. *Journal of Proteomics and Bioinformatics*, 2, 445–454.

**Wangsa-Wirawan** ND, Linsenmeier RA (2003) Retinal oxygen. *Fundamental and clinical aspects*. *Archives of Ophthalmology*, 121, 547–557.

**Waxman** AB and **Kolliputi** N (2009) IL-6 Protects against Hyperoxia-Induced Mitochondrial Damage via Bcl-2–Induced Bak Interactions with Mitofusions. *American Journal of Respiratory Cell and Molecular Biology*, 41, 385–396.

**Weis** M, Wildhirt SM, Schulze C (1999) Modulation of coronary vasomotor tone by cytokines in cardiac transplant recipients. *Transplantation*, 68, 1263–1267.

**Weisz** G, Lavy A, Adir Y et al (1997). Modification of in Vivo and in Vitro TNF- $\alpha$ , IL-1, and IL-6 Secretion by Circulating Monocytes during Hyperbaric Oxygen treatment in patients with perianal Crohn's disease. *Journal of Clinical Immunology*, 17, 154-159.

**Wells** L and **Hart** G (2003) O-GlcNAc turns twenty: functional implications for posttranslational modification of nuclear and cytosolic protein with a sugar. *FEBS Letters*, 546, 154–158.

**Wells-Knecht** K, Zyzak D, Litchfield J et al (1995) Mechanism of autoxidative glycosylation: identification of glyoxal and arabinose as intermediates in the autoxidative modification of proteins by glucose. *Biochemistry*, 34, 3702–3709.

**Wilkinson** D, Chapman IM, Heilbronn (2012) Hyperbaric oxygen therapy improves peripheral insulin sensitivity in humans. *Diabetic Medicine*, 03587, 1464-5491.

**Williamson** JR, Chang K, Frangos M et al (1993) Hyperglycaemic pseudohypoxia and diabetic complications. *Diabetes*, 42, 801-813.

**Winer** J, Jung CK, Shackel I et al (1999) Development and Validation of Real-Time Quantitative Reverse Transcriptase-Polymerase Chain Reaction for Monitoring Gene Expression in Cardiac Myocytes in Vitro. *Analytical Biochemistry* 270, 41-49.

**Witte** MH, Bernas MJ, Martin CP et al CL (2001) Lymph angiogenesis and lymphangio-dysplasia: from molecular to clinical lymphology. *Microscopy Research and Techniques*, 55, 122–145.

**Woodfin** A, Voisin MB, Nourshargh S (2007) PECAM-1: A Multi-Functional Molecule in Inflammation and Vascular Biology. *Arteriosclerosis, Thrombosis, and Vascular Biology*, 27, 2514–2523.

**World Health Organisation (WHO)** (1999) Definition, diagnosis and classification of diabetes mellitus and its complications, Part 1. Report of a WHO Consultation.



## X

**Xiang** MJ, Namani A, Wu SJ et al (2014) Nrf2: bane or blessing in cancer? *Journal of Cancer Research and Clinical Oncology*, 140, 1251-1259.

**Xiao** G Harhaj EW, Sun SC (2001) NF-kappa B-inducing kinase regulates the processing of NF-kappaB2 p100. *Molecular Cell*, 7, 401-409.

**Xiao** H, Gu Z, Wang G et al (2013) The Possible Mechanisms Underlying the Impairment of HIF-1 $\alpha$  Pathway Signaling in Hyperglycaemia and the Beneficial Effects of Certain Therapies. *International Journal of Medical Sciences*, 10, 1412-1421.

**Xu** B, Chibber R, Ruggiero D et al (2003) Impairment of vascular endothelial nitric oxide synthase activity by AGEs. *FASEB Journal*, 17, 1289-1291.

**Xu** Z, Wei Y, Gong J et al (2014) NRF2 plays a protective role in DR in mice. *Diabetologia*, 57, 204–213.

**Xu** N, Brodin P, Wei T (2011) MiR-125b, a microRNA downregulated in psoriasis, modulates keratinocyte proliferation by targeting FGFR2. *Journal of Investigative Dermatology*, 131: 1521–1529.

**Xue** M, Qian Q, Antonysunil A et al (2008) Activation of NF-E2-related factor-2 reverses biochemical dysfunction of endothelial cells induced by hyperglycaemia linked to vascular disease. *Diabetes*, 67. <https://doi.org/10.2337/db06-1003>

## Y

**Yachie** A, Niida Y, Wada T et al (1999) Oxidative stress causes enhanced endothelial cell injury in human heme oxygenase-1 deficiency. *Journal of Clinical Investigation*, 103, 129–135.

**Yagihashi** S, Mizukami H, Sugimoto K (2011) Mechanism of DN: Where are we now and where to go? *Journal of Diabetic Investigation*, 2, 18-32.

**Yan** SF, Ramasamy R, Naka Y et al (2003) Glycation, Inflammation, and RAGE: A Scaffold for the Macrovascular Complications of Diabetes and Beyond. *Circulation Research*, 93, 1159-1169.

**Yan** J, Zhang Z, Shi H (2012) HIF-1 is involved in high glucose-induced paracellular permeability of brain endothelial cells. *Cellular and Molecular Life Sciences*, 69, 115–128.

**Yang** QH, Zhang Y, Jiang J (2018) Protective effects of a novel drug RC28-E blocking both VEGF and FGF2 on early diabetic rat retina. *International Journal of Ophthalmology*, 11, 935–944.

**Yokota** T, Ma RC, Park JY, Isshiki K, Sotiropoulos KB et al (2003). Role of protein kinase C on the expression of platelet-derived growth factor and endothelin-1 in the retina of diabetic rats and cultured retinal capillary pericytes. *Diabetes*, 52, 838–845.

**Yoshida** T and **Sato** M (1989) Posttranslational and direct integration of heme oxygenase into microsomes. *Biochemical and Biophysical Research Communications*, 163, 1086-1092.

**Yoshida T**, Ishikawa K, Sato M (1991) Degradation of heme by a soluble peptide of heme-oxygenase obtained from rat liver microsomes by mild trypsinization. *European Journal of Biochemistry*, 199, 729-733

**Yu CH**, Suriguga A, Gong M et al (2017) High glucose induced endothelial to mesenchymal transition in human umbilical vein endothelial cell. *Experimental and Molecular Pathology*, 102, 377–383

**Yu PK**, Yu DY, Cringle SJ et al (2005) Endothelial F-actin cytoskeleton in the retinal vasculature of normal and diabetic rats. *Current Eye Research*, 30, 279– 290.

**Yu DY**, Cringle SJ (2001) Oxygen distribution and consumption within the retina in vascularised and avascular retinas and in animal models of retinal disease. *Progress in Retinal and Eye Research*, 20, 175–208.

**Yuen DY**, Dwyer RM, Matthews VB et al (2009) Interleukin-6 Attenuates Insulin-Mediated Increases in Endothelial Cell Signaling but Augments Skeletal Muscle Insulin Action via Differential Effects on Tumor Necrosis Factor- $\alpha$  Expression. *Diabetes*, 58, 1086-1095.

## Z

**Zakkar M**, Van der Heiden K, Luong LA et al (2009) Activation of Nrf2 in endothelial cells protects arteries from exhibiting a proinflammatory state. *Arteriosclerosis, Thrombosis, and Vascular Biology*, 29, 1851-1857.

**Zalata AA**, Lammertijn N, Christophe A et al (1998) The correlates and alleged biochemical background of the Resazurin reduction test in semen. *International journal of andrology*, 21, 289-294

**Zhang WJ** and **Frei B** (2001). Alpha-lipoic acid inhibits TNF-alpha-induced NF-kappa B activation and adhesion molecule expression in human aortic endothelial cells. *FASEB Journal*, 15, 2423-2432.

**Zhang T**, Wu DM, X G (2011) The electrotonic architecture of the retinal microvasculature: modulation by angiotensin II. *Journal of Physiology*, 589, 2383-2399.

**Zhao D**, Lu S, Xu W (2017) Efficacy and Safety of Hyperbaric Oxygen Therapy Used in Patients With Diabetic Foot: A Meta-analysis of Randomized Clinical Trials. *Clinical Therapeutics*, 39, 2088-2094.e2

**Zhong H**, Agani F, Baccala AA et al (1998) Increased expression of hypoxia inducible factor-1 $\alpha$  in rat and human prostate cancer. *Cancer Research*, 58, 5280-5284.

**Zhongwei L** and **Khalil R** (2018) Evolving mechanisms of vascular smooth muscle contraction highlight key targets in vascular disease. *Biochemical Pharmacology*, 153, 91-122

**Zhu C**. (2013) AR inhibitors as potential therapeutic drugs of diabetic complications. *Diabetes Mellitus-Insights and Perspectives*, 17-46.

**Ziello JE**, Jovin IS, Huang Y (2007) Hypoxia-Inducible Factor (HIF)-1 Regulatory Pathway and its Potential for Therapeutic Intervention in Malignancy and Ischaemia. *Yale Journal of Biology and Medicine*, 80, 51-60.

**Zilahi** E, Tarr T, Papp G et al (2012) Increased microRNA-146a/b, TRAF6 gene and decreased IRAK1 gene expressions in the peripheral mononuclear cells of patients with Sjögren's syndrome. *Immunology Letters*, 141, 165–168.

**Zykova** SN, Jenssen TG, Berdal M (2000) Altered cytokine and nitric oxide secretion in vitro by macrophages from diabetic type II-like db/db mice. *Diabetes*, 49, 1451–58.

**Zong** Y, Xu H, Yu J et al (2017) Retinal Vascular Autoregulation during Phase IV of the Valsalva Manoeuvre: An Optical Coherence Tomography Angiography Study in Healthy Chinese Adults. *Frontiers in Physiology*, <https://doi.org/10.3389/fphys.2017.00553>.